

APPLICATION OF ACTIVE CONTROLS TECHNOLOGY
TO AIRCRAFT RIDE SMOOTHING SYSTEMS

Technical Report

Grant No. NGR 47-005-202

Submitted to:

National Aeronautics and Space Administration
Scientific and Technical Information Facility
P.O. Box 8757
Baltimore/Washington International Airport
Baltimore, Maryland 21240

Submitted by:

Maris Lapins

and

Ira D. Jacobson

SCHOOL OF ENGINEERING AND
APPLIED SCIENCE

RESEARCH LABORATORIES FOR THE ENGINEERING SCIENCES

UNIVERSITY OF VIRGINIA

CHARLOTTESVILLE, VIRGINIA 22901



Report No. ESS-4039-106-75

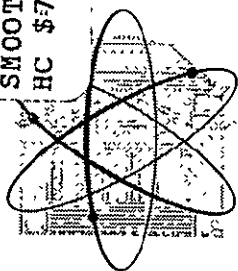
May, 1975



(NASA-CR-145980) APPLICATION OF ACTIVE
CONTROLS TECHNOLOGY TO AIRCRAFT RIDE
SMOOTHING SYSTEMS. (Virginia Univ.), 211 p.
HC \$7.75 CSDL 01C

N76-14138

Unclas
G3/08 07409



RESEARCH LABORATORIES FOR THE ENGINEERING SCIENCES

The School of Engineering and Applied Science of the University of Virginia has long believed that strong research capabilities go hand in hand with effective teaching. Early in the development of its graduate training program, the School also recognized that men and women engaged in research should be as free as possible of the administrative chores involved in sponsored research. In 1959, therefore, the Research Laboratories for the Engineering Sciences (RLES) was established and assigned the administrative responsibility for such research within the School.

Currently, approximately 60 members of the faculty, who also teach at the undergraduate and graduate levels, and 30 additional professional engineers and scientists, whose primary responsibility is research, generate and conduct the investigations that make up a vigorous and wide-ranging program. The Director of RLES, a faculty member and active researcher himself, maintains familiarity with the support requirements of all research under way. He is aided by an RLES Academic Advisory Committee made up of one faculty representative from each academic department of the School. This Committee serves to inform RLES of the needs and perspectives of the research community.

In addition to administrative support, RLES is charged with providing technical assistance where it is needed. Because it is not practical for each department of the School to become self-sufficient in all phases of the supporting technology essential to present-day research, RLES makes services available through the following support groups: Machine Shop, Instrumentation, Facilities Services, Publications (including photographic facilities), and Computer Terminal Maintenance.

The purpose of RLES, then, is to provide administrative and technical assistance for sponsored research carried out within the School of Engineering and Applied Science of the University of Virginia. Such research has played an important part in the University's contribution to scientific knowledge and service to the community and continues the successful partnership of University, government, and industry.

For information on current programs and capabilities, write to Director, Research Laboratories for the Engineering Sciences, Thornton Hall, University of Virginia, Charlottesville, Virginia 22901.

APPLICATION OF ACTIVE CONTROLS TECHNOLOGY
TO AIRCRAFT RIDE SMOOTHING SYSTEMS

Technical Report
Grant No. NGR 47-005-202

Submitted to:
National Aeronautics and Space Administration
Scientific and Technical Information Facility
P.O. Box 8757
Baltimore/Washington International Airport
Baltimore, Maryland 21240

Submitted by:
Maris Lapins
and
Ira D. Jacobson

DEPARTMENT OF ENGINEERING SCIENCE AND SYSTEMS
SCHOOL OF ENGINEERING AND APPLIED SCIENCE
UNIVERSITY OF VIRGINIA
CHARLOTTESVILLE, VIRGINIA

Report No. ESS-4039-106-75
May 1975

ABSTRACT

A critical review of past efforts in the design and testing of ride smoothing and gust alleviation systems is presented. Design trade-offs involving sensor types, choice of feedback loops, human comfort and aircraft handling-qualities criteria are discussed. Synthesis of a system designed to employ direct-lift and side-force producing surfaces is reported. Two STOL-class aircraft and an executive transport are considered. Theoretically-predicted system performance is compared with hybrid simulation and flight test data. Pilot opinion rating, pilot workload, and passenger comfort rating data for the basic and augmented aircraft are included.

TABLE OF CONTENTS

		Page
ABSTRACT.		iii
LIST OF TABLES.		ix
LIST OF FIGURES		xi
NOMENCLATURE.		xv
Chapter		
I	INTRODUCTION.	1
	1.1 Problem Statement.	1
	1.2 Historical Perspective	3
	1.3 Research Objectives.	11
II	PROBLEM DEFINITION.	13
	2.1 Equations of Motion.	13
	2.2 Description of Atmospheric Turbulence and Calculation of Aircraft Response	16
	2.3 Ride Smoothing System Criteria	16
	2.3.1 Passenger Comfort	16
	2.3.2 Design Level of Turbulence.	17
	2.3.3 Surface Activity.	19
	2.3.4 Handling Qualities.	19
	2.3.5 Failure Modes	20
	2.3.6 Feasibility	20
	2.3.7 The Optimal Control Performance Index	20
	2.4 Selection of Sensors, Control Surfaces, and Feedbacks.	21

PRECEDING PAGE BLANK NOT FILMED

TABLE OF CONTENTS (Continued)

Chapter		Page
III	ANALYSIS AND SYNTHESIS.	25
	3.1 Order of Presentation.	25
	3.2 Demonstration Aircraft	25
	3.3 Method of Analysis	28
	3.4 Longitudinal Ride Smoothing Systems.	28
	3.4.1 The Basic JetStar--Longitudinal Case.	28
	3.4.2 Baseline Longitudinal Ride Smoothing System	33
	3.4.3 Effect of Inner Loop Closures	35
	3.4.4 Basic Multi-Loop Longitudinal Ride Smoothing System.	35
	3.4.5 Analytic Model of Longitudinal Ride Smoothing System.	43
	3.4.6 Longitudinal Ride Smoothing System I.	50
	3.4.7 Longitudinal Ride Smoothing System II	62
	3.5 Lateral Ride Smoothing Systems	65
	3.5.1 The Basic JetStar--Lateral Case	65
	3.5.2 Lateral Ride Smoothing System	69
	3.5.3 Analytic Model of Lateral Ride Smoothing System.	82
	3.5.4 Alternate Lateral Ride Smoothing System	85
	3.6 Overall Effectiveness of Combined Axis Ride Smoothing System	89
IV	SIMULATION EXPERIMENTS.	91
	4.1 Order of Presentation.	91
	4.2 The Simulator Facility	91
	4.3 Digital Computer Program	93
	4.4 Analog Circuits.	95

TABLE OF CONTENTS (Continued)

Chapter		Page
IV	4.5 Hybrid Simulation Verification	95
	4.6 Simulation Evaluation Pilots	100
	4.7 Handling Qualities Evaluation.	104
	4.7.1 General Instructions.	104
	4.7.2 Longitudinal Task	105
	4.7.3 Lateral Task.	108
	4.7.4 Combined Axes Task.	109
	4.7.5 Smooth Air Evaluation, Conclusions.	111
	4.7.6 Instrument Landing System Approach Task . . .	111
	4.7.7 Simulation of Straight and Level Flight . . .	122
	4.8 Conclusions.	126
V	FLIGHT TEST PROGRAM	129
	5.1 Planned Program.	129
	5.2 Implementation of RSS Aboard the JetStar	129
	5.3 Ground Tests	131
	5.4 Data Acquisition and Reduction	133
	5.5 Summary of Flight Test Data.	134
	5.6 Conclusions.	138
VI	EXTENSION OF RIDE SMOOTHING SYSTEM CONCEPT TO STOL AIRCRAFT	143
	6.1 Selected Aircraft.	143
	6.2 Synthesis of Ride Smoothing Systems.	145
	6.2.1 Longitudinal RSS.	145
	6.2.2 Lateral RSS	153
	6.2.3 Improvement in Passenger Comfort.	159

TABLE OF CONTENTS (Continued)

Chapter		Page
VI	6.3 Simulator Evaluation of STOL Ride Smoothing Systems	159
	6.4 Conclusions	161
VII	CONCLUSIONS AND RECOMMENDATIONS	163
Appendix		
A	DEFINITION OF STABILITY DERIVATIVES	165
	A.1 Axis Systems	165
	A.2 Definition of Nondimensional Stability Derivatives	166
	A.3 Transformation of Stability Axis Derivatives to Body Axis	166
	A.3.1 Longitudinal Derivatives	166
	A.3.2 Lateral Derivatives	167
	A.4 Dimensional Stability Derivative Definitions	168
	A.4.1 Longitudinal Derivatives	168
	A.4.2 Lateral Derivatives	169
B	TURBULENCE FILTERS AND INPUT-OUTPUT RELATIONSHIPS	173
C	JETSTAR DATA	177
D	FORMULATION OF TRANSFER FUNCTIONS FOR MULTI-LOOP FEEDBACK CONTROL SYSTEMS	181
E	STOL DATA	187
	REFERENCES	191

LIST OF TABLES

Table		Page
I	Longitudinal Competing Systems.	23
II	Performance of Baseline Longitudinal RSS.	34
III	Characteristics of Longitudinal Ride Smoothing System I .	60
IV	Characteristics of Longitudinal Ride Smoothing System II.	67
V	Effect of Feedbacks on Roll Subsidence and Spiral Modes .	74
VI	Characteristics of Lateral Ride Smoothing System.	80
VII	Comparison of Lateral Ride Smoothing Systems.	88
VIII	Cooper-Harper Rating Scale.	106
IX	Average Cooper-Harper Pilot Ratings, Longitudinal Task. .	107
X	Average Cooper-Harper Pilot Ratings, Lateral Task	109
XI	Average Cooper-Harper Pilot Ratings, Combined Axis Task .	110
XII	Average Cooper-Harper Pilot Ratings, ILS Task	113
XIII	Simulation Results, ILS Tracking Task	123
XIV	Ride Smoothing System Flight Test Results	136
XV	Comparison of JetStar and STOL Longitudinal Ride Smoothing Systems	149
XVI	Comparison of JetStar and STOL Lateral Ride Smoothing Systems	156
XVII	Average Cooper-Harper Pilot Ratings, STOL ILS Approach Task	160

LIST OF FIGURES

Figure		Page
1	Open-Loop Control System.	3
2	Closed-Loop Control System.	3
3	Passenger Satisfaction Criteria	18
4	NASA General Purpose Airborne Simulator (GPAS).	26
5	Schematic of NASA General Purpose Airborne Simulator. . .	27
6	Handling Qualities Specification for n/α	30
7	Power Spectra of a_z Due to Turbulence for Basic JetStar .	31
8	Partitioned Power Spectra of a_z for Basic JetStar	32
9	Baseline Longitudinal Ride Smoothing System	33
10	Root Locus for Baseline Longitudinal RSS.	36
11	Root Locus for $\theta \rightarrow \delta_e$ Loop Closure.	37
12	Basic Longitudinal Ride Smoothing System	38
13	Root Locus for Basic Longitudinal RSS	39
14	Performance of Basic Longitudinal RSS; σ_{a_z} as a Function of K_{a_z} and K_θ	40
15	Performance of Basic Longitudinal RSS; σ_q as a Function of K_{a_z} and K_θ	41
16	Performance of Basic Longitudinal RSS; σ_{δ_f} as a Function of K_{a_z} and K_θ	42
17	Performance of Basic Longitudinal RSS; σ_{a_z} as a Constrained Function of K_{a_z} and K_θ	44
18	Comparison of Digitally Calculated σ_{a_z} with Analytic Expression	48
19	Power Spectra for w_g Due to Λ	49
20	Root Locus of Effect on Short-Period Dynamics of Filters in $a_z \rightarrow \delta_f$ Feedback Loop.	51

LIST OF FIGURES (Continued)

Figure		Page
21	Root Locus of Effect on Short-Period Dynamics of a Lead Filter in $\theta \rightarrow \delta_e$ Feedback Loop.	53
22	Longitudinal Ride Smoothing System I.	54
23	Performance of Longitudinal RSS I; σ_{a_z} as a Function of K_{a_z} and K_θ	55
24	Performance of Longitudinal RSS I; σ_q as a Function of K_{a_z} and K_θ	56
25	Performance of Longitudinal RSS I; σ_{δ_f} as a Function of K_{a_z} and K_θ	57
26	Performance of Longitudinal RSS I; σ_{a_z} as a Constrained Function of K_{a_z} and K_θ	58
27	Root Locus for Longitudinal RSS I	59
28	Comparison of a_z Power Spectra for Basic and Longitudinal RSS I Augmented ^Z JetStar	61
29	Longitudinal Ride Smoothing System II	63
30	Bode Magnitude Plot of Notch Filter	64
31	Root Locus of Effect on Short-Period Dynamics of a Notch Filter in $a_z \rightarrow \delta_f$ Feedback Loop	66
32	Comparison of a_z Power Spectra for Basic and Longitudinal RSS II Augmented JetStar.	68
33	Power Spectra of a_y Due to Turbulence for Basic JetStar .	70
34	Lateral Ride Smoothing System	72
35	Dutch Roll Root Locus for Lateral RSS	73
36	Performance of Lateral RSS; σ_{a_y} as a Function of K_{a_y} and K_r	75
37	Performance of Lateral RSS; σ_r as a Function of K_{a_y} and K_r	76
38	Performance of Lateral RSS; σ_p as a Function of K_{a_y} and K_r	77

LIST OF FIGURES (Continued)

Figure		Page
39	Performance of Lateral RSS; $\sigma_{\delta_{sfg}}$ as a Function of K_{a_y} and K_r	78
40	Performance of Lateral RSS; σ_{a_y} as a Constrained Function of K_{a_y} and K_r	79
41	Comparison of a Power Spectra for Basic and Lateral RSS Augmented JetStar	81
42	Comparison of Digitally Calculated σ_{a_y} with Analytic Expression	86
43	Alternate Lateral Ride Smoothing System.	87
44	Simulation Cockpit	92
45	GPAS Test Pilot's Instrumentation.	94
46	Analog Equalization Circuit Diagram; $a_z \rightarrow \delta_f$ Feedback Loop.	96
47	Analog Equalization Circuit Diagram; $\theta \rightarrow \delta_e$ Feedback Loop	97
48	Analog Equalization Circuit Diagram; $r \rightarrow \delta_r$ Feedback Loop	98
49	Simulation Laboratory.	99
50	Power Spectra of Simulated α_g	101
51	Power Spectra of Simulated β_g	102
52	Power Spectra of Simulated p_g	103
53	Altitude Track; Basic JetStar in Design Turbulence Field (Pilot A).	115
54	Deviation from Localizer; Basic JetStar in Design Turbulence Field (Pilot A)	116
55	Simulation Time History; JetStar in Design Turbulence Field (Pilot A).	117
56	Power Spectra of a_z Due to Turbulence, Simulation Data .	124

LIST OF FIGURES (Continued)

Figure		Page
57	Power Spectra of a_y Due to Turbulence, Simulation Data .	125
58	Airborne Analog Computer	130
59	Comparison of a_z Power Spectra for Basic and Longitudinal RSS I Augmented JetStar (Flight Data) . . .	137
60	Time History; Basic and Longitudinal RSS I Augmented JetStar in Turbulence (Flight Data).	139
61	Buffalo Longitudinal RSS	147
62	S-11 Longitudinal RSS.	148
63	Comparison of a_z Power Spectra for Basic and Longitudinal RSS Augmented Buffalo	151
64	Comparison of a_z Power Spectra for Basic and Longitudinal RSS Augmented S-11.	152
65	Buffalo Lateral RSS.	154
66	S-11 Lateral RSS	155
67	Comparison of a_y Power Spectra for Basic and Lateral RSS Augmented Buffalo	157
68	Comparison of a_y Power Spectra for Basic and Lateral RSS Augmented S-11.	158
69	Axis Systems	165

NOMENCLATURE

a	speed of sound in air
a_x	longitudinal acceleration along the X-body axis at the center of gravity (positive forward)
a_y	lateral acceleration along the Y-body axis at the center of gravity (positive out right wing)
a_y^i	lateral acceleration parallel to the Y-body axis at a distance l_x and l_z from the center of gravity; $a_y^i = l_x \dot{r} - l_z \dot{p}$
a_z	normal acceleration along the Z-body axis at the center of gravity (positive down)
a_z^i	normal acceleration parallel to the Z-body axis at a distance l_x from the center of gravity; $a_z^i = a_z - l_x \dot{q}$
b	reference wing span
\bar{c}	reference wing chord
C	comfort rating (Equation 2.3.1)
C_{L_0}	steady-state lift coefficient; $C_{L_0} \equiv \frac{L}{\frac{1}{2} \rho V_{T_0}^2}$
D	aerodynamic drag force along total velocity vector (positive aft)
g	acceleration due to gravity
G_i^j	transfer function of output j due to input i
h	altitude
I_x, I_y, I_z	moments of inertia referred to body axes
I_{xz}	product of inertia referred to body axes
$j\omega$	imaginary part of complex variable; $s = \sigma \pm j\omega$
K_i	feedback gain particularized by subscript

NOMENCLATURE (Continued)

l_x	distance along the X-body axis from the center of gravity (positive forward)
l_z	distance along the Z-body axis from the center of gravity (positive down)
L	rolling moment about the X-axis due to aerodynamic torques (positive right wing down)
L	aerodynamic lift force perpendicular to the total velocity vector in the aircraft's plane of symmetry (positive up)
L_i	characteristic gust length, particularized by subscript
m	aircraft mass
M	Mach number
M	pitching moment about the Y-axis due to aerodynamic torques (positive nose up)
n/α	handling qualities parameter (Figure 6)
\hat{N}	aerodynamic normal force along the Z-body axis (positive up)
N	yawing moment about Z-axis due to aerodynamic torques (positive nose right)
N_i^j	numerator of transfer function G_i^j
$N_{\delta_k \delta_l}^{q_i q_j}$	coupling numerator of first kind: outputs q_i and q_j due to inputs δ_k and δ_l
p	roll rate; angular velocity about X-axis (positive right wing down)
q	pitch rate; angular velocity about Y-axis (positive nose up)

NOMENCLATURE (Continued)

r	yaw rate; angular velocity about Z-axis (positive nose right)
s	Laplace operator, $\sigma + j\omega$
S	reference wing area
$T_{\frac{1}{2}}$	time to $\frac{1}{2}$ amplitude
T_2	time to double amplitude
u	linear perturbed velocity along X-axis (positive forward)
U_0	linear steady-state velocity along the X-axis (positive forward)
v	linear perturbed velocity along the Y-axis (positive out right wing)
V_{T_0}	total linear steady-state velocity (positive forward)
w	linear perturbed velocity along the Z-axis (positive down)
W	weight
W/S	wing loading parameter
W_0	linear steady-state velocity along the Z-axis (positive down)
X	aerodynamic force along the X-axis (positive forward)
Y	aerodynamic force along the Y-axis (positive out right wing)
Z	aerodynamic force along the Z-axis (positive down)

NOMENCLATURE (Continued)

$1/C_{1/10}$	handling qualities parameter: inverse cycles to 1/10 amplitude of short-period mode
α	perturbation angle of attack
α_0	steady-state (trim) angle of attack relative to fuselage reference line; $\alpha_0 = \cos^{-1}(w_0/V_{T_0}) = \sin^{-1}(u_0/V_{T_0})$
γ	flight path angle
β	sideslip angle
δ_a	aileron deflection (positive for positive rolling moment)
δ_f	direct lift flap deflection (positive for trailing edge down)
δ_e	elevator surface deflection from trim (positive for nose down pitching moment for aft surface)
δ_r	rudder deflection (positive for nose-left yawing moment (negative N))
δ_{sfg}	side force generator deflection (positive for trailing edge left)
Δ	denominator of free aircraft transfer function
Δ'	denominator of augmented aircraft transfer function
ξ	inclination of thrust axis relative to fuselage reference line
ζ_i	damping ratio of linear second-order mode particularized by subscript
λ	complex root of characteristic equation
Λ	white noise
θ	perturbation pitch angle (positive nose up)
θ_0	steady-state (trim) pitch angle

NOMENCLATURE (Continued)

ρ	mass density of air
σ	real portion of complex variable; $s = \sigma \pm j\omega$
σ_i	root-mean-square intensity of motion quantity, forcing function, or surface deflection particularized by subscript
τ_i	time constant of first-order mode particularized by subscript
ϕ	roll angle (positive right wing down)
$\Phi(i)$	power spectral density of quantity (i)
ψ	heading angle
ω	spectral frequency
ω_i	undamped natural frequency of second-order mode particularized by subscript

Special Subscripts

c	control surface actuator command
dr	Dutch Roll mode
g	gust
ph	phugoid mode
R	roll subsidence mode
s	spiral mode
sp	short-period mode
ST	static

Superscripts

(\cdot)	indicates differentiation with respect to time
-------------	--

NOMENCLATURE (Continued)

Abbreviations

GLAS	Gust Load Alleviation System
GPAS	General Purpose Airborne Simulator
ILS	Instrument Landing System
MSS	Mode Suppression System
NASA	National Aeronautics and Space Administration
PIO	Pilot Induced Oscillation
RSS	Ride Smoothing System
SAS	Stability Augmentation System
STOL	Short Take-off and Landing

CHAPTER 1

INTRODUCTION

1.1 Problem Statement

This dissertation reports on the analysis, synthesis, and experimental evaluation of a Ride Smoothing System for aircraft flying in atmospheric turbulence. Both longitudinal and lateral systems were investigated. Multiple design criteria, intended to satisfy the requirements of all components of the aircraft/pilot/passenger system, were established. Three Ride Smoothing System designs, two for the longitudinal and one for the lateral case, all of a multiloop feedback type, were developed. Two sets of unique control surfaces, direct-lift flaps and side-force generators, were used in addition to elevator and rudder for the mechanization. Predicted system performance was verified in a fixed-base ground simulator. The systems were also mechanized aboard the National Aeronautics and Space Administration (NASA) General Purpose Airborne Simulator (GPAS). Limited flight tests were conducted to evaluate two of the Ride Smoothing Systems.

Before discussing the motivation for this research, it is necessary to define several concepts: Ride Smoothing System (RSS), Gust Load Alleviation System (GLAS), Mode Suppression System (MSS), and Stability Augmentation System (SAS). The first three systems are designed primarily to attenuate aircraft response to atmospheric turbulence, but differ considerably in design criteria.

A Ride Smoothing System can be defined as one which proposes to improve passenger and flight crew comfort. It is generally designed to

suppress aircraft motion induced by moderate to heavy continuous turbulence ($\sigma_{w_g} = 2.1$ m/sec). Attenuation is achieved by damping rigid body modes, changing their natural frequency and/or deflecting control surfaces to counteract transient loads.

A Gust Load Alleviation System is designed to protect the aircraft structure from exceeding load limits. Transport class aircraft are typically stressed to ± 2.5 g. At low speeds, lift loads induced by large "sharp-edged" gusts ($w_g = 15$ m/sec) can exceed the design limit. Such aircraft are termed "gust-critical." Significant extension of the load-factor envelope or an equivalent reduction in structural weight are possible if an active GLAS is incorporated.

A Mode Suppression System is designed to counteract turbulence-induced flexible-body mode excitation. The design objective for a MSS is usually twofold: improvement of ride qualities at the pilot station and improvement of the fatigue life of the airframe.

Both the Gust Load Alleviation System and Mode Suppression System may include the functions of a Ride Smoothing System. Successful implementation of any of the three, the RSS, GLAS and MSS, may require the addition of a Stability Augmentation System in order to restore or improve the aircraft handling qualities.

Unfortunately, the above terms, and a number of variations, are often used interchangeably in the literature. Similarly, the terms turbulence (herein considered continuous) and gusts (discrete) have, in the past, been used synonymously. This report will deal only with the investigation of a Ride Smoothing System designed to operate in continuous turbulence as defined above.

1.2 Historical Perspective

Past Ride Smoothing System designs have used two general approaches: open- and closed-loop design philosophies. The essential difference between the two can be illustrated by simple block diagrams:

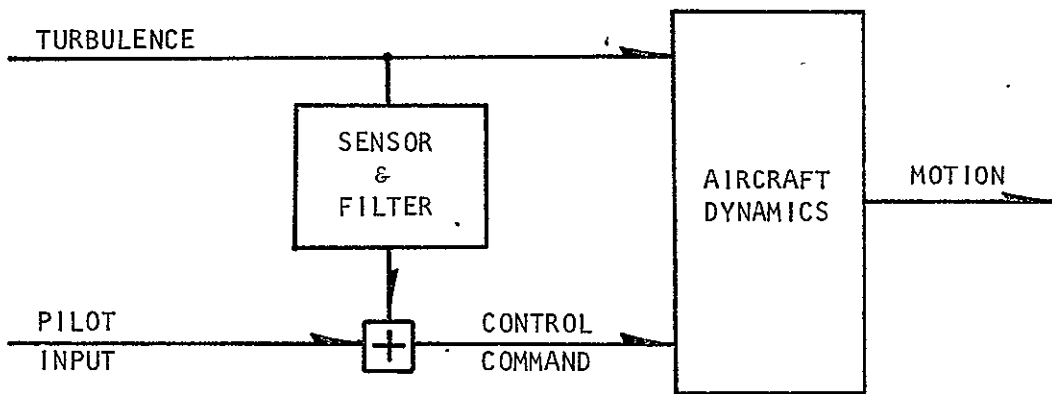


FIGURE 1. OPEN-LOOP CONTROL SYSTEM

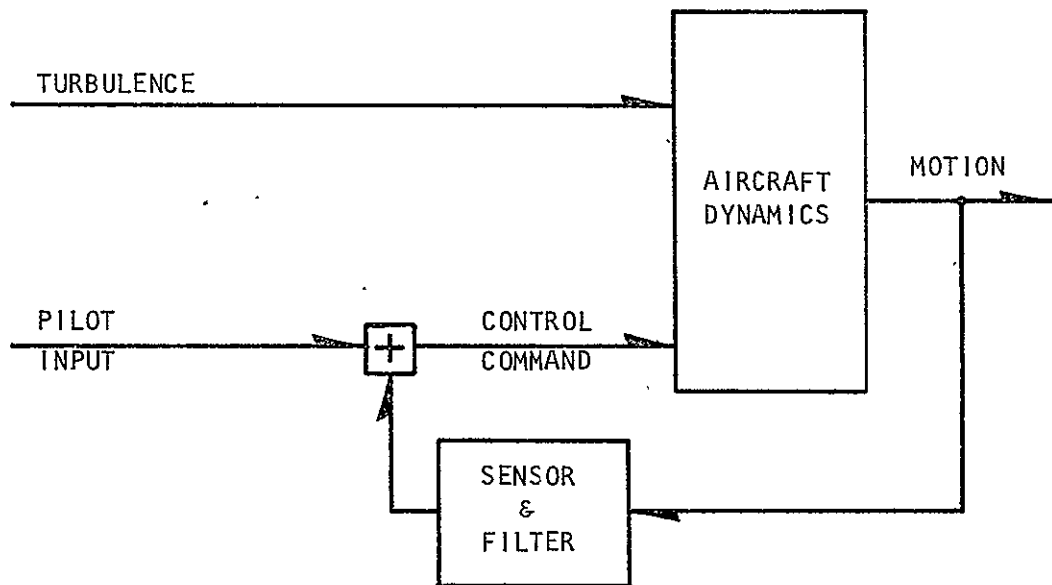


FIGURE 2. CLOSED-LOOP CONTROL SYSTEM

The open-loop scheme (Figure 1) has one very desirable feature: in principle, the aircraft dynamics remain unchanged as a result of the control. Practical difficulties, however, abound. In order to optimize the control law, a precise mathematical formulation of the turbulence field and aircraft dynamics is required. An adequate gust angle of attack sensor is difficult to mechanize. The most popular sensor has been the nose-boom mounted angle of attack vane. Unfortunately, an angle of attack vane measures not only variations in the remote wind, but responds to aircraft motion as well. Unless the vane measurements are accurately corrected for aircraft motion, an "aerodynamic feedback" results--and the characteristic equation is modified. Finally, if the overall gain of the system is high; i.e., almost total alleviation of, say, normal acceleration is achieved, the pilot will be unable to command a change in flight path by conventional means. With modern analog circuitry, servosystems and analytic techniques, an open-loop design can be implemented, but the resulting system is quite complex.

The closed-loop RSS is shown as a classical feedback system (Figure 2). As compared to the open-loop scheme, the main advantage of a feedback system is that no explicit knowledge of the turbulence field and its effect on the aircraft response is required. Careful analysis of the effect of feedback on the characteristic equation roots must, however, be undertaken. The effect of high gain systems on control is, of course, the same as for the open-loop case. The simplification in terms of sensor requirements afforded by the closed-loop system makes this approach more attractive from the practical viewpoint.

Not surprisingly, the first attempts at providing aircraft with a ride smoothing or gust alleviation capability ended in failure. Phillips, in a survey article (1), describes several of these pioneering efforts. Waterman, about 1930, built an airplane with wings attached to the fuselage by skewed hinges. Steady lift forces were balanced by pneumatic struts. Unsteady lift loads caused the wings to deflect, thus reducing the local angle of attack. A modern equivalent of this mechanism is found in the flexible, swept-wing aircraft. The biggest drawback in Waterman's design was lack of adequate lateral control: deflection of ailerons would cause deflection of the wings in opposition to the desired rolling moment.

In 1953, results of a series of ride smoothing flight tests conducted with a Lancaster bomber by the British Royal Aircraft Establishment were published (2). The Lancaster system was designed to operate essentially in an open-loop sense: the vertical component of turbulence was sensed by a "wind incidence meter" mounted on a boom ahead of the nose of the aircraft. The derived electrical analog signal was then used to command symmetric aileron deflection so as to reduce the anticipated lift increment. Flight data, however, indicated an amplification of aircraft response. The preliminary explanation, confirmed in a 1961 report (3), blamed the failure on incomplete analysis: the system design had neglected the adverse effect of aileron-induced pitching moment on system performance.

In 1950, the Douglas Aircraft Company conducted flight tests with a C-47 aircraft configured for gust alleviation. The feedback control used a linkage system which caused symmetric aileron deflection as a

function of wing bending. As with the British effort, and for the same reasons, flight tests were inconclusive (1).

Another essentially open-loop GLAS/RSS design, also summarized by Phillips (1), was developed by the Frenchman René Hirsch about 1938 and successfully flight-tested aboard a specially-fabricated light aircraft during the period 1954-1967 (4). Hirsch's clever mechanization of both a longitudinal and lateral system is mechanically too complex to fully discuss here. The many free aerodynamic surfaces, cables, bellcranks, etc., that were critical to the success of his design would have to be replaced by modern sensors and servosystems if the design were to be implemented aboard a larger aircraft.

Numerous NACA/NASA Technical Notes document the investigation of a longitudinal Ride Smoothing System at the NASA Langley Research Center. The first of these, published in 1951 by Phillips and Kraft (5), sets forth the basic design philosophy of the open-loop system. The sensing element is an angle of attack vane. Two control surfaces are driven by this signal: direct lift flaps and, through fixed gearing, the elevator. In order to counter the flap-induced change in downwash at the tail, it was proposed that a small inboard portion of the flaps be driven in opposition to the main flaps. In principle, the proposed system was capable of total alleviation of turbulence-induced vertical acceleration and pitching moment. Pilot control of flight path was provided by connecting the control stick to both the direct lift flaps and elevator. Concurrent research established the feasibility of using a single angle of attack vane to provide an adequate measure of the average angle of attack perturbation over the entire wing span (6).

Subsequent analytic work and analog computer simulation indicated that adequate static stability could be insured by providing a small static margin at the expense of some alleviation capability (7). Initial flight tests were conducted aboard a C-45 aircraft flying at a single airspeed. A reduction in acceleration of 40 to 50% at specific frequencies was realized (8). Pilot opinion of longitudinal control adequacy was reported favorable.

Results of a more complex flight test program were reported in 1961 by Hunter, et al. (9)(10). Additional alleviation capability had been achieved by slaving the ailerons to the direct lift flaps. Another modification was the incorporation of a negative feedback loop in the flap position command circuit. The feedback was mechanized using a mechanical/electrical integrator. This feature permitted longitudinal trim changes and minimized phugoid mode excitation. Performance of the system was improved to a maximum acceleration attenuation of 60% at the short-period frequency. Somewhat lower performance was recorded when the command signal was generated by a c.g.-mounted normal accelerometer rather than the angle of attack vane. Curiously, Hunter, et al. do not discuss the effect on aircraft dynamics of changing from an essentially open-loop (angle of attack vane) to a close-loop (accelerometer) system, except to state that the latter system was known to approach instability at high gains.

Following completion of these experiments, the C-45 project was terminated. In 1971, Phillips' original design received renewed attention (11 - 16). Barker and Sparrow (11) explain the decade-long hiatus in development as being the result of the relative insensitivity

of the 1960's generation of aircraft to atmospheric turbulence. It was the advent of Short Take-off and Landing (STOL) aircraft that provided motivation for continuation of research in Ride Smoothing Systems.

Several reasons can be cited for the poor ride quality anticipated aboard STOL aircraft. The sensitivity of an aircraft to turbulence is, to first order, inversely proportional to wing-loading (W/S). Yet, a number of STOL designs rely on low wing-loading in order to achieve required short field performance. In addition, STOL aircraft are intended to operate at low altitudes where atmospheric turbulence is most severe.

Several other investigations of open-loop RSS/GLAS have been reported in the literature. One of these, a 1957 report by Tobak (17), is particularly interesting in that he was the first to apply the Weiner optimum filter theory to the problem of minimization of aircraft response to turbulence. Tobak's analysis validated some of the classical analysis results of Phillips and Kraft (5), as well as establishing the form of the optimum command circuit filter. Tobak assumed that a sensor signal proportional purely to fluctuations in angle of attack was available, the turbulence field could be described by the Dryden model, and a single control surface was available.

A very similar analysis, culminating in 1971 flight tests with a Dassault Mirage III delta-wing fighter by the Office National d'Etudes et de Recherches Aérospatiales (ONERA), was reported by Couptry (18). Initial data indicated that substantial reduction in the normal acceleration levels at the pilot-station was achieved.

A series of studies of closed-loop, longitudinal RSS Smoothing System designs has been carried out by a group at the University of

Osaka in Japan (19)(20). In the first of these papers, three systems were postulated; all depending on feedback of normal acceleration and pitch attitude, rate and acceleration to the elevator and direct lift flaps of a conventional subsonic aircraft. The first system; designated a "Linkage-Control System," summed all feedback signals before generating a command signal for the two control surfaces. The second, "Noninteracting System," made provision for separate equalization in each feedback path. The last, "Split-Control System," commanded the direct lift flaps in response to vertical acceleration and the elevator in response to pitch rate only. Within the limits of the assumptions of the study, the authors concluded that the "Split-Control System" was not only the simplest, but also the most effective in reducing c.g. acceleration. Stability of the aircraft system was substantially increased but the short-period frequency was decreased. The authors did not comment on the effect of such a shift on the handling qualities of the vehicle, although the possibility of introducing an integrating circuit in the feedback loops in order to improve control was postulated. The second paper reported on the calculation of an optimal feedback system, and showed the performance of the optimal and simplified ("Split Control") systems to be equivalent.

A closed-loop design approach, almost identical to that of the Osaka group, was adopted by Holloway, et al. of Boeing (21) for a feasibility study of a STOL Ride Smoothing System. Vertical acceleration was fed back to the direct lift flap through a low-pass filter and pitch rate to the elevator through an integrator circuit. Well-defined operating criteria were established, including the design turbulence level,

attenuation requirement for passenger acceptance, and a handling qualities specification. In addition, a lateral ride smoothing system was designed based on feedback of filtered yaw rate and lateral acceleration to the rudder. The same general system was adapted for installation aboard a deHavilland DHC-6 Twin Otter aircraft (22).

Several theoretical studies based on the application of optimal control theory to closed-loop Ride Smoothing Systems have also appeared in the literature. Hess (23) investigated a system that drove the elevator in response to the sum of three signals: normal acceleration, pitch rate, and angle of attack. One of his major conclusions was that the performance of the optimal controller was insensitive to characteristics of the turbulence field; in particular, the "characteristic gust length." In subsequent investigations, the feedforward loop was eliminated because of the difficulty in mechanizing a practical angle of attack sensor. The resulting system, identical in form to an "acceleration autopilot," was shown to have an alleviation capability nearly equivalent to the optimal controller (24)(25). A similar configuration had been studied earlier by McClean (26).

Probably the most ambitious study of an aircraft gust alleviation system designed to suppress longitudinal rigid-body response was undertaken by Iliff (27). His research involved the application of stochastic identification theory to a system (the aircraft) contaminated by state noise (turbulence). Not only did Iliff's technique successfully extract almost exact values of aircraft stability derivatives, it also yielded a good approximation of the root mean square turbulence intensity. Iliff also demonstrated application of stochastic control theory to

solving the gust alleviation problem; minimizing either vertical acceleration or pitch rate. Unfortunately, no research aircraft equipped with an onboard digital computer capable of performing the required calculations is available to prove Hiff's concepts in flight.

A great deal of research effort since the early 1960's has dealt with the problem of structural mode alleviation for flexible aircraft. A good survey of this work is presented in a paper by Swaim (28). Solutions to this problem are generally attempted through the application of linear optimal control theory. An example of this approach is discussed by Smith, et al. (29). Since this dissertation does not consider the effect of turbulence on non-rigid aircraft, detailed review of Mode Alleviation Systems will be omitted.

1.3 Research Objectives

As mentioned previously, the ride quality aboard STOL-class aircraft might be improved by the incorporation of a Ride Smoothing System. In fact, several conceptual studies of STOL designs (e.g., Reference 30) assumed that a Gust Alleviation and/or Ride Smoothing System would be an integral part of the aircraft design. Although several flight investigations of open-loop RSS performance have been conducted, no closed-loop systems have been so tested. It was the ultimate purpose of this research to provide such an evaluation for both a longitudinal and lateral Ride Smoothing System. Furthermore, previous designs often neglected to consider the effect of such systems on aircraft handling qualities, both in terms of stability and control characteristics. Such consideration is most important for STOL aircraft, since they will be expected to maneuver extensively in the airport terminal area. An

evaluation of the interaction of the pilot with the RSS-augmented aircraft was, therefore, identified as a critical area in need of investigation. The most critical flight regime for piloted flight is the approach for landing. For this reason, the handling-qualities evaluation was conducted with the aircraft in the approach configuration. By approaching the analysis and synthesis of a Ride Smoothing System from a comprehensive, systems engineering viewpoint, it was hoped that not only the above major objectives could be accomplished, but a better understanding of inherent engineering trade-offs would be achieved.

CHAPTER II

PROBLEM DEFINITION

2.1 Equations of Motion

It is assumed that the motion of the aircraft can be adequately described by standard, linearized, separable, small perturbation equations of motion. In order to simplify the formulation of feedback quantities obtained from aircraft sensors (e.g., accelerometers), the equations are written with respect to body fixed axes. The coefficients of these differential equations are in dimensional form (see Appendix A). Derivations of the equations of motion can be found in any standard text on airplane flight mechanics (e.g., Reference 31). Validity of these expressions is subject to the following major assumptions:

1. The airframe is a rigid body;
2. The earth is an inertial reference frame;
3. The mass and mass distribution of the vehicle are constant;
4. The XZ plane is a plane of symmetry;
5. Disturbances from steady flight conditions are small;
6. Initial conditions are straightline flight with forces and moments balanced;
7. Longitudinal forces and moments due to lateral perturbations are negligible and vice versa;
8. The flow is quasi-steady; and
9. The effect of engine gyroscopics is negligible.

Furthermore, the airframe may be subject to forces and moments caused by control surface (direct lift flap, elevator, side force

generator and rudder) deflections. Thrust is assumed constant. The effects of turbulence are included by assuming uniform immersion of the aircraft and applying the disturbances in terms of vertical and lateral velocity perturbations (w_g and v_g) and the related angular velocity increments in pitch rate, roll rate and yaw rate (q_g , p_g , and r_g) at the center of gravity through the appropriate aerodynamic coefficients (32). The effect of the longitudinal turbulence, u_g , is neglected.

In matrix form, the resulting Laplace transformed equations of motion for the aircraft are:

Longitudinal

$$\begin{bmatrix} (1 - X_{\dot{u}})s - X_{u^*} & -(X_{\dot{w}}s + X_w) & (-X_q + W_0)s + g \cos \theta_0 \\ -Z_{\dot{u}}s - Z_{u^*} & (1 - Z_{\dot{w}})s - Z_w & (-Z_q - U_0)s + g \sin \theta_0 \\ -M_{\dot{u}}s - M_{u^*} & -(M_{\dot{w}}s + M_w) & s^2 - M_q s \end{bmatrix} \begin{bmatrix} u \\ w \\ \theta \end{bmatrix} =$$

$$\begin{bmatrix} X_{\delta_e} & X_{\delta_f} & X_w & X_q \\ Z_{\delta_e} & Z_{\delta_f} & Z_w & Z_q \\ M_{\delta_e} & M_{\delta_f} & M_w & M_q \end{bmatrix} \begin{bmatrix} \delta_e \\ \delta_f \\ w_g \\ q_g \end{bmatrix} \quad (2.1.1)$$

$$q = s\theta \quad (2.1.2)$$

$$a_z = sw - U_0q + (g \sin \theta_0)\theta \quad (2.1.3)$$

$$a_z' = a_z - 1_x s^2 \theta \quad (2.1.4)$$

Lateral

$$\begin{bmatrix} (s - Y_V) & -\frac{W_0 s + g \cos \theta_0}{V_{T_0}} & \frac{U_0 s - g \sin \theta_0}{V_{T_0} s} \\ -L_{\beta}' & s(s - L_p') & -L_r' \\ -N_{\beta}' & -N_p' s & (s - N_r') \end{bmatrix} \begin{bmatrix} \beta \\ p/s \\ r \end{bmatrix} =$$

$$\begin{bmatrix} Y_{\delta_r}^* & Y_{\delta_{sfg}}^* & Y_V & 0 & 0 \\ L_{\delta_r}' & L_{\delta_{sfg}}' & L_{\beta}' & L_r' & L_p' \\ N_{\delta_r}' & N_{\delta_{sfg}}' & N_{\beta}' & N_r' & N_p' \end{bmatrix} \begin{bmatrix} \delta_r \\ \delta_{sfg} \\ \beta_g \\ r_g \\ p_g \end{bmatrix} \quad (2.1.5)$$

$$v = V_{T_0} \beta \quad (2.1.6)$$

$$\phi = p/s + (r/s) \tan \theta_0 \quad (2.1.7)$$

$$\psi = (1/\cos \theta_0)(r/s) \quad (2.1.8)$$

$$a_y = sv + U_0 r - W_0 p - g(\cos \theta_0)\phi \quad (2.1.9)$$

$$a_y' = a_y + l_x sr - l_z sp \quad (2.1.10)$$

The stability derivatives ($X_{\dot{u}}$, $X_{\dot{u}}^*$, etc.) are defined in Appendix A.

2.2 Description of Atmospheric Turbulence and Calculation of Aircraft Response

Atmospheric turbulence is generally random in time; being both intermittent and variable in intensity. Thus, the input-output relationship of aircraft response to turbulence is described in terms of statistical quantities defined by random process theory. A concise treatment of the important concepts of this theory as applicable to the aircraft problem can be found in an article by Pratt (33). Short "patches" of turbulence are assumed to satisfy certain statistical properties: stationarity, homogeneity, isotropy, ergodicity, and normality in the Gaussian sense. In addition, Taylor's hypothesis is assumed valid: the turbulent velocity pattern is frozen in space. Thus, a relationship defined on the aircraft velocity exists between the spatial and spectral frequencies of turbulence.

Mathematical expressions for the input-output relationship in terms of statistical quantities as well as definitions of turbulence transfer functions are given in Appendix B. Additional relationships, needed to include the effect of closing feedback control loops, are developed as required in the discussion.

2.3 Ride Smoothing System Criteria

2.3.1 Passenger Comfort

It is generally recognized that the comfort of aircraft passengers is affected by numerous physical and psychological factors (34); of these, the motion environment is believed to be one of the important variables. Although no comprehensive criteria for predicting comfort

is available, several mathematical models of subjective passenger response to aircraft motion have been developed by Jacobson, et al. (35). The simplest form, valid for motion dominated by vertical acceleration, predicts a comfort rating:

$$C = 2 + 11.9 a_{z_{rms}} + 7.6 a_{y_{rms}} \quad (2.3:1)$$

where

C = 1; Very Comfortable

C = 2; Comfortable

C = 3; Neutral

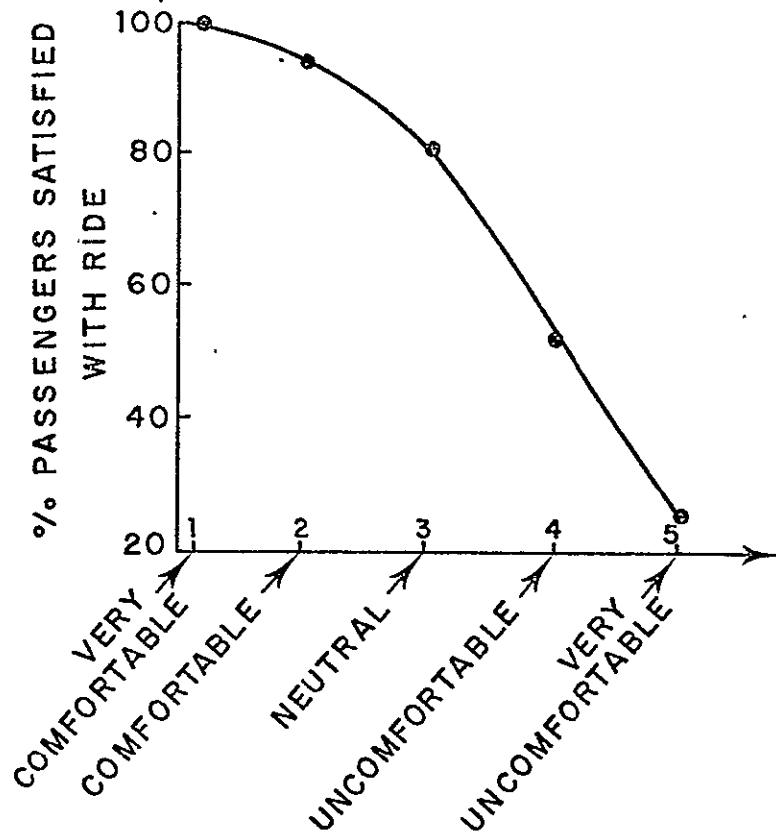
C = 4; Uncomfortable

C = 5; Very Uncomfortable

and the acceleration levels are expressed in units of acceleration due to gravity (g's). This subjective reaction to an aircraft motion environment has also been correlated to passenger satisfaction with the "quality" of the ride (Figure 3).

2.3.2 Design Level of Turbulence

Because all of the work discussed herein is concerned with an aircraft flying in the approach flight regime, the nominal aircraft operating altitude was defined as 305 meters (1000 feet). The corresponding characteristic gust lengths are $L_w = 305$ meters (1000 ft) and $L_v = 442$ meters (1450 ft). A value of the root-mean-square vertical gust velocity corresponding to a 1% probability of exceedance was chosen as the standard; thus, $\sigma_{w_g} \equiv 2.1$ m/s (7 ft/sec) (Equation B.8) and $\sigma_{v_g} \equiv 2.6$ m/s (8.4 ft/sec) (Equation B.9).



MATHEMATICAL FIT TO THE CURVE

$$\% = \frac{-B - \sqrt{B^2 - 4C(A - CR)}}{2C} \quad CR < 3$$

$$A = -159/11$$

$$B = 26/55$$

$$C = -0.035/11$$

$$\% = 162.5 - 27.5 CR \quad CR \geq 3$$

FIGURE 3. PASSENGER SATISFACTION CRITERIA
(From Jacobson and Kuhithau, unpublished data, 1973)

2.3.3 Surface Activity

For a zero mean Gaussian process it can be shown that 99% of the time a random variable can be expected to fall within $\pm 2.6\sigma$, where σ is the standard deviation. In order not to violate the mathematical assumption of linearity, gains of feedback control loops in a Ride Smoothing System mechanization must be limited such that the root-mean-square control surface deflection does not exceed approximately 38% of the available range.

2.3.4 Handling Qualities

The current, industry accepted, standards for handling qualities of aircraft in smooth air are contained in Military Specification F-8785B (36). As pointed out by Barnes (37), the requirements are vague on the subject of handling qualities for flight in turbulence. The criteria of MIL-F-8785B can, however, be applied to both the baseline and RSS augmented aircraft in order to determine compatibility with minimum acceptable levels of aircraft dynamic mode parameters (e.g., $\omega_{n_{sp}}$, ζ_{sp} , τ_R , etc.). For this purpose, the aircraft under consideration for augmentation with a Ride Smoothing System was assumed to fall in the Class II ("medium weight, low to medium maneuverability") category. Level I ("clearly adequate") flying qualities were sought for the category C ("terminal") flight phase.

In addition to the possible detrimental effect of a Ride Smoothing System on the dynamics of an aircraft, the effect on control power is of concern (e.g., n/α). Thus, final evaluation of handling qualities must be accomplished in piloted simulation using the Cooper-Harper criteria (38).

2.3.5 Failure Modes

Any automatic control system is subject to failure. In the case of a Ride Smoothing System, it can be argued that system operation is not critical to the integrity of the airframe or flight safety. For non-self-monitoring mechanizations, however, unrecognized failures in multi-loop feedback systems could result in significant changes in the aircraft stability characteristics. Thus, a system of this type must be constrained to failure modes that do not catastrophically alter handling qualities. Compatibility with this requirement is again best tested in piloted simulation.

2.3.6 Feasibility

Any system design must be implementable. Few aircraft are equipped with an extensive onboard digital computing capability. Thus, any system command signal processing requirement must be met with analog devices. As with most engineering solutions, feasibility and reliability of a Ride Smoothing System is to a great degree a function of simplicity and economy of design. As a quantifiable criterion, feasibility is difficult to describe--it is the art of engineering design.

2.3.7 The Optimal Control Performance Index

The optimal control theory performance index is customarily expressed as an integral of the weighted sum of squared state variables. Most optimal control theory solutions to either the longitudinal Ride Smoothing System or Gust Alleviation design problems have included a combination of a_z , q , δ_e , or δ_f as the integrands in the performance index. From the preceding discussion, it should be evident that not all design criteria are so satisfied. Although minimization of a_z is

a desirable goal, total alleviation is not an absolute prerequisite for satisfactory system performance. For any given aircraft flying in a given level of turbulence, only a level of alleviation compatible with the passenger comfort (satisfaction) criterion need be provided. Furthermore, compatibility with the handling qualities criteria, especially in a system failure mode, cannot be adequately included in the classical performance index formulation. Finally, optimal filters, in the case of feedback of all state variables to all control surfaces, tend to be overly complex for mechanization by analog devices. For a Ride Smoothing System, i.e., one proposed to attenuate rigid body response to turbulence, successful design to the above-mentioned criteria dictates a classical (suboptimal), rather than optimal control theory, approach.

2.4 Selection of Sensors, Control Surfaces, and Feedbacks

Having, in the interests of design simplicity, chosen to limit the number of feedback loops, the system analyst/designer is faced with the task of choosing which control surfaces to use and deciding what signals are needed to implement a useful feedback control law. A rational approach to this problem has been proposed by Stapleford, et al (39). The technique involves the identification of essential feedbacks.

Quoting:

"The essential feedbacks...derive from one or both of two basic flight control system purposes:

- To establish and maintain certain specified equilibrium states of vehicle motion.
- To remedy aircraft handling quality deficiencies.

The establishment and maintenance of an equilibrium state of motion requires an outer control loop pertinent to the vehicle motion quantity defining that state." (Reference 39, page 8.)

A Ride Smoothing System essentially fits the above definition. Note the implication that an inner control loop (of a multi-loop feedback system) may be required to satisfy handling qualities requirements.

For the longitudinal Ride Smoothing System problem, i.e., the reduction of a_z response to vertical gusts, three outer loop closures are possible (see Table 1).

No equivalent guidelines are available for a lateral Ride Smoothing System design. Lateral autopilot functions have classically involved the use of yaw dampers ($r \rightarrow \delta_r$ feedback) or roll attitude hold devices (ϕ or $p \rightarrow \delta_a$ feedback) to reduce aircraft response to turbulence. The recent Ride Smoothing System Feasibility Study by Gordon and Dodson (22) reports on the performance of a lateral system using yaw rate and c.g. transverse acceleration feedback to the rudder (r and $a_y \rightarrow \delta_r$). The major difficulty encountered with such a mechanization is explained by conflicting requirements on the rudder: significant side force cannot be generated without inducing large yawing moments that counter the aircraft's natural tendency to weather-vane into the remote wind. Thus, lateral acceleration in response to turbulence can successfully be suppressed only at a given fuselage station. Application of the essential feedback concept points to a solution to this dilemma: feedback of transverse acceleration to a pure side-force generating control surface ($a_y \rightarrow \delta_{sfg}$). Clearly, any number of other feedback loops might serve to implement a Ride Smoothing System.

TABLE I

LONGITUDINAL COMPETING SYSTEMS

<u>Feedback</u>	<u>Primary Function Performed</u>	<u>Equalization Requirements</u>	<u>Practical Design Problems</u>
$a_z + \delta_e$	<ol style="list-style-type: none"> Increase ζ_{sp} and $\omega_{n_{sp}}$ Reduce h and a_z response to gusts 	<ol style="list-style-type: none"> Gain $K_{a_z} \propto \frac{m l y}{\rho^2 V_{T0}^4 C_{L\alpha} C_{m\delta_e}}$ Lead/lag element desirable 	<ol style="list-style-type: none"> Severe gain adjustment with flight condition. Sensor location adequate for all flight conditions. Structural mode feedback. Increase θ response to vertical gusts.
$\alpha + \delta_e$	<ol style="list-style-type: none"> Increase ζ_{sp} and $\omega_{n_{sp}}$ Reduce h and a_z response to gusts 	<ol style="list-style-type: none"> Gain $K_\alpha \propto \frac{1}{M\delta_e}$ Lead/lag element desirable 	<ol style="list-style-type: none"> Gain adjustment with flight condition. Sensor instrumentation <ol style="list-style-type: none"> Determination of operating point. Errors due to aerodynamic interference. Elaborate sensor complex required to suppress gust inputs.
$a_z + \delta_{dlc}$	<ol style="list-style-type: none"> Reduce h and a_z response to gusts 	<ol style="list-style-type: none"> Gain $K_{a_z} \propto \frac{.m^2}{\rho^2 V_{T0}^3 C_{L\alpha} C_{L\delta_f}}$ Crossfeed $\delta_f \rightarrow \delta_e$ desirable to adjust effective $M_{\delta_{dlc}} / Z_{\delta_{dlc}}$ 	<ol style="list-style-type: none"> Severe gain adjustment with flight condition. Sensor location adequate for all flight conditions. Structural mode feedback. Probable drag penalty due to direct lift control surface.

(Reference 39, page 14)

CHAPTER III

ANALYSIS AND SYNTHESIS

3.1 Order of Presentation

In this section of the report, the analysis and synthesis of Ride Smoothing Systems consistent with the criteria of Chapter II is presented. Development of longitudinal systems is contained in Section 3.4. Lateral systems are discussed in Section 3.5.

3.2 Demonstration Aircraft

To provide the flight evaluation of a closed-loop Ride Smoothing System, the NASA General Purpose Airborne Simulator (GPAS) was chosen. GPAS is a Lockheed JetStar (C-140) light utility transport modified for variable stability experiments by the Cornell Aeronautical Laboratory, Inc. (Figures 4 and 5).

Two basic GPAS modes of operation are possible: model following and response feedback (40). For this study, the basic Jetstar was used as the model aircraft. Thus, the model-following capability was not required and only some elements of the response feedback system were used. These included the sensor package (accelerometers, attitude and rate gyros) and onboard analog computer (Electronic Associates, Inc. PC-12). All of the fully-powered control surfaces of the aircraft (elevator, direct-lift flaps, ailerons, rudder and side-force generators) can be commanded by the response feedback system.

The RSS design flight condition was for the aircraft in the power approach configuration. As mentioned previously, because an instrument



FIGURE 4. NASA GENERAL PURPOSE AIRBORNE SIMULATOR (GPAS)

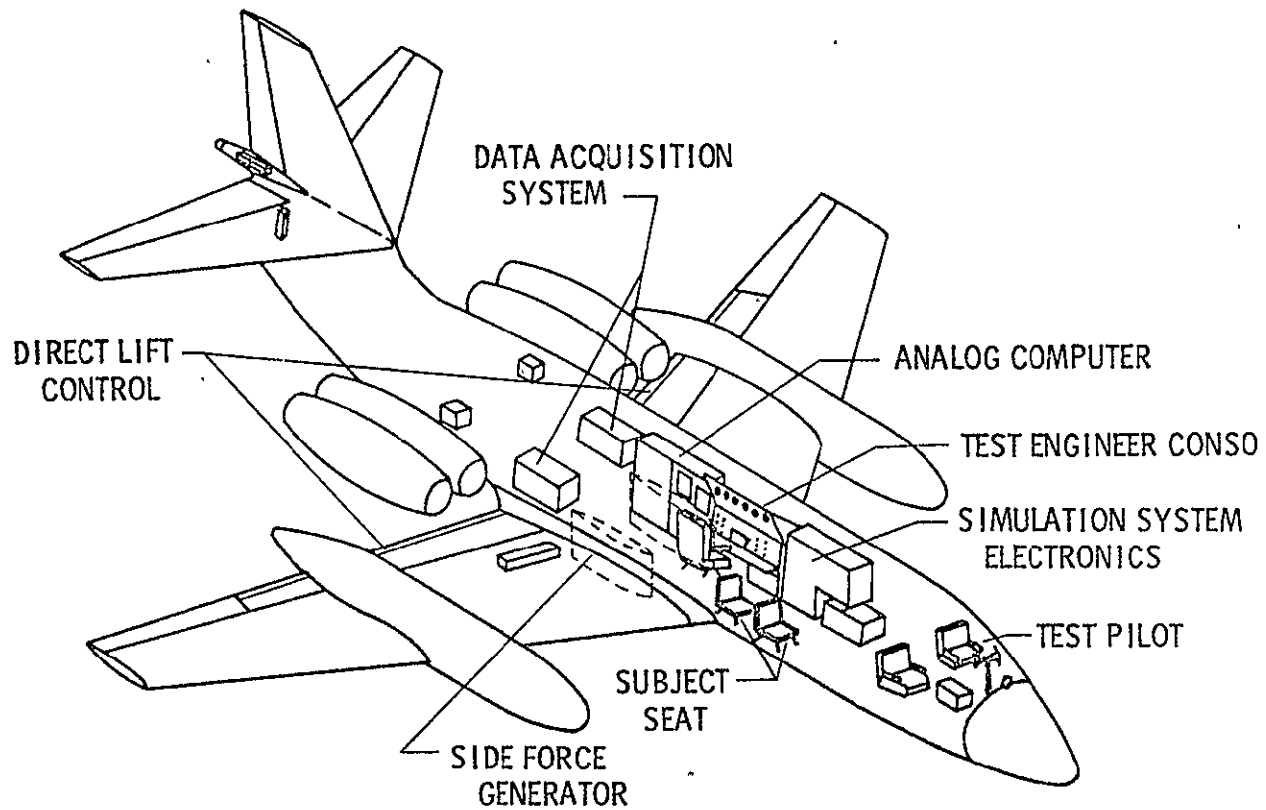


FIGURE 5. SCHEMATIC OF NASA GENERAL PURPOSE AIRBORNE SIMULATOR

landing approach is the most difficult flight phase from a pilot's point of view, it is the best condition for evaluation of aircraft handling qualities. Operational parameters, aircraft stability derivatives, and control surface actuator dynamics for this configuration and flight condition are summarized in Appendix C.

3.3 Method of Analysis

Throughout the analysis and synthesis portion of this research extensive use was made of the digital computer program "CONTROL" written by J. W. Edwards of NASA Flight Research Center. "CONTROL" permits analysis of open- and closed-loop continuous systems by frequency response, transient response, and root locus techniques. The plant is specified in state variable form, but the feedback loops and equalization may be specified in block diagram (frequency domain) form.

3.4 Longitudinal Ride Smoothing Systems

3.4.1 The Basic JetStar--Longitudinal Case

In the power approach configuration, the longitudinal dynamics of the basic JetStar are characterized by the following parameters:

$$\begin{aligned} \text{Short Period Mode: } \lambda_{sp} &= -0.9123 \pm j 1.3948 \\ \zeta_{sp} &= 0.546 && (0.35) \\ \omega_{n_{sp}} &= 0.266 \text{ Hz} && (0.11) \end{aligned}$$

$$\begin{aligned}
\text{Phugoid mode: } \lambda_{\text{ph}} &= -0.00923 \pm j 0.1714 \\
\zeta_{\text{ph}} &= 0.054 && (0.04) \\
P_{\text{ph}} &= 36.6 \text{ sec} \\
T_{\frac{1}{2}} &= 74.8 \text{ sec.}
\end{aligned}$$

$$\text{Control Authority (see Figure 6): } \frac{n}{\alpha} = 6.22 \text{ g /rad. } (2.0)$$

The numbers in parenthesis refer to minimum values of the given parameter as specified in MIL-F-8785B (36). The basic aircraft clearly meets all longitudinal handling qualities specifications. Only the phugoid mode damping is marginal.

At the design turbulence condition ($\sigma_{w_g} = 2.1 \text{ m/sec}$), the root-mean-square vertical acceleration was computed to be $\sigma_{a_z} = 0.1178 \text{ g}$. Throughout this report, calculation of root-mean-square values is accomplished by integrating the appropriate power spectra over the frequency range of interest: $0.01 \leq \omega \leq 100.0 \text{ rad/sec}$. The mean-square acceleration distribution by frequency (power spectra) is depicted in Figure 7.

Although the comfort model (Equation 2.3.1) is given only in terms of total σ_{a_z} , it is known that, depending on the frequency band over which oscillatory excitation occurs, the effect on human comfort is quite different (34). Low frequency oscillations tend to cause motion sickness. Resonance of body organs, leading to annoyance and pain, is possible in the frequency range between 2 and 8 Hertz. For the JetStar, a significant percentage of the total mean-square acceleration is in the low frequency range. Consider the partitioned power spectrum for the basic JetStar (Figure 8). The "power" in

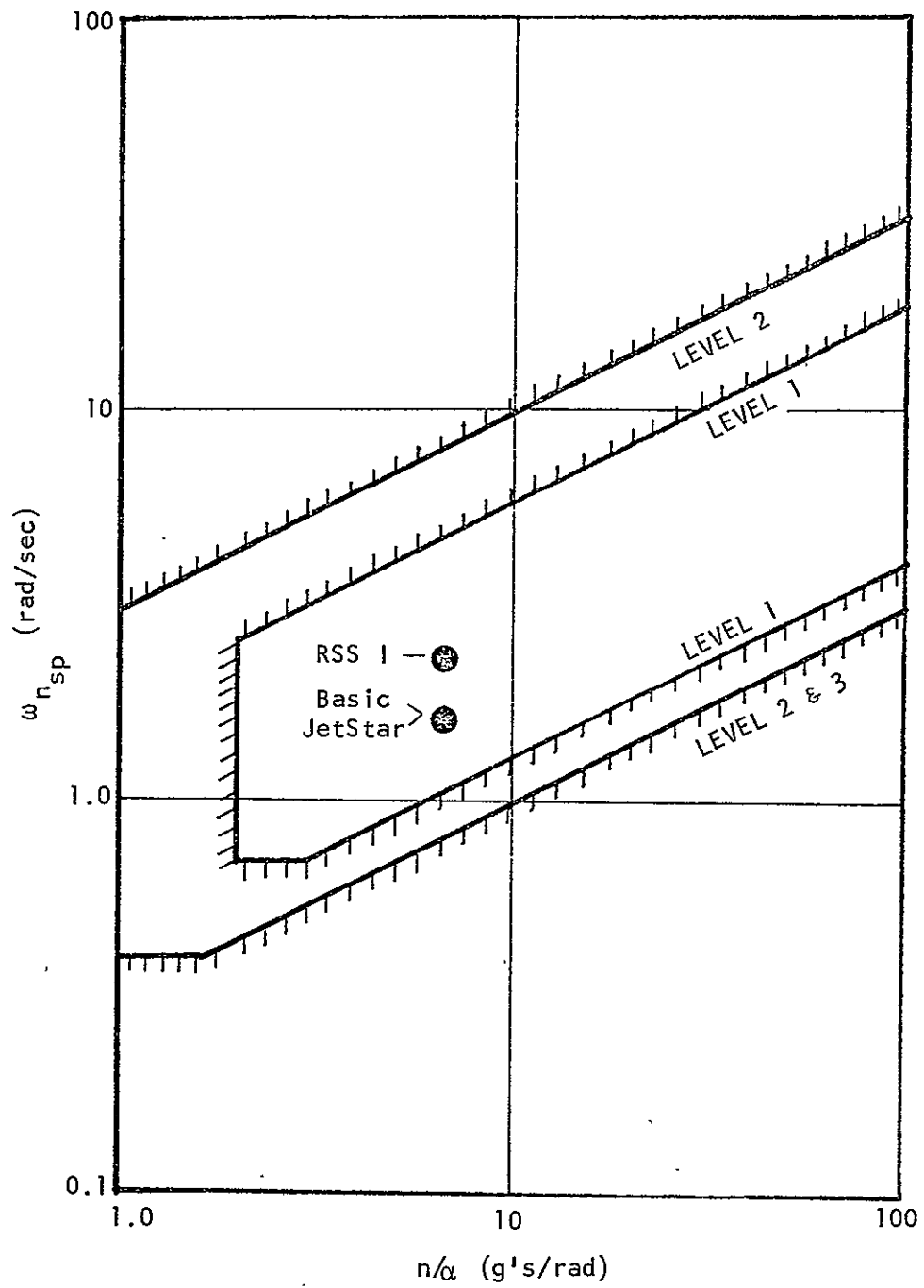


FIGURE 6. HANDLING QUALITIES SPECIFICATION FOR n/α

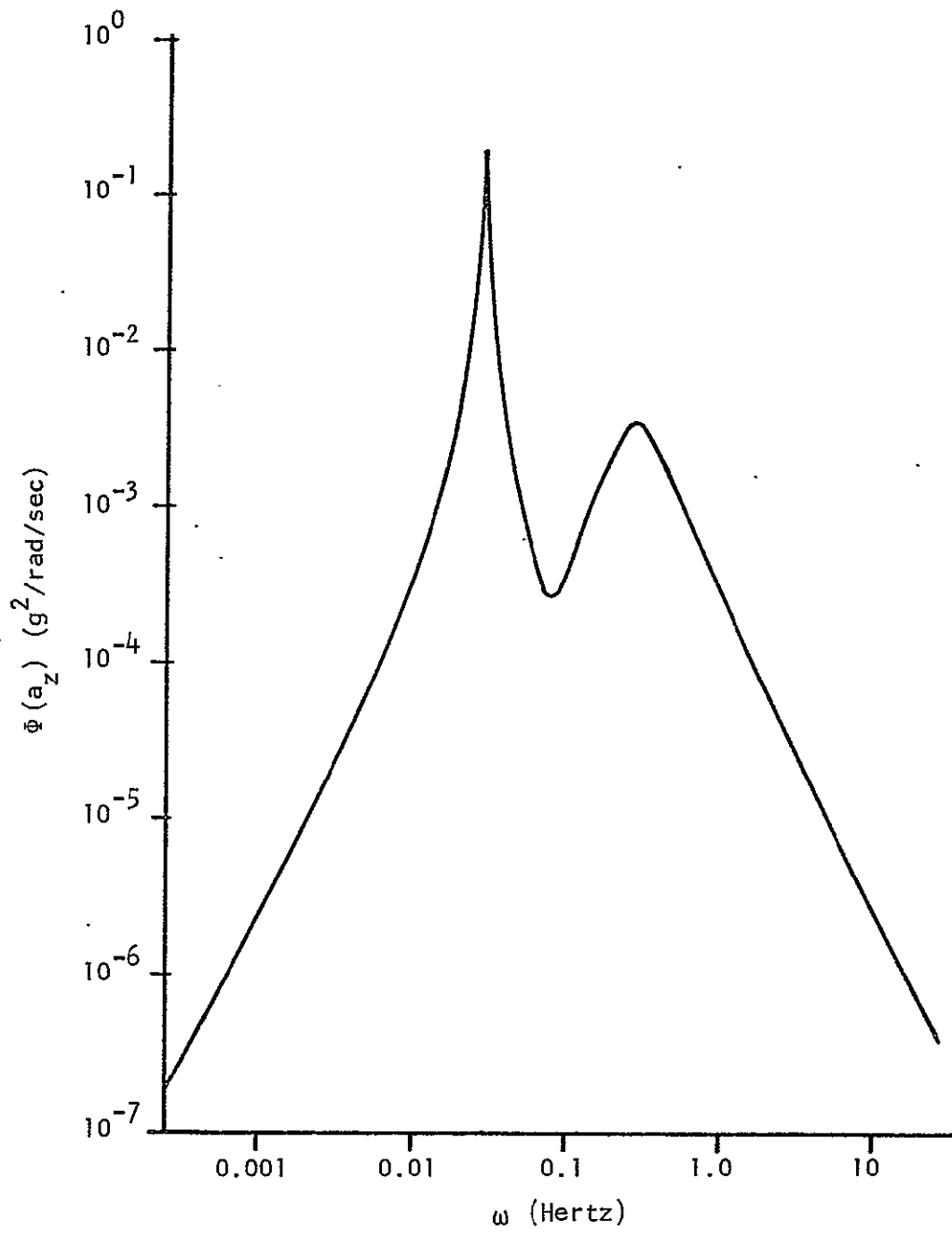


FIGURE 7. POWER SPECTRA OF a_z DUE TO TURBULENCE FOR BASIC JETSTAR

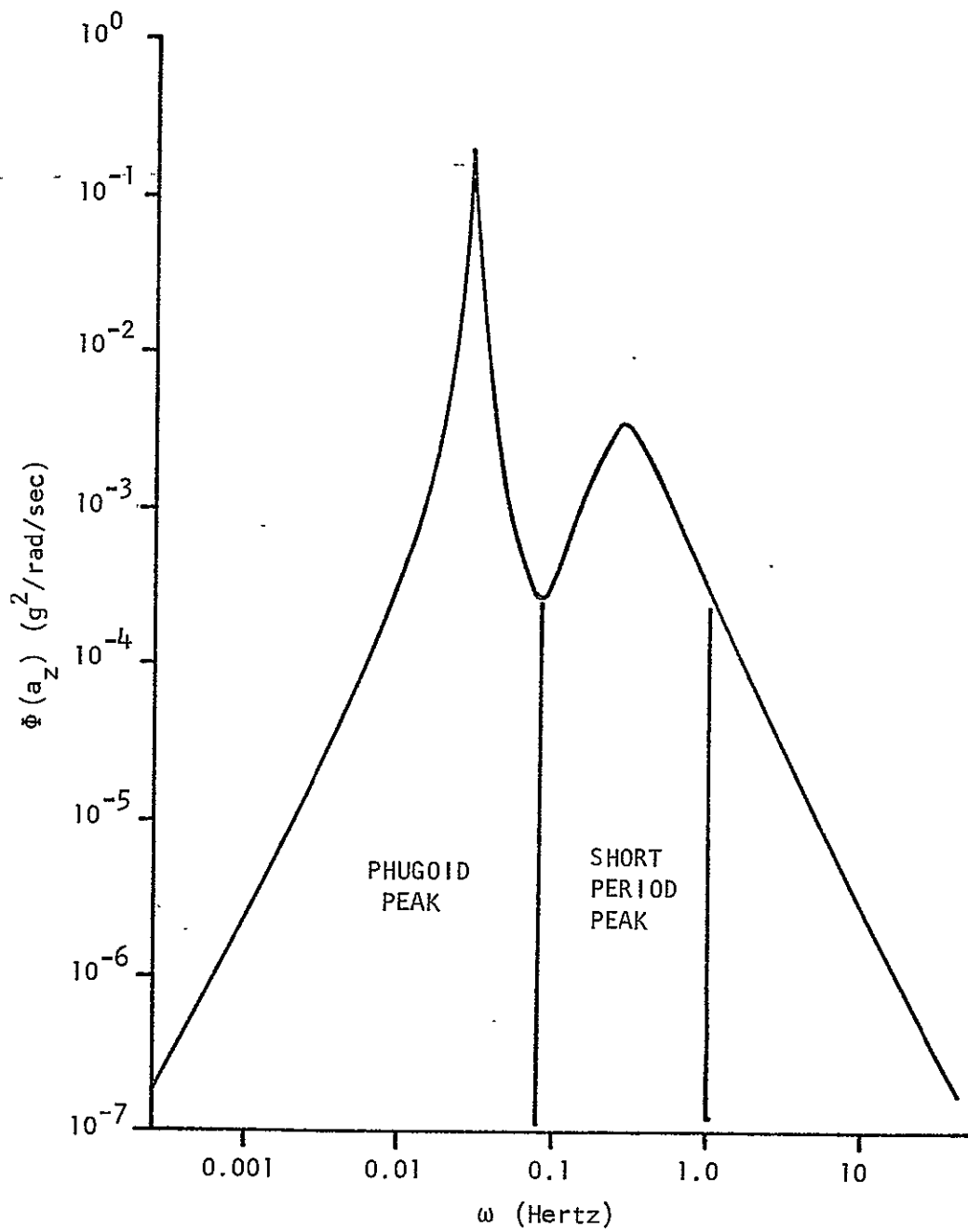


FIGURE 8. PARTITIONED POWER SPECTRA OF a_z FOR BASIC JETSTAR

the lowest frequency band (phugoid peak) is approximately 38% of the total. Only 9% of the total mean-square acceleration occurs at frequency above 1 Hz; the remainder is concentrated in the short-period peak.

3.4.2 Baseline Longitudinal Ride Smoothing System

Based on the concept of an essential feedback, a baseline longitudinal Ride Smoothing System employing feedback of vertical acceleration to the direct-lift flaps was analyzed. In simplified block diagram form:

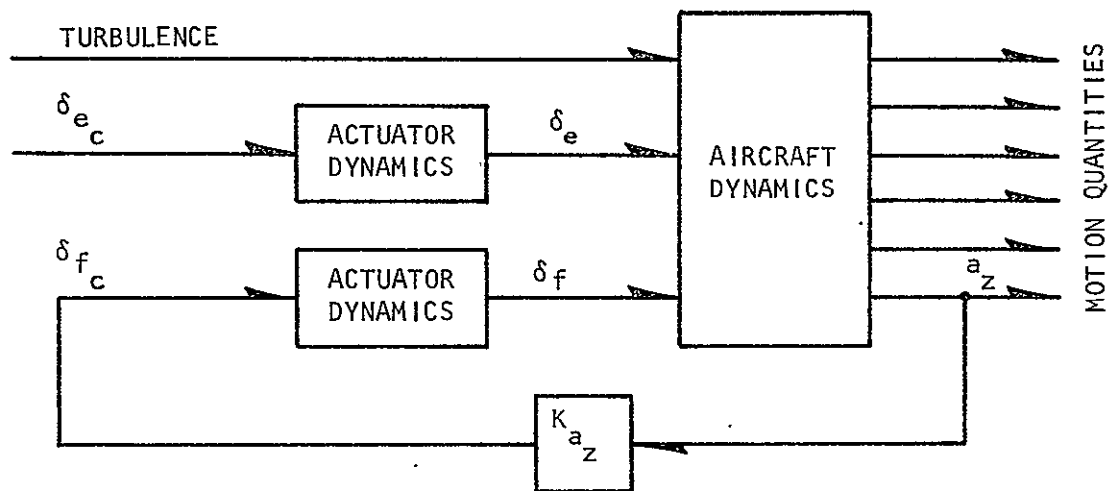


FIGURE 9. BASELINE LONGITUDINAL RIDE SMOOTHING SYSTEM

$$a_z \rightarrow \delta_f$$

The feedback loop has associated with it only a gain: K_{a_z} (no equalization). Performance of this system at the design turbulence condition is summarized in Table II.

TABLE II
 PERFORMANCE OF BASELINE LONGITUDINAL RSS

$$a_z \rightarrow \delta_f$$

<u>(rad/m/sec²)</u>	<u>K_{a_z} (rad/ft/sec²)</u>	<u>σ_{a_z} (g)</u>	<u>% Alleviation</u>	<u>σ_{δ_f} (°)</u>	<u>n/α (g/rad)</u>
0	0	0.1178	0	0	6.22
0.1	0.03	0.1024	13	5.6	3.94
0.2	0.06	0.0938	20	10.2	2.91
0.3	0.09	0.0892	24	14.5	2.28
0.4	0.12	0.0903	23	19.6	1.88

The locus of roots of the aircraft characteristic equation for this system is presented as a function of feedback gain K_{a_z} in Figure 10.

Several deficiencies in the simple $a_z \rightarrow \delta_f$ system are immediately apparent. At reasonable levels of flap activity ($\sigma_{\delta_f} \cong 10^0$), the degree of vertical acceleration alleviation is small. Both the natural frequency of the short-period mode and the magnitude of the handling qualities parameter n/α are rapidly reduced to marginal values as K_{a_z} is increased. Phugoid damping remains low. Consequently, an "inner" loop closure to augment the essential feedback is indicated.

3.4.3 Effect of Inner Loop Closure

A number of feedbacks will serve to increase short-period frequency: angle of attack to elevator ($\alpha \rightarrow \delta_e$), pitch attitude to elevator ($\theta \rightarrow \delta_e$), or normal acceleration to elevator (a_z or $a_z' \rightarrow \delta_e$). The first of these, $\alpha \rightarrow \delta_e$, can be eliminated from consideration because of the difficulty in providing an adequate sensor. Feedback of $a_z \rightarrow \delta_e$ has a minor effect on phugoid damping and tends to increase pitch response to turbulence (31) (39). The best compromise appears to be incorporation of the classical "pitch damper" or $\theta \rightarrow \delta_e$ feedback. The root locus for this closure is depicted in Figure 11.

3.4.4 Basic Multi-loop Longitudinal Ride Smoothing System

The basic multi-loop longitudinal Ride Smoothing System in simplified block diagram form is depicted below:

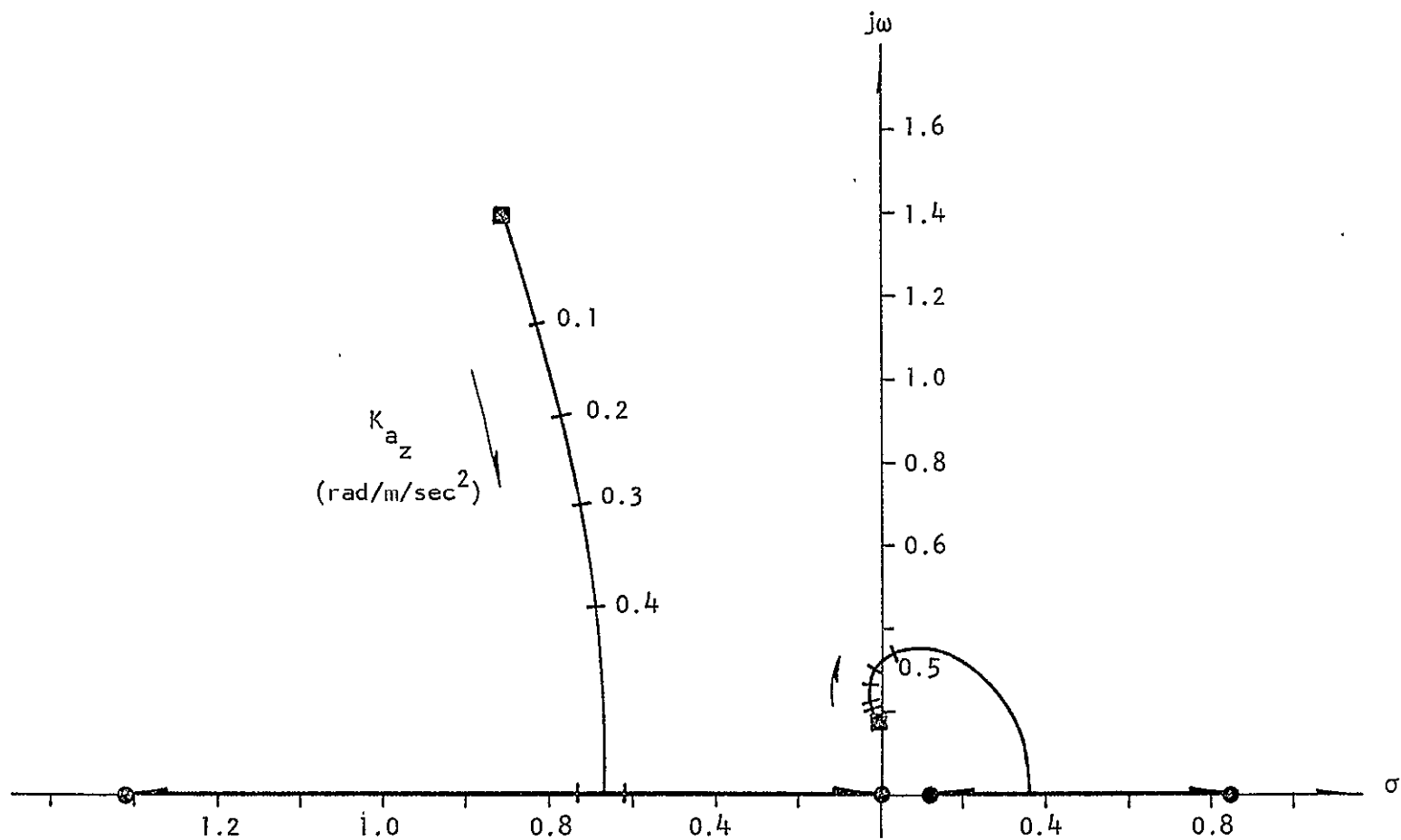


FIGURE 10. ROOT LOCUS FOR BASELINE LONGITUDINAL RSS

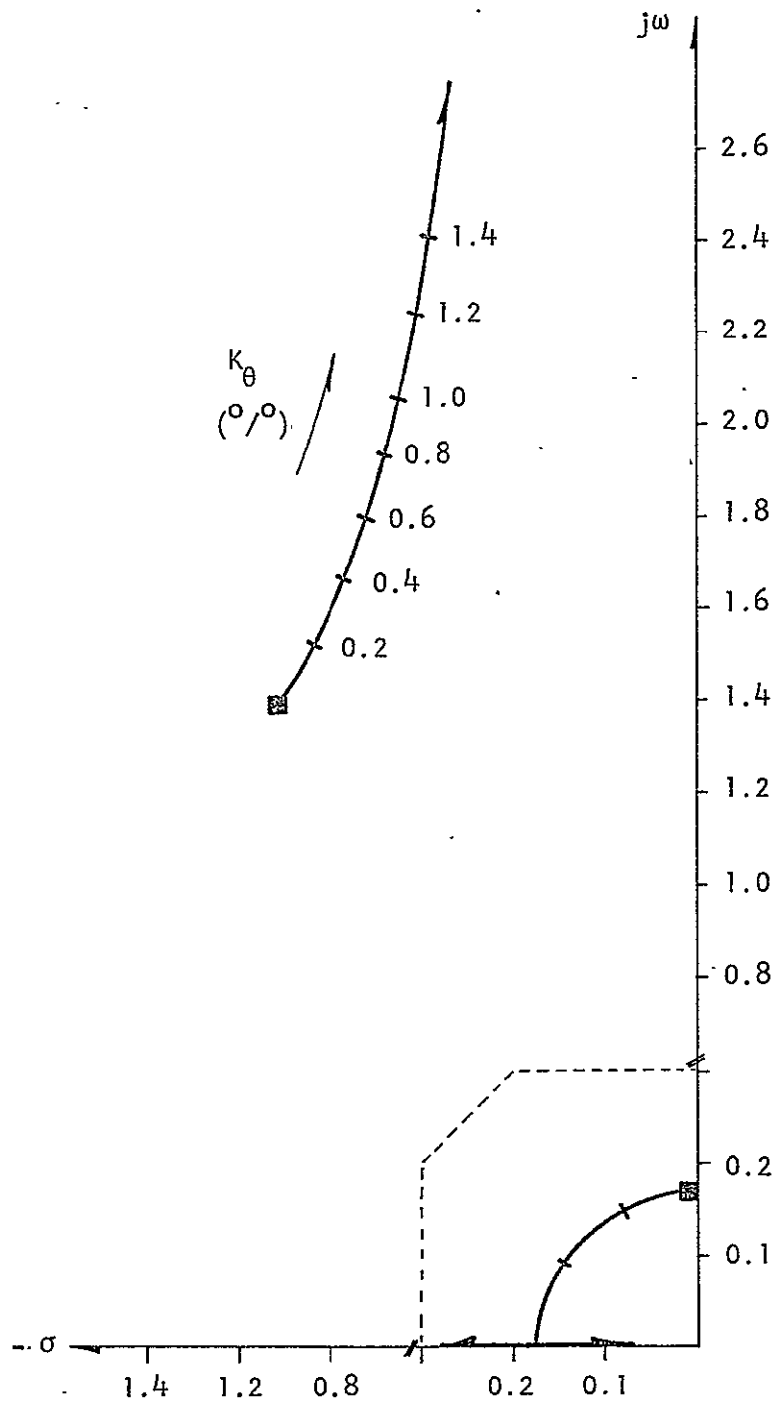


FIGURE 11. ROOT LOCUS FOR $\theta \rightarrow \delta_e$ LOOP CLOSURE

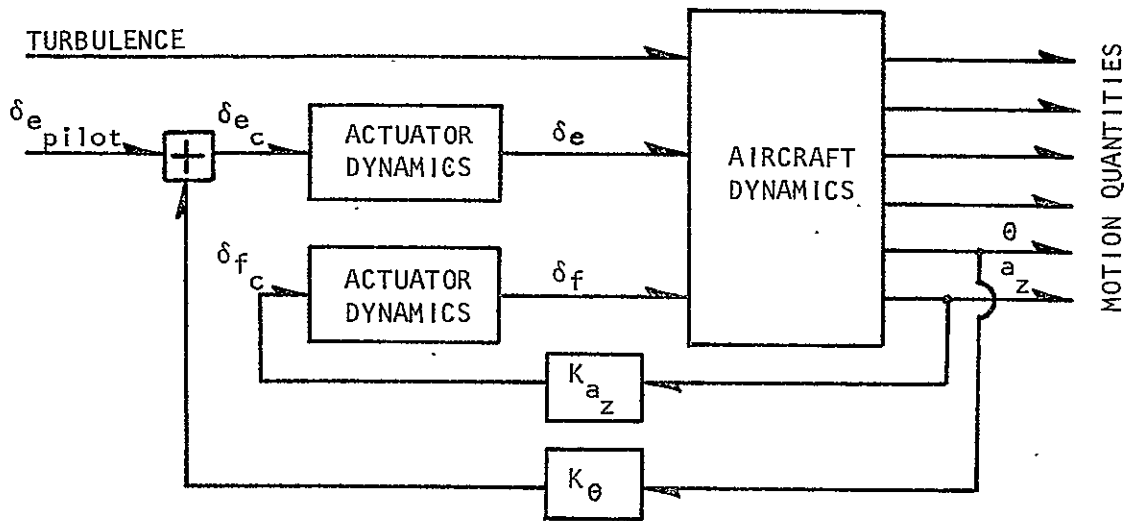


FIGURE 12. BASIC LONGITUDINAL RIDE SMOOTHING SYSTEM

K_{a_z} and K_{θ} are pure gains.

The effect on aircraft short period and phugoid dynamics is presented as a function of the two feedback gains in Figure 13. Note that the phugoid mode is rapidly stabilized by feedback of θ for any value of K_{a_z} . Any desired value of short-period frequency can also be attained. Some degradation in the short-period damping ratio, however, results.

Performance of the Ride Smoothing System, in terms of percent reduction in σ_{a_z} and σ_q , is depicted as a function of the feedback gains in Figures 14 and 15. Root-mean-square direct-lift flap activity is similarly presented in Figure 16. Maximum permissible root-mean-square flap deflection, consistent with the constraint of Section 2.3.3, is 10° . No plot is presented for elevator activity since $\sigma_{\delta_e} < 1.2^\circ$ for all levels of feedback gains considered and is thus well within available

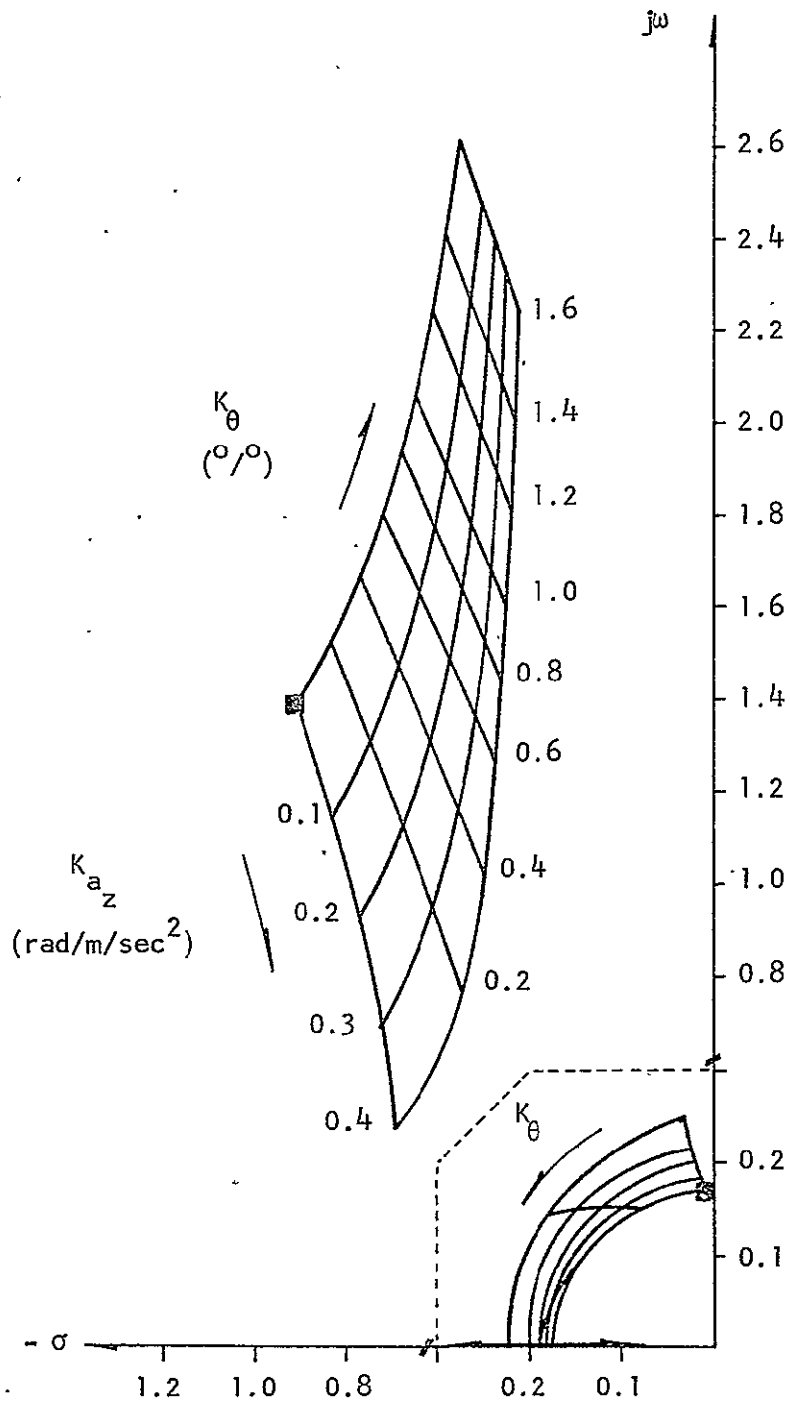


FIGURE 13. ROOT LOCUS FOR BASIC LONGITUDINAL RSS

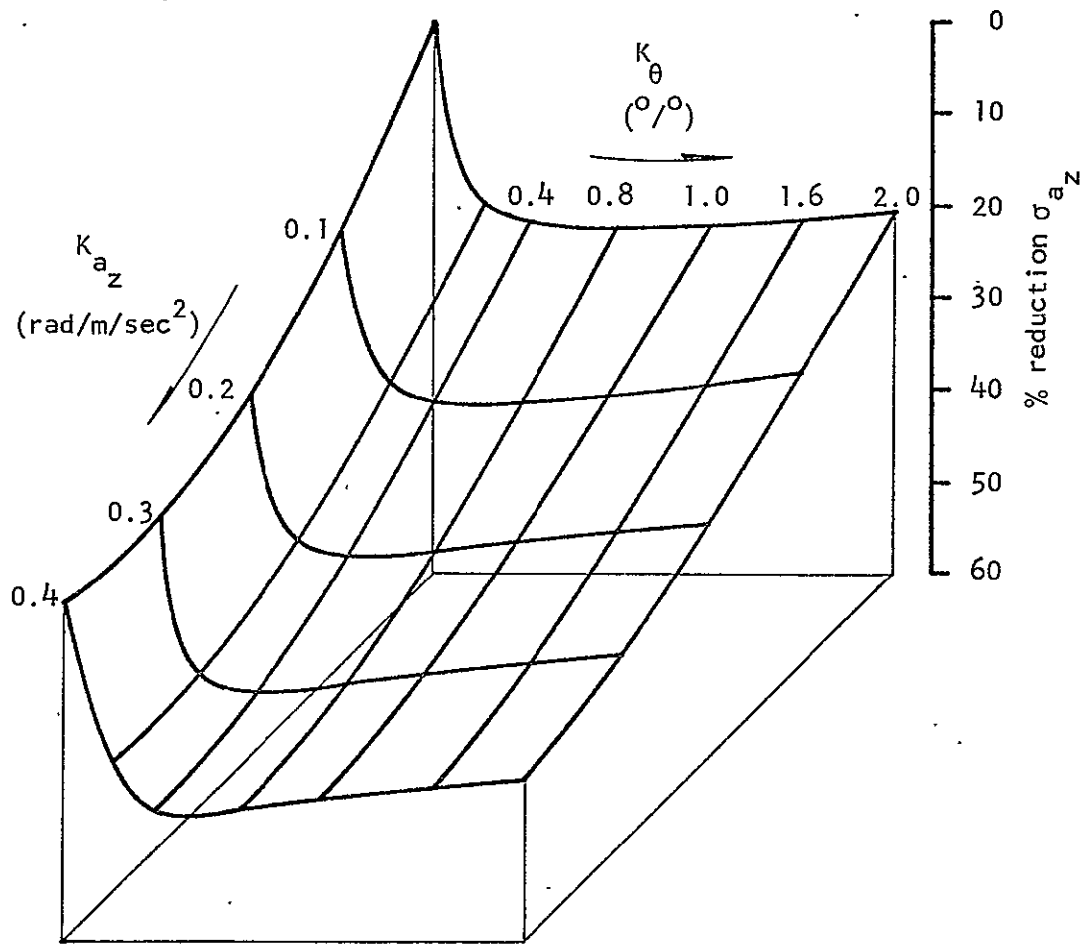


FIGURE 14. PERFORMANCE OF BASIC LONGITUDINAL RSS;
 σ_{a_z} AS A FUNCTION OF K_{a_z} AND K_{θ}

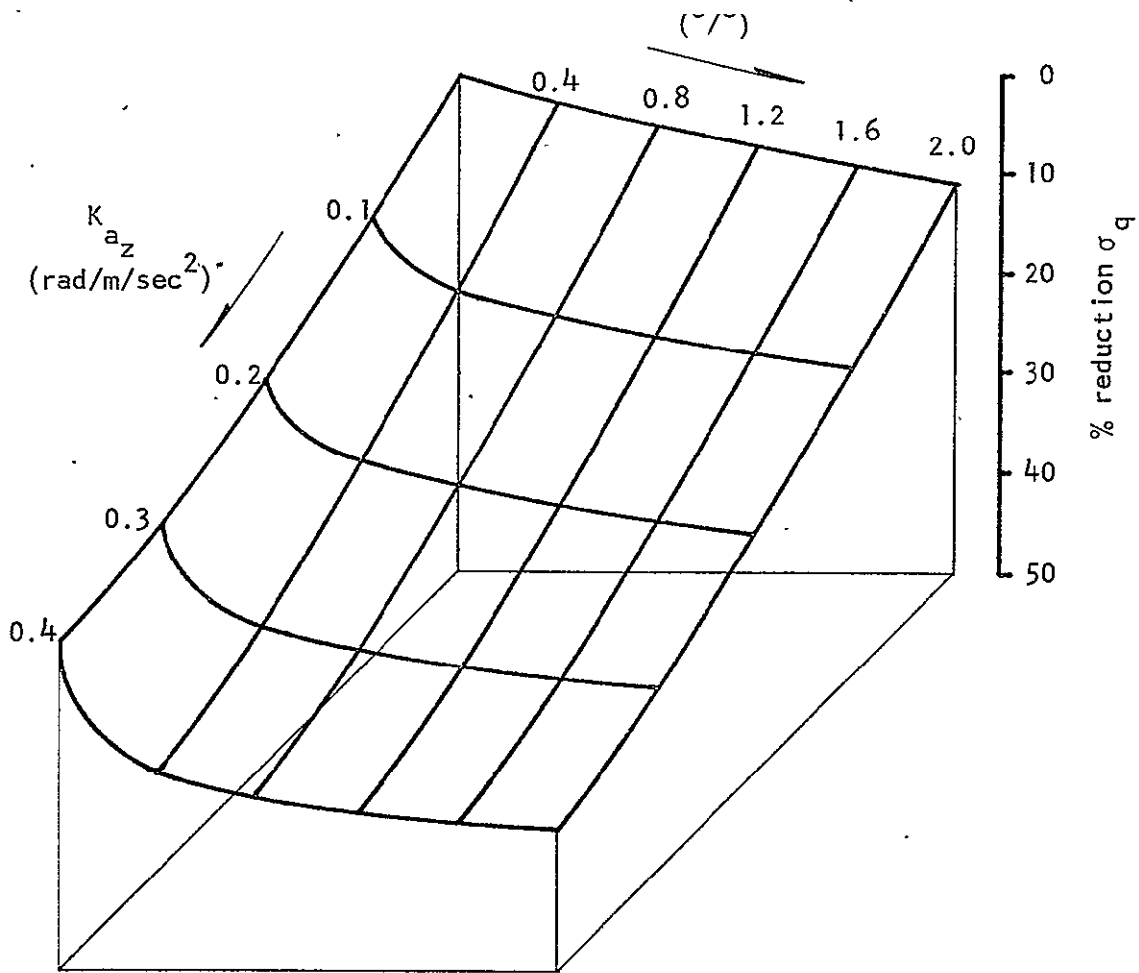


FIGURE 15. PERFORMANCE OF BASIC LONGITUDINAL RSS;
 σ_q AS A FUNCTION OF K_{az} AND K_{θ}

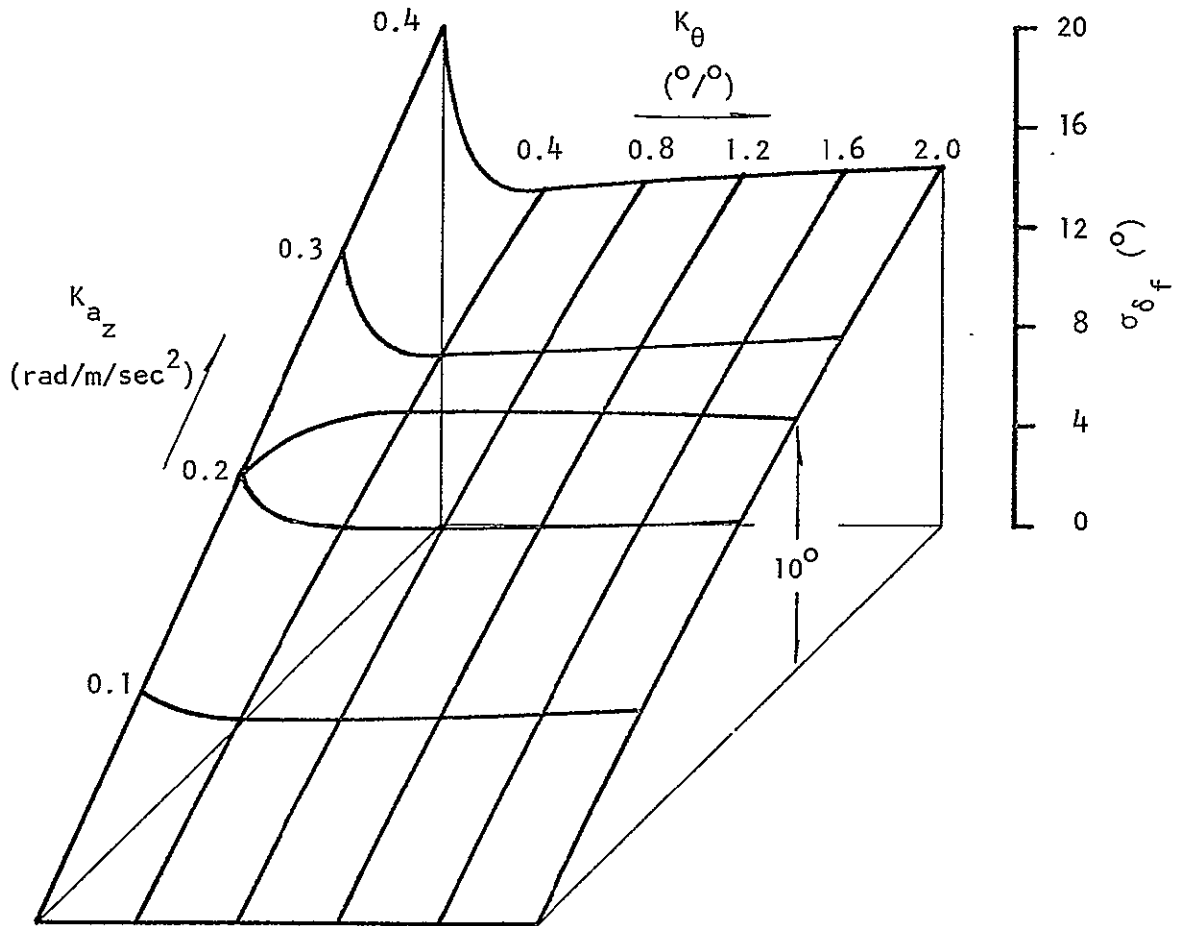


FIGURE 16. PERFORMANCE OF BASIC LONGITUDINAL RSS;
 σ_{δ_f} AS A FUNCTION OF K_{a_z} AND K_{θ}

JetStar limits ($-20^\circ \leq \delta_e \leq +16^\circ$). Figure 17 was constructed by superimposing the flap deflection criteria and lines of constant short-period damping ratio (ζ_{sp}) and frequency ($\omega_{n_{sp}}$) on Figure 14. The resulting surface can be interpreted as a rudimentary graphical representation of a RSS performance index. By referring to this plot, the system designer can choose any combination of gains K_{a_z} and K_θ to minimize σ_{a_z} and simultaneously satisfy a handling-qualities criterion based on short-period mode characteristics. Note that no combination of feedback gains will permit a return to the free aircraft short-period characteristics. The limit on permissible K_{a_z} as established by surface activity considerations is also shown.

In order to maximize the performance of this system, K_{a_z} should be chosen so as to take complete advantage of the available direct-lift flap authority. Choice of K_θ is then limited to a narrow band $0.4 < K_\theta < 0.5$; the lower limit being based on system performance considerations, the upper, on handling qualities criteria ($\zeta_{sp} > 0.35$). A typical design point might then be chosen at $K_{a_z} = 0.26 \text{ rad/m/sec}^2$, $K_\theta = 0.4 \text{ rad/rad/sec}$ resulting in a 41% reduction in σ_{a_z} .

3.4.5 Analytic Model of Longitudinal Ride Smoothing System

Significant insight into the mechanisms underlying the performance of the baseline longitudinal RSS can be gained by examining a simplified analytic expression for aircraft root-mean-square vertical acceleration due to turbulence. As the first step in the derivation, the appropriate aircraft transfer function is required (see Appendix D). Although the development is conceptually straightforward, the resulting equations are extremely lengthy. Considerable simplification results

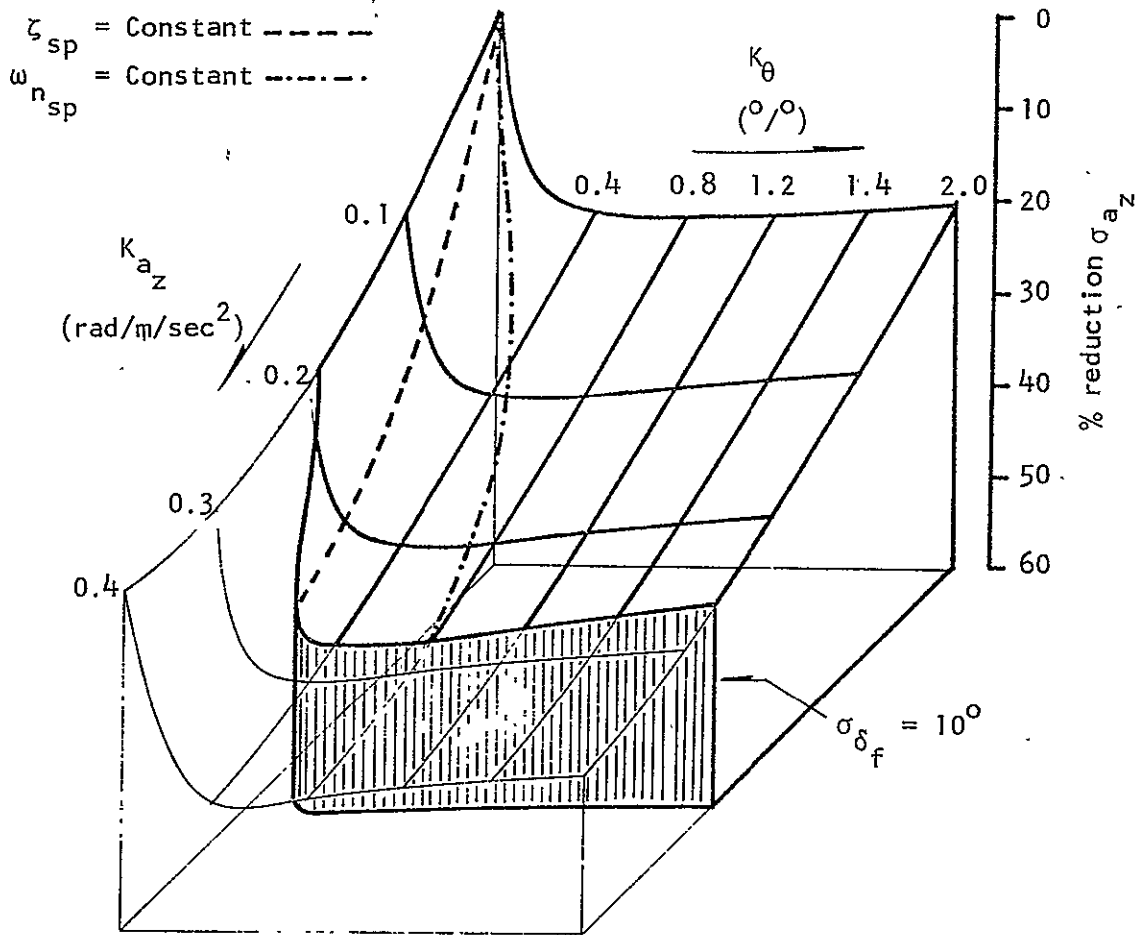


FIGURE 17. PERFORMANCE OF BASIC LONGITUDINAL RSS;
 σ_{a_z} AS A CONSTRAINED FUNCTION OF K_{a_z} AND K_{θ}

if several assumptions are made:

1. Effect of pitch gust, q_g , on vertical acceleration, a_z , is small as compared to the effect of vertical gust, w_g ;
2. The dynamics of the aircraft can be approximated by setting the phugoid mode frequency equal to zero; and
3. All actuators are perfect.

If only the highest order terms (based on JetStar aerodynamics only) in each power of the Laplace variable are retained, the transfer function for a_z due to w_g can be written in terms of the aircraft stability derivatives as

$$G_{w_g}^{a_z} \approx K_{ST} \left\{ \frac{s^2(s^2 - M_q s - K_{\theta} M_{\delta_e})}{s^2(s^2 + 2\zeta_{sp} \omega_{n_{sp}} s + \omega_{n_{sp}}^2)} \right\}, \quad (3.4.1)$$

where the static gain, K_{ST} , is

$$K_{ST} \equiv \frac{Z_w}{(1 - K_{a_z} Z_{\delta_f})}; \quad (3.4.2)$$

the short-period damping is given by

$$-2\sigma_{sp} = 2\zeta_{sp} \omega_{n_{sp}} \approx -M_q - K_{ST}; \quad (3.4.3)$$

and the short-period natural frequency

$$\omega_{n_{sp}}^2 \approx -U_0 M_w - K_{\theta} M_{\delta_e} + K_{ST} (M_q - K_{a_z} U_0 M_{\delta_f}). \quad (3.4.4)$$

With the additional assumption that the transfer function of w_g due to turbulence, Λ , can be approximated by a first-order filter

$$G_{\Lambda}^w \approx \frac{1}{s} , \quad (3.4.5)$$

we can write

$$G_{\Lambda}^z = K_{ST} \cdot \left\{ \frac{s^2 - M_q s - K_{\theta} M_{\delta_e}}{s(s^2 + 2\zeta_{sp} \omega_{n_{sp}} s + \omega_{n_{sp}}^2)} \right\} , \quad (3.4.6)$$

and (from Equation B.2)

$$\sigma_{a_z}^2 = \int_0^{\infty} |G_{\Lambda}^z|^2 \Phi(\Lambda) d\omega . \quad (3.4.7)$$

The integration can be performed in the complex plane to yield:

$$\sigma_{a_z} \propto \frac{K_{ST}}{\omega_{n_{sp}}^2} \left\{ \frac{(K_{\theta} M_{\delta_e})^2}{\omega_0} + \frac{\pi}{4\zeta_{sp}} \left[(K_{\theta} M_{\delta_e})^2 (4\zeta_{sp}^2 - 1) - \omega_{n_{sp}}^2 (\omega_{n_{sp}}^2 + M_q^2 + 2K_{\theta} M_{\delta_e}) \right] \right\}^{\frac{1}{2}} \quad (3.4.8)$$

where ω_0 is the lower limit for a truncated input turbulence (white noise) power spectra.

Several comments about the deficiencies of this approximation are in order. Note that the expression for σ_{sp} (Equation 3.3.3) does not properly account for the reduction in short-period damping with increasing K_{θ} (Figure 13). A value of $\omega_0 > 0$ is clearly required for

the integration to be bounded. If ω_0 is arbitrarily chosen as $\omega_0 = 0.56$ rad/sec, the approximation predicts system performance in good agreement with the digitally-calculated results (Figure 18).

The critical parameters affecting the acceleration alleviation capability of this system are the constants outside the radical: K_{ST} and $\omega_{n_{sp}}^2$. From the definition of K_{ST} (Equation 3.4.2), it is clear that, for a given lift curve slope Z_w , the overall system performance is determined by the flap effectiveness term Z_{δ_f} . Conceptually, this conclusion is intuitively obvious. The fact that system performance is improved as $\omega_{n_{sp}}^2$ is increased can be explained by considering the exact input power spectra (Figure 19). Above the break frequency, $\omega = 0.236$ rad/sec, the input power decays at the rate of 40 dB/decade; thus, the higher the aircraft effective short-period resonant frequency, the lower the magnitude of response to turbulence. Finally, the effect of changing the damping ratio of the short-period mode, ζ_{sp} , is contained within the second term inside the radical. At $\zeta_{sp} = 0.5$, this term contributes nothing to σ_{a_z} ; for $\zeta_{sp} < 0.5$, however, the magnitude of σ_{a_z} is increased as K_{θ} is increased.

Note that the performance of the baseline longitudinal RSS, to first order, depends only on a single dynamic derivative: M_q . Generally, dynamic derivatives are more difficult to estimate or measure than static stability derivatives. In order to be most successful, any RSS design should be minimally sensitive to errors in estimation of the plant parameters. Calculations, based on the simplified model, showed that variations of $\pm 25\%$ in the magnitude of M_q resulted in less than 1% change in the performance of the baseline longitudinal RSS.

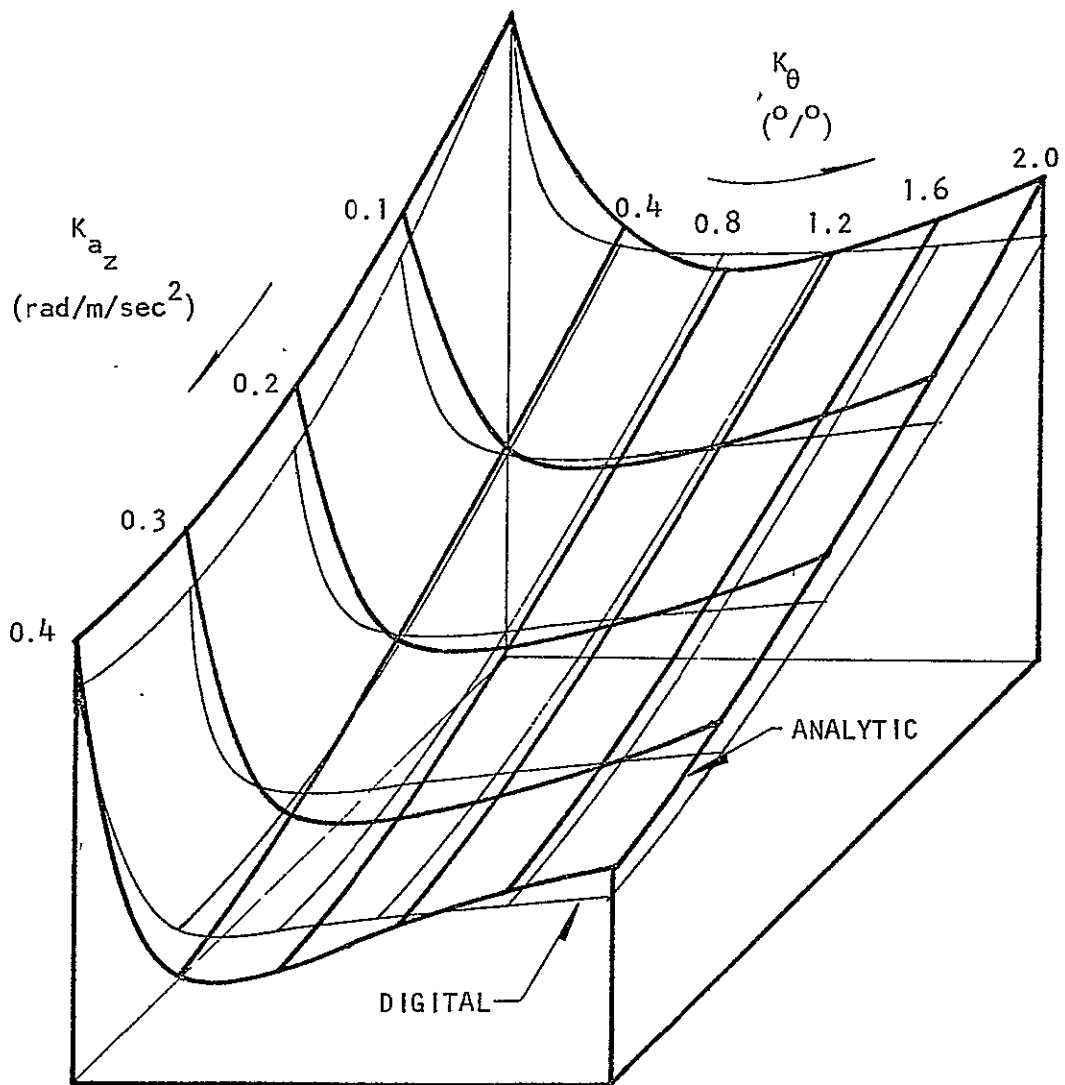


FIGURE 18. COMPARISON OF DIGITALLY CALCULATED σ_{a_z} WITH ANALYTIC EXPRESSION

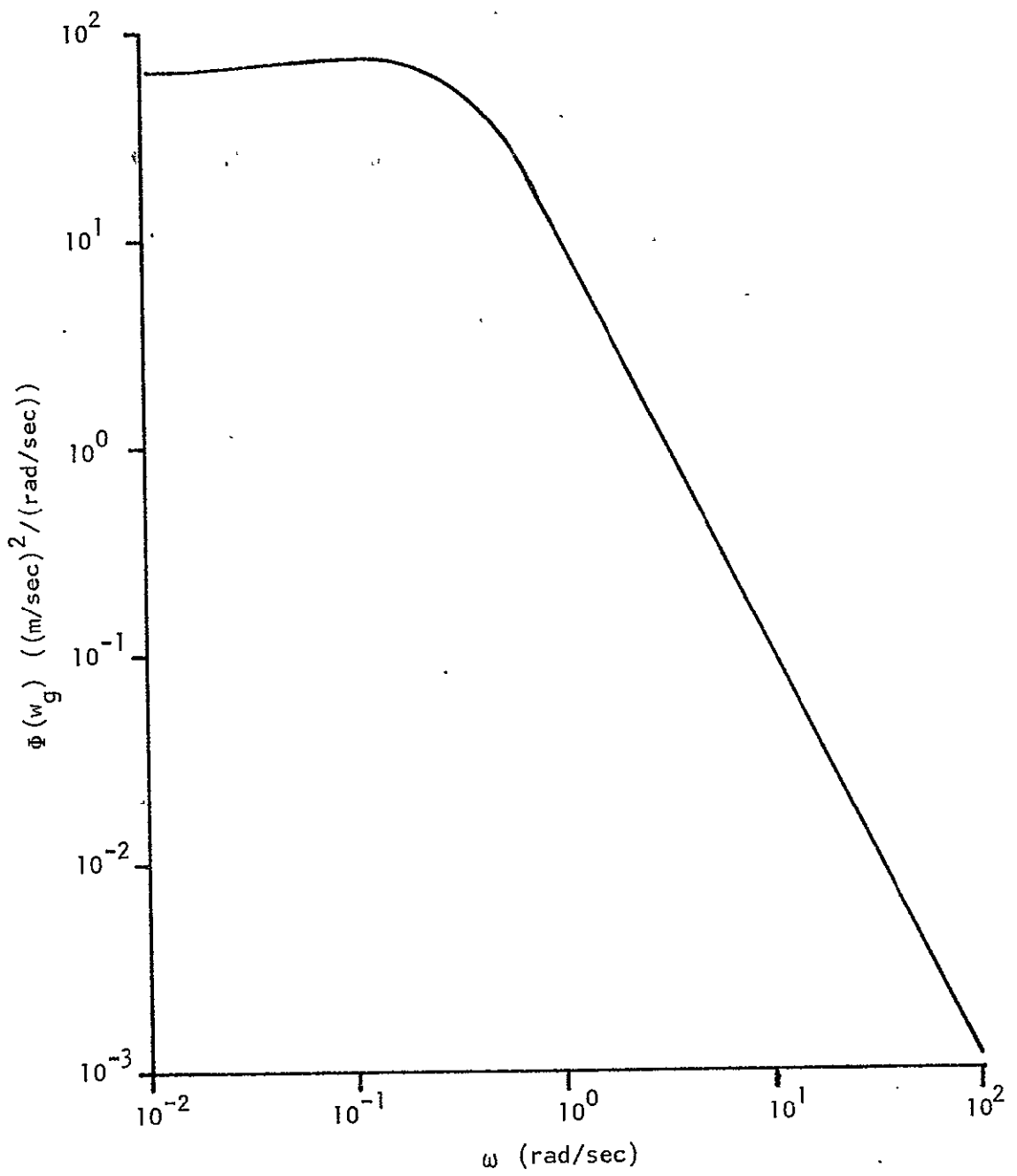


FIGURE 19. POWER SPECTRA FOR w_g DUE TO A

3.4.6 Longitudinal Ride Smoothing System I

Although the baseline longitudinal RSS provides a measure of acceleration alleviation while meeting design criteria, several improvements are desirable. First, the simple mechanization results in narrow limits for the choice of K_θ . Secondly, no choice of feedback gain permits recovery of the basic aircraft short-period characteristics. Finally, the pilot's control of flight path, as represented by the parameter n/α , is degraded.

The inclusion of proper equalization in the feedback paths can eliminate all of these shortcomings while improving system performance. Consider first the feedback of $a_z \rightarrow \delta_f$. For the two feedback loop systems ($a_z \rightarrow \delta_f$, $\theta \rightarrow \delta_e$), it can be shown that (see Appendix D):

$$\frac{n}{\alpha} \approx \frac{U_0}{g} \cdot \frac{-Z_w}{1 - G_{a_z} Z_{\delta_f}} \quad (\text{g/rad}) \quad (3.4.9)$$

If a filter of the form $\frac{s}{s + \tau_{w_0}^{-1}}$ (washout) is included in the $a_z \rightarrow \delta_f$ feedback path, the steady state n/α will be the same as for the basic aircraft. A more rapid decrease in σ_{sp} with K_{a_z} than for a pure gain feedback, however, results. Introduction of a lag filter $(\frac{s+a}{s+b}, a < b)$ in series with the washout tends to offset this undesirable trend. A short-period root locus depicting the effect of these filters is shown in Figure 20. The filter parameters were chosen so as to permit the construction of feasible analog circuits. In the case of lag circuits, the ratio of a/b is customarily restricted to be greater than or equal to 0.1 by circuit noise considerations.

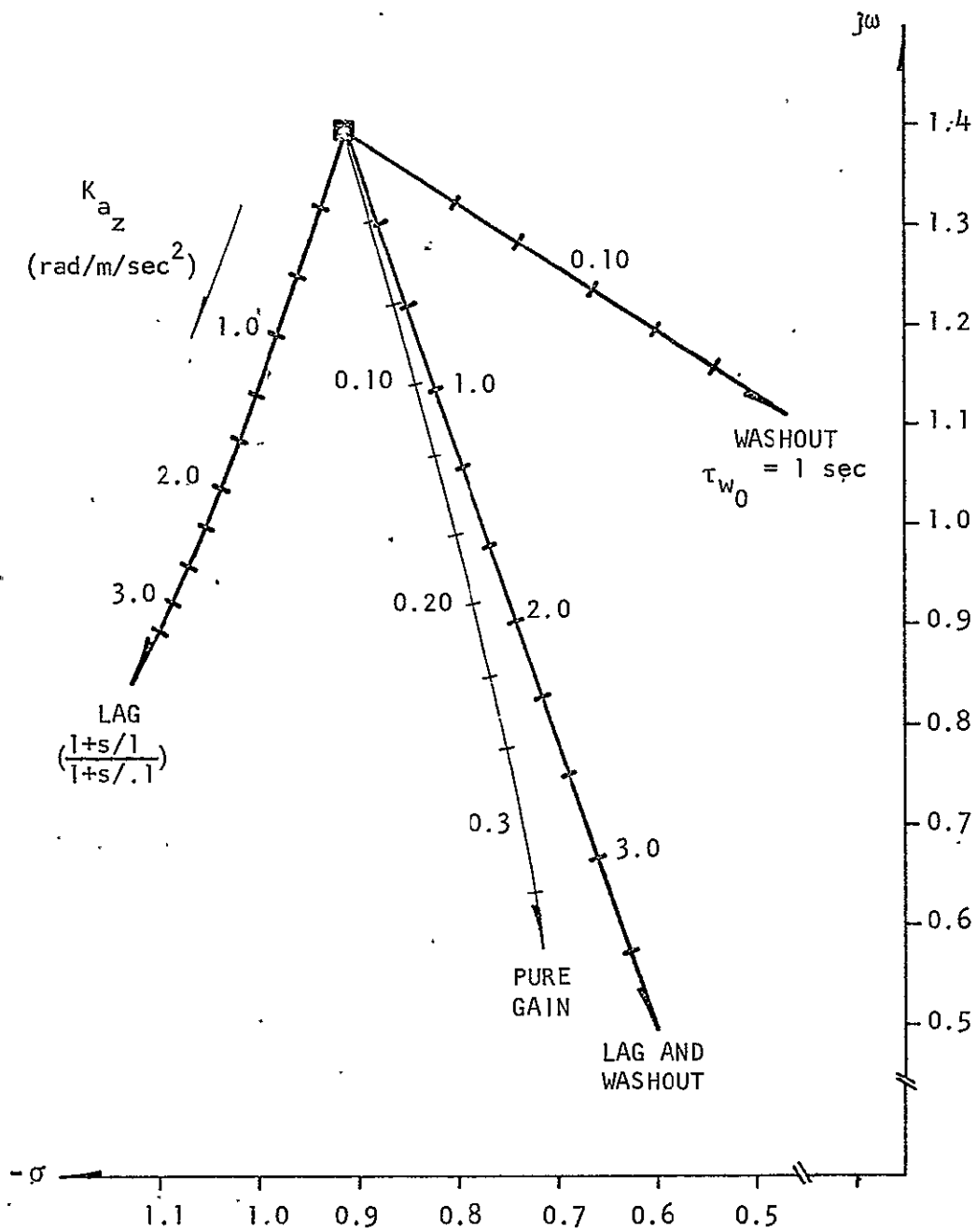


FIGURE 20. ROOT LOCUS OF EFFECT ON SHORT-PERIOD DYNAMICS OF FILTERS IN $a_z \rightarrow \delta_f$ FEEDBACK LOOP

Additional short-period damping can be provided by incorporating a lead filter $(\frac{s+c}{s+d}, d > c)$ in the $\theta \rightarrow \delta_e$ feedback loop. In essence, this filter provides a pseudo-differentiation or feedback of a component of pitch rate at very low frequencies (Figure 21). The maximum ratio c/d is again limited by feasibility considerations to values equal to or less than 10.0.

For both the lead and lag filters, the desired break frequencies were determined by inspecting a number of root locus plots. The system resulting from the incorporation of these filters is depicted in block diagram form in Figure 22 and designated Longitudinal Ride Smoothing System I. System performance surfaces, equivalent to those shown for the baseline system are presented in Figures 23 through 26. The complete root locus carpet plot is given in Figure 27.

Based on the procedures outlined in Section 3.3.4, the system design point was chosen at $K_{a_z} = 3.3$, $K_{\theta} = 0.14$. The aircraft dynamics and system performance parameters for this configuration at $\sigma_{wg} = 2.1$ m/sec are summarized in Table III.

Figure 28 compares the power spectral density of vertical acceleration for the basic and longitudinal RSS I augmented aircraft. Note that the response to turbulence is heavily attenuated at both the phugoid and short-period frequencies, as well as in the range above the short-period peak. A slight amplification in a narrow frequency band, however, results.

Compared to the baseline system, Longitudinal RSS I is clearly superior both in terms of acceleration alleviation capability and closed-loop short-period mode characteristics. As pointed out

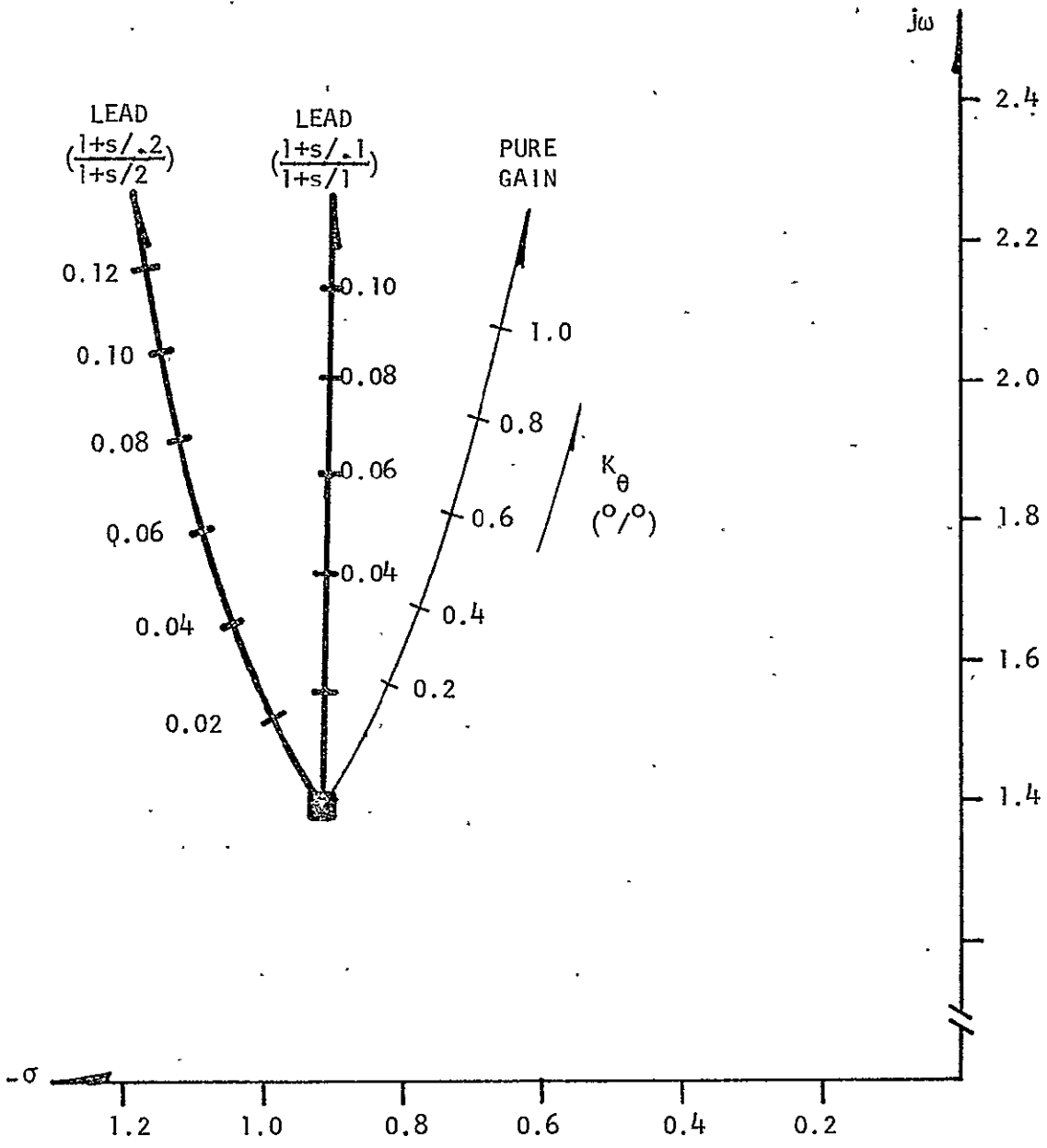


FIGURE 21. ROOT LOCUS OF EFFECT ON SHORT-PERIOD DYNAMICS OF A LEAD FILTER IN $\theta \rightarrow \delta_e$ FEEDBACK LOOP

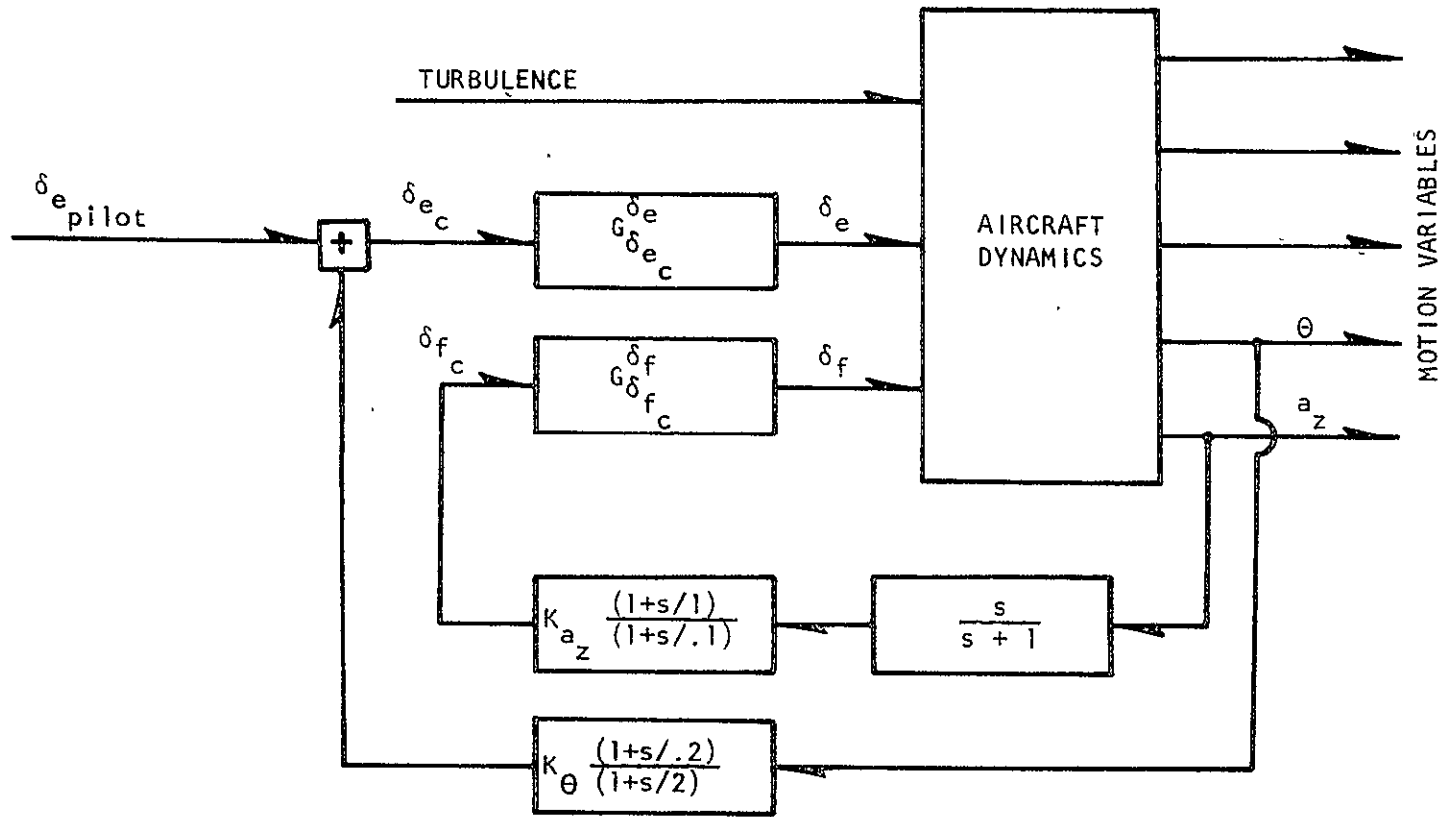


FIGURE 22. LONGITUDINAL RIDE SMOOTHING SYSTEM I
 (Design Point: $K_{a_z} = 3.3 \text{ rad/m/sec}^2$, $K_\theta = 0.14 \text{ }^\circ/\text{o}$)

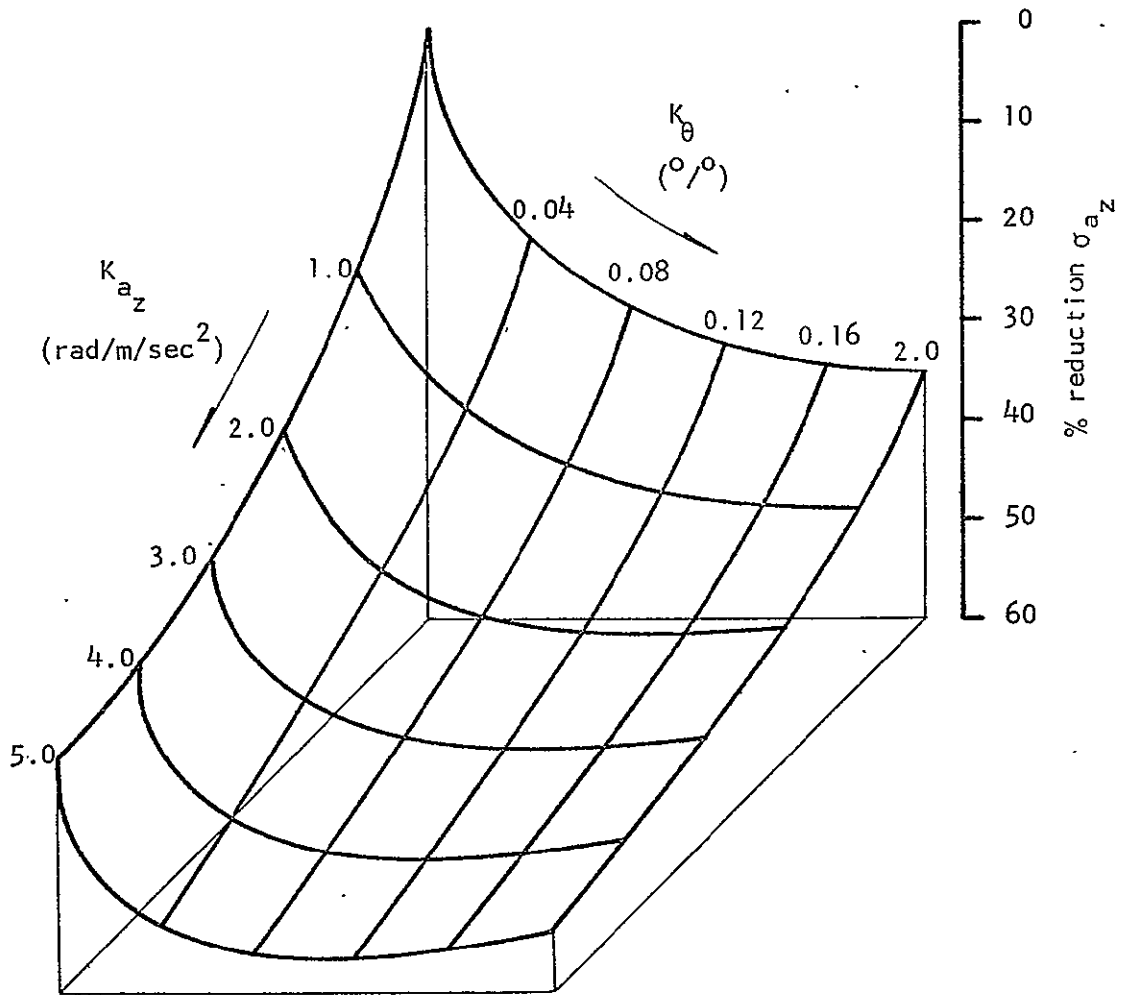


FIGURE 23. PERFORMANCE OF LONGITUDINAL RSS I;
 σ_{a_z} AS A FUNCTION OF K_{a_z} AND K_{θ}

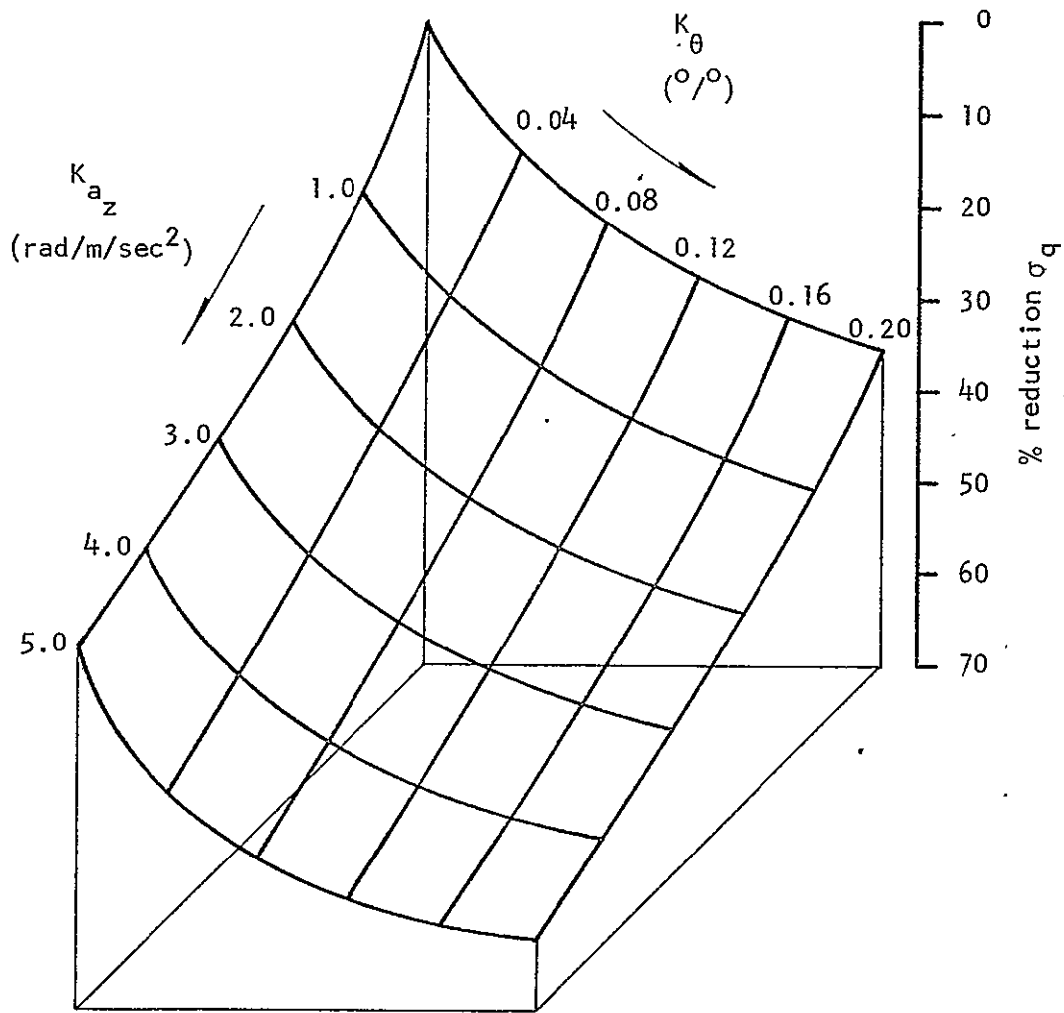


FIGURE 24. PERFORMANCE OF LONGITUDINAL RSS I;
 σ_q AS A FUNCTION OF K_{a_z} AND K_{θ}

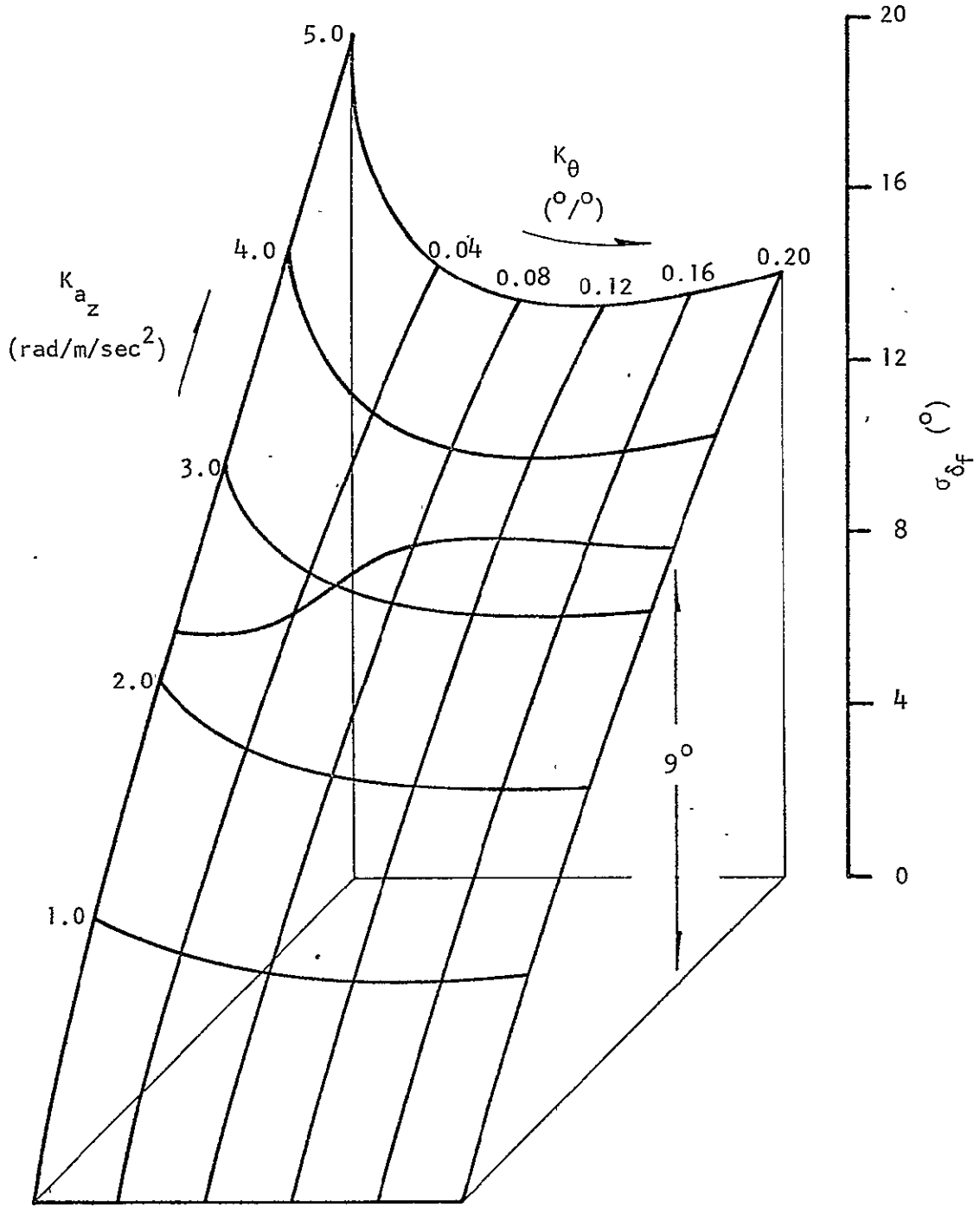


FIGURE 25. PERFORMANCE OF LONGITUDINAL RSS 1;
 σ_{δ_f} AS A FUNCTION OF K_{a_z} AND K_{θ}

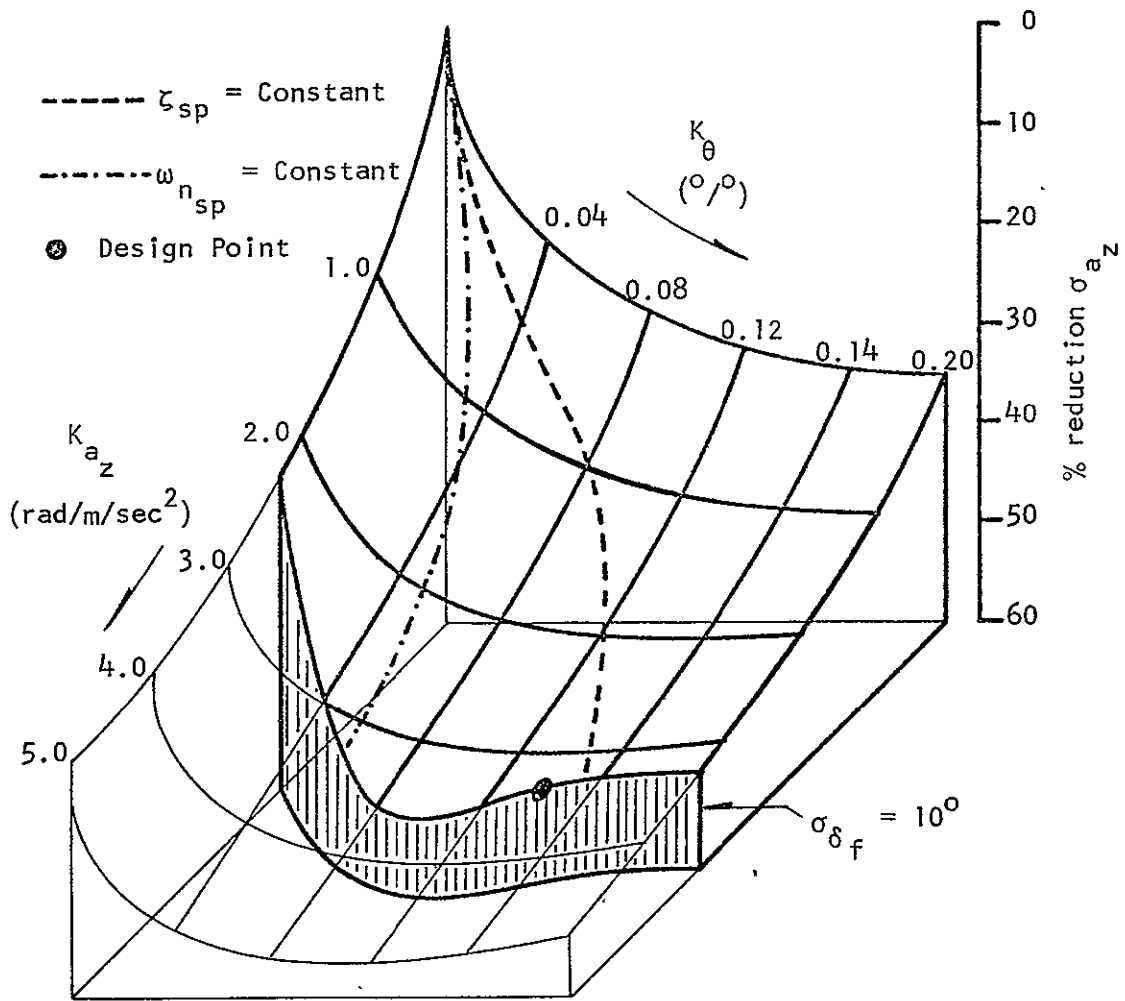


FIGURE 26. PERFORMANCE OF LONGITUDINAL RSS I;
 σ_{a_z} AS A CONSTRAINED FUNCTION OF K_{a_z} AND K_{θ}

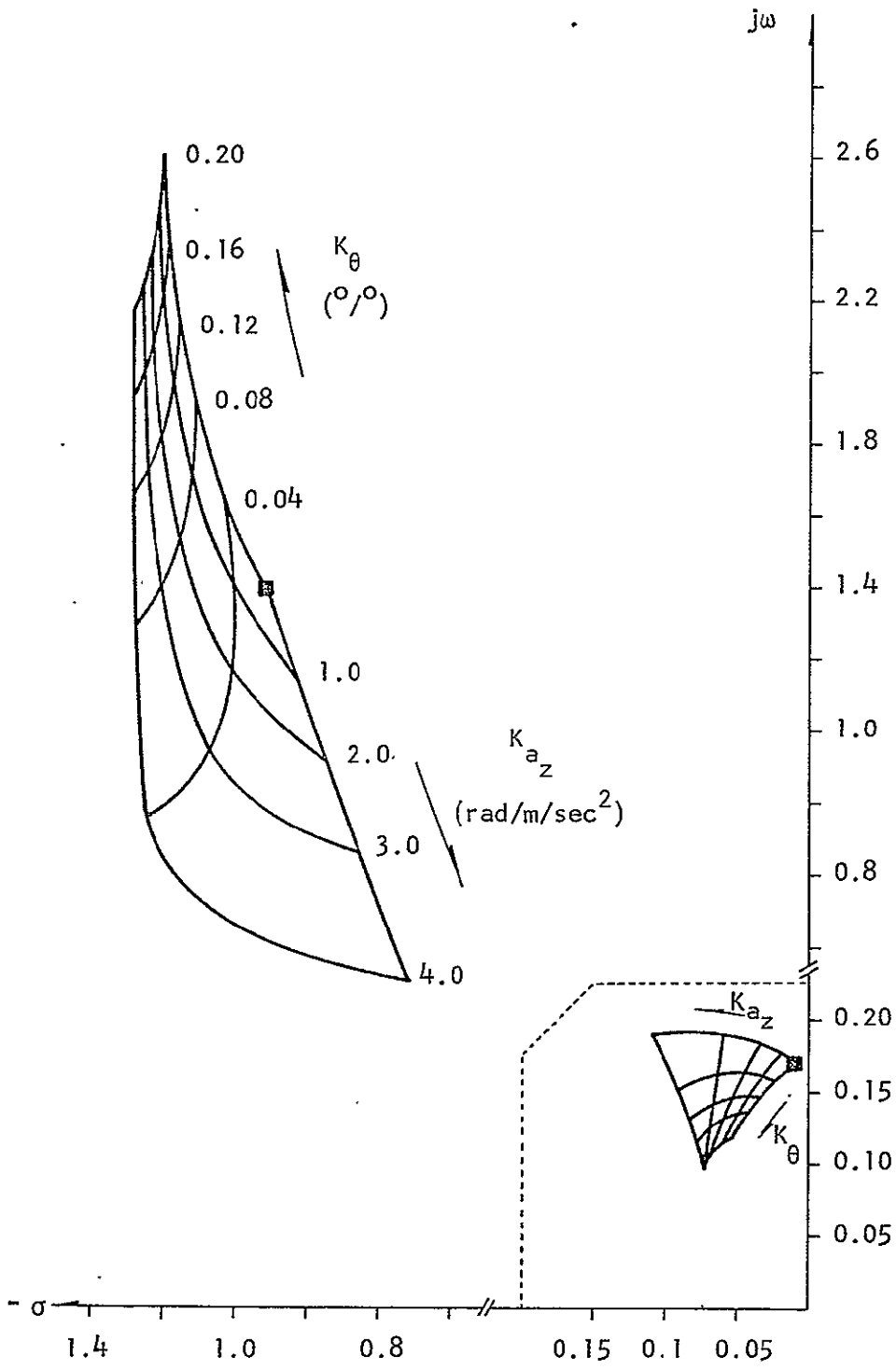


FIGURE 27. ROOT LOCUS FOR LONGITUDINAL RSS I

TABLE III

CHARACTERISTICS OF LONGITUDINAL RIDE SMOOTHING SYSTEM I

	<u>Basic JetStar</u>	<u>Longitudinal RSS I</u>
ζ_{sp}	0.546	0.567
$\omega_{n_{sp}}$	0.266 Hz	0.356 Hz
ζ_{ph}	0.054	0.522
P_{ph}	36.6 sec	53.2 sec
$T_{\frac{1}{2}ph}$	74.8 sec	9.6 sec
σ_{a_z}	0.1178 g	0.0572 g
σ_{a_x}	0.0112 g	0.0040 g
σ_q	1.44 °/sec	0.70 °/sec
σ_{δ_f}	--	9.9 °
σ_{δ_e}	--	0.4 °
% reduction σ_{a_z}	--	51.8%
% reduction σ_{a_x}	--	64.6%
% reduction σ_q	--	51.3%

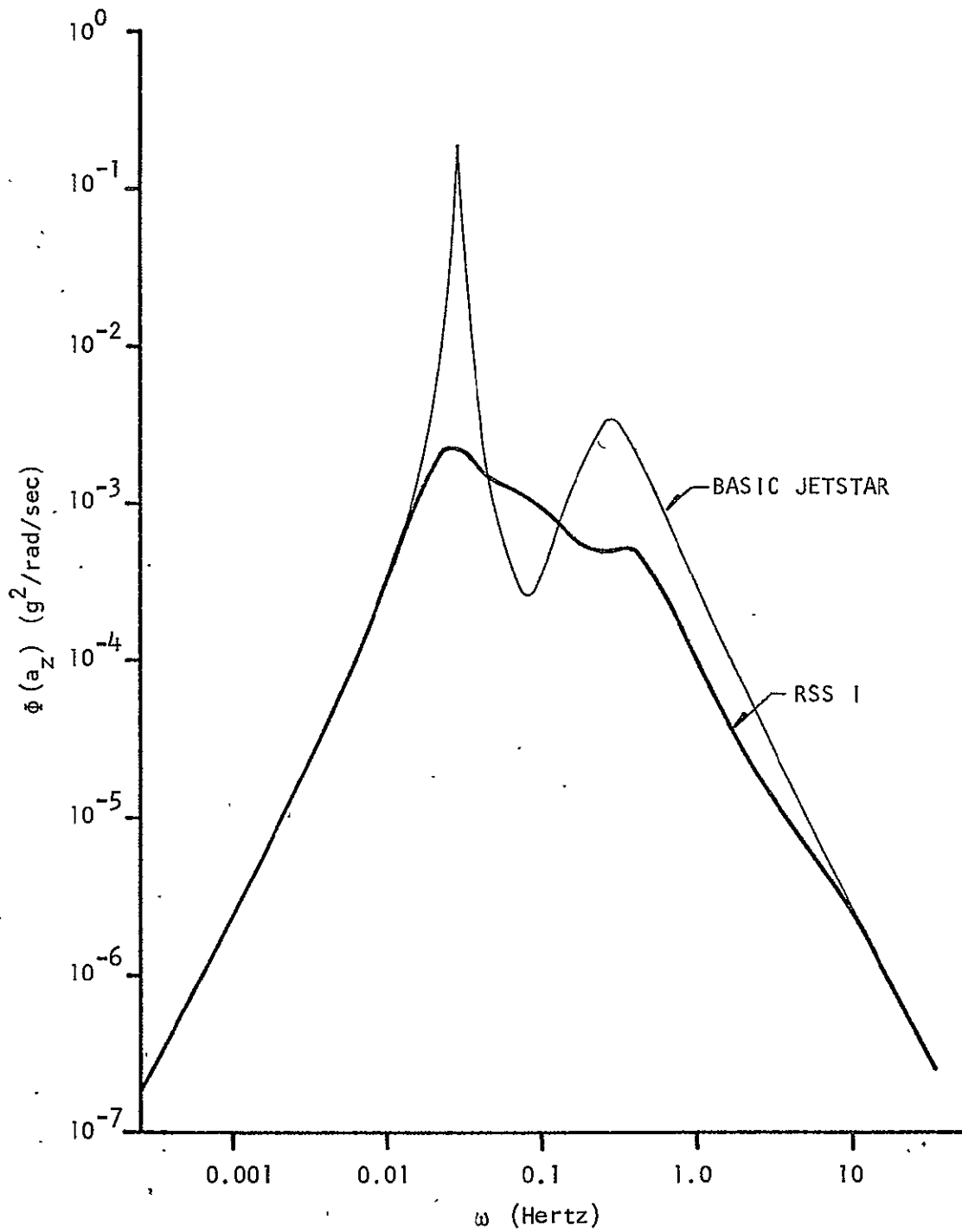


FIGURE 28. COMPARISON OF a_z POWER SPECTRA FOR BASIC AND LONGITUDINAL RSS I AUGMENTED JETSTAR

previously, the presence of a washout circuit in the $a_z \rightarrow \delta_f$ feedback path prevents degradation of the handling qualities parameter n/α . From the pilot's point of view, the only noticeable effects of the RSS might be some reduction in the speed of normal acceleration response to a stick input and the slightly greater stick deflection required to produce a given change in pitch attitude. The degree of these potential handling qualities problems was left to be considered in the ground-based simulation phase of this research.

Also to be evaluated in simulation was the effect of a failure of the stabilizing $\theta \rightarrow \delta_e$ feedback on the controllability of the augmented vehicle. From the root locus diagram (Figure 27), it is clear that with only the acceleration feedback operational, the short-period natural frequency would drop to marginal values ($\omega_{n_{sp}} \approx 0.14$ Hz).

3.4.7 Longitudinal Ride Smoothing System II

An alternate mechanization, designated Longitudinal RSS II, is depicted in block diagram form in Figure 29. It differs from the previous system only in the form of equalization in the $a_z \rightarrow \delta_f$ feedback path. A Bode magnitude plot of this filter is given in Figure 30. At the phugoid frequency, this circuit acts to heavily attenuate the feedback signal (notch filter). For all other frequencies, the magnitude response characteristics are similar to that of the lag filter used in System I. The lightly damped quadratic numerator of the filter introduces a pair of stable, very low-frequency roots which help delay the onset of short-period instability as K_{a_z} is increased. When the inner, $\theta \rightarrow \delta_e$, loop is closed, this artificially-introduced mode as well as the phugoid

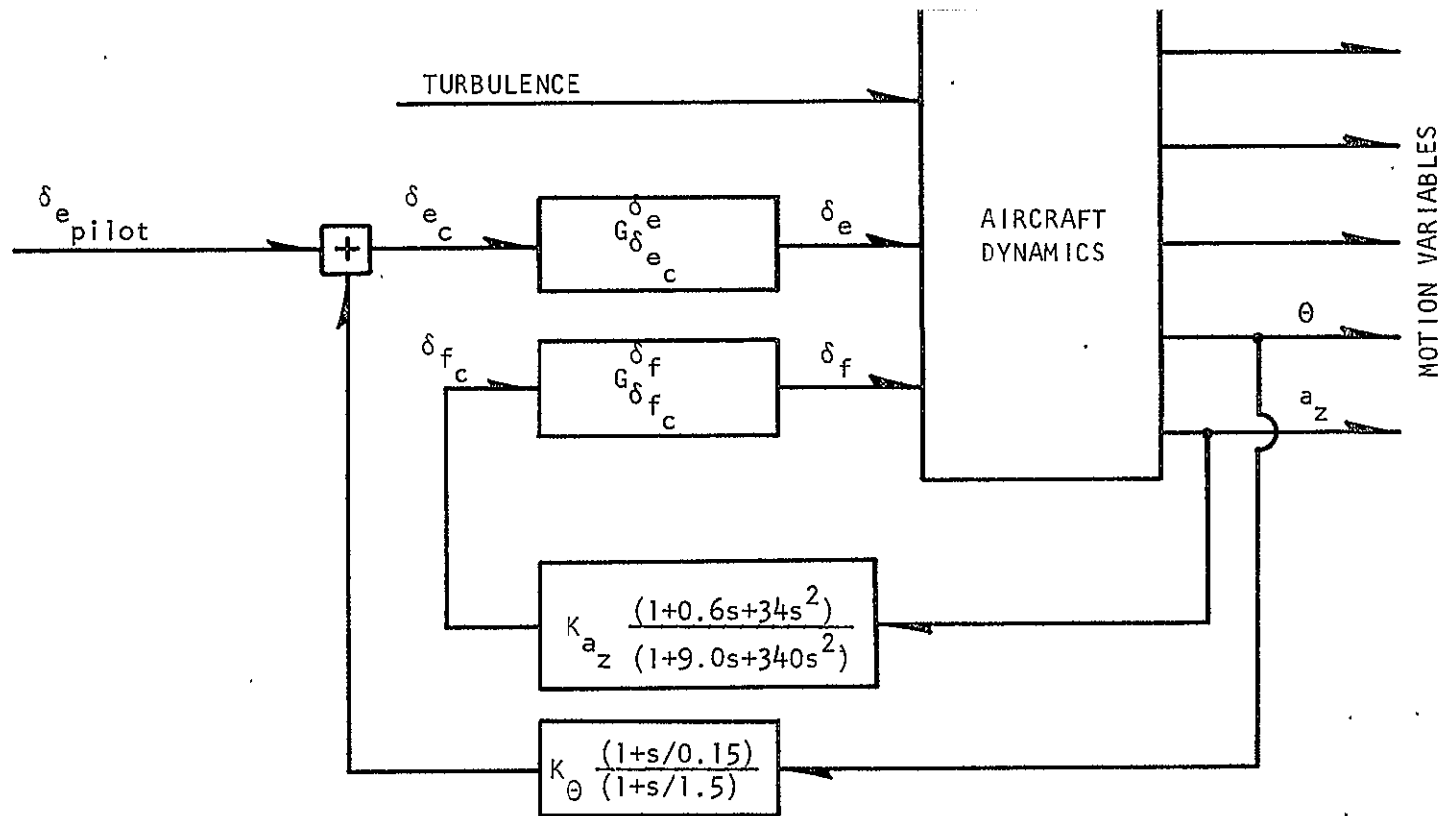


FIGURE 29. LONGITUDINAL RIDE SMOOTHING SYSTEM II
 (Design Point: $K_{a_z} = 3.3 \text{ rad/m/sec}^2$, $K_{\theta} = 0.1 \text{ }^\circ/\text{o}$)

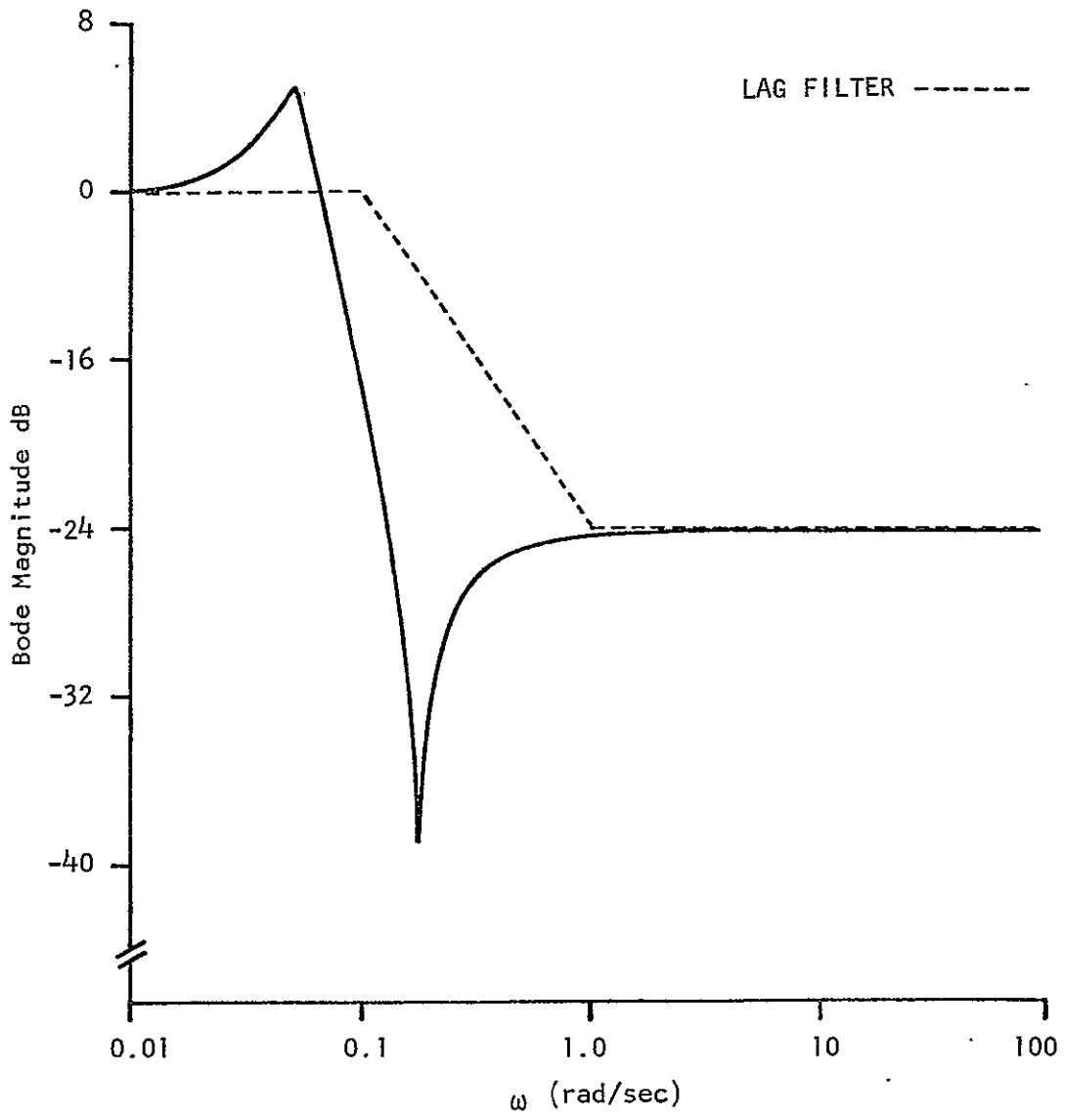


FIGURE 30. BODE MAGNITUDE PLOT OF NOTCH FILTER

are rapidly stabilized. The effect of the inner loop closure on the short-period roots is almost identical as for System I (Figure 31).

In order to provide a comparison of Systems I and II, the same value, $K_{a_z} = 3.3$, was selected for the design point. By setting the pitch attitude feedback gain at $K_\theta = 0.1$, the short-period damping ratio is made approximately equivalent to that of the basic aircraft. Table IV compares the key metrics of the basic and RSS augmented JetStar.

Although System II appears, from Table IV, to be somewhat inferior to System I in all respects, an examination of the power spectral density plots shows that the alleviation capability of System II is almost identical to that of System I for frequencies above the phugoid peak (Figure 32). Thus, the only major difference between the two mechanizations is in the handling qualities parameter n/α . Since handling qualities criteria were postulated as an important consideration in the design of Ride Smoothing Systems, both System I and II were retained for simulation experiments where pilot opinion was solicited. As with System I, failure of the $\theta \rightarrow \delta_e$ feedback loop will cause $\omega_{n_{sp}}$ to be reduced to a marginal value, and simulator studies were carried out to evaluate the severity of this deficiency.

3.5 Lateral Ride Smoothing Systems

3.5.1 The Basic JetStar--Lateral Case

The lateral dynamics of the basic JetStar in the approach configuration are characterized by the following parameters:

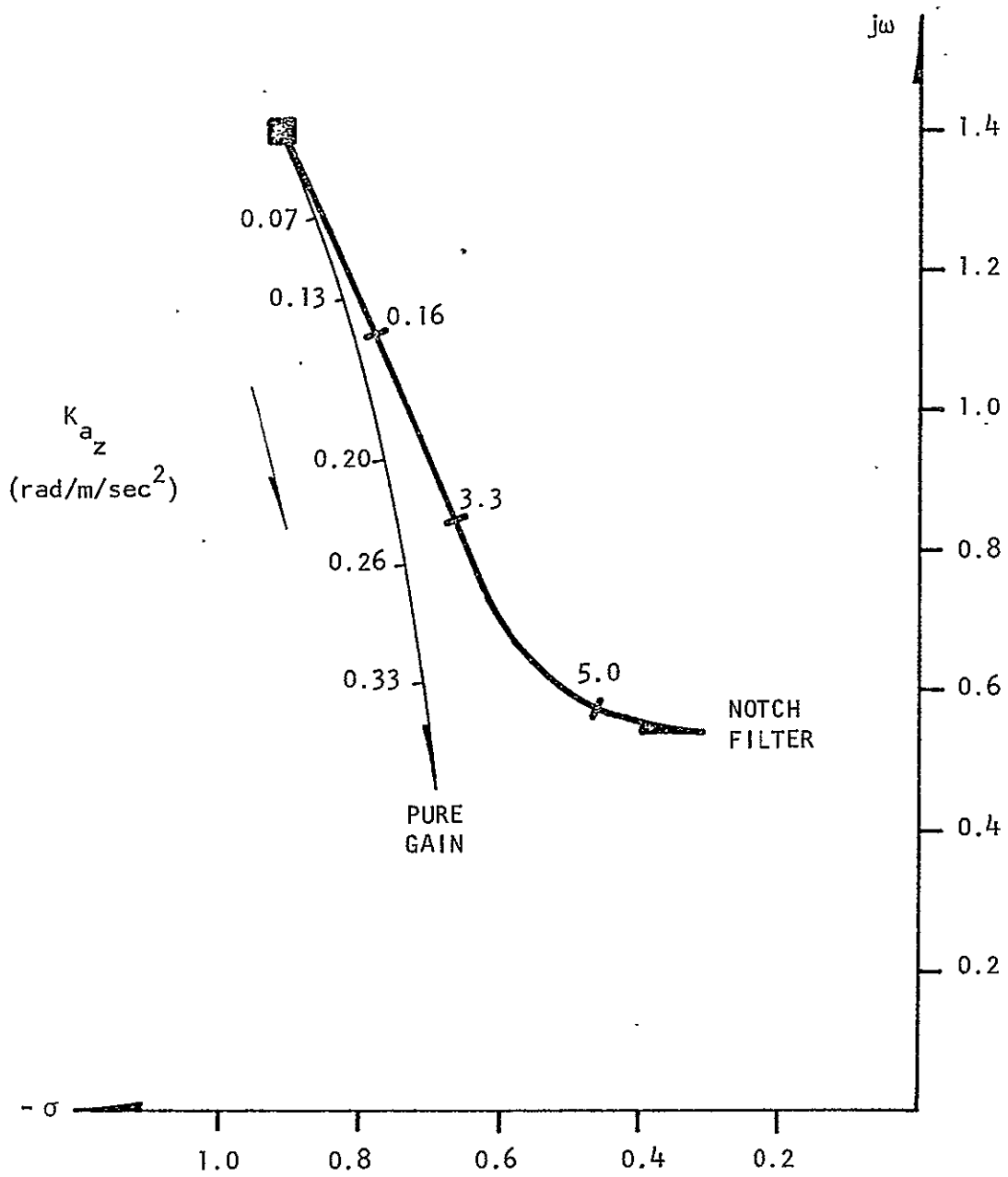


FIGURE 31. ROOT LOCUS OF EFFECT ON SHORT-PERIOD DYNAMICS OF A NOTCH FILTER IN $a_z \rightarrow \delta_f$ FEEDBACK LOOP

TABLE IV

CHARACTERISTICS OF LONGITUDINAL RIDE SMOOTHING SYSTEM II

	<u>Basic JetStar</u>	<u>Longitudinal RSS I</u>	<u>Longitudinal RSS II</u>
ζ_{sp}	0.546	0.567	0.534
$\omega_{n_{sp}}$	0.266 Hz	0.356 Hz	0.312 Hz
ζ_{ph}	0.054	0.522	0.158
P_{ph}	36.6 sec	53.2 sec	52.9 sec
$T_{\frac{1}{2}ph}$	74.8 sec	9.6 sec	36.8 sec
n/α	6.22 g/rad	6.22 g/rad	4.03 g/rad
σ_{a_z}	0.1178 g	0.0572 g	0.0607 g
σ_{a_x}	0.0112 g	0.0040 g	0.00454 g
σ_{δ_f}	--	9.7 °	12.2 °
σ_{δ_e}	--	0.4 °	0.4 °
% reduction σ_{a_z}	--	51.8%	49.4%
% reduction σ_{a_x}	--	64.6%	59.5%

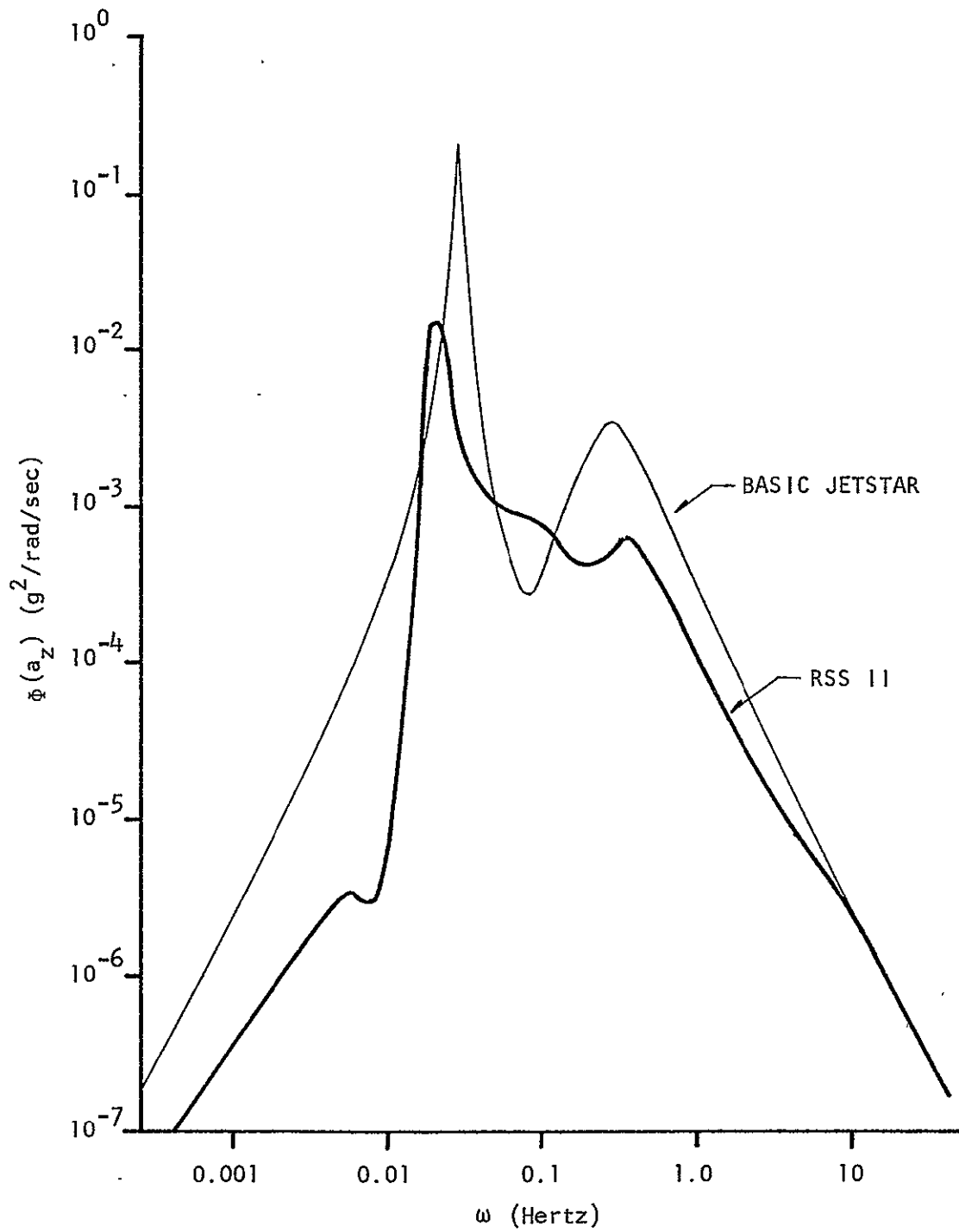


FIGURE 32. COMPARISON OF a_z POWER SPECTRA FOR BASIC AND LONGITUDINAL RSS II AUGMENTED JETSTAR

Dutch Roll Mode:	λ_{dr}	=	$-0.0615 \pm j 1.36$	
	ζ_{dr}	=	0.045	($\zeta > 0.08$)
	$\omega_{n_{dr}}$	=	1.36 rad/sec	($\omega_n > 0.4$)
	$\zeta_{dr} \omega_{n_{dr}}$	=	0.061 rad/sec	($\zeta \omega > 0.15$)
Roll Subsidence:	τ_R	=	0.87 sec	($\tau_R < 1.0$)
	$T_{\frac{1}{2}R}$	=	0.61 sec	
Spiral Mode:	$T_{\frac{1}{2}}$	=	418 sec	($T_2 > 20$)

where the inequalities in brackets are criteria of MIL-F-8785B (36).

Note that the Dutch Roll mode damping fails to meet these requirements.

At the design turbulence level $\sigma_{v_g} = 2.65$ m/sec (8.45 ft/sec), $\sigma_{a_y} = 0.0312$ g. As in the longitudinal case, the transverse acceleration power spectral density was integrated over the frequency range $0.01 \leq \omega \leq 100.0$ rad/sec (Figure 33).

3.5.2 Lateral Ride Smoothing System

Compared to the longitudinal case, mechanization of a lateral ride smoothing system is considerably easier. The essential feedback is transverse acceleration. The obvious control surface is a pure transverse force control; i.e., the outer loop becomes lateral acceleration to side-force generator deflection $a_y \rightarrow \delta_{sfg}$. A number of inner loop closures are possible, but since the aircraft exhibits insufficient Dutch Roll damping, a yaw damper ($r \rightarrow \delta_r$) is the conventional solution. Also customary is the inclusion of a washout circuit in the $r \rightarrow \delta_r$ feedback path so that pilot commands to the rudder are not suppressed.

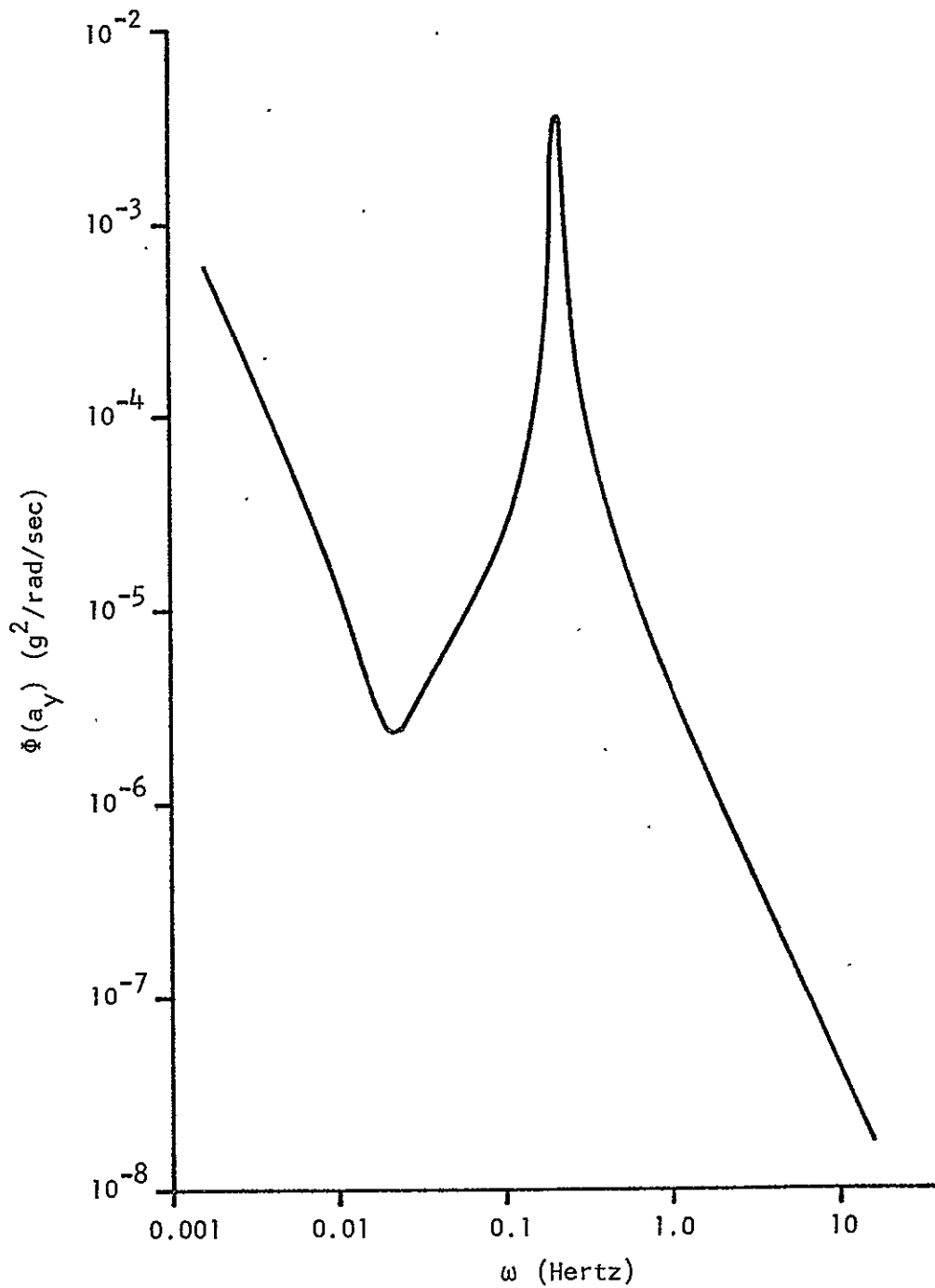


FIGURE 33. POWER SPECTRA OF a_y DUE TO TURBULENCE FOR BASIC JETSTAR

The resulting system is depicted in block diagram form in Figure 34. Note that the washout time constant was chosen as $\tau_{w0} = 1$ sec. Increasing τ_{w0} tends to increase ζ_{dr} at the expense of τ_R without significantly altering system alleviation performance.

The locus of Dutch Roll roots is plotted as a function of K_{a_y} and K_R in Figure 35. Note that the $a_y \rightarrow \delta_{sfg}$ feedback has almost no effect on either $\omega_{n_{dr}}$ or ζ_{dr} , whereas $r \rightarrow \delta_r$ increases ζ_{dr} while slightly lowering $\omega_{n_{dr}}$. The effect of the two feedbacks on the roll subsidence and spiral modes is summarized in Table V.

The effectiveness of the Lateral Ride Smoothing System in terms of reduction of root-mean-square lateral acceleration (σ_{a_y}), yaw rate (σ_r), and roll rate (σ_p) is presented graphically as a function of feedback gains K_{a_y} and K_r in Figures 36 through 38. Root-mean-square side-force generator activity is similarly presented in Figure 39. The limit on permissible side-force generator activity, determined by linearity considerations, is $\sigma_{\delta_{sfg}} \leq 9^\circ$. A system performance surface, with the limits $\sigma_{\delta_{sfg}} = 9^\circ$, $(\zeta\omega_n)_{dr} = 0.16$ superimposed, is presented as Figure 40. As in the case of the Longitudinal RSS, this surface allows the designer to choose feedback gains that satisfy all design criteria.

For this study, the selected design point was for $K_{a_y} = -3.3$ rad/m/sec² (1.0 rad/ft/sec²), $K_r = 1$ rad/rad/sec. The aircraft dynamics and system performance parameters for this choice of feedback gains are summarized in Table VI.

A comparison of the power spectral density of lateral acceleration in response to turbulence with the RSS on and off is shown in Figure 41. Alleviation is provided over the entire range of

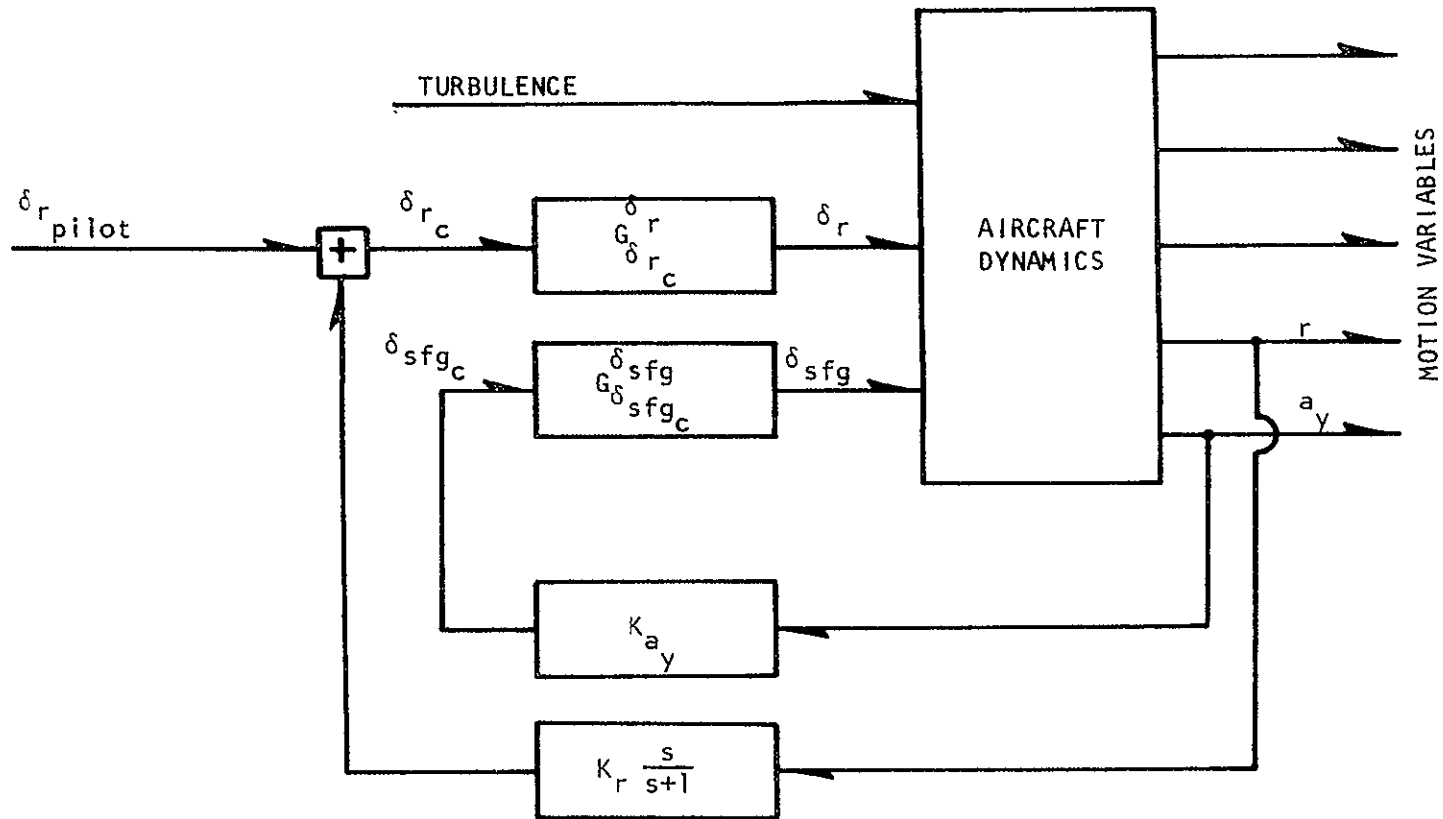


FIGURE 34. LATERAL RIDE SMOOTHING SYSTEM
 (Design Point: $K_{a_y} = -3.3 \text{ rad/m/sec}^2$, $K_r = 1 \text{ }^\circ/\text{ }^\circ/\text{sec}$)

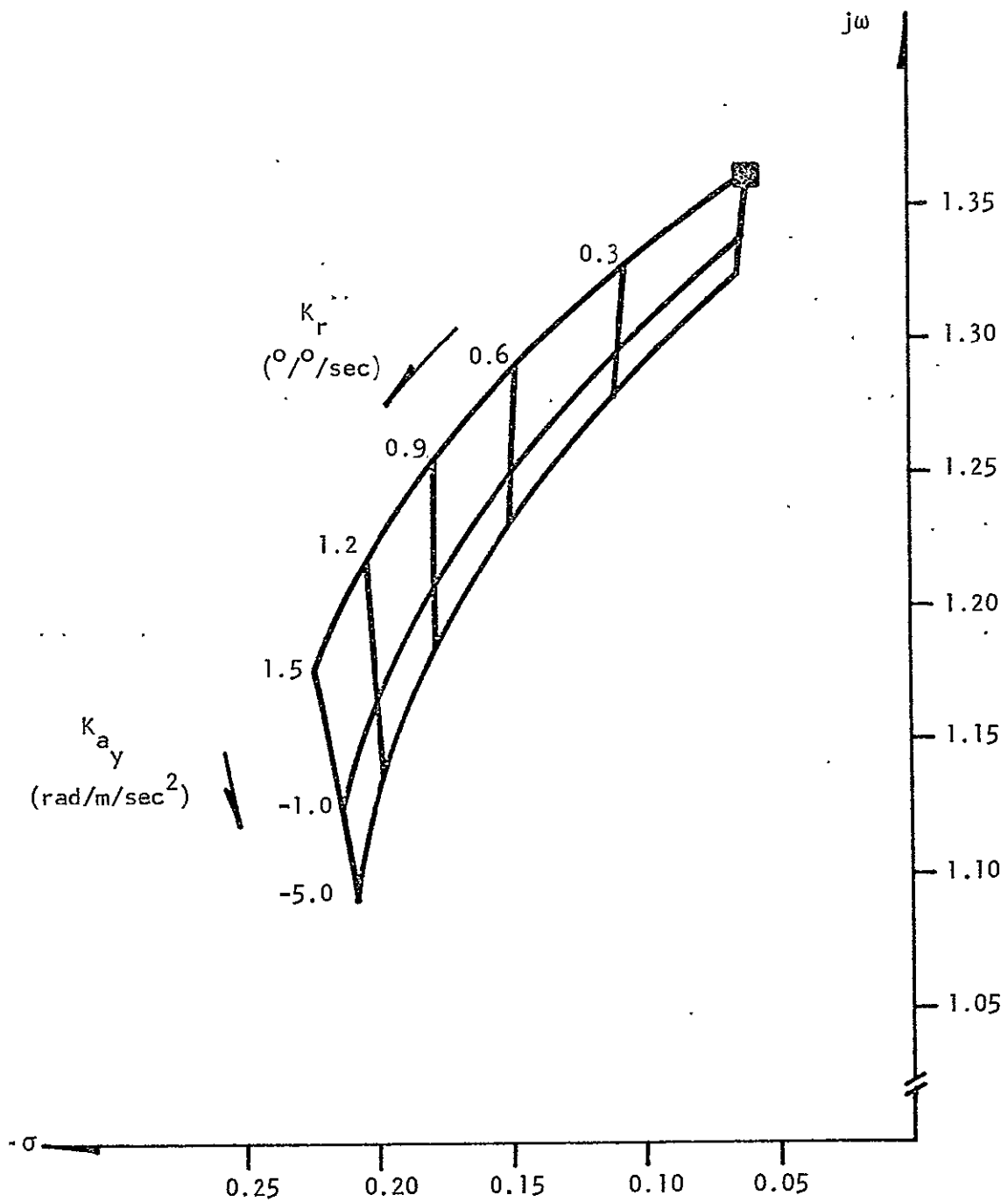


FIGURE 35. DUTCH ROLL ROOT LOCUS FOR LATERAL RSS

TABLE V

EFFECT OF FEEDBACKS ON ROLL SUBSIDENCE
AND SPIRAL MODES

$K_r \backslash K_y$	0	Fixed >0	Variable >0
0			+
Fixed >0			+
Variable >0	-	+	

$K_r \backslash K_y$	0	Fixed >0	Variable >0
0			-
Fixed >0			+
Variable >0	-	-	

where + → stabilizing effect

- → destabilizing effect

blank → no effect

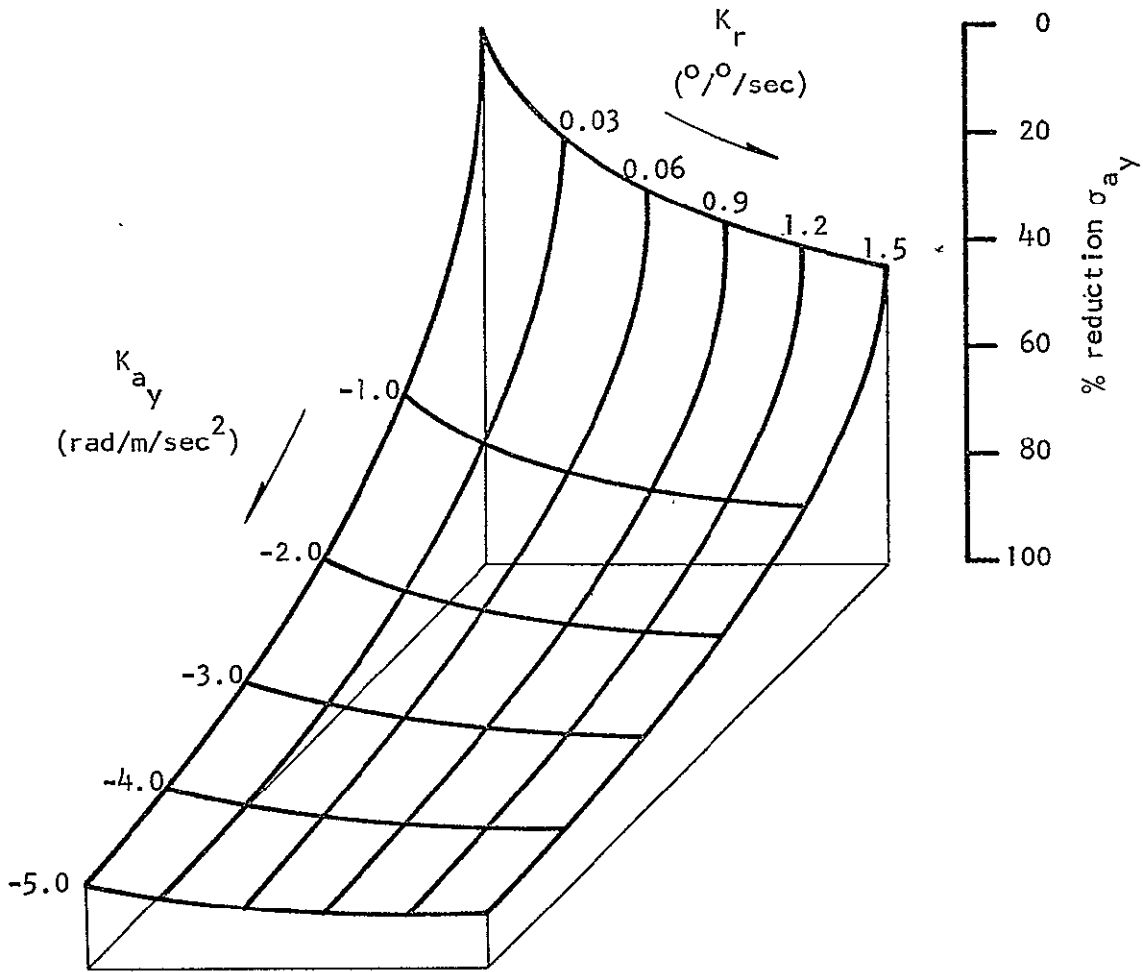


FIGURE 36. PERFORMANCE OF LATERAL RSS;
 σ_{a_y} AS A FUNCTION OF K_{a_y} AND K_r

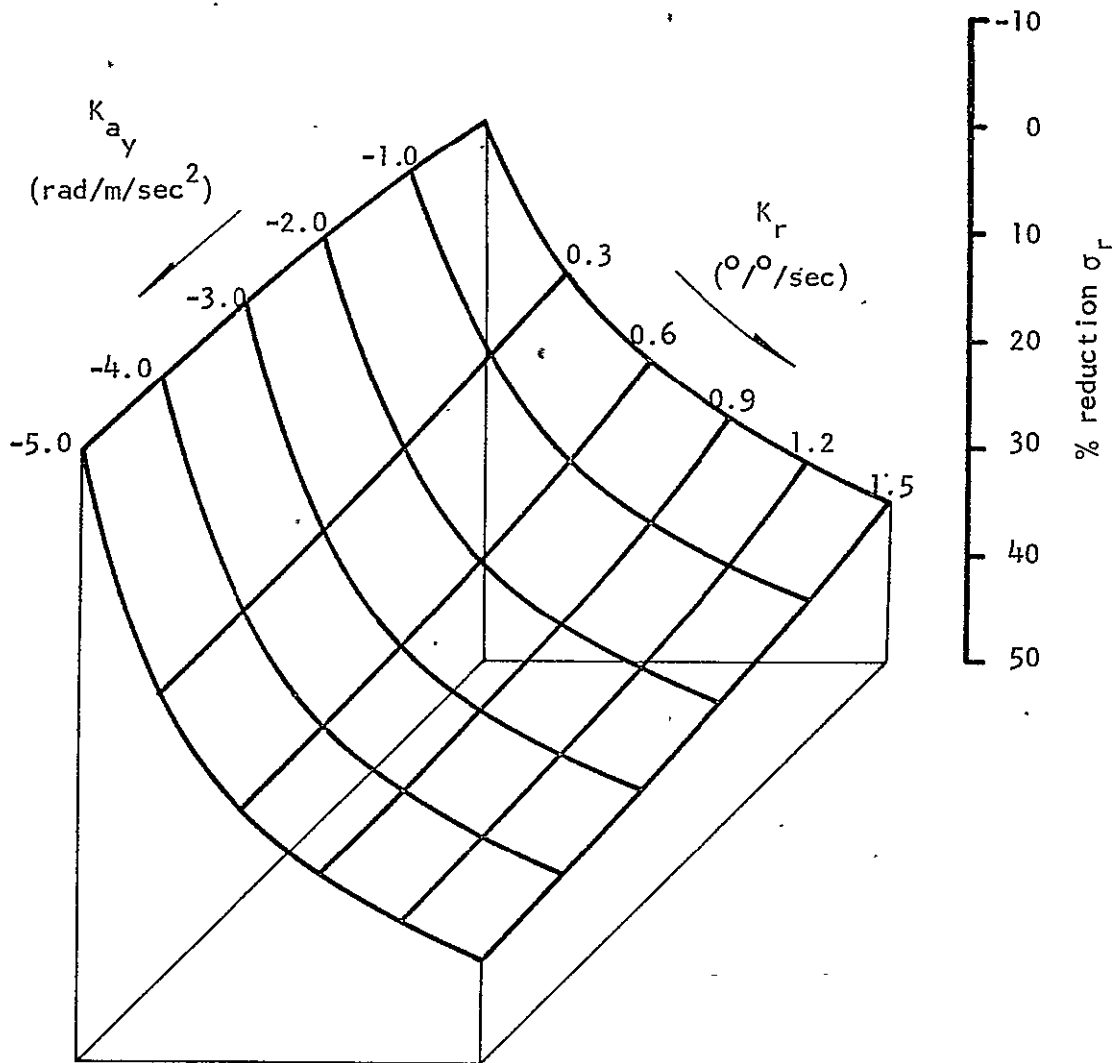


FIGURE 37. PERFORMANCE OF LATERAL RSS;
 σ_r AS A FUNCTION OF K_{a_v} AND K_r

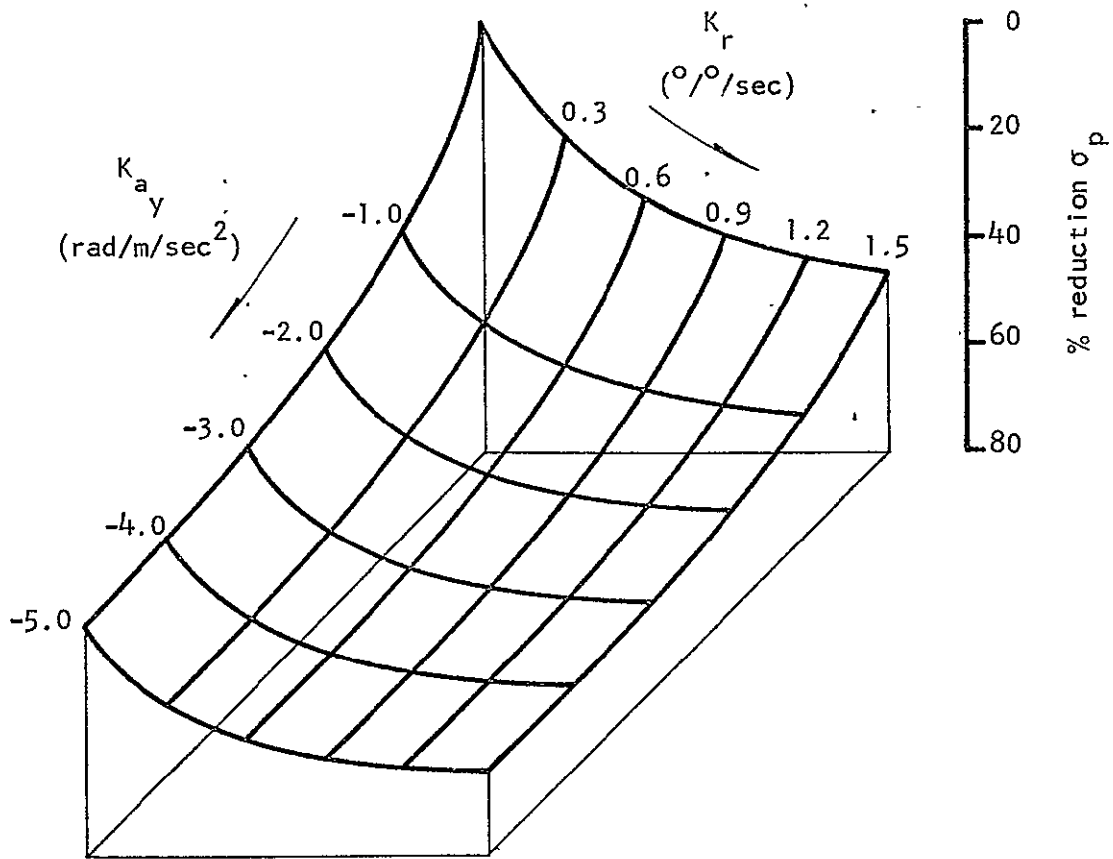


FIGURE 38. PERFORMANCE OF LATERAL RSS;
 σ_p AS A FUNCTION OF K_{a_y} AND K_r

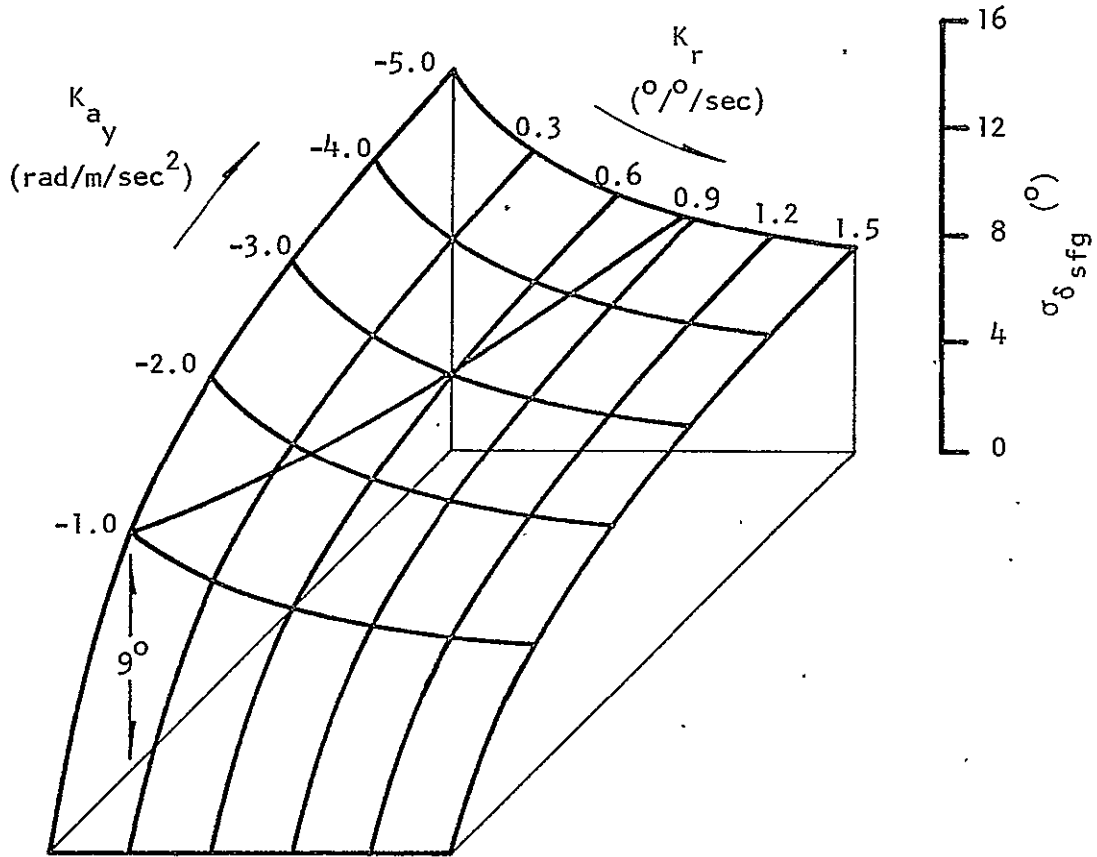


FIGURE 39. PERFORMANCE OF LATERAL RSS;
 $\sigma_{\delta \text{ sfg}}$ AS A FUNCTION OF K_{a_y} AND K_r

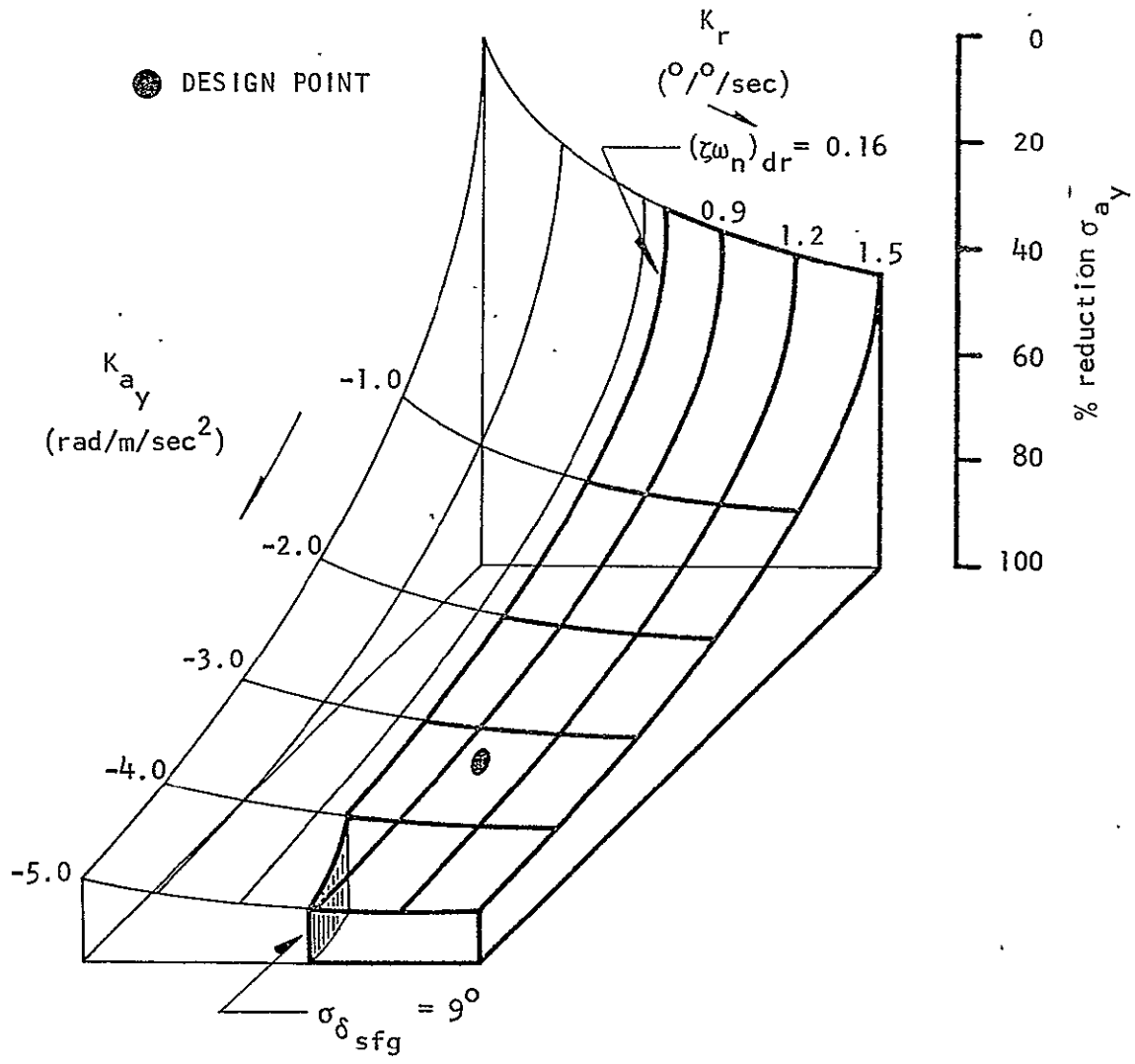


FIGURE 40. PERFORMANCE OF LATERAL RSS; σ_{a_y} AS A CONSTRAINED FUNCTION OF K_{a_y} AND K_r

TABLE VI

CHARACTERISTICS OF LATERAL RIDE SMOOTHING SYSTEM

	<u>Basic JetStar</u>	<u>Lateral RSS</u>
ζ_{dr}	0.045	0.155
$\omega_{n_{dr}}$	1.36 rad/sec	1.195 rad/sec
τ_R	0.87 sec	0.61 sec
$T_{\frac{1}{2}R}$	0.61 sec	0.42 sec
$T_{\frac{1}{2}S} (T_2)_S$	418 sec	(37.5) sec
σ_{a_y}	0.0312 g	0.0047 g
σ_r	2.35 °/sec	1.56 °/sec
σ_p	5.01 °/sec	1.95 °/sec
$\sigma_{\delta_{sfg}}$	--	7.8 °
σ_{δ_r}	--	0.92 °
% reduction σ_{a_y}	--	84.5%
% reduction σ_r	--	43.5%
% reduction σ_p	--	61.0%

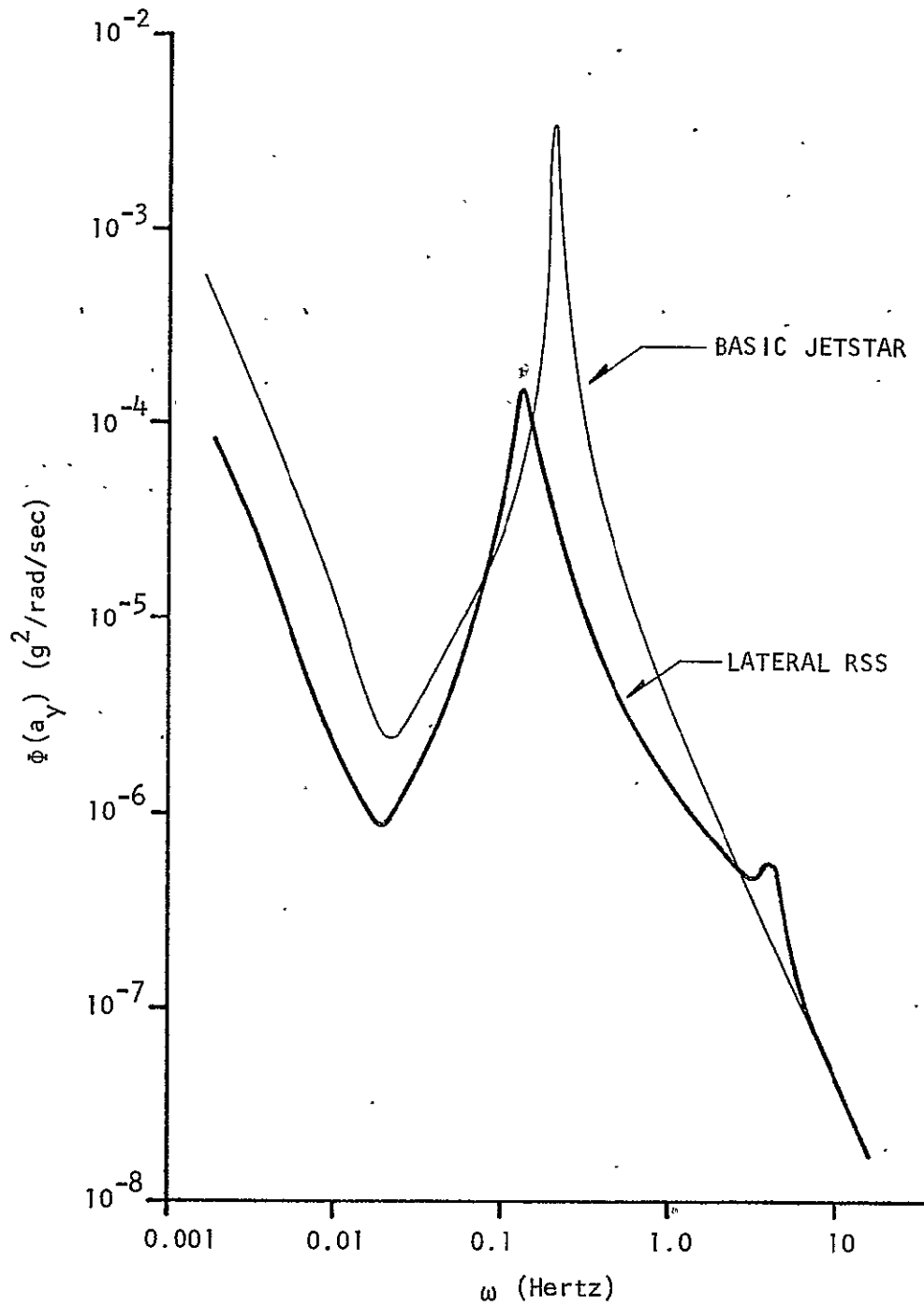


FIGURE 41. COMPARISON OF a_y POWER SPECTRA FOR BASIC AND LATERAL RSS AUGMENTED JETSTAR

frequencies of interest with the exception of a small resonance peak at the side-force generator damped natural frequency.

No investigation of the effect of additional equalization in the feedback loops was undertaken since the system appears highly effective as mechanized. The greatest potential problem with the system was expected to be achievement of the very high gain required in the lateral acceleration feedback loop. If the lateral accelerometer is mounted on a structural member that can be excited by the action of the side force generators, the control system may become unstable. In such an event, extensive equalization or a change in sensor mounting location would be required.

Finally, it should be noted that the degree of acceleration alleviation obtainable at the aircraft center of gravity by use of the rudder alone (yaw damper) is considerably less than when a side-force generator is employed (see Figure 36).

3.5.3 Analytic Model of Lateral Ride Smoothing System

In order to gain some insight into the effect of lateral stability derivatives on the performance of the RSS, a simplified mode comparable to the one developed for the longitudinal case was sought.

The following assumptions were made:

1. Effects of r_g and p_g on a_y are small as compared to the effect of β_g ;
2. The dynamics of the aircraft can be approximated by setting the spiral mode root equal to zero;
3. All actuators are perfect;
4. The washout time constant $\tau_{w0} \rightarrow 0$;

5. The transfer function of β_g due to turbulence (Λ) can be approximated by a first-order filter $1/s$.

If only the highest order terms (based on JetStar data) are retained, the transfer function of a_y due to Λ can be written as:

$$G_{\Lambda}^{a_y} \approx K_{ST}^1 \left\{ \frac{s^2(s^2 - L_p^1 s)}{s^2(s + R)(s^2 + 2\zeta_{dr}\omega_{n_{dr}}s + \omega_{n_{dr}}^2)} \right\}, \quad (3.5.1)$$

where the static gain K_{ST}^1 is defined as:

$$K_{ST}^1 \equiv \frac{V_{T_0} Y_v}{(1 + K_{a_y} \frac{V_{T_0} Y_{\delta_r}^*}{sfg})}, \quad (3.5.2)$$

and

$$R \equiv 1/\tau_R. \quad (3.5.3)$$

From Table V (page 74), it is clear that the value of the roll subsidence root (R) is a complex function of the gains K_{a_y} and K_r . The same is true of the Dutch Roll mode damping. In fact, both modes are, as was pointed out above, also sensitive to the choice of the washout filter time constant, τ_{w_0} . The following expressions were derived for the Lateral Ride Smoothing System with $\tau_{w_0} = 1$.

$$\omega_{n_{dr}}^2 \approx L_p^1 N_r^1 - N_p^1 L_r^1 + \cos \theta_0 N_{\beta}^1 - \sin \theta_0 L_{\beta}^1 \quad (3.5.4)$$

$$2\zeta_{dr}\omega_{n_{dr}} \approx Y_v - K_r N_{\delta_r}^1 \cdot f \quad (3.5.5)$$

$$R \cong -L_p - N_r - K_r N_{\delta_r} (1 - f) + Y_v - \frac{Y_v - K_{a_y} K_r V_T N_{\delta_{sfg}}^* Y_{\delta_r}^*}{(1 + K_{a_y} V_T Y_{\delta_{sfg}}^*)} \quad (3.5.6)$$

where f was empirically chosen to be 0.375. The factor f is numerically equivalent to the ratio of the numerators of the transfer functions G_{Λ}^r and G_{Λ}^p at the steady state ($s = 0$). Inclusion of this factor, then, essentially prorates the yaw damper effectiveness between the roll subsidence and Dutch Roll modes. The expressions for $\omega_{n_{dr}}^2$, $2\zeta_{dr}\omega_{n_{dr}}$, and R are accurate to within 22% over the range of interest.

Evaluation of the integral

$$\sigma_{a_y}^2 = \int_0^{\infty} |G_{\Lambda}^a|^2 \Phi(\Lambda) d\omega \quad (3.5.7)$$

yields:

$$\sigma_{a_y}^2 \propto \frac{K_{ST}^2}{(R^2 + \omega_{n_{dr}}^2)^2 - 4R^2\sigma_{dr}^2} \left\{ R(R^2 - L_p^2) - \frac{1}{2\zeta_{dr}\omega_{n_{dr}}} \left[(\omega_{n_{dr}}^2 + R^2)(\omega_{n_{dr}}^2 - L_p^2) + R^2 2\omega_{n_{dr}}^2 (2\zeta_{dr}^2 - 1) \right] \right\} \quad (3.5.8)$$

A number of similarities between this expression and its analog for the longitudinal case (Equation 3.4.8) are apparent. The critical parameters affecting the acceleration alleviation capability of the Lateral RSS are the constants outside the brackets. System effectiveness can be increased by:

1. Increasing K_{a_y} or, alternatively, increasing the side-force generator effectiveness ($Y_{\delta_{sfg}}^*$);

2. Increasing the damping of the roll subsidence mode
($1/\tau_R$);

3. Increasing the frequency of the Dutch Roll mode ($\omega_{n_{dr}}$).
Increasing Dutch Roll damping (ζ_{dr}) without simultaneously increasing
the Dutch Roll natural frequency would appear to degrade system
performance. Terms inside the brackets have little effect on σ_{a_y} .

Figure 42 compares the RSS performance as calculated by
the simplified expression (Equation 3.5.8) to the digitally calculated
results. Agreement is seen to be excellent at fairly high levels of K_{a_y} .

As in the case of the Longitudinal Ride Smoothing Systems,
failure of the stabilizing feedback loop ($r \rightarrow \delta_r$) can be expected to
degrade the handling qualities of the aircraft. The degree to which
this was the case was left to be examined in the simulation phase.

3.5.4 Alternate Lateral Ride Smoothing System

Several authors cited in Chapter 1 (References 21 and 22)
proposed the use of rudder alone to provide lateral ride smoothing.
For purposes of comparison with the performance of the system developed
above, a calculation was carried out for such a mechanization adapted
to the JetStar (Figure 43).

The feedback gains were set at $K_{a_y} = -0.26 \text{ rad/m/sec}^2$ (0.08
 rad/ft/sec^2) and $K_r = 4.0 \text{ rad/rad/sec}$ so as to yield Dutch Roll dynamics
approximately comparable to those with the baseline Lateral RSS. Note
that the $r \rightarrow \delta_r$ feedback signal is filtered by some washout ($\tau_{w0} = 1 \text{ sec}$).
A comparison of the performance of the two systems is given in Table VII.

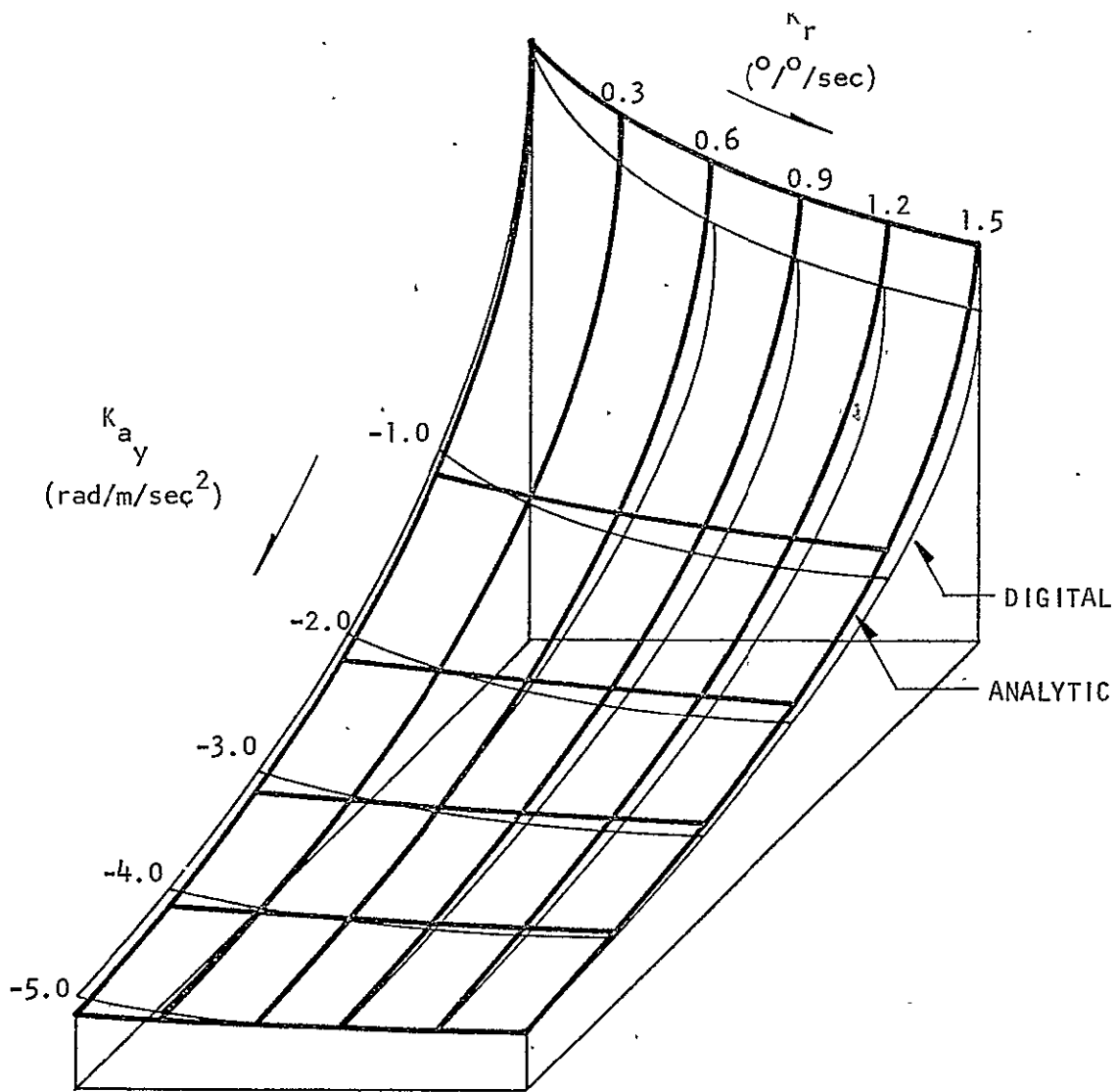


FIGURE 42. COMPARISON OF DIGITALLY CALCULATED σ_{ay} WITH ANALYTIC EXPRESSION

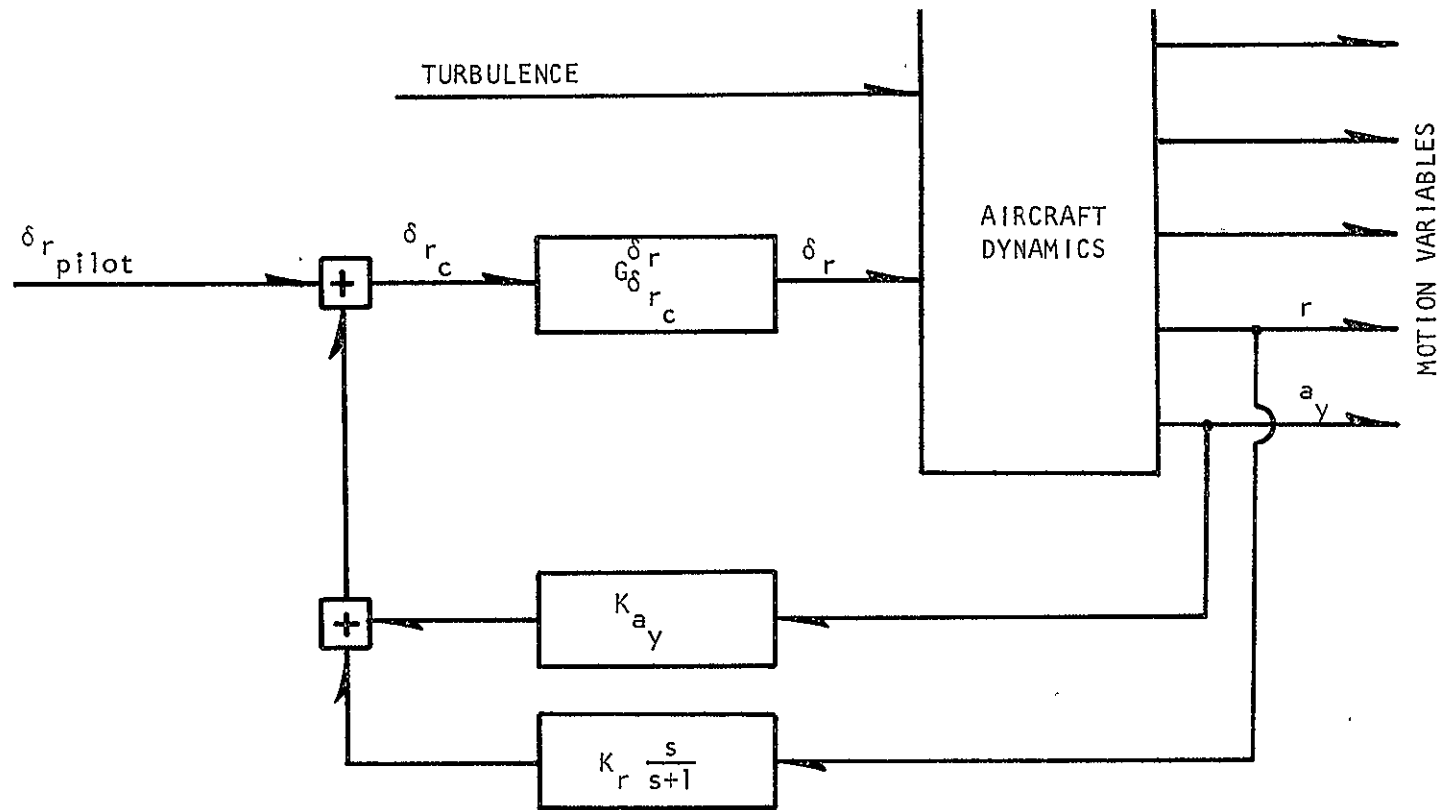


FIGURE 43. ALTERNATE LATERAL RIDE SMOOTHING SYSTEM
 (Design Point: $K_{a_y} = -0.26 \text{ rad/m/sec}^2$, $K_r = 4 \text{ }^\circ/\text{/sec}$)

TABLE VII

COMPARISON OF LATERAL RIDE SMOOTHING SYSTEMS

	<u>Basic JetStar</u>	<u>Baseline RSS</u>	<u>Rudder RSS</u>
ζ_{dr}	0.045	0.155	0.131
$\omega_{n_{dr}}$	1.36 rad/sec	1.195 rad/sec	0.86 rad/sec
τ_R	0.87 sec	0.61 sec	0.44 sec
$T_{\frac{1}{2}s} (T_{2s})$	418 sec	(37.5) sec	23.0 sec
σ_{a_y}	0.0312 g	0.0047 g	0.0145 g
σ_r	2.35 °/sec	1.56 °/sec	0.68 °/sec
σ_p	5.01 °/sec	1.95 °/sec	3.98 °/sec
$\sigma_{\delta_{sfg}}$	--	7.8 °	--
σ_{δ_r}	--	0.92 °	3.12 °
% reduction σ_{a_y}	--	84.5%	53.4%
% reduction σ_r	--	43.5%	71.1%
% reduction σ_p	--	61.0%	20.6%

Although substantial acceleration alleviation can be obtained with the single control surface Lateral RSS, several practical considerations would make it difficult to mechanize the system aboard the JetStar. First, operation at the design feedback gain levels places severe demands on the rudder servo-actuator. The servo in the aircraft would be operating at a damping ratio $\zeta_{\delta_r} = 0.17$ ($\zeta_{\delta_r} = 0.24$ for the baseline Lateral RSS). Secondly, failure of the yaw damper ($r \rightarrow \delta_r$ feedback loop) would result in a marginally stable Dutch Roll oscillation. Any attempt to improve the acceleration alleviation capability of the system by increasing the K_{a_y} feedback gain, would, under the failure condition, drive ζ_{dr} negative. These reasons alone were sufficient to reject the single control Lateral RSS in favor of the baseline mechanization.

3.6 Overall Effectiveness of Combined Axis Ride Smoothing System

The prototype Longitudinal and Lateral Ride Smoothing Systems synthesized in the preceding sections meet, with the possible exception of failure mode and structural resonance (feasibility) criteria, all the conditions for a successful design as set forth in Chapter II. The command signals that are required are readily available from typical aircraft instruments. The equalization circuits are all easily mechanized on an analog computer. Minimal handling qualities specifications are satisfied.

But what of the passenger and his comfort? For locations at or near the center of gravity, under the design turbulence conditions, the comfort model (Equation 2.3.1) predicts:

1. For the basic JetStar: $C \cong 3.6$;
2. For Longitudinal RSS I and Lateral RSS: $C \cong 2.7$;
3. For Longitudinal RSS II and Lateral RSS: $C \cong 2.8$;

or approximately a 1-point increase in the comfort rating with the RSS operating. More important, the overall level of passenger satisfaction can be expected to increase from 63.5% to ~85% (Figure 3). In the case of the model aircraft, the Jetstar, only the relatively small size of direct-lift flaps prevent an even more substantial improvement in ride quality.

CHAPTER IV

SIMULATION EXPERIMENTS

4.1 Order of Presentation

This section of the report deals with the ground-based simulation of the dynamics and evaluation of handling qualities of the basic and RSS augmented JetStar. A brief description of the experimental facility, simulation mechanization, and operational verification is presented. A summary of the evaluation pilot's experience is followed by a detailed description of the evaluation tasks. Results of the handling qualities evaluations in smooth air are presented in terms of subjective pilot opinion. Both subjective and objective measures of handling qualities are presented for evaluations conducted in simulated turbulence.

4.2 The Simulator Facility

The ground facility used in this study was the NASA Flight Research Center fixed-based, six-degree-of-freedom, hybrid computer controlled transport aircraft simulator. The aircraft equations of motion were mechanized on a Xerox Model 9300 digital computer and the Ride Smoothing Systems were programmed on an Electronics Associates, Inc. Model 231 R-V analog computer.

The simulation cockpit, shown in Figure 44, contained the following instruments (from left to right):

Top row: Sideslip (β) meter,
 Angle of attack (α) meter,

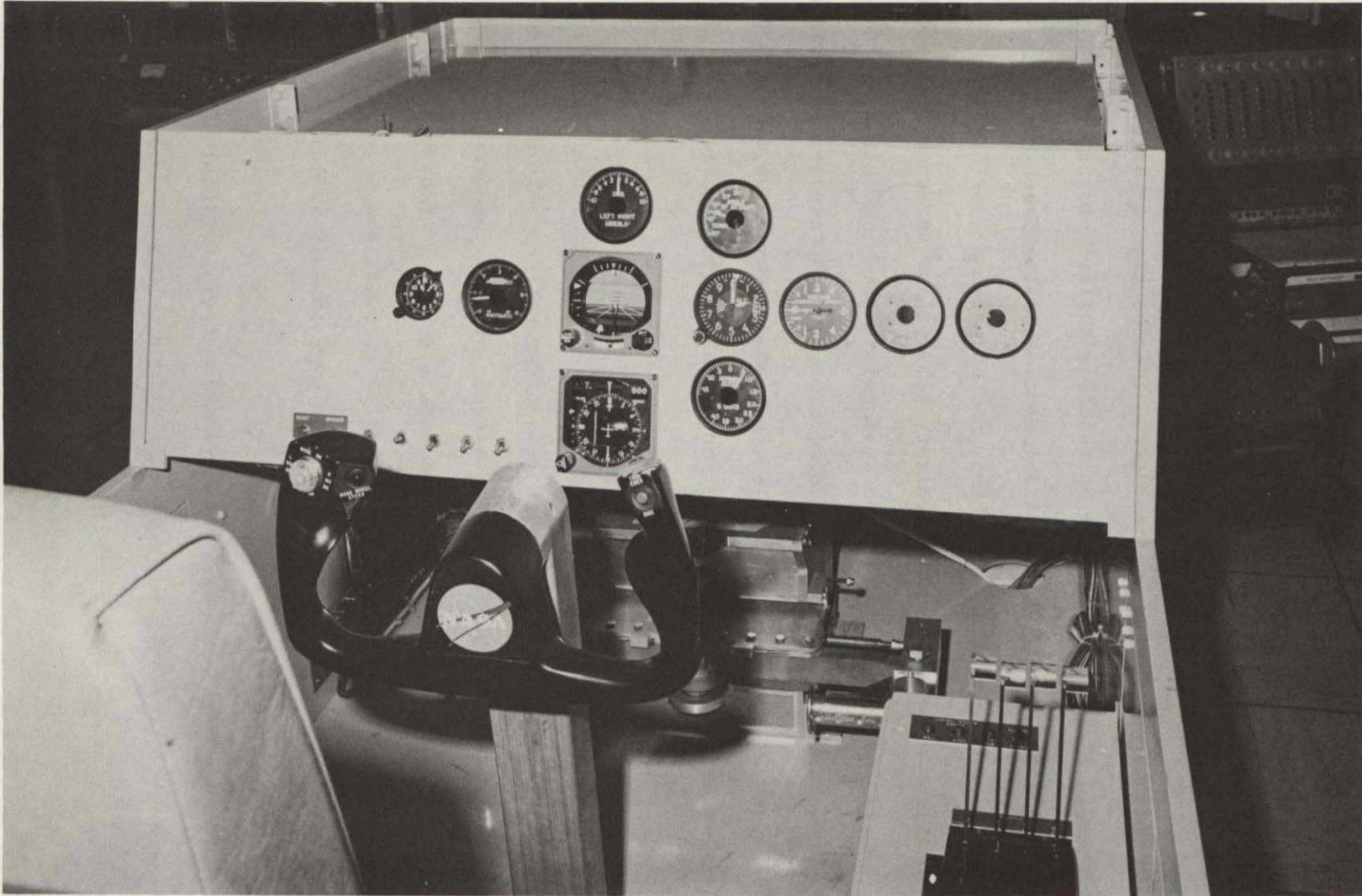


FIGURE 44. SIMULATION COCKPIT

Second row: Clock,
Airspeed indicator,
Flight director (Collins FD-108G)
Altimeter,
Instantaneous vertical speed indicator,
Two engine power level meters,
Bottom row: Horizontal situation indicator (Collins 331-6A)
Normal acceleration meter.

This instrument panel mockup is almost identical to that provided the command pilot in the GPAS (Figure 45).

Both the yoke and the rudder pedals were provided with a feel system that permitted adjustment of apparent linear control force, breakout force, friction, and damping (41). A four-way trim button on the yoke allowed adjustment of pitch and roll trim. Rudder trim was controlled by a console-mounted switch. Although four throttle levers were mechanized, an asymmetric thrust condition could not be simulated. Selected cockpit control characteristics, gains, and trim rates were chosen by one of the pilots to be representative of the JetStar.

4.3 Digital Computer Program

The real-time digital computer program was based on the six-degree-of-freedom routine (SIM II) of Myers and Evans (42). This program solved the aircraft equations of motion (including the control surface actuator dynamics) as well as generating the turbulence quantities α_g , β_g , and p_g in real time. The cockpit display signals were calculated digitally with a repetition rate of 25 calculations per second.



FIGURE 45. GPAS TEST PILOT'S INSTRUMENTATION

The basic program was modified to calculate statistical properties of 20 channels of data and to store the sampled time history of any one variable of interest. The variables consisted of angular rigid body rates (p, q, r) inertial orientation angles (ϕ, θ, ψ), aerodynamic angles (α, β), total velocity (V), control surface deflections ($\delta_a, \delta_e, \delta_r, \delta_f, \delta_{sfg}$), power setting, vertical and lateral acceleration (a_z, a_y) and turbulence intensity (α_g, β_g, p_g). The mean, variance, probability distribution, and probability histogram of these quantities were calculated in real time. Power spectral density of the stored variable time history could be calculated following a simulation run.

4.4 Analog Circuits

The analog computer provided the interface between the digitally-computed motion quantities and cockpit displays. Cockpit control commands were summed with signals generated by the simulated Ride Smoothing Systems before being transmitted to the digital computer. Schematics of the Ride Smoothing System analog mechanization are given in Figure 46 through 48.

In addition to digital data, 16 channels of analog data could be recorded. Variables monitored varied with the simulation task assigned the pilots, but were generally chosen to provide a check on systems during a run. During simulation of an Instrument Landing System (ILS) approach task, glideslope and localizer tracking were monitored on dual X-Y plotters. The analog computer and recorders are shown in Figure 49.

4.5 Hybrid Simulation Verification

Qualitative verification of the accuracy of the hybrid simulation

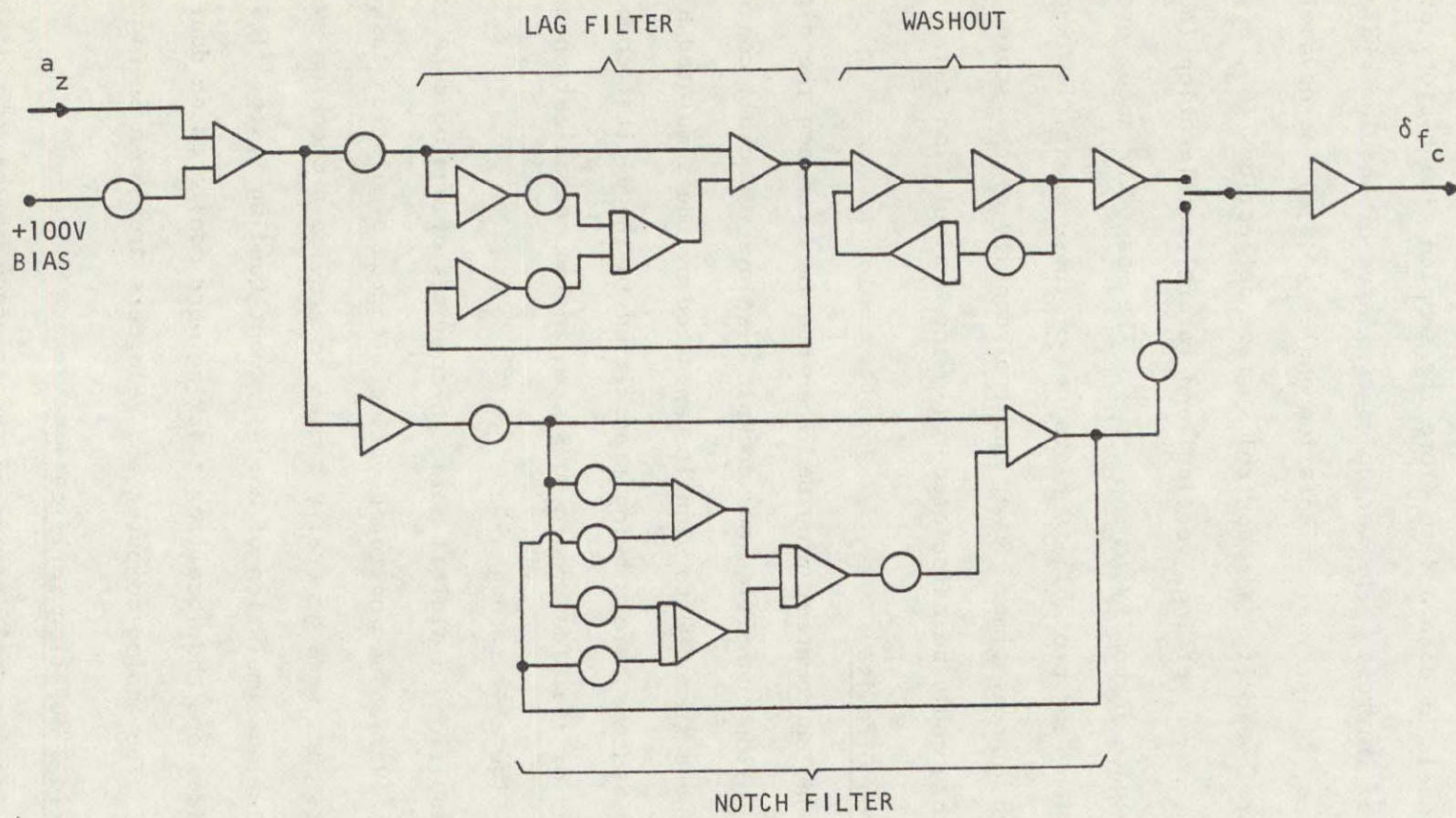


FIGURE 46. ANALOG EQUALIZATION CIRCUIT DIAGRAM;
 $a_z \rightarrow \delta_f$ FEEDBACK LOOP

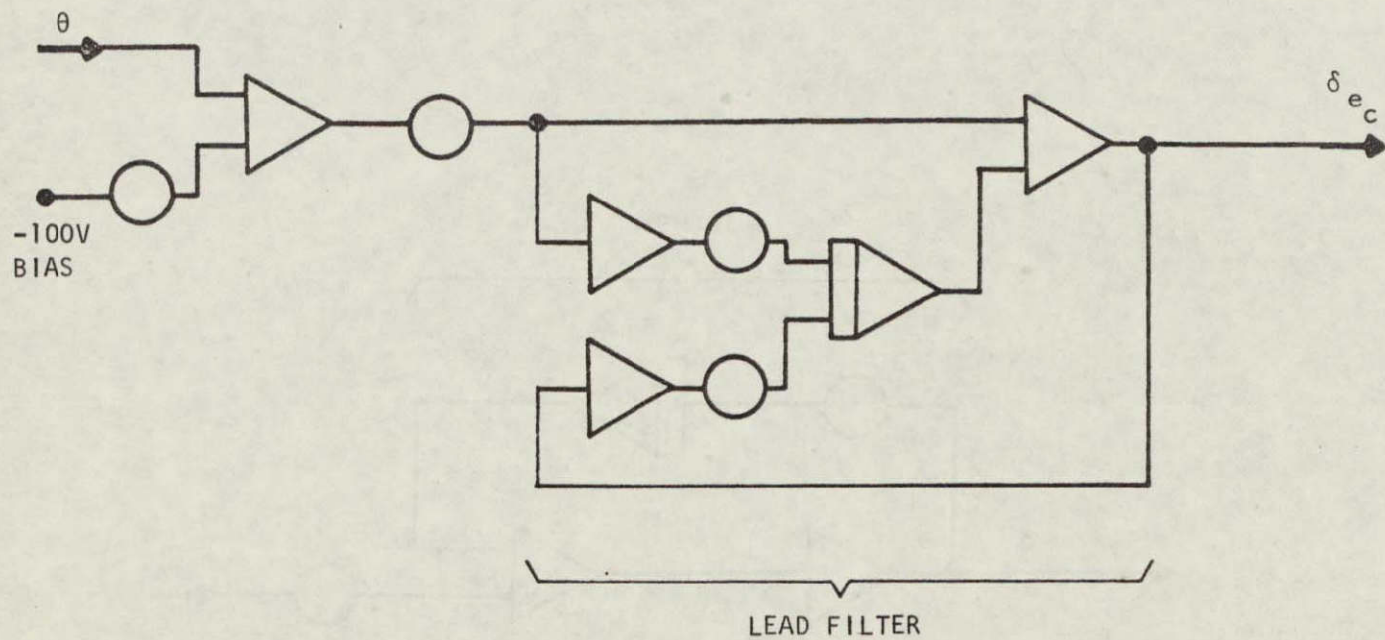


FIGURE 47. ANALOG EQUALIZATION CIRCUIT DIAGRAM;
 $\theta \rightarrow \delta_e$ FEEDBACK LOOP

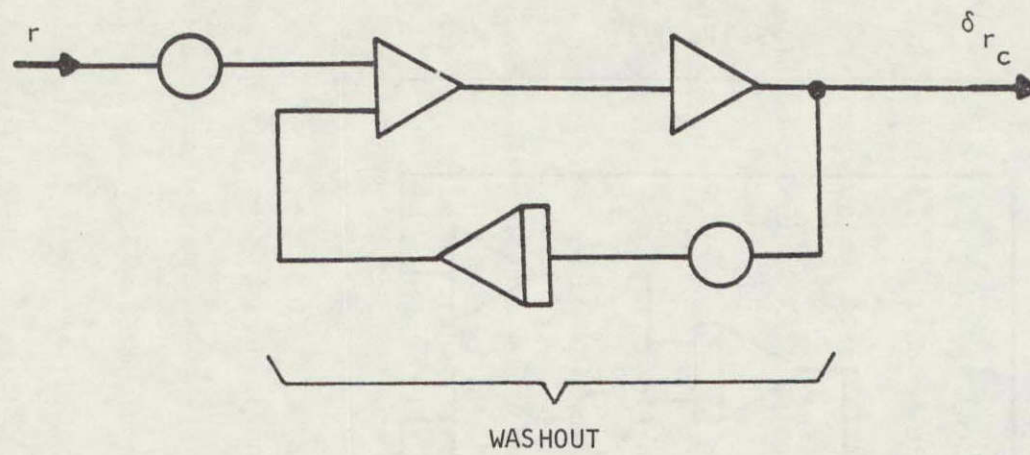


FIGURE 48. ANALOG EQUALIZATION CIRCUIT DIAGRAM;
 $r \rightarrow \delta r_c$ FEEDBACK LOOP

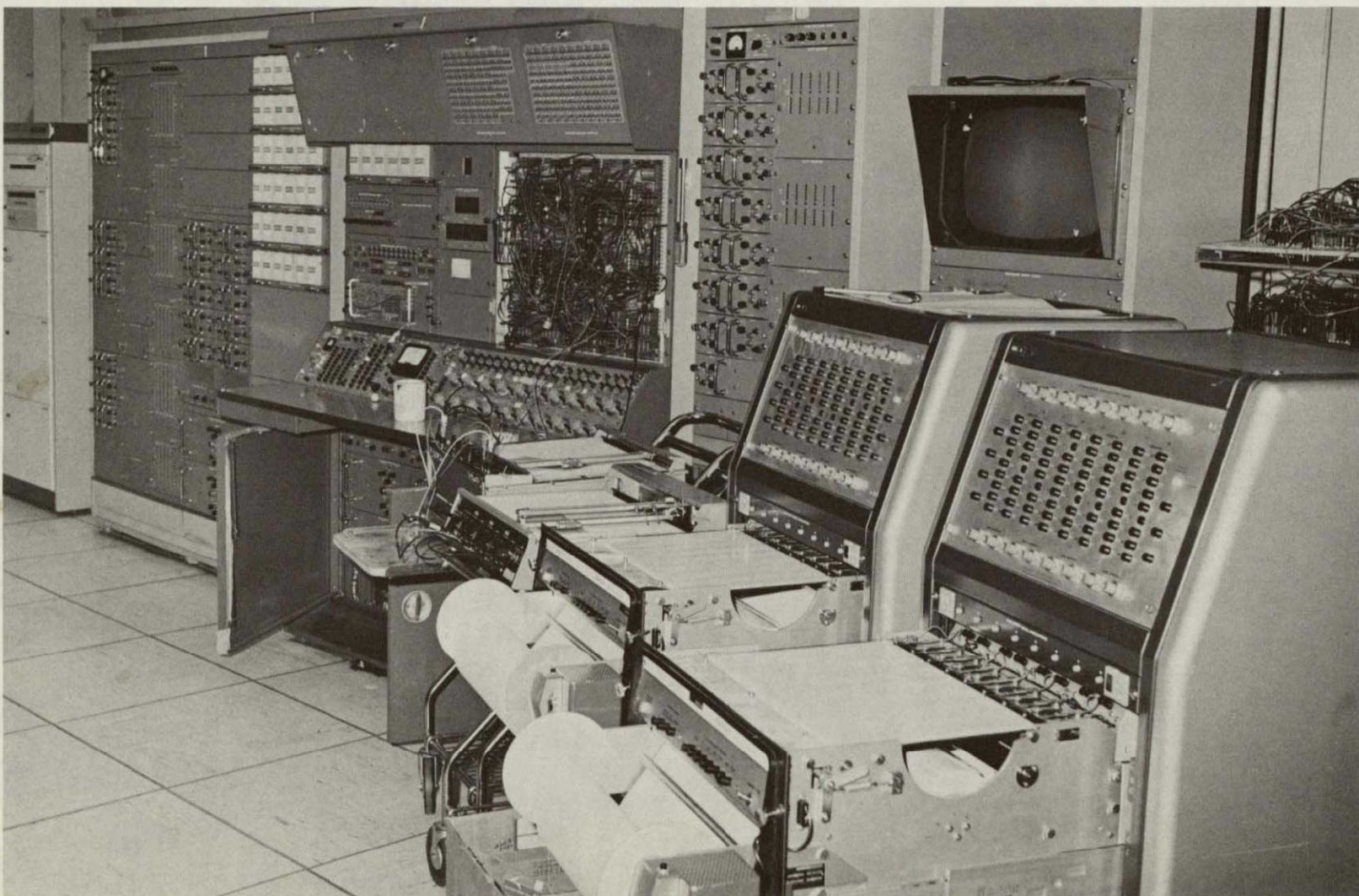


FIGURE 49. SIMULATION LABORATORY

of JetStar dynamics was performed by applying inputs to the control surfaces and observing the time history of aircraft response. Frequency and damping of the longitudinal oscillatory modes compared favorably with calculated values. A 25% increase in the value of N_r' was required to approximately achieve the numerically-calculated frequency and damping of the Dutch Roll mode. Also, pilot A evaluated the simulation and reported the simulated aircraft dynamics to be generally representative of the JetStar in the approach configuration.

Power spectral densities were calculated for the turbulence fields α_g , β_g , and p_g . These spectra (Figure 50 through 52) are reasonable approximations to the Dryden spectra asymptotes shown.

Feedback loop filters (lead, lag, and notch) compared well in amplitude and phase characteristics over the frequency range of interest with digitally-calculated values. Washout circuits were verified by measuring the decay time for step inputs.

4.6 Simulation Evaluation Pilots

Five pilots participated in the simulation experiments. Pilots A, B, and C are professional research pilots with 9000, 6500, and 12,000 hours of flight time, respectively. Pilots A and B have logged considerable time in the JetStar. Pilot D has more than 10,500 hours of airline transport experience, and Pilot E is a military aviator with total experience of 3500 hours as well as approximately 100 hours in simulator handling-qualities evaluation time.

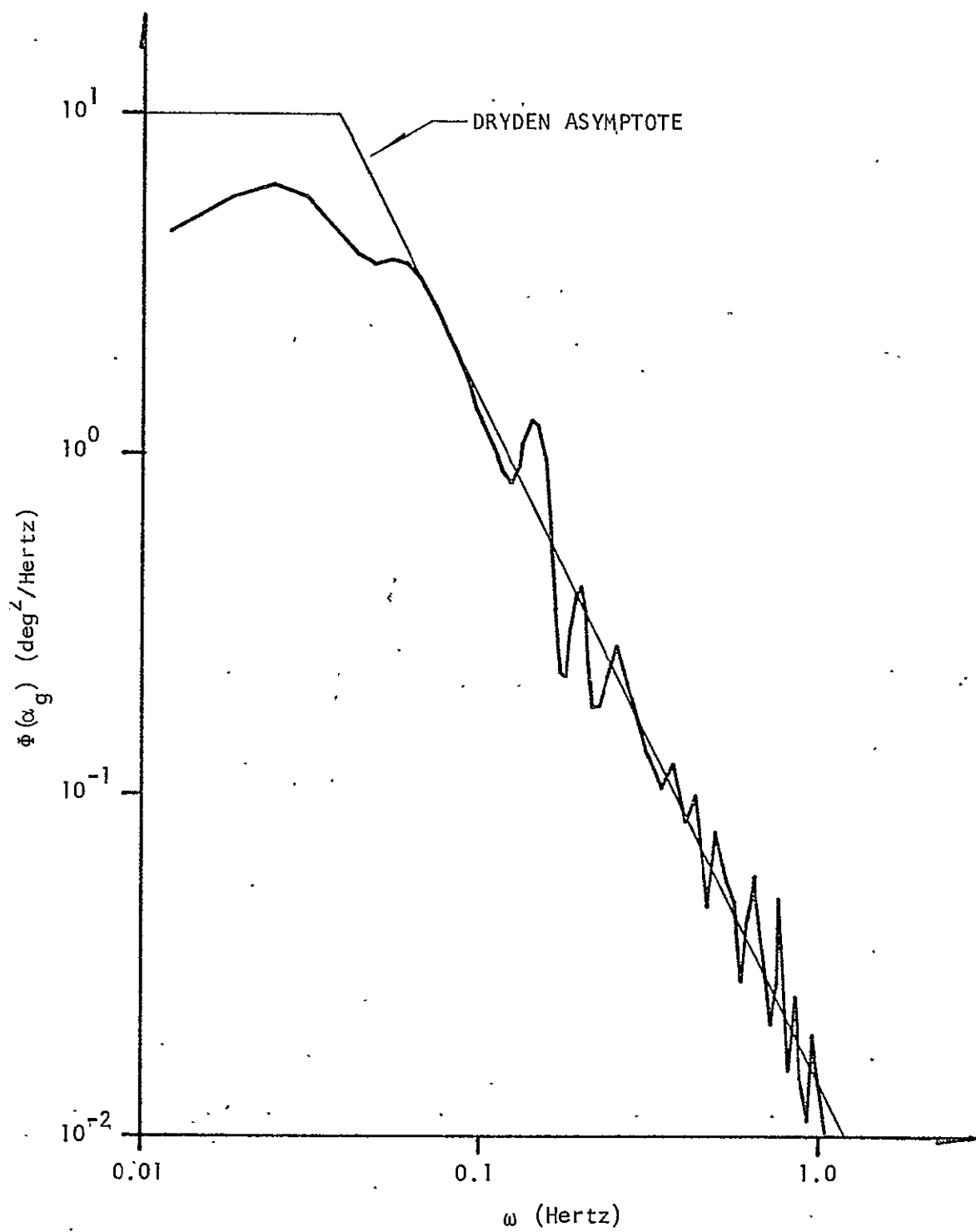


FIGURE 50. POWER SPECTRA OF SIMULATED α_g

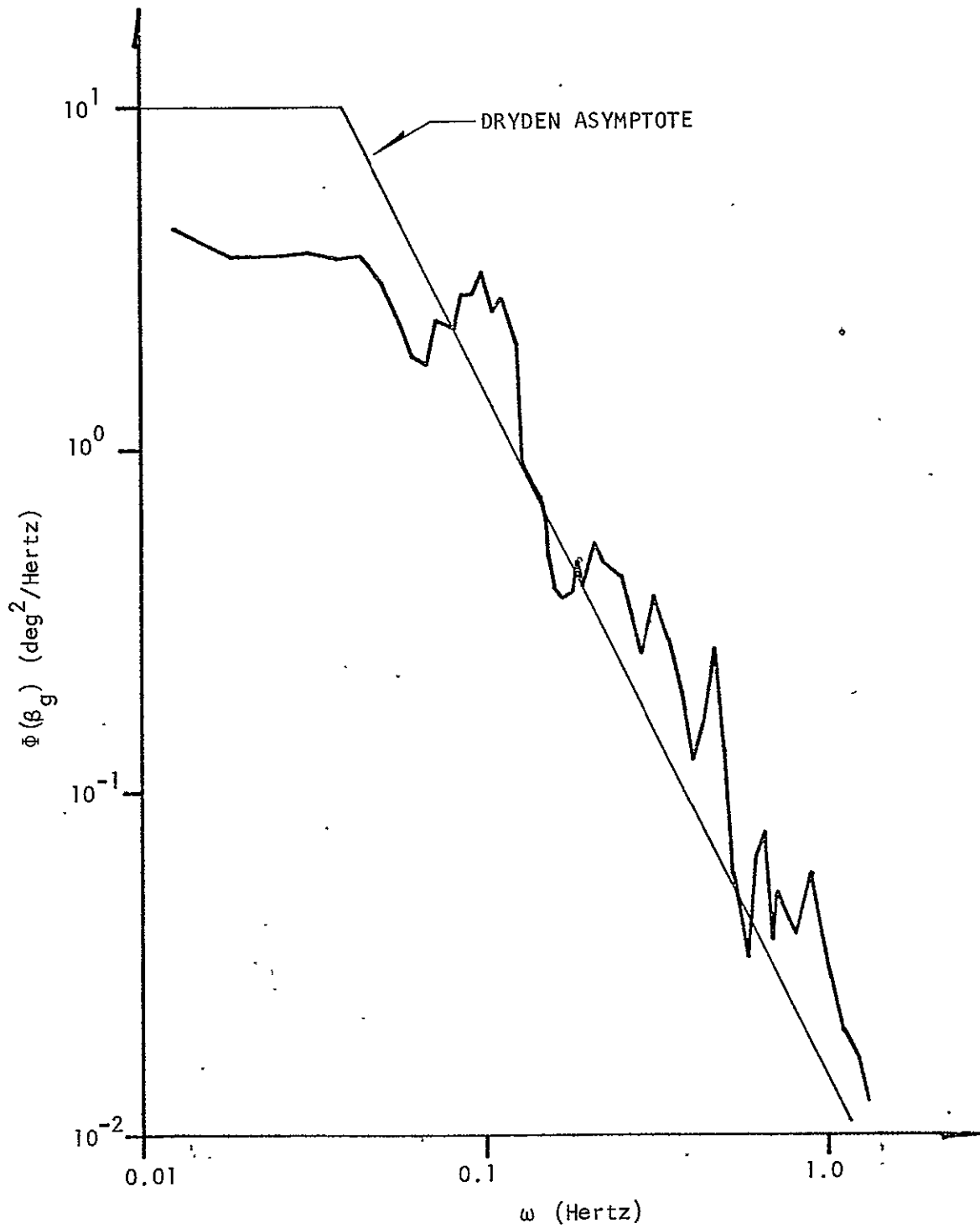


FIGURE 51. POWER SPECTRA OF SIMULATED β_g

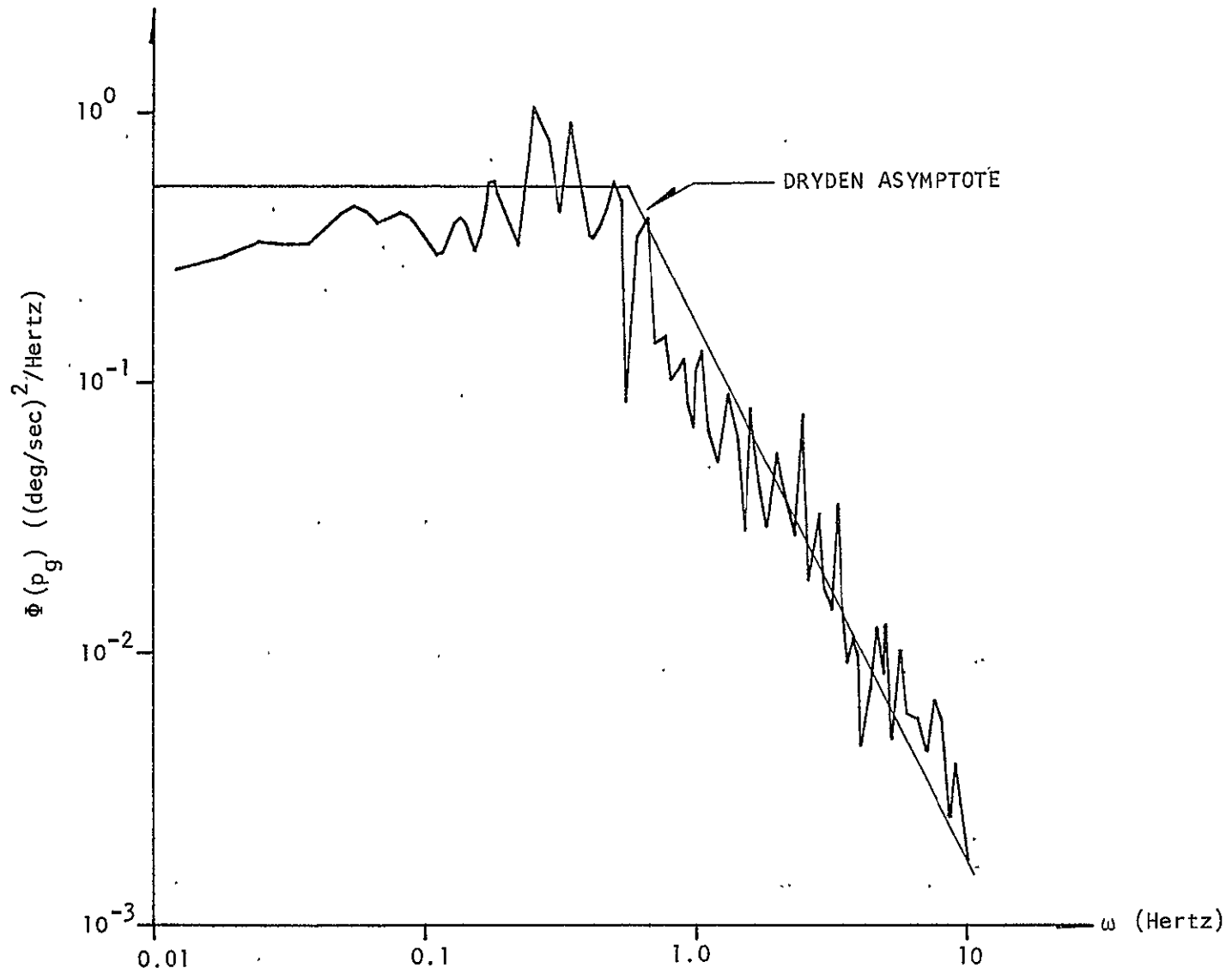


FIGURE 52. POWER SPECTRA OF SIMULATED n

4.7 Handling Qualities Evaluation

4.7.1 General Instructions

Four problems were flown by all five pilots in the handling-qualities evaluation of the basic and RSS augmented JetStar: a longitudinal axis task, lateral axis task, combined axes task, and an Instrument Landing System (ILS) approach task. General instructions to the pilot were as follows: "The simulated aircraft is to be assumed a transport type and should be flown in a manner consistent with airline operational procedures, i.e., passenger comfort considerations are paramount. Load factor, bank angle, etc., are to be kept small; tight control, however, should be maintained." For all problems, the aircraft was in the landing approach configuration: gear down and flaps at the approach setting.

Initial conditions for all problems were:

Altitude	610 meters (2000 feet)
Indicated airspeed	260 kilometers/hr (140 knots)
Angle of attack	11 degrees
Displayed pitch attitude	7 degrees
Heading	0 degrees
Power setting for level flight	48%.

For the ILS task, the following additional information was provided:

Field elevation	0 meters (0 feet)
Runway heading	0 degrees
Runway length	3050 meters (10,000 feet)
Runway width	92 meters (300 feet)

Initial distance to threshold	15.2 kilometers (8.25 nautical miles)
Initial offset from runway centerline	0.61 kilometers (0.33 nautical miles)
Time to threshold	3:45 minutes
Glideslope	3 degrees
Required rate of sink	213 m/min (700 ft/min)
Required power setting	32%
Breakout altitude	61 meters (200 feet)

Pilots evaluated handling qualities on the basis of the Cooper-Harper Rating Scale (38) depicted in Table VIII.

4.7.2 Longitudinal Task

The longitudinal axis task, repeated five times, was a timed, smooth air problem defined as follows:

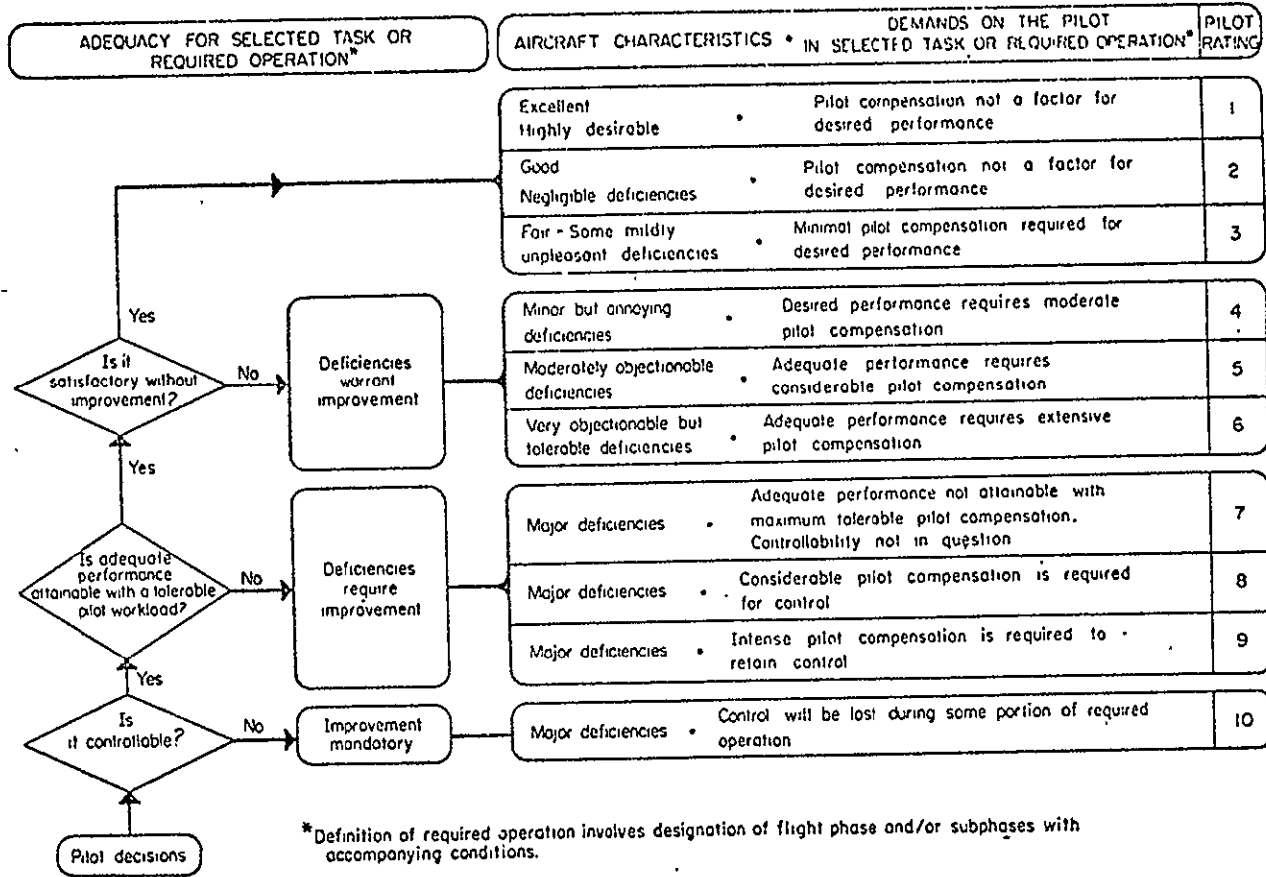
	<u>End Time</u>
1. Stabilize aircraft at initial conditions.	0:30
2. Climb to 3000 feet in 60 seconds.	1:30
3. Stabilize aircraft at 3000 feet and hold altitude for 30 seconds.	2:00
4. Descend to 2000 feet in 60 seconds.	3:00
5. Stabilize aircraft at 2000 feet.	3:30

Throughout the maneuver heading and airspeed were to be held constant. One run each was made for the basic JetStar, the two longitudinal RSSs engaged, and each longitudinal RSS with the stabilizing ($\theta \rightarrow \delta_e$) feedback loop open to simulate a system failure condition. Failure was initiated approximately 60 seconds after problem initiation. Pilots were not informed of the configuration they were flying. In addition to Cooper-Harper ratings, pilot comments were solicited on:

ORIGINAL PAGE IS
OF POOR QUALITY

TABLE VIII

COOPER-HARPER RATING SCALE



1. Ease of establishing trim conditions;
2. Ease of initiating desired climb and descent gradients;
3. Ease of maintaining airspeed; and
4. Presence of undesirable pitch or rate of climb/sink excursions.

A summary of pilot ratings for this task is presented in Table IX, below.

TABLE IX

AVERAGE COOPER-HARPER PILOT RATINGS, LONGITUDINAL TASK
(Smooth Air)

	<u>Case</u>	<u>Rating</u>	<u>Standard Deviation</u>
1	Basic JetStar	2.4	0.33
2	Longitudinal RSS I	2.5	0.45
3	Longitudinal RSS II	2.1	0.20
4	Longitudinal RSS I ($\theta \rightarrow \delta_e$ loop failed)	2.3	0.24
5	Longitudinal RSS II ($\theta \rightarrow \delta_e$ loop failed)	2.7	0.31

Generally, the pilots found no significant differences between the first three configurations and reported no problems in performing the assigned task. Surprisingly, Longitudinal RSS II, with a value of n/α , lower than that of the basic aircraft and RSS I configuration, was rated equally good. Since the configurations were not presented in the same order for each pilot, the "learning curve" phenomenon was not a factor in the average ratings. Although numerically the simulated failure conditions were not significantly penalized, all pilots

indicated that a higher work load had resulted due to slight pitch excursions. One pilot reported a tendency toward pilot-induced oscillations (PIO) in pitch response and accurately identified the source of the problem as an excessively low short-period mode frequency.

4.7.3 Lateral Task

The lateral evaluation task, repeated three times, was a timed problem flown in smooth air and defined as follows:

	<u>End Time</u>
1. Stabilize aircraft at initial	0:30
2. Execute 90-degree right turn in 60 seconds.	1:30
3. Stabilize aircraft on new heading and hold for 30 seconds.	2:00
4. Execute 90-degree left turn in 60 seconds.	3:00
5. Stabilize aircraft at initial conditions.	3:30

Airspeed and altitude were to be held constant for the basic JetStar, the Lateral RSS engaged, and a simulated failure of the RSS yaw damper occurring approximately 60 seconds into the problem. Pilots were asked to comment on the following:

1. Use of rudder in order to coordinate the turns;
2. Ease of turn coordination;
3. Ease of initiating and maintaining desired turn rate;
4. Presence of undesirable Dutch Roll characteristics; and
5. Ease of maintaining heading.

A summary of the subjective pilot evaluations is given in Table X, below.

TABLE X

AVERAGE COOPER-HARPER PILOT RATINGS, LATERAL TASK
(Smooth Air)

	<u>Case</u>	<u>Rating</u>	<u>Standard Deviation</u>
1	Basic JetStar	3.1	0.77
2	Lateral RSS	2.5	0.45
3	Lateral RSS ($r \rightarrow \delta_r$ loop failed)	3.0	0.35

An examination of the root locus for the Lateral RSS (Figure 35, page 72) indicates that the Dutch Roll characteristics of the aircraft with the yaw damper ($r \rightarrow \delta_r$) failed are almost identical to those of the basic JetStar. Thus it is not surprising that the pilot ratings for the two cases are almost identical. Not all of the pilots attempted to coordinate their turns by use of rudder. All, however, agreed that the turns were essentially coordinated with the RSS engaged. Only one pilot, using the rudder, reported that coordinated turns could be maintained even with the yaw damper failed. All five evaluation pilots recognized the improved Dutch Roll characteristics with the RSS engaged and reported improved turn-entry and heading-hold characteristics.

4.7.4 Combined Axes Task

The combined axes task, repeated three times, was a timed climbing/descending turn in smooth air defined as follows:

	<u>End Time</u>
1. Stabilize aircraft at initial conditions.	0:30
2. Descend to 1000 feet while turning right 90 degrees in 1 minute.	1:30

	<u>End Time</u>
3. Stabilize on new heading and altitude and hold for 30 seconds.	2:00
4. Climb to 2000 feet while turning left 90 degrees in 1 minute.	3:00
5. Stabilize aircraft at initial conditions.	3:30

Airspeed was to be held constant. The runs were for the basic JetStar configuration and for the Longitudinal Systems I and II with the Lateral RSS engaged. Pilots were asked to give an overall Cooper-Harper rating for the task and make any comments regarding handling qualities as appropriate. The evaluation results are summarized in Table XI.

TABLE XI

AVERAGE COOPER-HARPER RATINGS, COMBINED AXES TASK
(Smooth Air)

	<u>Case</u>	<u>Rating</u>	<u>Standard Deviation</u>
1	Basic Jetstar	3.1	0.71
2	Longitudinal RSS I and Lateral RSS	2.5	0.45
3	Longitudinal RSS II and Lateral RSS	2.9	0.57

In verbal comments, three pilots remarked on the obvious increase in workload due to the more difficult task, but none found any particular difficulty with the Longitudinal RSS I plus Lateral RSS configuration. There was no agreement among the pilots about the cause of the reported relative degradation of handling qualities of the Longitudinal RSS II plus Lateral RSS configuration. Although the lateral/directional characteristics for the aircraft were identical for Cases 2 and 3, two

pilots reported control of heading to be more difficult. Two other pilots found pitch control to be somewhat too sensitive. One pilot preferred the configuration of Case 3 to that of Case 2. According to the average pilot opinion ratings, the basic JetStar would appear to possess the poorest handling qualities of the three simulated configurations. Three pilots reported control of vertical speed and pitch attitude as more difficult, one pilot noticed a slightly annoying Dutch Roll oscillation, but one pilot felt the basic JetStar to be slightly superior to the RSS-augmented configurations.

4.7.5 Smooth Air Evaluations, Conclusions

Examination of the results of the first three evaluations leads to the conclusion that the incorporation of the Ride Smoothing Systems makes little difference in the handling qualities of the JetStar for maneuvering flight in smooth air. For the lateral axis control task some improvement in Dutch Roll characteristics was detected by the pilots. During the combined axes task, a subtle improvement in pitch characteristics with the RSS engaged resulted in the augmented aircraft configurations being rated better than the basic aircraft. The numerical differences in ratings, however, are so slight that statistically they are insignificant. More important is the conclusion that even with the stabilizing loops ($\theta \rightarrow \delta_e$, $r \rightarrow \delta_r$) failed for the RSS-augmented cases, the average pilot opinion rating is approximately three (3). According to the Cooper-Harper scale, a rating of three (3) represents an aircraft with satisfactory handling qualities requiring no improvement.

4.7.6 Instrument Landing System Approach Task

The final simulation evaluation task was an Instrument

Landing System approach problem. The pilots were asked to capture and track the localizer and glideslope to a 61 meter (200 foot) breakout altitude. A total of four runs were made by each pilot. The first run was with the basic JetStar configuration in smooth air. During the next three runs (basic JetStar, Longitudinal RSS I plus Lateral RSS, Longitudinal RSS II plus Lateral RSS) simulated turbulence was introduced with components scaled to a vertical gust field of $\sigma_{w_g} \approx 1.2$ meters/sec (4 ft/sec). The simulation turbulence level was chosen below the design condition after a preliminary evaluation at $\sigma_{w_g} = 2.1$ m/s (7 ft/sec) resulted in a pilot opinion rating of seven (7) for the basic JetStar. Ratings of seven (7) or greater imply a workload level that precludes the pilot from devoting attention to detailed evaluation of handling qualities.

Pilots were requested to comment on the following specific handling qualities considerations:

1. Ability to maintain desired airspeed and attitude;
2. Ability to acquire and track the glideslope;
3. Tendency to PIO in pitch/airspeed;
4. Adequacy of roll control;
5. Precision of heading control;
6. Ability to acquire and track the localizer; and
7. Tendency to PIO in roll/heading.

In addition, a separate Cooper-Harper rating was recorded for the longitudinal and lateral control aspects of the task. The subjective evaluations are summarized in Table XII.

TABLE XII

AVERAGE COOPER-HARPER PILOT RATINGS, ILS TASK

<u>Case</u>	<u>Longitudinal</u>		<u>Lateral</u>	
	<u>Rating</u>	<u>Standard Deviation</u>	<u>Rating</u>	<u>Standard Deviation</u>
<u>Smooth Air</u>				
1 Basic JetStar	3.2	0.3	2.6	0.4
<u>Turbulent Air</u>				
2 Basic JetStar	4.3	0.9	5.5	1.4
3 Longitudinal RSS I + Lateral RSS	2.8	0.9	3.1	1.7
4 Longitudinal RSS II + Lateral RSS	2.9	0.7	3.6	2.3

Whereas no significant effect on handling qualities in smooth air could be attributed to the incorporation of a Ride Smoothing System, the effect of such systems for flight in turbulence is beneficial. Although the standard deviations of Pilot Opinion Ratings are large, ratings by individual pilots were all improved when the RSSs were engaged. Note especially that at the simulated turbulence level the longitudinal handling qualities of the aircraft with a RSS in turbulence are rated equivalent to those of the basic aircraft in smooth air. The improvement in the lateral axis is not quite as great.

Verbal comments by the pilots generally indicated few problems with longitudinal axis control for the RSS-augmented configurations. With the basic aircraft, however, all pilots reported some tendency toward PIO in pitch. It was in the lateral-directional task

that a tendency of the aircraft to "wander" in heading and oscillate in roll angle was observed. For the RSS-augmented cases, such oscillation was characterized by three of the pilots as typical of flight in turbulence. When the RSSs were disengaged, however, these motions were reported to result in serious difficulties in holding desired heading and maintaining the localizer. In all cases, the pilots indicated that the level of turbulence appeared moderate to heavy for the approach with the basic JetStar. When the Ride Smoothing Systems were engaged, the level of turbulence was judged to be from very light to light to moderate.

Perhaps the best summary of the effect on handling qualities of a Ride Smoothing System for the JetStar was given by Pilot A. After having flown a simulated approach in the unaugmented aircraft with a turbulence level of $\sigma_{wg} = 2.1$ m/s (7 ft/sec), he compared the experience to the previous run where Longitudinal RSS I and the Lateral RSS had been engaged:

"General comment: [compared to the previous run] this is an awful condition to fly--laterally, directionally, and in pitch. Could not maintain airspeed. Had to keep adding power because [the aircraft] was sashaying around so much. Attitude: I was just herding it around the best I could... Could not hold heading because of the [large] roll excursions... Looked like the ship didn't have much stability... Definite tendency to PIO... Roll control was very poor due to adverse yaw. Initial roll response was low... [Apparent] level of turbulence compared to the previous run--almost double."

Despite these comments, the pilot's tracking error was small (Figure 53 and 54). The differences in workload, however, are apparent in the strip-chart recordings (Figure 55a-e) of aileron activity

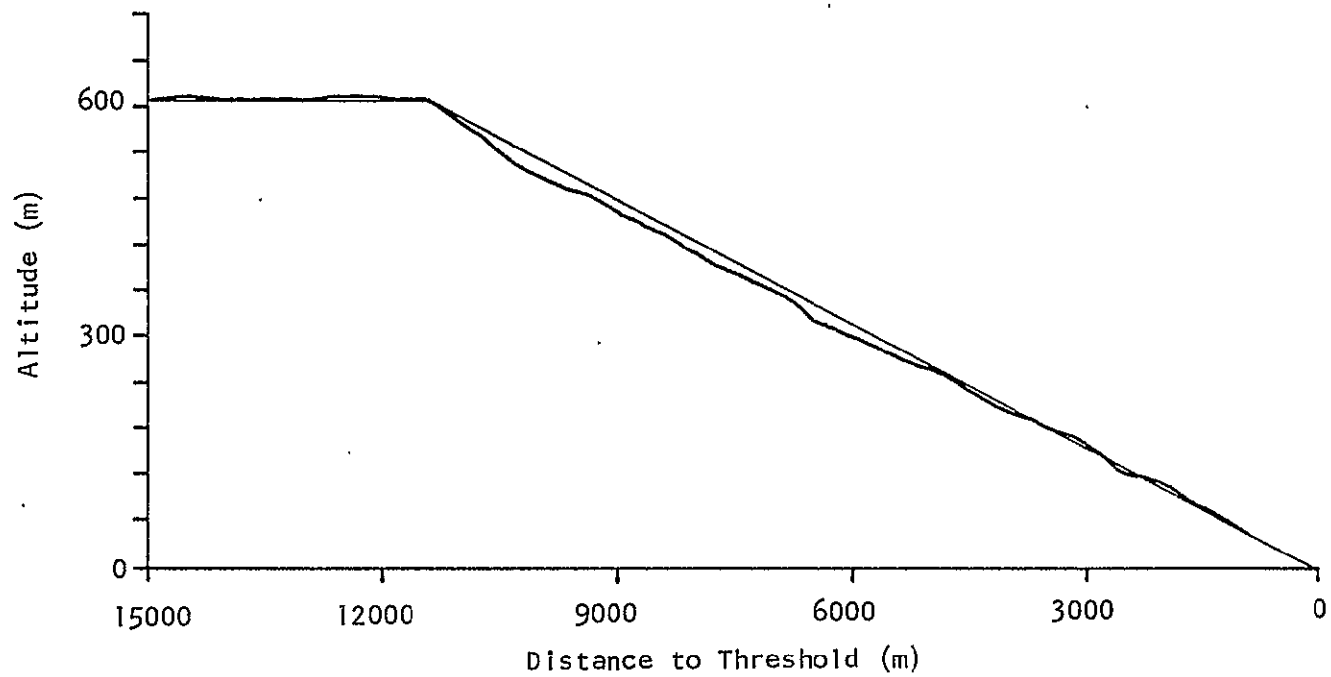


FIGURE 53. ALTITUDE TRACK; BASIC JETSTAR IN DESIGN
TURBULENCE FIELD (PILOT A)

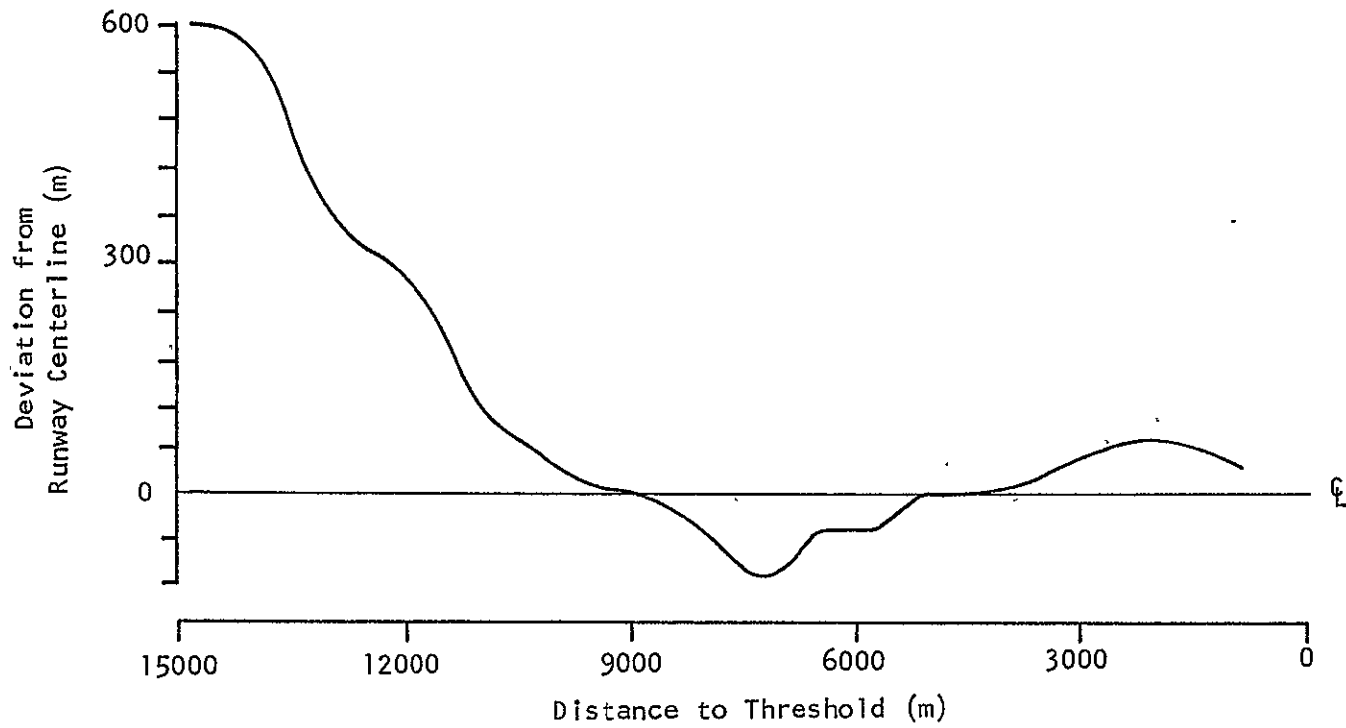


FIGURE 54. DEVIATION FROM LOCALIZER; BASIC JETSTAR IN DESIGN TURBULENCE FIELD (PILOT A)

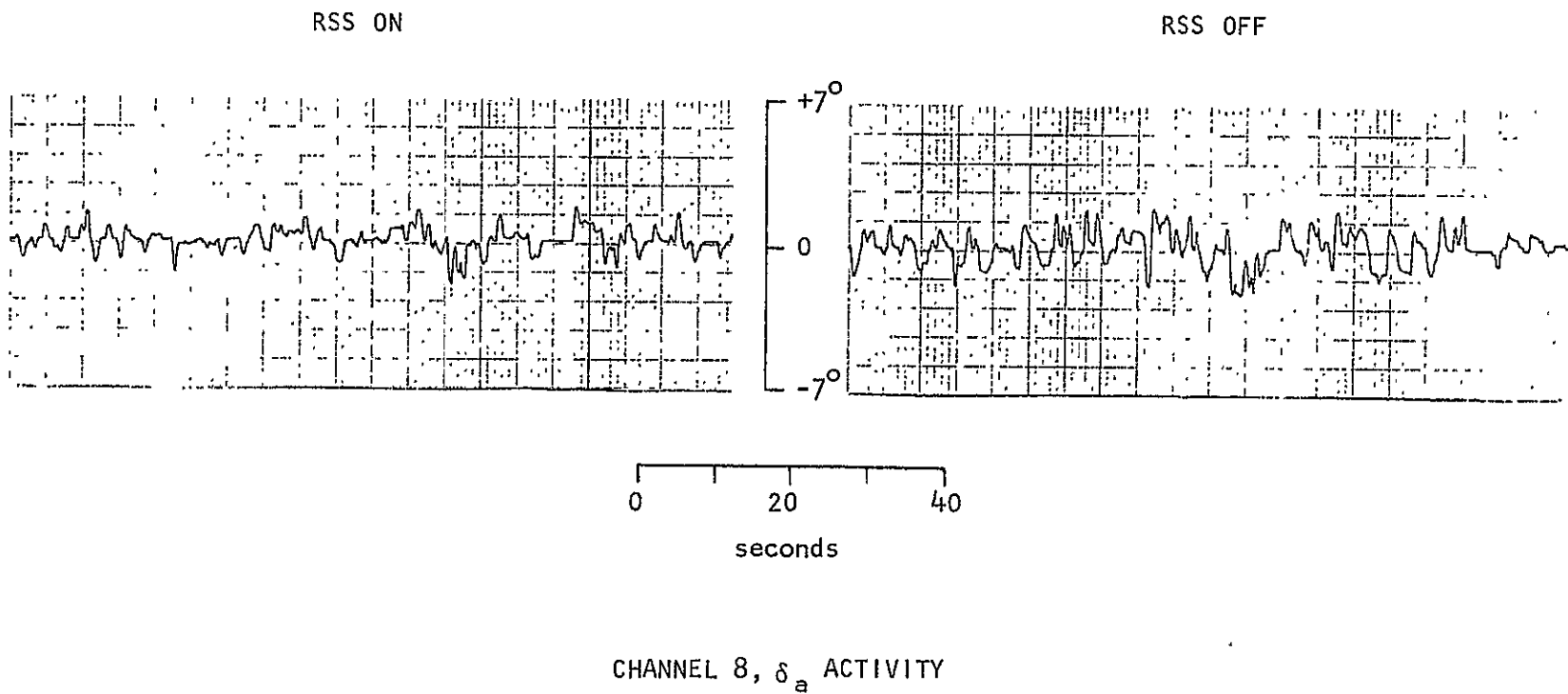
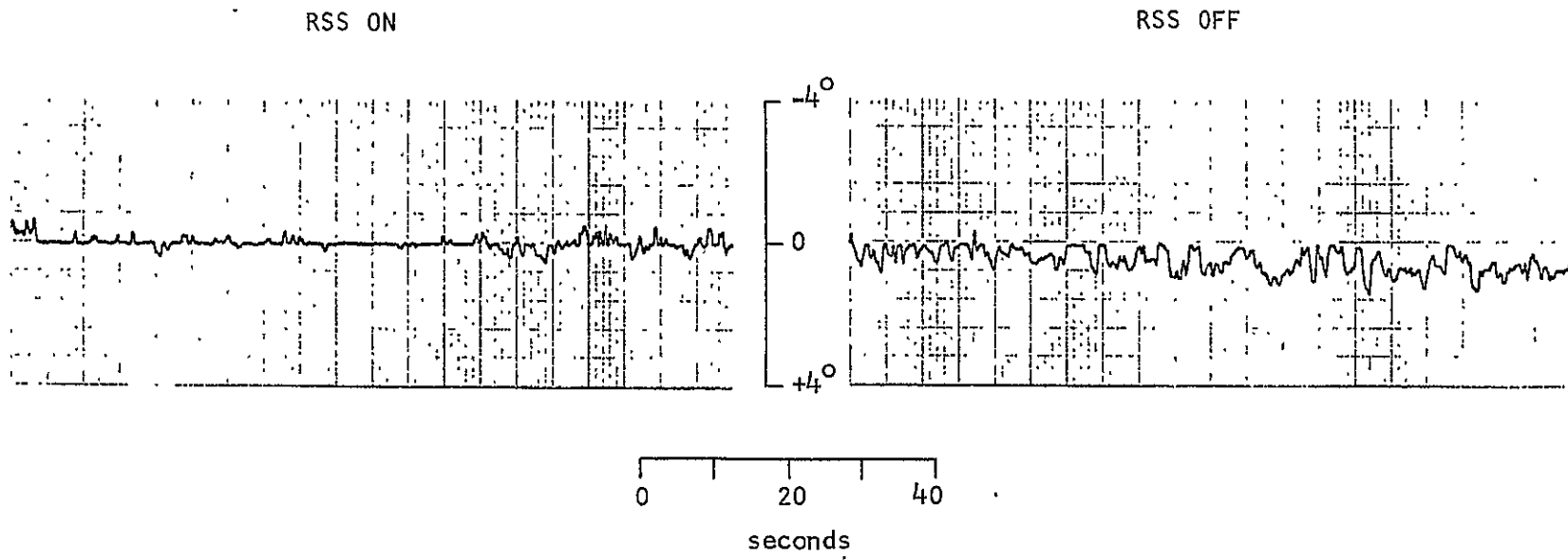


FIGURE 55. SIMULATION TIME HISTORY; JETSTAR IN DESIGN TURBULENCE FIELD (PILOT A)

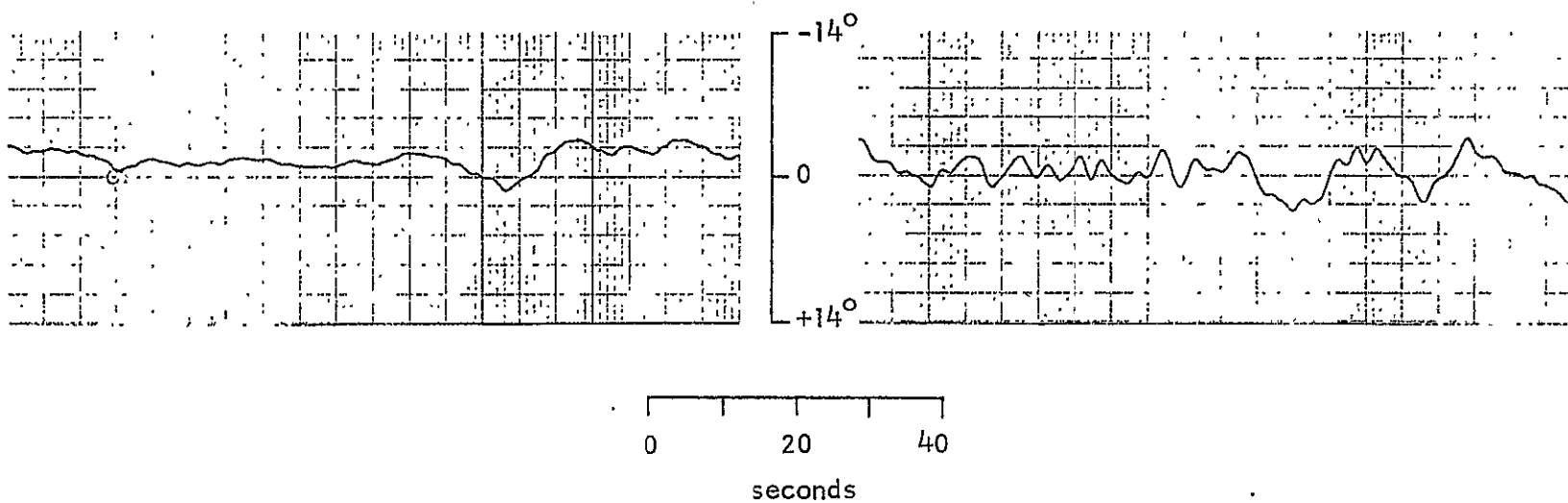


CHANNEL 4, $\delta_{e_{pilot}}$

FIGURE 55. CONTINUED

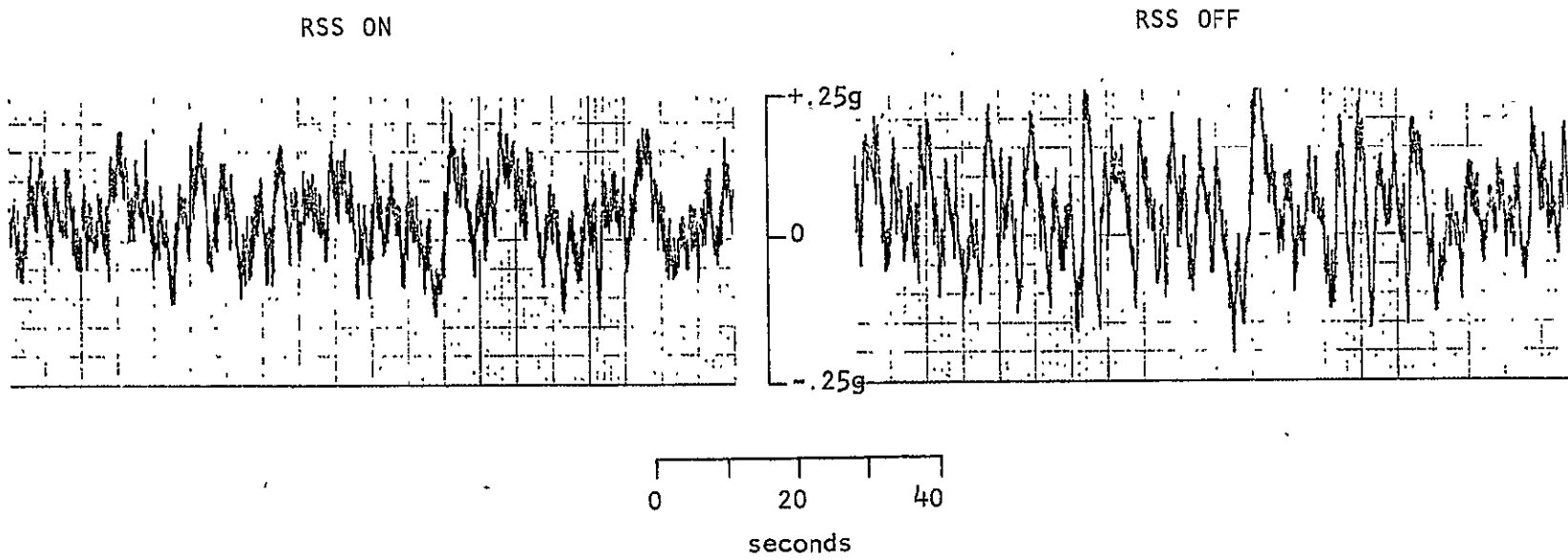
RSS ON

RSS OFF



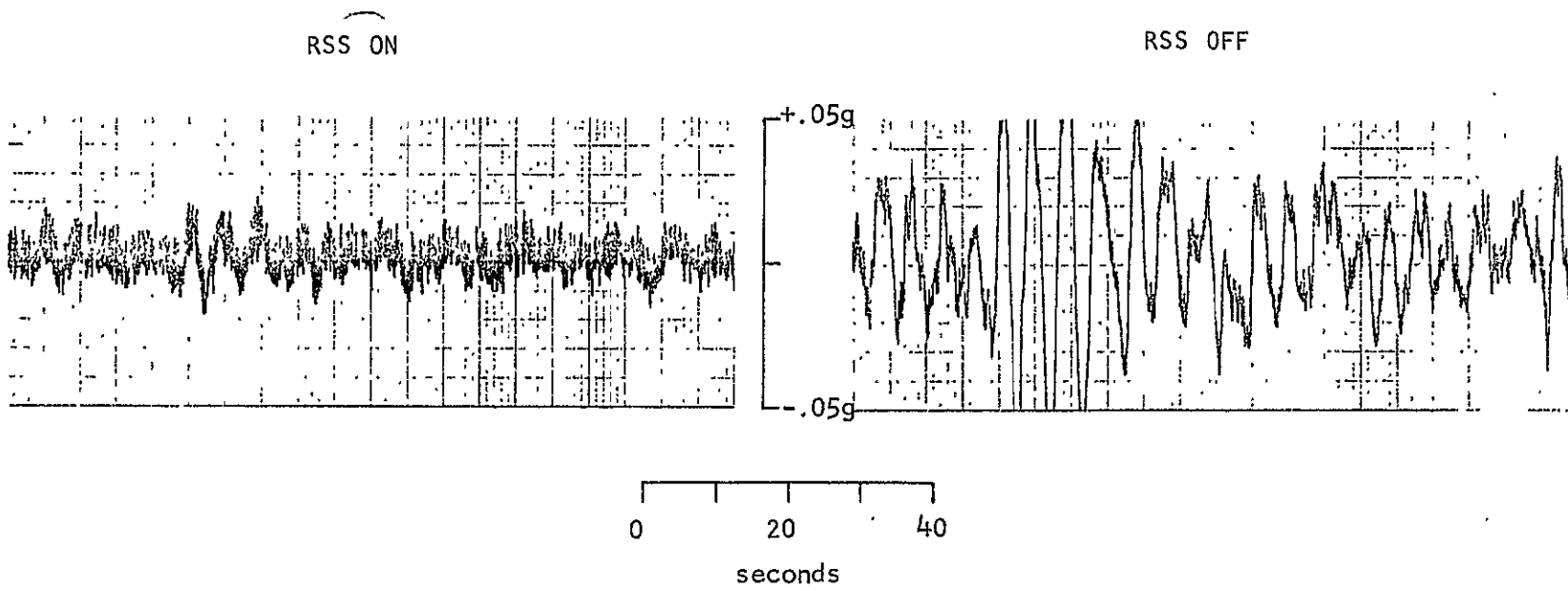
CHANNEL 5, $\Delta\theta$

FIGURE 55. CONTINUED



CHANNEL 1, a_z

FIGURE 55. CONTINUED



CHANNEL 3, a_y

FIGURE 55. CONCLUDED

(Channel 8) and pilot inputs to the elevator (Channel 4). Note also that the pitch attitude trace (Channel 5) was considerably smoother when the RSS was engaged. Vertical acceleration at the aircraft center of gravity is displayed on Channel 1. With the RSS operating, the sharp acceleration spikes were suppressed. The effectiveness of the Lateral RSS is displayed in Channel 3, the transverse acceleration at the aircraft center of gravity. With the system engaged, the lateral acceleration was reduced to very small amplitude.

Digitally-calculated data for these two runs are summarized in Table XIII. The calculated root-mean-square turbulence levels for both runs were as follows: $\sigma_{w_g} \approx 1.89$ m/s (6.21 ft/sec), $\sigma_{\beta_g} \approx 1.32^\circ$, $\sigma_{p_g} \approx 2.23^\circ$ /sec.

Despite the fact that the measured quantities include maneuvering loads, the agreement between theoretically-calculated parameters and their experimental values is reasonably good. Only the measured performance of the Longitudinal RSS is considerably inferior to the predicted value. Several additional runs were made to investigate the reason for this discrepancy.

4.7.7 Simulation of Straight and Level Flight

Several data runs were made for a straight and level flight condition. Pilot control was "loose." At this condition, a 32.5% reduction in σ_{a_z} and a 80.5% reduction in σ_{a_y} were measured when Longitudinal RSS 1 and the Lateral RSS were engaged. Power spectral density plots for these experiments are shown in Figure 56 and 57. Note that the power spectral density for the basic aircraft does not show the sharp peak at the phugoid frequency that was predicted by the theoretical

TABLE XIII

SIMULATION RESULTS, ILS TRACKING TASK

	<u>Basic Aircraft</u>		Longitudinal RSS + <u>Lateral RSS</u>	
	<u>Experimental</u>	<u>Calculated</u>	<u>Experimental</u>	<u>Calculated</u>
σ_q	1.00 °/sec	1.28 °/sec	0.48 °/sec	0.62 °/sec
σ_p	5.07 °/sec	3.32 °/sec	2.68 °/sec	1.29 °/sec
σ_r	1.59 °/sec	1.56 °/sec	1.27 °/sec	1.04 °/sec
σ_α	1.60 °	--	1.34 °	--
σ_β	2.20 °	--	1.87 °	--
σ_ψ	4.87 °	--	4.69 °	--
σ_{δ_e}	0.84 °	--	0.44 °	0.35 °
σ_{δ_f}	--	--	10.59 °	8.8 °
σ_{δ_r}	--	--	0.80 °	0.61 °
$\sigma_{\delta_{sfg}}$	--	--	7.59 °	5.18 °
σ_{δ_a}	2.98 °	--	2.40 °	--
σ_{a_z}	0.0963 g	0.104 g	0.0634 g	0.0508 g
σ_{a_y}	0.0273 g	0.0207 g	0.0061 g	0.0031 g
Comfort Rating	3.4	3.4	2.8	2.6
% reduction σ_{a_z}			33.2 %	51.8 %
% reduction σ_{a_y}			77.7 %	84.5 %
% reduction σ_q			52.0 %	51.3 %
% reduction σ_p			47.2%	61.0 %
% reduction σ_r			20.2%	43.5 %

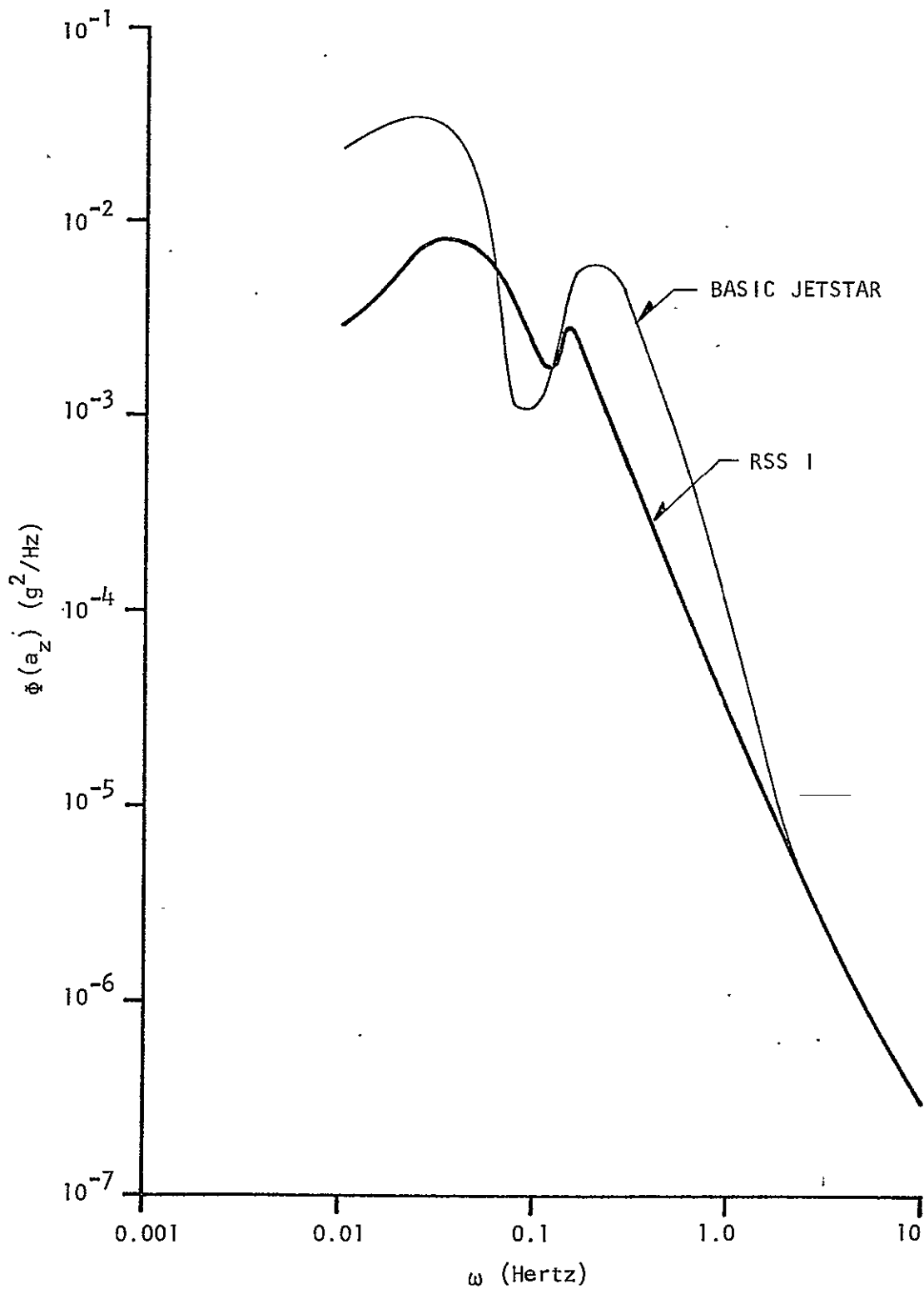


FIGURE 56. POWER SPECTRA OF a_z DUE TO TURBULENCE, SIMULATION DATA

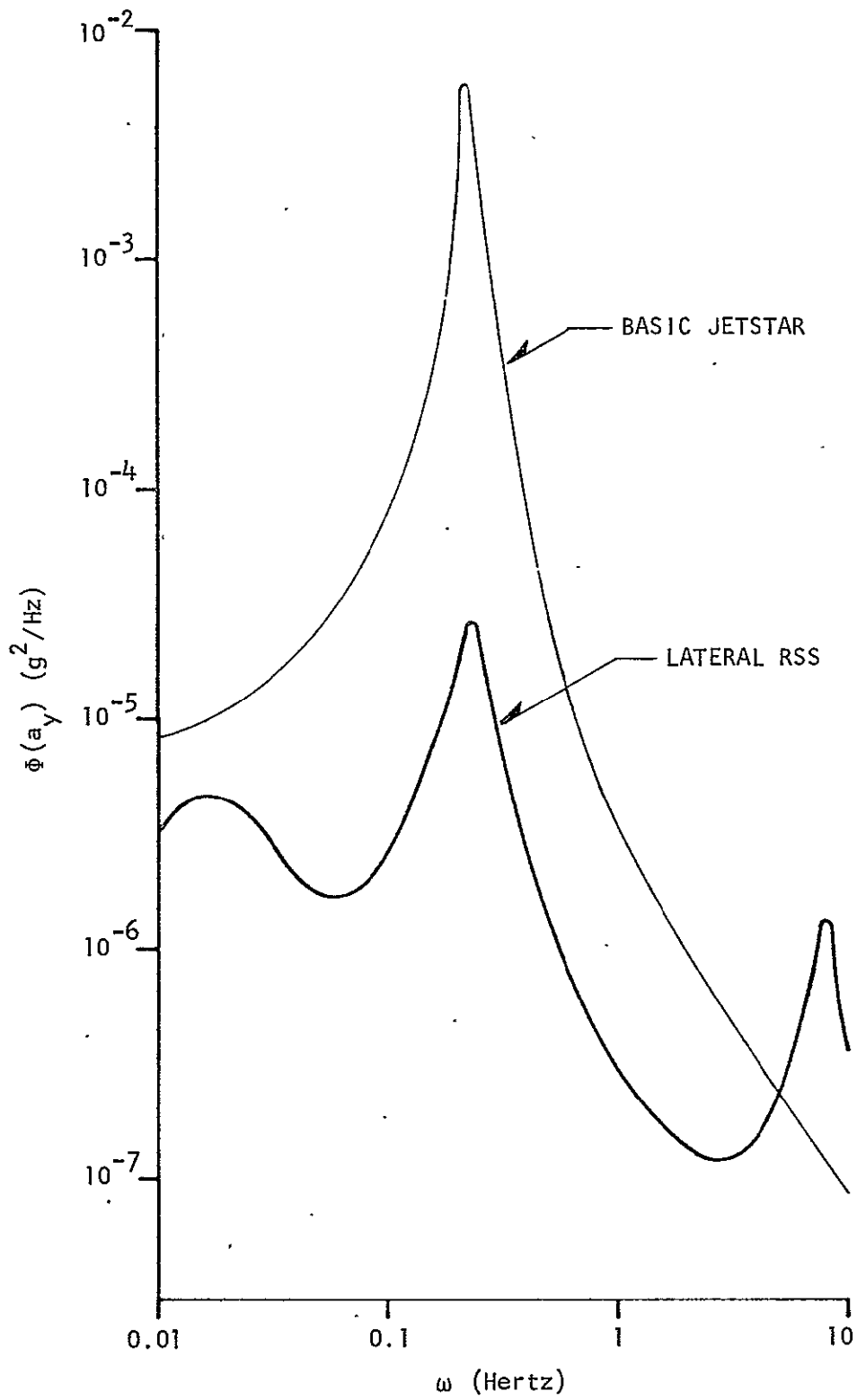


FIGURE 57. POWER SPECTRA OF a_y DUE TO TURBULENCE, SIMULATION DATA

calculations (see Figure 28, page 60). In Section 3.4.1 it was shown that a considerable amount of energy is associated with this peak. Thus it can be concluded that the apparent loss of longitudinal system effectiveness is the result of calculation errors at low frequencies in the simulation data. At higher frequencies, the shapes of the power spectral density plots closely match the theoretically calculated curves.

4.8 Conclusions

The ground-based simulation program had, as its primary objective, the evaluation of the effect of the synthesized Ride Smoothing Systems on the handling qualities of the JetStar. It is concluded that, for maneuvering flight in smooth air, the incorporation of these systems yields a slight improvement in pilot opinion ratings. Under the postulated system failure conditions, handling qualities are not catastrophically degraded. Thus, the Ride Smoothing Systems meet two of the most important design criteria set forth in Section 2.3: maintenance of adequate handling qualities and insensitivity to system failure.

For precision instrument flight in turbulence, incorporation of a RSS significantly improves the handling qualities of the basic aircraft by reducing pilot workload. Parenthetically, it should be noted that when subject to a severe turbulence environment, the handling qualities of a reasonably "well-behaved" aircraft such as the JetStar may deteriorate to unacceptable levels. Thus, the handling qualities criteria of MIL-F-8785B (36) appear to be inadequate.

Finally, the simulator experiments provided a measure of confidence in the performance estimates for the ride quality improvement provided by Ride Smoothing Systems and, based on the anticipated improvement in comfort rating, justification for flight test experiments.

CHAPTER V

FLIGHT TEST PROGRAM

5.1 Planned Program

JetStar flight tests of the Ride Smoothing Systems were planned to be conducted in three phases. First, a series of developmental flights during which feedback gains were to be increased incrementally to their nominal levels were to be flown. A rudimentary handling-qualities evaluation and acquisition of baseline system performance data was to be accomplished. When a reasonable level of confidence in system operation had been achieved, Phase II, a repetition of the ground-based simulation flight, was to be performed. The final flight test phase was to obtain subjective evaluations of RSS performance.

Following a GPAS system failure unrelated to the RSS operation, the JetStar was grounded. Consequently, only two test flights were made and only some of the objectives of Phase I were accomplished. Results of these very limited experiments are discussed below.

5.2 Implementation of RSS Aboard the JetStar

Implementation of the Longitudinal and Lateral Ride Smoothing Systems aboard the JetStar was a straightforward extension of the ground-based simulator mechanization. The feedback equalization circuits wired on the airborne PC-12 analog computer were identical to those used on the simulator (Figure 46 through 48, page 96ff). The airborne analog computer is shown in Figure 58.

System-driving signals were obtained from standard GPAS instrumentation. Yaw rate and pitch attitude gyro outputs were input to

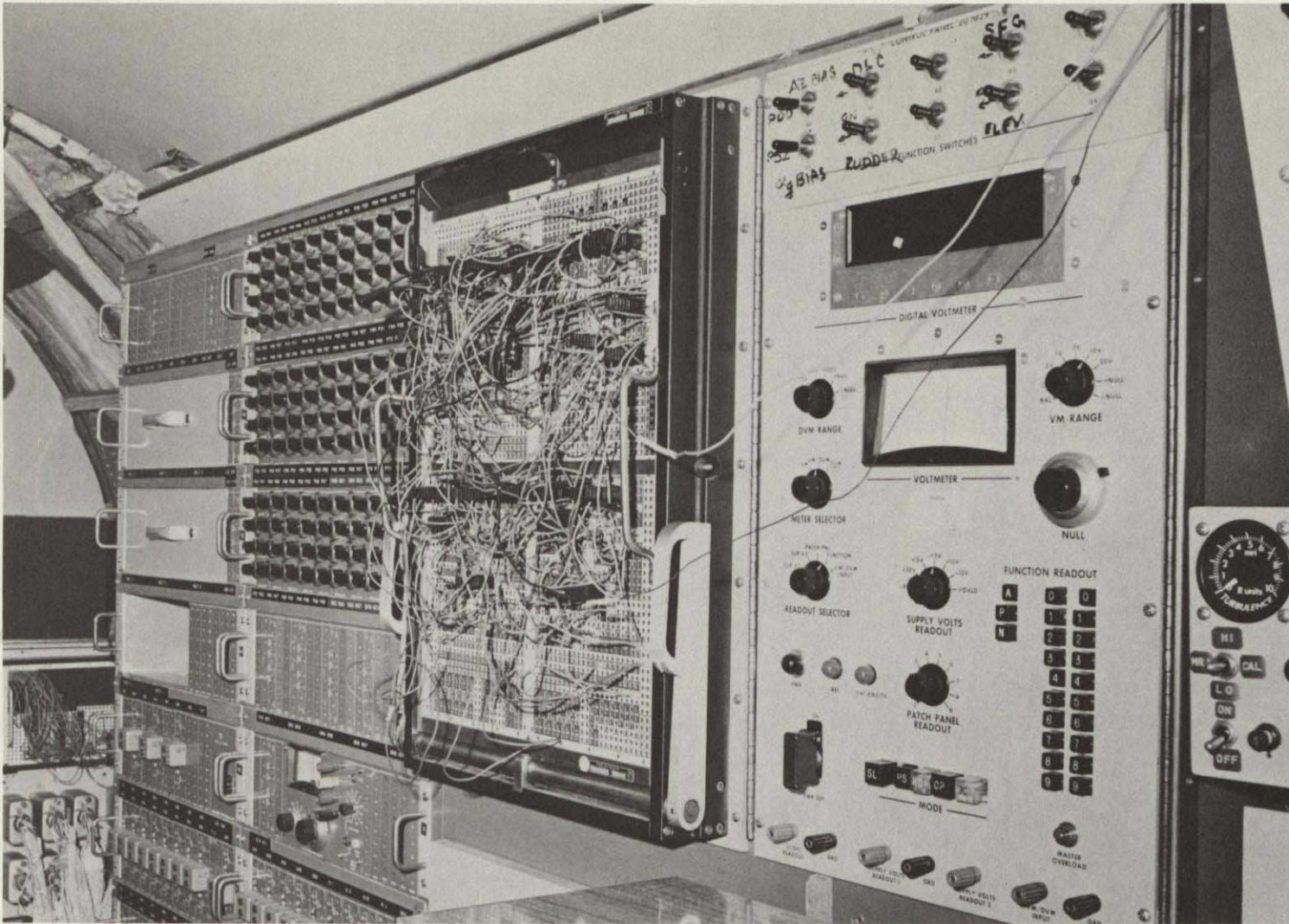


FIGURE 58. AIRBORNE ANALOG COMPUTER

the PC-12 patchboard directly from GPAS signal-conditioning circuits. Upon engagement of the GPAS mode, the pitch attitude signal was automatically nulled by the Response Feedback System circuitry. The vertical and lateral acceleration signals for operation of the Ride Smoothing Systems were provided by a pair of accelerometers bolted to the cabin floor slightly ahead of the nominal aircraft center of gravity. Outputs of these accelerometers were input directly to the PC-12 board, bypassing the GPAS signal-conditioning circuits, requiring the normal accelerometer signal to be nulled manually prior to RSS engagement.

Ride Smoothing System commands to the elevator and rudder were summed with pilot commands from the aircraft left seat controls. RSS commands to the direct-lift flaps and side-force generators were applied directly to the surface servos.

5.3 Ground Tests

As with the ground-based simulation, performance of the airborne analog circuits was verified by observing the frequency and magnitude response of the RSS filters to sinusoidal inputs. Response of the PC-12 computer circuits was comparable to those of the ground-based analog computer. Proper phasing of the command signals was verified by pressurizing the GPAS system, tilting individual sensors, and observing the deflection of the appropriate control surface.

Prior to the implementation of the Ride Smoothing Systems, feedback of acceleration to the direct-force surfaces had never been attempted aboard the JetStar. Several experiments were, therefore, conducted to determine the stability (structural coupling) of these

feedback loops. With the GPAS system pressurized, the acceleration feedback gains were slowly increased to their nominal values and the surface position transducer signals monitored on a strip-chart recorder. In the case of the direct lift-flaps, no instability was detected. The flaps would, however, respond to movement by personnel about the aircraft cabin. Thus, although the accelerometer mounting was adequate for the Phase I investigation, ultimately a more suitable accelerometer location would have had to have been found. Increasing the lateral acceleration feedback gain above approximately 20% of the nominal value resulted in limit cycling of the side-force generators. This phenomenon was attributed to significant free play in the side-force generator linkages. The feedback gain of this loop was, therefore, set well below nominal during the flight test program. Although the linkages were readjusted, the flight program was terminated before another ground resonance test could be accomplished.

A final pre-flight operational test of the airborne RSS consisted of operating the system in a closed-loop sense. The aircraft equations of motion were solved on three slaved Electronics Associates, Inc. (two Model TR 58 and a TR 10) analog computers. Calculated motion parameters were fed to left-seat cockpit displays and the airborne PC-12 analog computer. Pilot control inputs and RSS system commands were fed to the appropriate control surfaces of the aircraft. Surface position transducer outputs were fed back to the auxiliary ground computers to complete the closure. Hydraulic pressure for the control surfaces was supplied by a ground system. Signals proportional to components of actual atmospheric turbulence that had been recorded on

analog tape were used to perturb the calculated angle-of-attack and sideslips signals in the ground analog computers. The aircraft was thus made a part of a ground-based simulator. Selected system parameters were monitored on strip-chart recorders during the simulation runs. Since operation of the GPAS in this ground mode adds to utilization time of aircraft hydraulic components, the experiment was conducted only long enough to qualitatively verify proper operation of the RSS.

5.4 Data Acquisition and Reduction

Acquisition of JetStar flight-test data was by means of a Pulse Code Modulation (PCM) System. Some 80 channels of data were available for analysis. All of the data presented below were sampled at a rate of 40 samples per second. Power spectral analysis of selected data channels was performed using the same digital computer program (PSDQR) employed in the ground-based simulation studies.

Calculation of the statistical properties of the true vertical gust field (w_g) was accomplished by correcting the nose-boom-mounted gust vane signal (α_v) for aircraft motion:

$$w_g = \cos \phi [V_{T_0} \alpha_v - V_{T_0} \theta + \ell_x q] + \int A_z dt \quad (5.4.1)$$

where ℓ_x is the distance from the aircraft center of gravity to the gust vane, and A_z is the vertical acceleration of the aircraft center of gravity with respect to inertial space. The value of A_z was determined from the aircraft center of gravity accelerometer outputs N_x , N_y , and N_z (in g's) by:

$$A_z = g \{ N_x \sin \hat{e} + \sin \phi \cos \theta (N_y + \sin \phi \cos \theta) + \cos \phi \cos \theta (N_z - \cos \phi \cos \theta) \} \quad (5.4.2)$$

Several channels of data were monitored on strip-chart recorders during the flight tests. In addition to providing a qualitative indication of system performance in real time, the time code on the strip-chart recordings provided identification of data segments for digital analysis.

5.5 Summary of Flight Test Data

Two flight tests of the Ride Smoothing Systems, #349 and #350, were conducted on 5 June and 11 June 1974, respectively. The aircraft was flown in the approach configuration. During Flight #349, the Lateral RSS and Longitudinal RSS I were engaged. Acceleration feedback gains for these systems were increased incrementally from 5% of their nominal values to 45% of nominal for the Longitudinal RSS and 15% of nominal for the Lateral RSS. A rudimentary examination of the aircraft handling qualities in smooth air for this configuration (flight path angle changes, "S" turns) was accomplished. The command pilot reported no objectionable aircraft characteristics. The aircraft was then flown in light to moderate natural turbulence for approximately 10 minutes with the Lateral and Longitudinal RSS I systems engaged. Heading was then reversed, and the same geographical area traversed with the systems shut down.

During Flight #350, the Longitudinal RSS I was operated at nominal design feedback gains in turbulent air for approximately 3 minutes before

a GPAS system anomaly resulted in system shut down. Approximately three minutes of turbulence data for the basic JetStar was recorded immediately following RSS disengagement.

Results of these experiments are summarized in Table XIV. Experimental values have been adjusted by multiplying by the ratio of the design turbulence level of $\sigma_{w_g} = 2.1$ m/sec (7 ft/sec) to the measured σ_{w_g} . The numbers in parenthesis are theoretically-predicted values.

The agreement between theoretical and measured acceleration levels for the baseline case is quite good. The theoretical calculation, however, significantly overestimates aircraft response in pitch rate and yaw rate. The measured performance of Longitudinal RSS 1, in terms of percent reduction in σ_{a_z} and σ_q at the design feedback gain levels, is in excellent agreement with predicted performance. The acceleration alleviation provided by the Lateral RSS, however, is significantly below the expected level, while the reduction in σ_r is very close to the predicted value. Had the acceleration feedback loop been open, the yaw damper ($r \rightarrow \delta_r$ feedback) alone would have provided a 38.3% reduction in σ_{a_y} and a 29.0% reduction in σ_r . Thus, it appears that the side-force generators provided no benefit at the very low level of K_{a_y} realized in the tests.

A comparative power spectral density plot (PSD) of the output of the center of gravity normal accelerometer is shown in Figure 59 for the baseline and Longitudinal RSS 1 nominal gain cases. This plot differs from previously-presented PSD's in that the individual curves have been normalized by their respective mean-square values. Since the areas under both curves are thus identical, the plot displays only relative

TABLE XIV

RIDE SMOOTHING SYSTEM FLIGHT TEST RESULTS

		<u>Longitudinal RSS I</u>		
		<u>Flight #349</u>	<u>Flight #349</u>	<u>Flight #350</u>
Baseline			$K_{a_z} = 1.4 \text{ rad/m/sec}^2$ $(0.43 \text{ rad/ft/sec}^2)$	$K_{a_z} = 3.3 \text{ rad/m/sec}^2$ $(1.0 \text{ rad/ft/sec}^2)$
			$K_{\theta} = 0.03^\circ/\circ$	$K_{\theta} = 0.14^\circ/\circ$
σ_{a_z}		0.1047 (0.1178) g	0.0788 (0.0794) g	0.0518 (0.0572) g
σ_q		0.933 (1.440) $^\circ/\text{sec}$	0.599 (1.12) $^\circ/\text{sec}$	0.402 (0.700) $^\circ/\text{sec}$
σ_{δ_f}		--	5.31 (5.95) $^\circ$	7.70 (9.90) $^\circ$
% reduction σ_{a_z}		--	24.7 (32.6) %	50.5 (51.8) %
% reduction σ_q		--	35.8 (22.3) %	56.9 (51.3) %
		<u>Lateral RSS</u>		
		<u>Flight #349</u>	<u>Flight #349</u>	
		Baseline	$K_{a_y} = 0.5 \text{ rad/m/sec}^2$ $(0.15 \text{ rad/ft/sec}^2)$	
			$K_r = 1.0^\circ/\circ/\text{sec}$	
σ_{a_y}		0.0307 (0.0350) g	0.0206 (0.0158) g	
σ_r		1.32 (2.35) $^\circ/\text{sec}$	0.88 (1.65) $^\circ/\text{sec}$	
$\sigma_{\delta_{sfg}}$		--	2.14 (2.67) $^\circ/\text{sec}$	
% reduction σ_{a_y}		--	32.9 (54.9) %	
% reduction σ_r		--	33.0 (30.0) %	

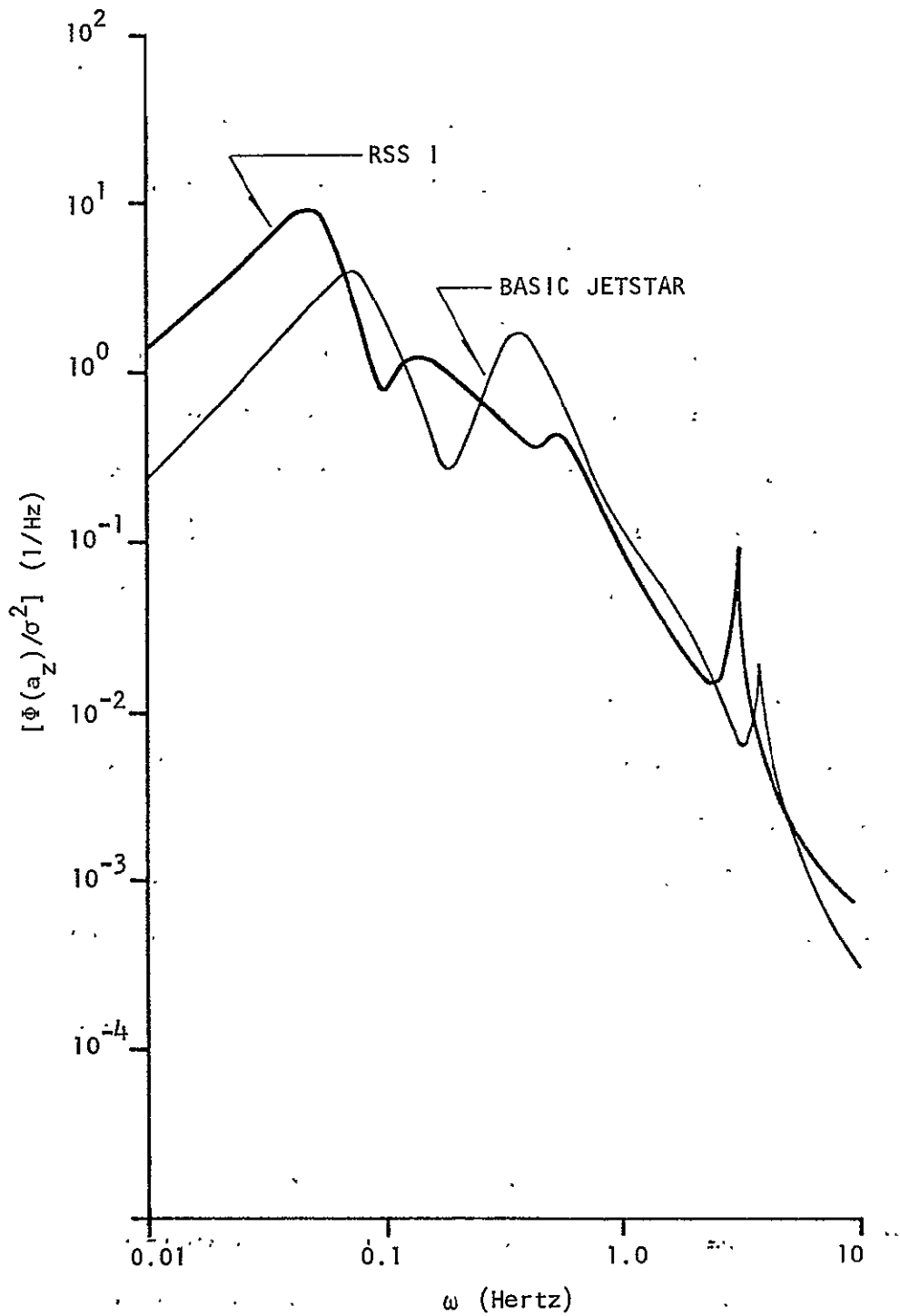


FIGURE 59. COMPARISON OF a_z POWER SPECTRA FOR BASIC AND LONGITUDINAL RSS 1 AUGMENTED JETSTAR (FLIGHT DATA)

RSS effectiveness at particular frequencies. The greatest acceleration alleviation can be seen to occur from frequencies somewhat below the short period peak to 1 Hertz. This conclusion is in clear agreement with the theoretical calculations (see Figure 28, page 60). The "spikes" in the experimental curves at approximately 3 to 4 Hertz are attributable to resonance of the accelerometer mounting plate.

A qualitative impression of the effectiveness of Longitudinal RSS I can be gained by referring to Figure 60. These strip-chart records are taken from Flight #350. The traces on the left side of the figures are for the time segment with the Longitudinal RSS I operating (13:44 to 13:45:40 hr) and those on the right for the baseline case (13:48 to 13:49:40 hr).

The β vane output was chosen as representative of the turbulence level since aircraft motion in the lateral axis is essentially unaffected by the Longitudinal RSS. Note that the magnitude of the turbulence field is approximately equivalent for both time segments. Excursions in vertical acceleration (a_z), however, were substantially reduced when the RSS was engaged.

5.6 Conclusions

Although the limited amount of available flight data makes categorical statements impossible, the data permit some tentative conclusions. First, the theoretical calculations of aircraft root-mean-square acceleration response to turbulence agree reasonably well with experimental values for both the Longitudinal RSS augmented and unaugmented configurations. Such agreement is most important since

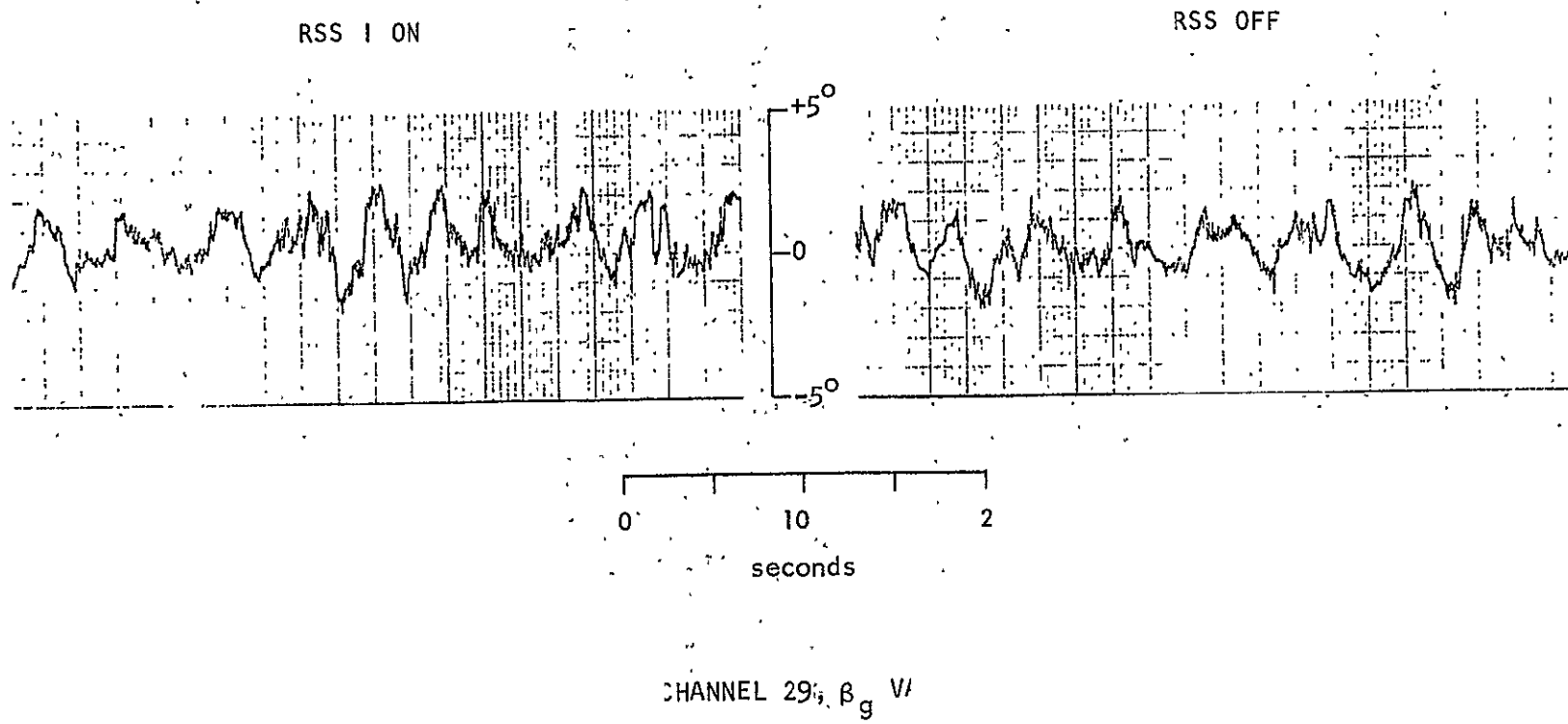
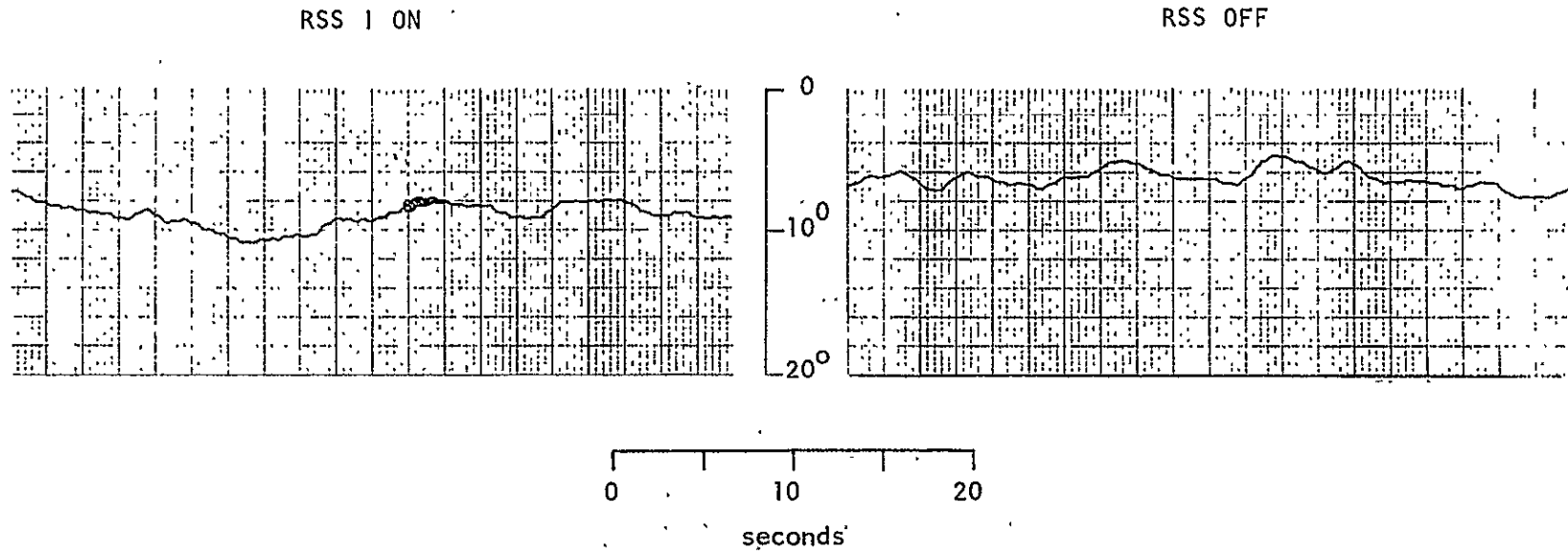


FIGURE 60. TIME HISTORY; BASIC AND LONGITUDINAL RSS I AUGMENTED
JETSTAR IN TURBULENCE (FLIGHT DATA)

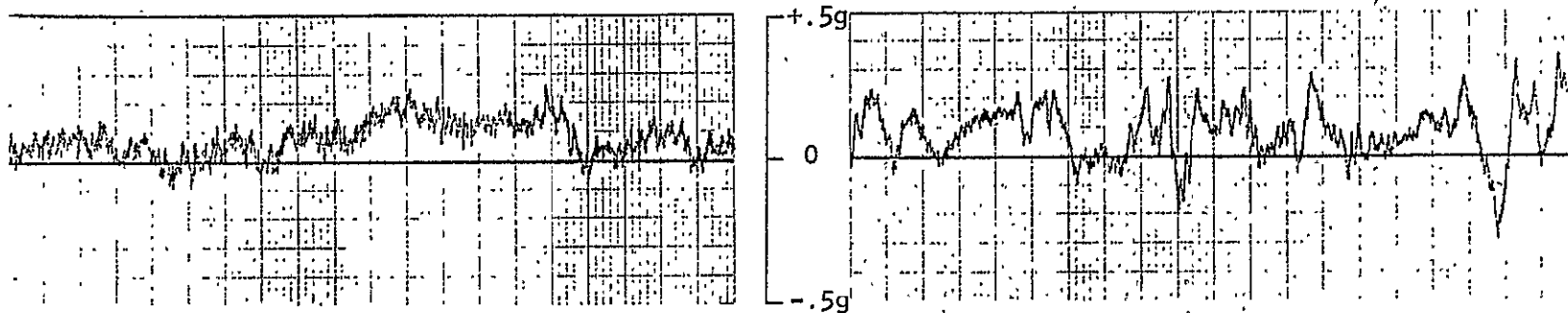


CHANNEL 5, θ

FIGURE 60. CONTINUED

RSS I ON

RSS OFF



0 10 20
seconds

CHANNEL 11, a_z

FIGURE 60. CONCLUDED

σ_{a_z} is the dominant term in the evaluation of passenger comfort.

Secondly, the theoretical prediction of lateral acceleration is also in good agreement with experiment for the baseline case. The failure of the experimentally-observed value of σ_{a_y} to fall to the theoretically-predicted level with the Lateral RSS engaged can probably be attributed to the low acceleration feedback gain level necessitated by mechanical difficulties. Finally, it would appear that mechanization of Longitudinal Ride Smoothing System I is feasible and that its incorporation would provide substantial improvement in passenger comfort. Had human subjects been on board the aircraft, the comfort model predicts that the percentage satisfied would have increased from 66.8% ($C = 3.5$) for the basic JetStar case to 84.5% ($C = 2.8$) when the RSSs were engaged.

CHAPTER VI

EXTENSION OF RIDE SMOOTHING SYSTEM CONCEPT TO STOL AIRCRAFT

6.1 Selected Aircraft

The success achieved in synthesizing ride smoothing systems for the JetStar prompted a brief theoretical and simulation investigation of the applicability of these systems to two radically different STOL-class aircraft of the same size as the JetStar. The first of these was the deHavilland of Canada DHC-5 Buffalo. The Buffalo relies on low-wing loading ($W/S \approx 1676 \text{ N/m}^2 = 35 \text{ lb/ft}^2$) to achieve short-field performance, but is otherwise similar in configuration to conventional aircraft. The other aircraft selected for this investigation was a conceptual design extensively studied at the NASA Langley and Flight Research Centers and designated LRC S-11. The wing loading of this aircraft is equivalent to typical modern jet transports ($W/S \approx 3830 \text{ N/m}^2 = 80 \text{ lb/ft}^2$). S-11 short-field performance is achieved through the operation of an externally-blown jet flap (43). As in the JetStar investigation, the selected design condition was the power approach in moderate to heavy turbulence ($\sigma_{w_g} = 2.1 \text{ m/sec}$).

The mechanization of a Longitudinal RSS for the STOL aircraft made use of the elevator and wing trailing edge flaps. In the case of the Buffalo, aerodynamic data were available only for the entire flap system. Thus, although these flaps are considerably more effective at the design condition than those on the JetStar, the entire surface had to be assumed as the direct-lift control. The S-11 configuration

has a more sophisticated system of wing-mounted control surfaces. These include spoilers, flaperons, symmetrically-deflecting ailerons, and a "direct-drag" flap system. Although the direct-drag flaps have an effective lift to drag ratio of only $(L/D)_f \cong 1.36$, their lift capability is equivalent to that of the JetStar system. Therefore, only the "direct-drag" flaps were mechanized in the RSS design.

The lateral axis RSS for the STOL aircraft was initially mechanized in the same way as that for the JetStar, i.e., using the rudder and side-force generators. The hypothetical side-force generators were scaled to produce the same lateral acceleration per unit deflection at the design velocity as those on the JetStar. The projected area for each of two surfaces was 4.9 m^2 (53 ft^2) and 8.0 m^2 (86 ft^2) for the Buffalo and S-11, as compared to 1.3 m^2 (14 ft^2) for the JetStar. The postulated STOL side-force generators are quite large; for the S-11, the area is 1.4 times that of the aircraft's vertical tail. Incorporation of such controls strictly for improvement of ride qualities would be hard to justify. One can, however, envision additional uses of large side-force generators, e.g., improvement of crosswind landing capability. Furthermore, some reduction in size might be possible if the surfaces are immersed in the propeller slipstream or jet efflux. Such tradeoffs, however, were not evaluated.

Dimensional stability derivatives and aircraft parameters for the Buffalo and S-11 power approach conditions are summarized in Appendix E. The Buffalo parameters were taken from the NASA Ames Research Center STOLAND program documentation; the S-11 data from NASA Flight

Research Center sources. Actuator characteristics for the control surfaces were assumed identical to those of the JetStar.

6.2 Synthesis of Ride Smoothing Systems

6.2.1 Longitudinal RSS

Whereas the basic JetStar longitudinal dynamics and control characteristics in the approach configuration (with the exception of ζ_{ph}) clearly meet the handling qualities requirements of MIL-F-8785B (36), those of the Buffalo and S-II do not. Thus, a direct adaptation of the Longitudinal RSS developed previously was not possible. In particular, the handling qualities parameter n/α is marginal in the case of the Buffalo ($n/\alpha = 2.9$ g/rad) and inadequate for the S-II ($n/\alpha = 1.57$ g/rad). Incorporation of Longitudinal RSS II would have further degraded this metric. Therefore, the applicability only of Longitudinal RSS I to the STOL configurations was studied.

The effect of the equalized essential feedback ($a_z \rightarrow \delta_f$ through cascaded washout and lag filters) on the dynamic modes of both STOL aircraft was substantially different from the short-period and phugoid-root location changes observed for the JetStar. First, for the range of acceleration feedback gains considered, the phugoid root remained essentially stationary. Secondly, the short-period root locus tended toward the imaginary axis (reduction in ζ_{sp}) at an almost constant level of damped natural frequency (ω_d). These variations, however, were also small. Consequently, the stabilizing feedback loop requirements were different than for the JetStar RSS. In the case of the Buffalo, no increase in short-period frequency was required, and

short-period damping was recovered by feedback of pitch rate to the elevator ($q \rightarrow \delta_e$) through a lag filter.

The short-period damped natural frequency ($\omega_{d_{sp}}$) for the basic S-11 was calculated to be only a factor of two higher than that of the phugoid (see Table XV, below). Under these conditions, considerable coupling between vertical velocity (angle of attack) and pitch attitude perturbations occurs at the phugoid frequency; modal ratio: $u:\alpha:\theta = 2.4 \text{ ft/sec}:0.7^\circ:1^\circ$. (At the short-period frequency: $u:\alpha:\theta = 0.2 \text{ ft/sec}:1.7^\circ:1^\circ$.) Consequently, both pitch attitude and pitch rate were fed back to the elevator ($\theta, q \rightarrow \delta_e$) to increase the short-period frequency and damping and to achieve a greater separation of the modes. Lead and lag filters were incorporated in the θ and q loops, respectively.

Block diagrams of the Longitudinal Ride Smoothing Systems for the Buffalo and S-11 are shown in Figures 61 and 62. Table XV compares the dynamic characteristics and Longitudinal RSS performance parameters at the design condition for the JetStar and the two STOL aircraft.

The numerical data of Table XV indicate a number of similarities between the RSS augmented aircraft. The vertical acceleration levels (underlined terms) for flight in the standard ($\sigma_{w_g} = 2.1 \text{ m/sec}$) turbulence field for the three augmented aircraft are essentially the same. From the pilot's viewpoint, the dynamics of the augmented aircraft, as expressed in terms of the parameters (time to half amplitude of the short-period mode, $T_{\frac{1}{2}sp}$, inverse cycles to the 1/10 amplitude $1/C_{1/10}$, and phugoid time to half amplitude,

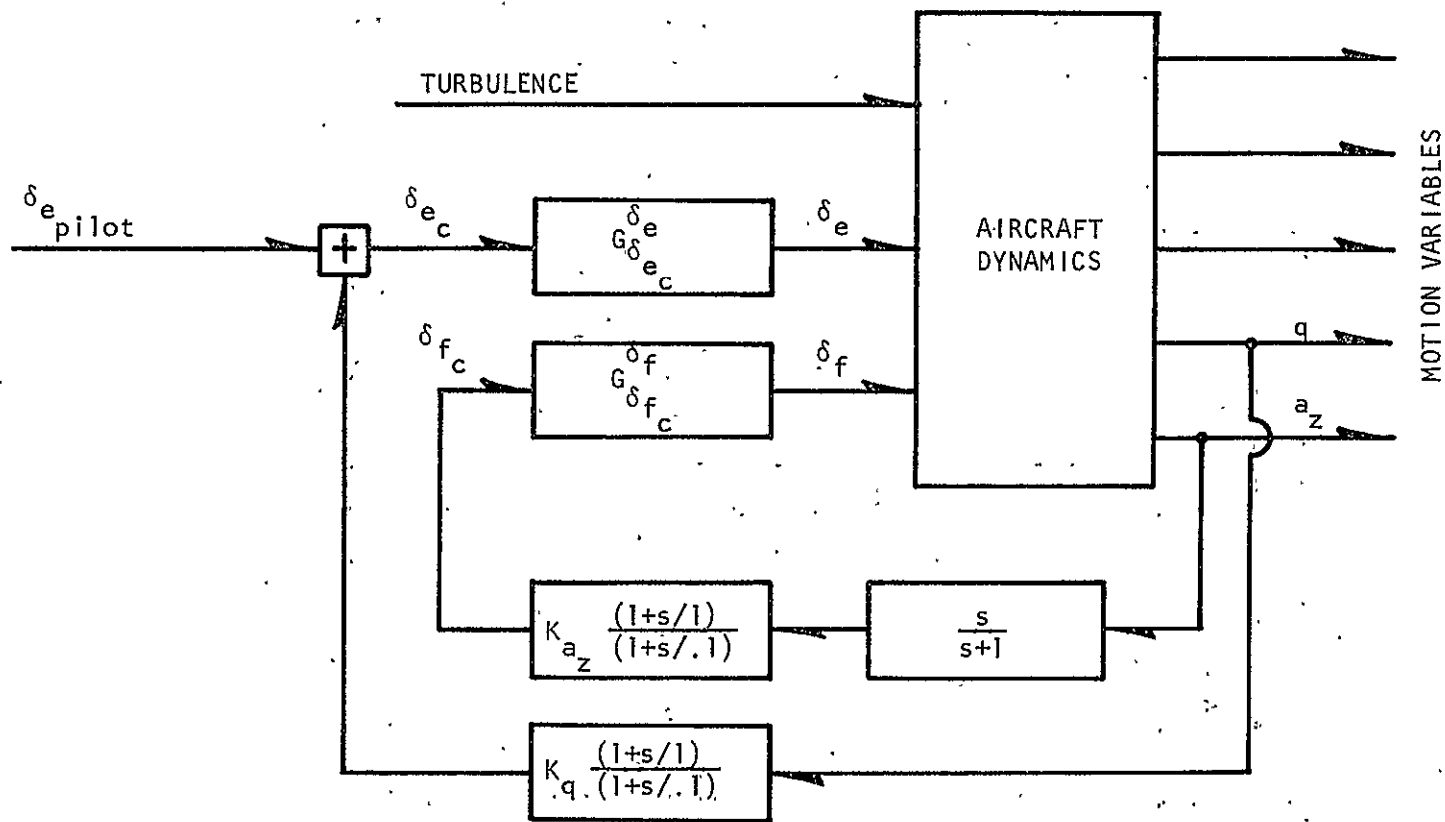


FIGURE 61. BUFFALO LONGITUDINAL RIDE SMOOTHING SYSTEM
 (Design Point: $K_{a_z} = 0.8 \text{ rad/m/sec}^2$, $K_q = 5 \text{ }^\circ/\text{sec}$)

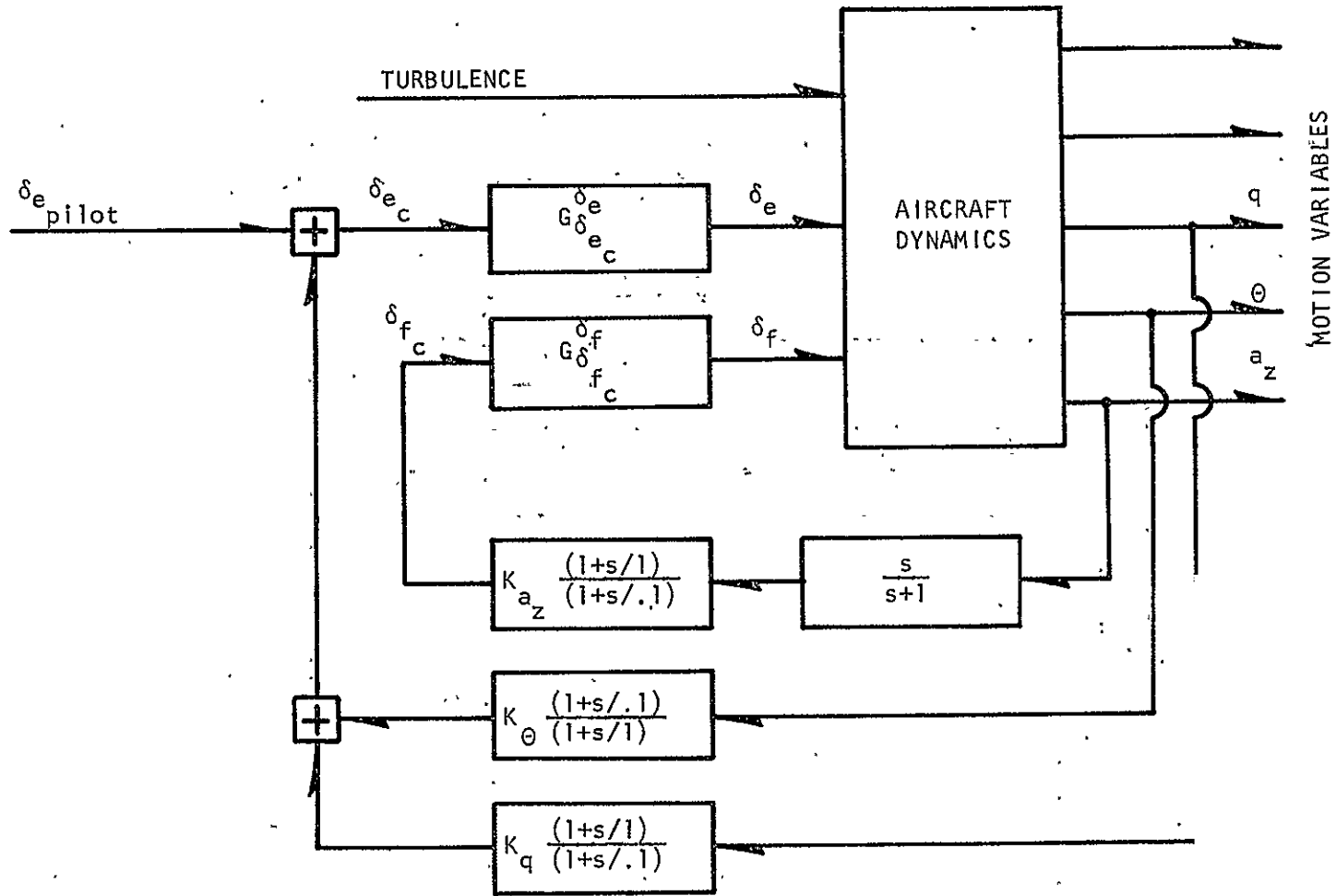


FIGURE 62. S-11 LONGITUDINAL RIDE SMOOTHING SYSTEM.
 (Design Point: $K_{a_z} = 0.8 \text{ rad/m/sec}^2$, $K_{\theta} = 0.6 \text{ } ^\circ/\text{ } ^\circ$, $K_q = 5 \text{ } ^\circ/\text{ } ^\circ/\text{sec}$)

TABLE XV

COMPARISON OF JETSTAR AND STOL LONGITUDINAL RIDE SMOOTHING SYSTEMS

	Basic JetStar	RSS-Augmented JetStar	Basic Buffalo	RSS-Augmented Buffalo	Basic S-11	RSS-Augmented S-11
ζ_{sp}	0.546	0.567	0.628	0.725	0.826	0.698
$\omega_{n_{sp}}$	0.266 Hz	0.356 Hz	0.282 Hz	0.310 Hz	0.136 Hz	0.262 Hz
$T_{\frac{1}{2}sp}$	0.76 sec	0.55 sec	0.62 sec	0.49 sec	0.98 sec	0.60 sec
$1/C_{1/10}$	2.21	2.35	2.81	3.77	5.41	3.46
ζ_{ph}	0.054	0.522	0.102	0.249	-0.005	0.371
P_{ph}	36.6 sec	53.2 sec	20.0 sec	22.8 sec	26.9 sec	31.6 sec
$T_{\frac{1}{2}ph} (T_{2_{ph}})$	74.8 sec	9.6 sec	21.4 sec	10.0 sec	(658) sec	8.7 sec
σ_{a_z}	0.1178 g	0.0572 g	0.1073 g	0.0622 g	0.805 g	0.0561 g
σ_{a_x}	0.0112 g	0.0040 g	0.0318 g	0.0251 g	0.270 g	0.0209 g
σ_q	1.44 °/sec	0.70 °/sec	2.28 °/sec	1.33 °/sec	10.8 °/sec	0.70 °/sec
σ_{δ_f}	--	9.9 °	--	2.6 °	--	2.4 °
σ_{δ_e}	--	0.4 °	--	1.2 °	--	0.9 °
% reduction σ_{a_z}	--	51.8%	--	42.8%	--	93.0%
% reduction σ_{a_x}	--	64.6%	--	34.1%	--	92.2%
% reduction σ_q	--	51.3%	--	41.5%	--	93.5%

$T_{\frac{1}{2}ph}$) are equivalent. In the landing approach, passenger comfort and previously-considered handling qualities criteria (with the exception of the aforementioned STOL deficiency in n/α) can, therefore, be met equally well for the three aircraft by the incorporation of a Ride Smoothing System.

Several differences between the STOL aircraft and the JetStar, should be noted, however. First, even with the RSS engaged, the root-mean-square longitudinal acceleration (σ_{a_x}) is significantly larger for the STOL aircraft than for the JetStar. Also, the values of the stability derivative Z_u^* are much greater. These observations suggest that the effect of the longitudinal component of turbulence (u_g) on the STOL aircraft acceleration response might be important and should be included in a more complete analysis. Second, the degree of flap activity (σ_f) required to achieve an equivalent level of σ_{a_z} for the STOL aircraft is only one-fourth that required for the JetStar. Part of the reason for this difference is, of course, the much lower approach speed of the Buffalo and S-11. Finally, because of the unstable phugoid mode of the basic S-11, the values calculated for σ_{a_z} , σ_{a_x} , and σ_q are very large. Almost all (99.7%) of the total calculated mean-square vertical acceleration occurs in the frequency band below 0.05 Hz. In practice, low frequency motion is easily suppressed by the pilot; the significance of the calculated root-mean-square values for this case is, therefore, debatable. A comparison of the a_z power spectra for the three aircraft, however, indicates that the RSS effect at higher frequencies is quite similar (Figures 28, 63, and 64).

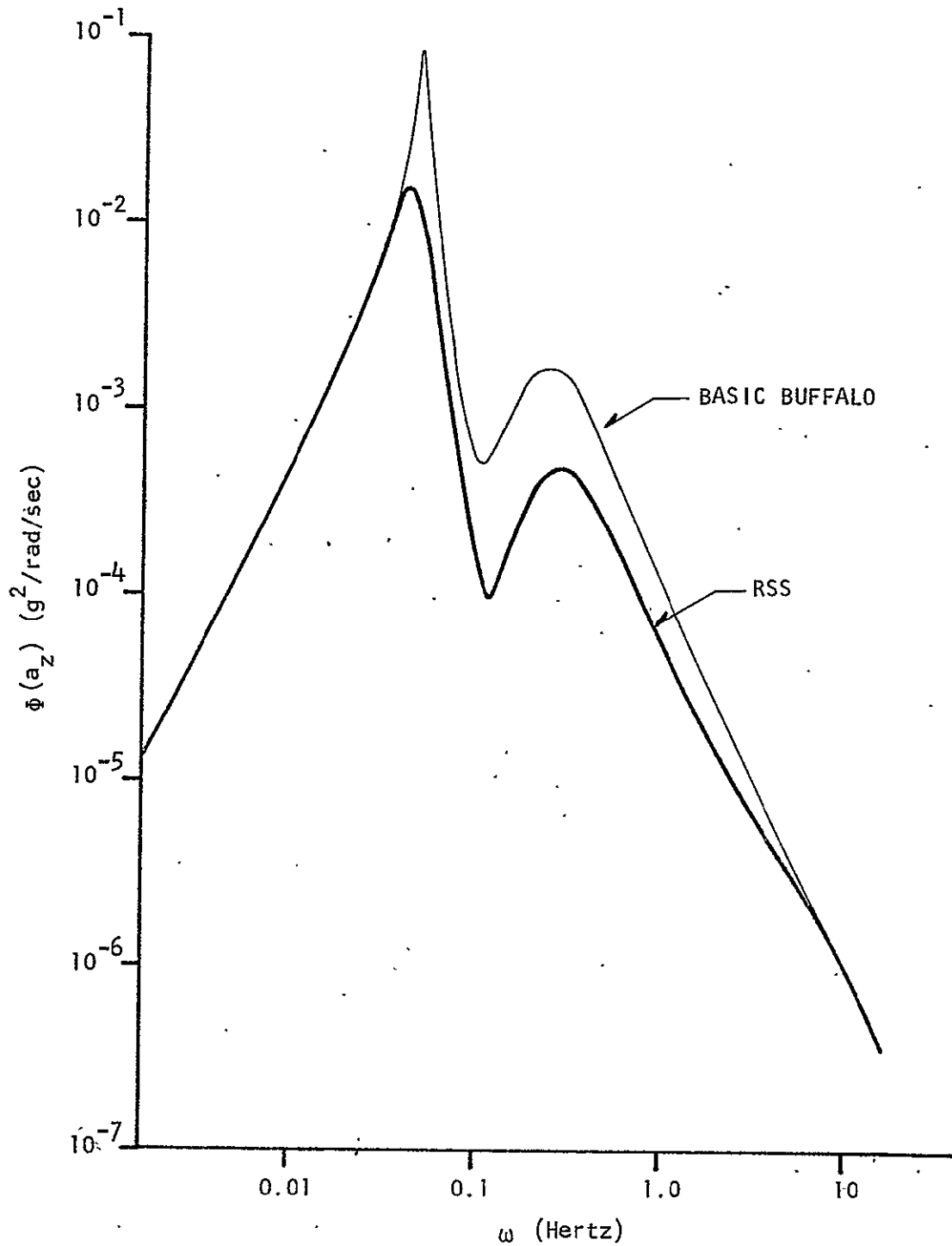


FIGURE 63. COMPARISON OF a_z POWER SPECTRA FOR BASIC AND LONGITUDINAL RSS AUGMENTED BUFFALO

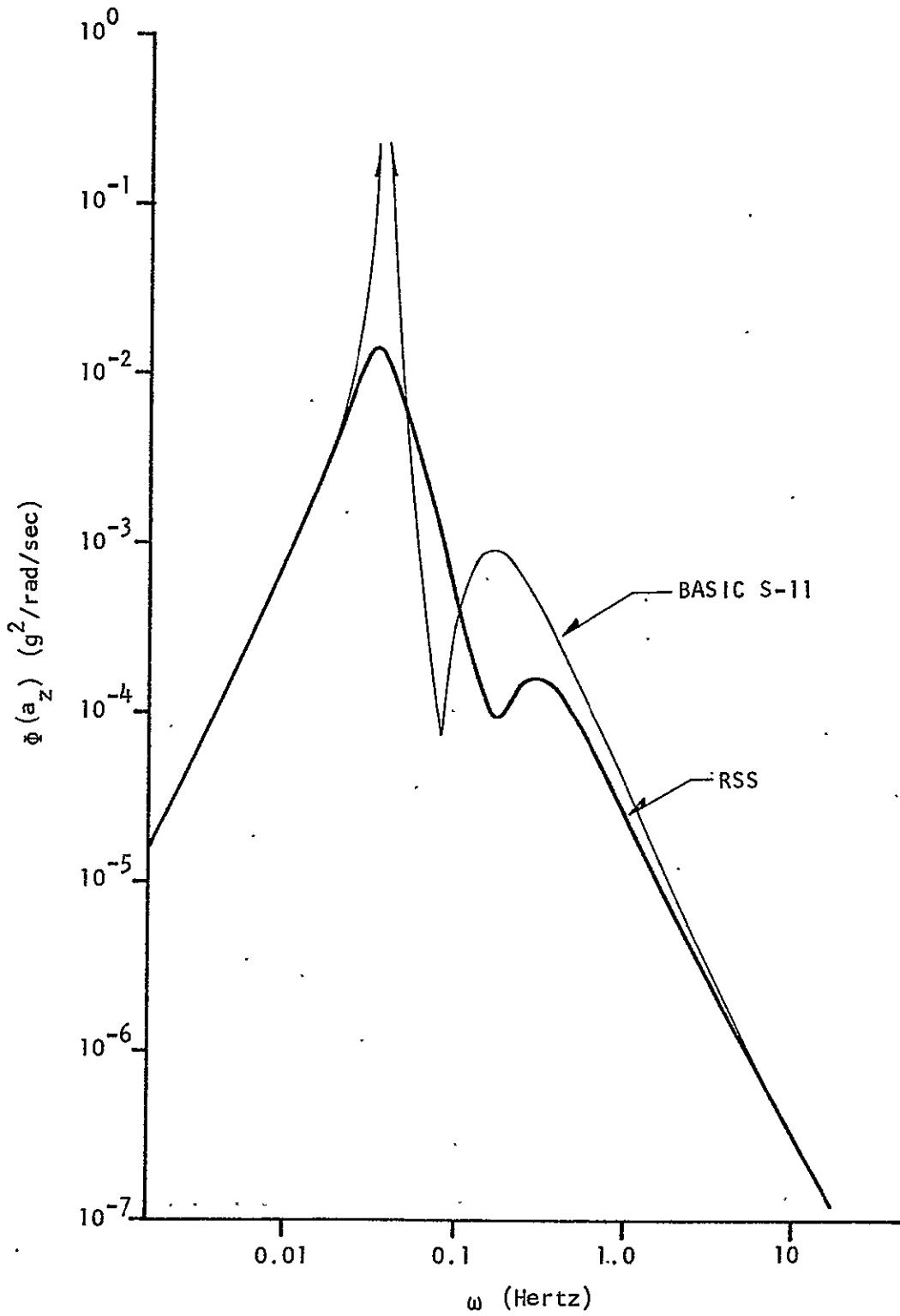


FIGURE 64. COMPARISON OF a_z POWER SPECTRA FOR BASIC AND LONGITUDINAL RSS AUGMENTED S-11

6.2.2 Lateral RSS

As in the longitudinal case, closure of the essential Lateral RSS feedback loop ($a_y \rightarrow \delta_{sfg}$) had a negligible effect on the characteristic modes of the STOL aircraft. The previously employed stabilizing loop, $r \rightarrow \delta_r$, however, was still desirable. Both the basic Buffalo and S-11 have an unstable spiral mode (see Table XVI). In addition, damping of the Dutch Roll mode of the basic S-11 is well below the level specified in MIL-F-8785. The incorporation of an unequalized yaw damper tends to alleviate both of these undesirable characteristics. A washout was not incorporated in the $r \rightarrow \delta_r$ loop since it was found to radically reduce both Dutch Roll damping and frequency. A third feedback loop, roll rate to aileron ($p \rightarrow \delta_a$), was added to the S-11 RSS mechanization in order to increase roll damping.

Block diagrams of the Lateral Ride Smoothing Systems for the Buffalo and S-11 are shown in Figures 65 and 66. Table XVI compares the dynamic characteristics and Lateral RSS performance parameters for the JetStar and the two STOL aircraft.

Comparative power spectral density plots for the lateral acceleration of the Buffalo and S-11 in the baseline and RSS-augmented configurations are given in Figure 67 and 68. In the case of the Buffalo; the RSS completely suppresses the Dutch Roll response peak in addition to reducing the acceleration level across the entire frequency band. In the case of the S-11 aircraft, the effect of the $p \rightarrow \delta_a$ feedback is clearly evident as a sharp dip at the maximum roll gust (p_g) input frequency. Although the Dutch Roll resonance is still apparent, the magnitude of response is sharply reduced. At higher

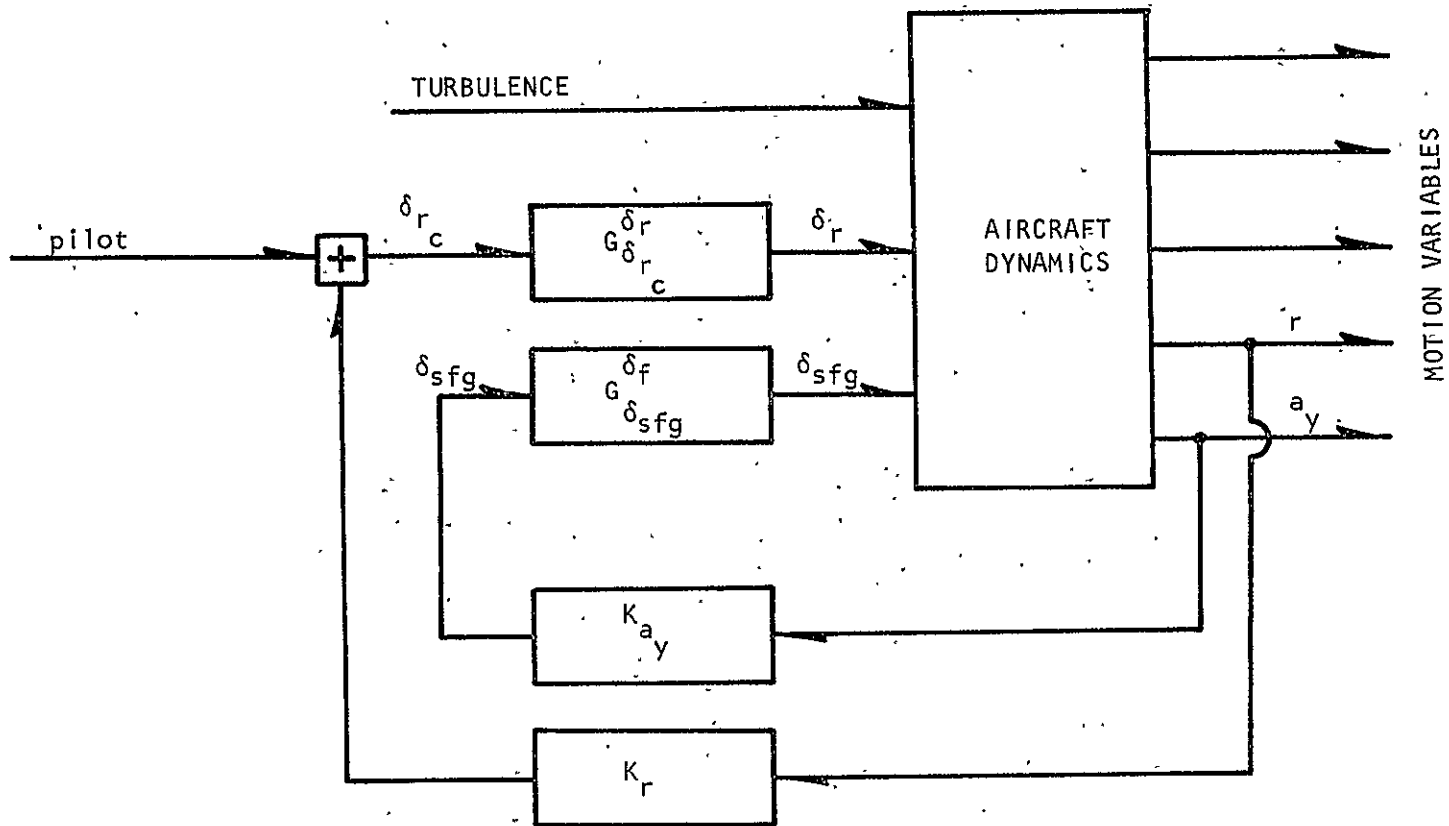


FIGURE 65. BUFFALO LATERAL RIDE SMOOTHING SYSTEMS
 (Design Point: $K_{a_y} = -3.3 \text{ rad/m/sec}^2$, $K_r = .1 \text{ }^\circ/\text{sec}$)

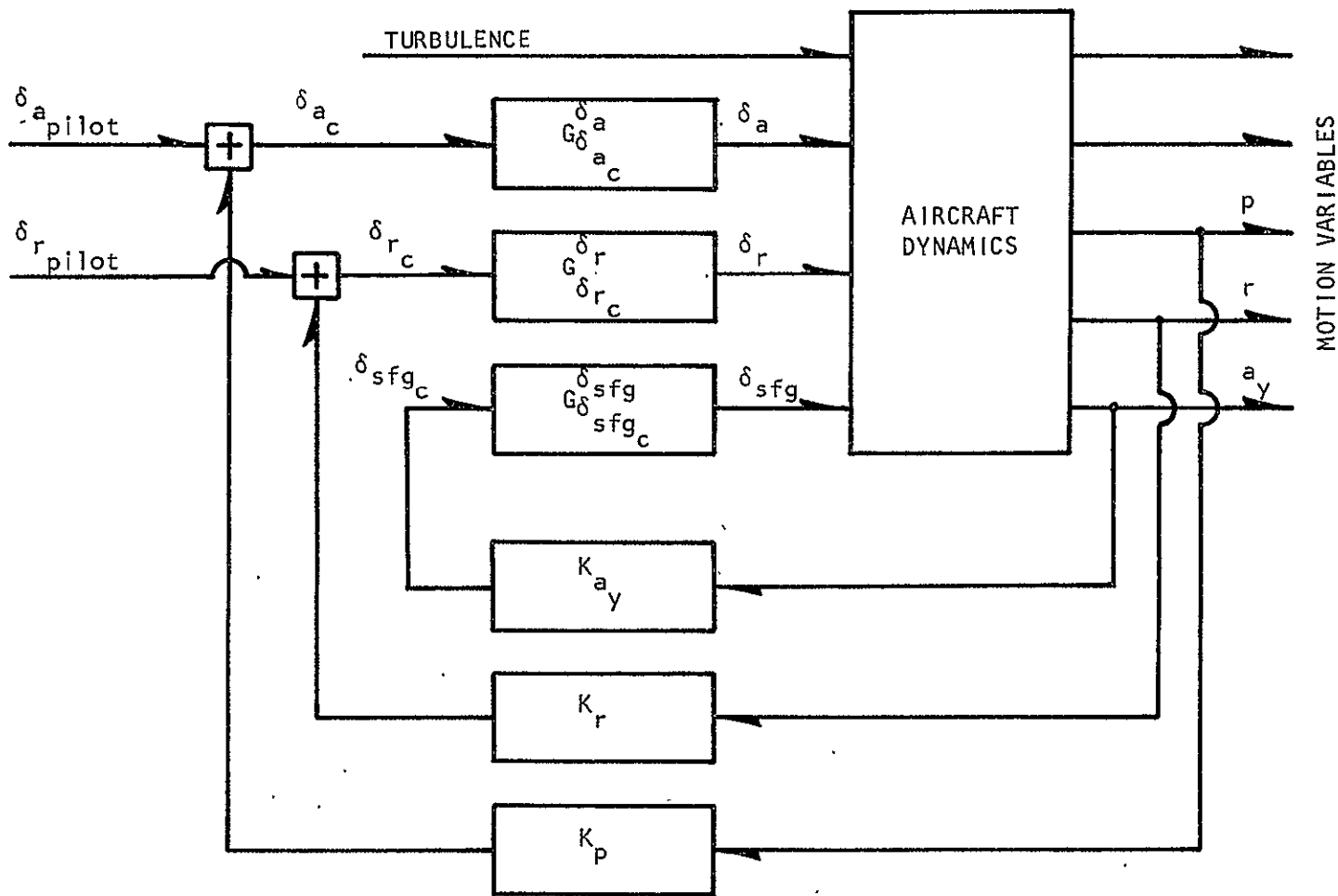


FIGURE 66. S-11 LATERAL RIDE SMOOTHING SYSTEM
 (Design Point: $K_{a_y} = -3.3 \text{ rad/m/sec}^2$, $K_r = 2 \text{ }^\circ/\text{sec}$, $K_p = -1 \text{ }^\circ/\text{sec}$)

TABLE XVI

COMPARISON OF JETSTAR AND STOL LATERAL RIDE SMOOTHING SYSTEMS

	<u>Basic JetStar</u>	<u>RSS-Augmented JetStar</u>	<u>Basic Buffalo</u>	<u>RSS-Augmented Buffalo</u>	<u>Basic S-11</u>	<u>RSS-Augmented S-11</u>
ζ_{dr}	0.045	0.155	0.266	0.710	0.003	0.403
$\omega_{n_{dr}}$	1.36 rad/s	1.20 rad/s	0.89 rad/s	0.83 rad/s	1.01 rad/s	0.67 rad/s
τ_R	0.87 sec	0.61 sec	0.66 sec	0.70 sec	1.37 sec	1.18 sec
$T_{\frac{1}{2}s} (T_2)_s$	418 sec	(37.5) sec	(20.7) sec	11.7 sec	(5.4) sec	14.3 sec
σ_{a_y}	0.0312 g	0.0047 g	0.0214 g	0.0060 g	0.0330 g	0.0054 g
σ_r	2.35 °/sec	1.56 °/sec	1.62 °/sec	1.46 °/sec	2.39 °/sec	2.44 °/sec
$\sigma_{\delta_{sfg}}$	--	7.8 °	--	11.2 °	--	9.3 °
σ_{δ_r}	--	0.92 °	--	1.47 °	--	4.9 °
% reduction σ_{a_y}	--	84.5%	--	72.0%	--	83.6%
% reduction σ_r	--	43.5%	--	9.9%	--	-2%

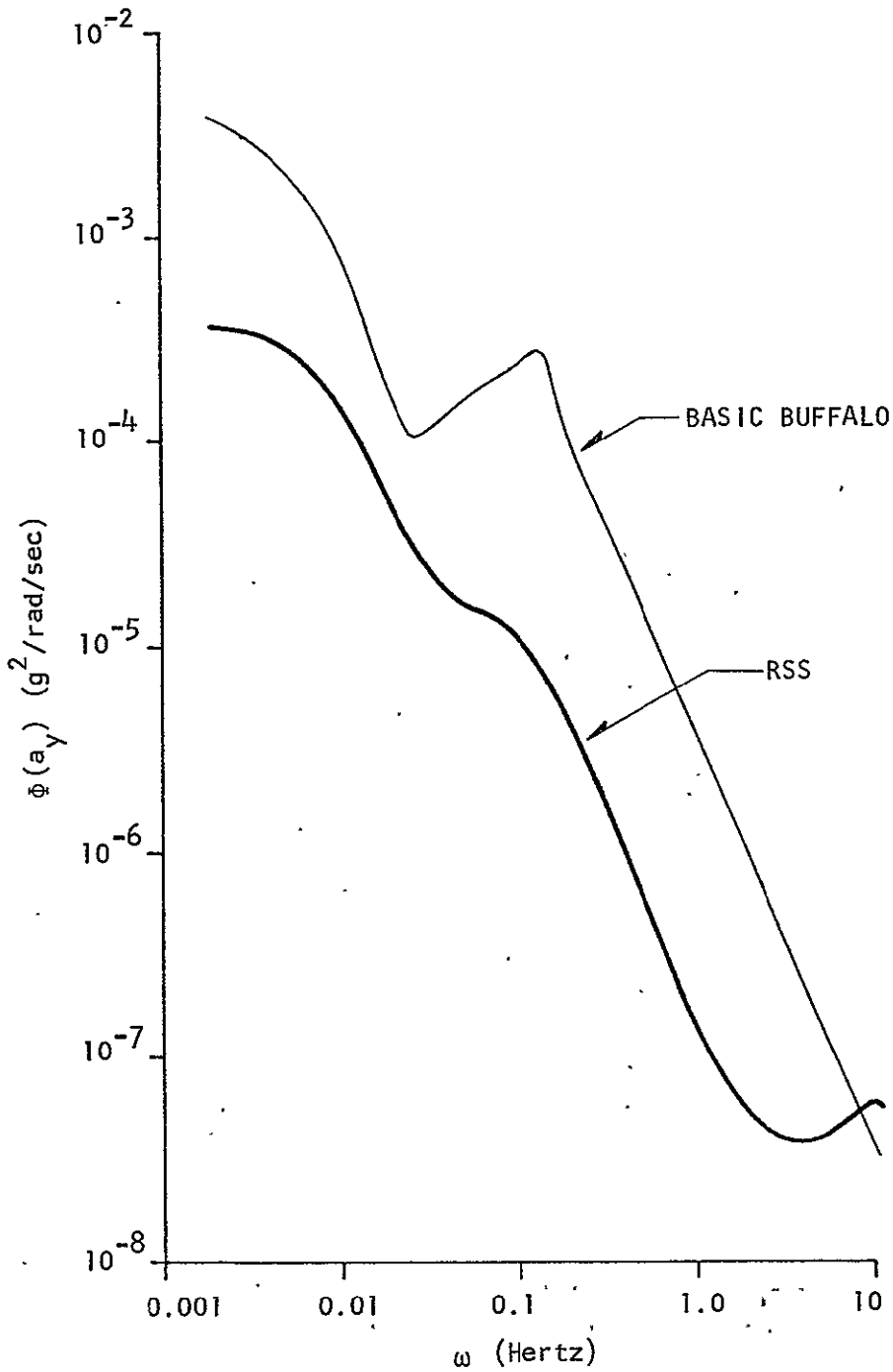


FIGURE 67. COMPARISON OF a_y POWER SPECTRA FOR BASIC AND LATERAL RSS AUGMENTED BUFFALO

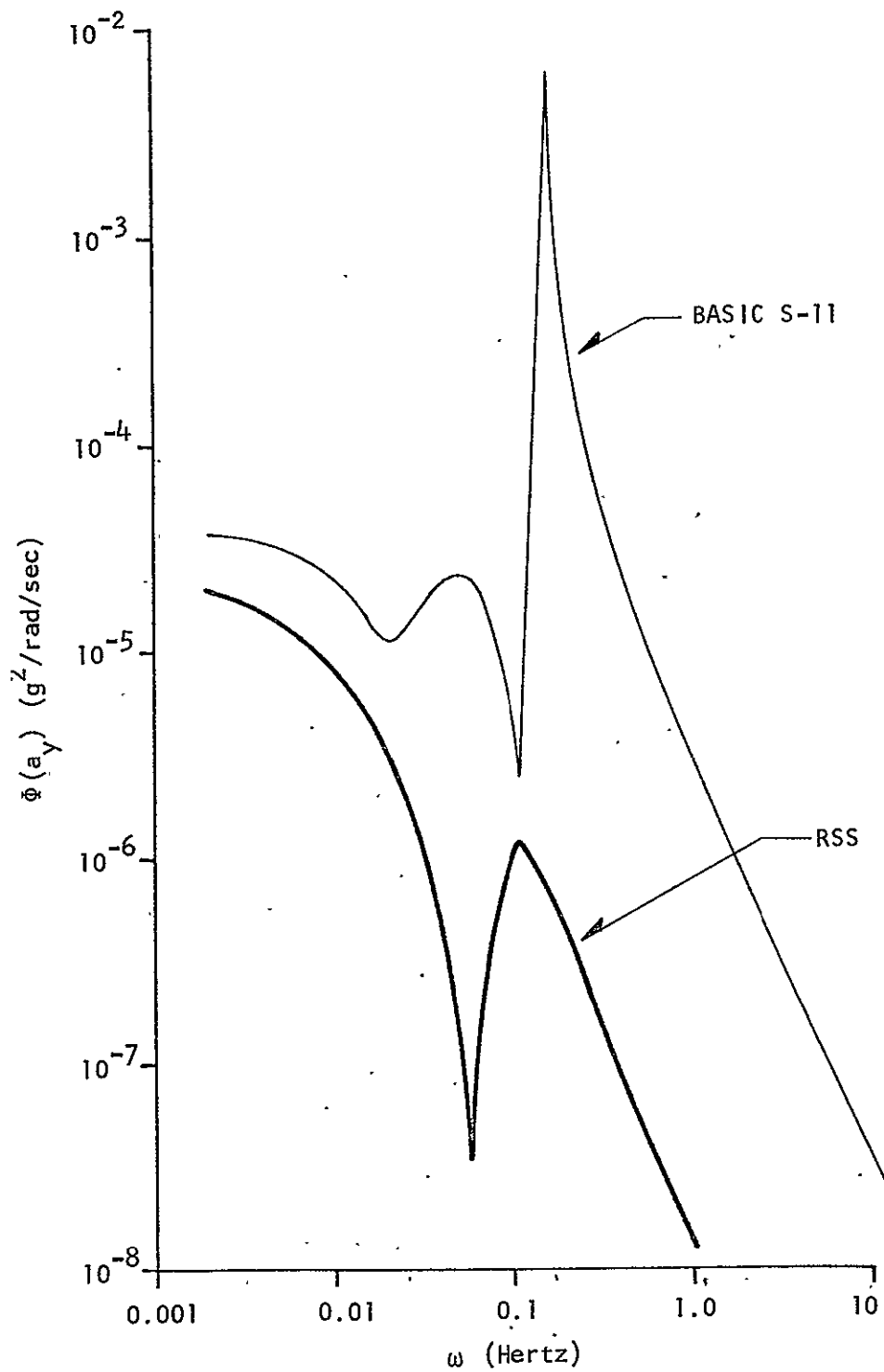


FIGURE 68. COMPARISON OF a_y POWER SPECTRA FOR BASIC AND LATERAL RSS AUGMENTED S-11

frequencies, a uniform reduction in acceleration response to turbulence was achieved. As with the Longitudinal RSS, the root-mean-square acceleration response for all three aircraft with the Lateral RSS engaged was reduced to comparable levels.

Although effective in suppressing the Dutch Roll mode, the yaw damper fails to provide any alleviation of σ_p for the Buffalo, and actually increases σ_p for the S-11. The yaw rate response of both aircraft remains dominated by a low-frequency heading instability which is unaffected by the RSS.

6.2.3 Improvement in Passenger Comfort

The improvement in passenger comfort resulting from the incorporation of a Ride Smoothing System aboard the STOL aircraft operating in the design turbulence environment is evident from predicted comfort ratings:

	<u>Buffalo</u>		<u>S-11</u>	
	<u>Comfort Rating</u>	<u>% of Passengers Satisfied</u>	<u>Comfort Rating</u>	<u>% of Passengers Satisfied</u>
Basic	3.4	69%	5.0	25%
RSS Augmented	2.8	84%	2.7	86%

6.3 Simulator Evaluation of STOL Ride Smoothing System

The simulator handling qualities evaluation of the RSS-augmented STOL aircraft was carried out in the same facility as used for the Jet-Star evaluation. Only the ILS problem was flown by the five evaluation pilots. Three runs were made for each of the aircraft: basic and RSS-augmented configuration in smooth air and RSS-augmented configuration in

moderate turbulence ($\sigma_{wg} \cong 1.2$ m/sec). No evaluation was made of the basic configurations in turbulence since a preliminary run with the S-11 resulted in a Pilot Opinion Rating of 10 (uncontrollable).

The simulated glideslope angle was increased from 3° to $7\frac{1}{2}^{\circ}$ to better simulate a typical STOL approach. The only noticeable effect of the steeper approach angle was to increase the pilot lead required to fly the simulated Buffalo, i.e., upon intercepting the glideslope, power had to be reduced to idle and a rapid pitch-over accomplished. Several of the pilots penalized the Buffalo because of this power/drag characteristic.

Results of the STOL handling qualities evaluation are summarized in Table XVII.

TABLE XVII

AVERAGE COOPER-HARPER PILOT RATINGS

STOL ILS APPROACH TASK

	<u>Longitudinal</u>		<u>Lateral</u>	
	<u>Rating</u>	<u>Standard Deviation</u>	<u>Rating</u>	<u>Standard Deviation</u>
Basic Buffalo	3.2	0.68	4.9	0.81
RSS-Augmented Buffalo	2.9	0.66	5.0	1.45
RSS-Augmented Buffalo in Turbulence	3.3	0.83	5.3	1.15
Basic S-11	*	*	8.5	0.74
RSS-Augmented S-11	3.0	0.00	4.7	1.54
RSS-Augmented S-11 in Turbulence	3.25	0.43	5.9	1.24

*No rating; task dominated by lateral problem.

In light of the aforementioned deficiencies of the STOL configurations with respect to the control parameter n/α , it is somewhat surprising that none of the evaluation pilots reported serious longitudinal handling qualities problems. One pilot did report a slight tendency toward PIO in pitch at the S-11 phugoid frequency.

The simulated lateral characteristics of both aircraft, even with the RSS engaged, however, were clearly unsatisfactory for the ILS tracking task. Three pilots stated that the basic S-11 could be landed only if a visual reference were available. Inadequate heading control and high adverse yaw were cited as the major deficiencies of this aircraft. Several pilots suggested incorporation of a heading/roll attitude command autopilot and aileron rudder interconnect. Heading precision was also cited as the major directional control problem with the Buffalo. Whether this characteristic is in fact representative of the operational aircraft would have to be established in a more extensive investigation.

6.4 Conclusions

Although incorporation of a Ride Smoothing System aboard the selected STOL aircraft would provide substantial improvements in ride quality, the simple systems investigated failed to meet the qualitative handling qualities criteria in terms of pilot opinion rating as set forth in Section 2.3. As was pointed out by the evaluation pilots, a number of elements normally associated with stability augmentation systems (SAS) would have to be incorporated in order to provide adequate handling qualities. Such an integration should not be

difficult. Recall that for both the Buffalo and S-11, the closure of the essential feedback loops $(a_z \rightarrow \delta_f, a_y \rightarrow \delta_{sfg})$ had negligible effect on aircraft dynamics. Reference 44 reports a Stability Augmentation System developed for the S-11 in the landing approach flight phase. An obvious extension of the present research would be an investigation of the compatibility of the proposed Ride Smoothing System with the SAS-augmented S-11.

CHAPTER VII

CONCLUSIONS AND RECOMMENDATIONS

The research reported herein is unique in the sense that the problem of analyzing, synthesizing and evaluating aircraft Ride Smoothing Systems was, for the first time, approached from a comprehensive viewpoint. The multiple criteria that were established, both subjective and objective, precluded the application of optimal control theory. Nevertheless, both Longitudinal and Lateral RSSs were successfully developed and were shown to be applicable to STOL aircraft, suggesting that the solution to the RSS problem is generic.

A significant amount of new information was generated. In particular, the feasibility of employing side force generators to attenuate rigid aircraft response to turbulence was demonstrated theoretically and in simulation. Such systems were shown to be more effective than systems using rudder control alone. Extensive fixed-based simulator experiments provided subjective, qualitative and quantitative data that indicate the improvement in turbulent flight handling qualities made possible by the incorporation of a Ride Smoothing System. The simple analytic models developed for the baseline Ride Smoothing Systems allow significant insight into the effect of individual aerodynamic parameters on the performance of these systems. The constrained "performance index" contours generated by these models, together with the "comfort model," permit a rational approach to the choice of feedback gains. The limited flight data that were generated generally support the theoretical

predictions of RSS performance. Finally, the data presented herein are sufficiently complete to permit independent evaluation and interpretation, thus contributing to the overall data base on Ride Smoothing System characteristics.

As with any broad scope research project, the results of this study suggest as many questions as may have been answered. Different forms of equalization for the various prototype RSS feedback loops should be examined. For comparison purposes, it would be interesting to develop optimal control laws for both the longitudinal and lateral axis control problem. The effectiveness of the proposed RSS should be examined at fuselage locations other than the center of gravity. The gain scheduling that would be required for system operation over the entire flight regime should be established. The interfacing of the RSS and SAS for the STOL configurations should be undertaken. Extension of the simplified analytic models to the STOL configurations should be attempted. Finally, additional flight testing of the proposed RSS would be most desirable.

APPENDIX A

DEFINITION OF STABILITY DERIVATIVES (45)

A.1 Axis Systems

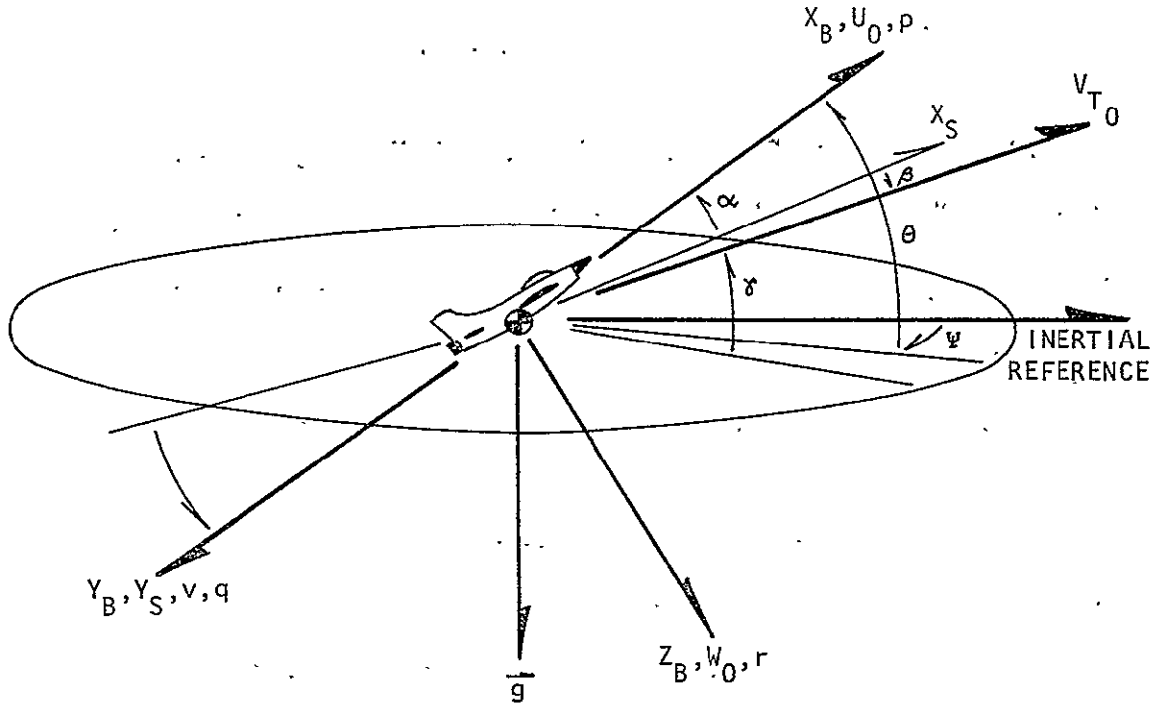


FIGURE 69. AXIS SYSTEMS

X_B, Y_B, Z_B - The Body Axis System consists of a right-handed, orthogonal axes whose origin is fixed at the nominal aircraft center of gravity. Its orientation remains fixed with respect to the aircraft, the X_B and Z_B axes being in the plane of symmetry. The exact alignment of X_B is arbitrary, herein it is taken along the body centerline reference.

X_S, Y_S, Z_S - The Stability Axis System is that particular body axis system for which the X_S axis is coincident with the projection of the total steady-state velocity vector (V_{T0}) on the aircraft's plane of symmetry. Its orientation remains fixed with respect to the aircraft.

A.2 Definition of Nondimensional Stability Derivatives

Nondimensional stability derivatives are defined with respect to body fixed stability axes in standard NASA form (e.g., (46)).

A.3 Transformation of Stability Axis Derivatives to Body Axis

A.3.1 Longitudinal Derivatives

$$C_N = C_L \cos \alpha_0 + C_D \sin \alpha_0$$

$$C_X = C_D \cos \alpha_0 - C_L \sin \alpha_0$$

$$C_{N_\alpha} = C_{L_\alpha} \cos \alpha_0 - C_L \sin \alpha_0 + C_{D_\alpha} \sin \alpha_0 + C_D \cos \alpha_0$$

$$C_{N_{\dot{\alpha}}} = C_{L_{\dot{\alpha}}} \cos \alpha_0$$

$$C_{N_q} = C_{L_q} \cos \alpha_0$$

$$C_{N_M} = C_{L_M} \cos \alpha_0 + C_{D_M} \sin \alpha_0$$

$$C_{N_\delta} = C_{L_\delta} \cos \alpha_0 + C_{D_\delta} \sin \alpha_0$$

$$C_{X\alpha} = C_{D\alpha} \cos \alpha_0 - C_D \sin \alpha_0 - C_{L\alpha} \sin \alpha_0 - C_L \cos \alpha_0$$

$$C_{X\alpha} = -C_{L\alpha} \sin \alpha_0$$

$$C_{Xq} = -C_{Lq} \sin \alpha_0$$

$$C_{X_M} = C_{D_M} \cos \alpha_0 - C_{L_M} \sin \alpha_0$$

$$C_{X\delta} = C_{D\delta} \cos \alpha_0 - C_{L\delta} \sin \alpha_0$$

$$C_m, C_{m_\alpha}, C_{m_\alpha}, C_{m_q}, C_{m_M}, C_{m_\delta} - \text{unchanged}$$

A.3.2 Lateral Derivatives

$$(C_{l_\beta})_B = C_{l_\beta} \cos \alpha_0 - C_{n_\beta} \sin \alpha_0$$

$$(C_{l_p})_B = C_{l_p} \cos^2 \alpha_0 - (C_{l_r} + C_{n_p}) \sin \alpha_0 \cos \alpha_0 + C_{n_r} \sin^2 \alpha_0$$

$$(C_{l_r})_B = C_{l_r} \cos^2 \alpha_0 - (C_{n_r} - C_{l_p}) \sin \alpha_0 \cos \alpha_0 - C_{n_p} \sin^2 \alpha_0$$

$$(C_{l_\delta})_B = C_{l_\delta} \cos \alpha_0 - C_{n_\delta} \sin \alpha_0$$

$$(C_{n_\beta})_B = C_{n_\beta} \cos \alpha_0 + C_{l_\beta} \sin \alpha_0$$

$$(C_{n_p})_B = C_{n_p} \cos^2 \alpha_0 - (C_{n_r} - C_{l_p}) \sin \alpha_0 \cos \alpha_0 - C_{l_r} \sin^2 \alpha_0$$

$$(C_{n_r})_B = C_{n_r} \cos^2 \alpha_0 + (C_{l_r} + C_{n_p}) \sin \alpha_0 \cos \alpha_0 + C_{l_p} \sin^2 \alpha_0$$

$$(C_{n_\delta})_B = C_{n_\delta} \cos \alpha_0 + C_{l_\delta} \sin \alpha_0$$

$$C_{y_\beta}, C_{y_\delta} - \text{unchanged}$$

A.4 Dimensional Stability Derivative Definitions

A.4.1 Longitudinal Derivatives

$$U_0 = V_{T_0} \cos \alpha_0$$

$$W_0 = V_{T_0} \sin \alpha_0$$

$$X_u = \frac{\rho S U_0}{m} \left(-\frac{M}{2} C_{X_M} - C_X + \frac{W_0}{2U_0} C_{X_\alpha} \right)$$

$$X_u^* = X_u + T_u \cos \xi_0$$

$$X_w = \frac{\rho S U_0}{2m} \left[-C_{X_\alpha} - 2 \frac{W_0}{U_0} \left(C_X + \frac{M}{2} C_{X_M} \right) \right]$$

$$X_\delta = -\frac{\rho S V_{T_0}^2}{2m} C_{X_\delta}$$

$$Z_u = \frac{\rho S U_0}{m} \left(-\frac{M}{2} C_{N_M} - C_N + \frac{W_0}{2U_0} C_{N_\alpha} \right)$$

$$Z_u^* = Z_u - T_u \sin \xi_0$$

$$Z_w = \frac{\rho S U_0}{2m} \left[-C_{N_\alpha} - 2 \frac{W_0}{U_0} \left(C_N + \frac{M}{2} C_{N_M} \right) \right]$$

$$Z_{\dot{w}} = -\frac{\rho S \bar{c}}{4m} \frac{U_0}{V_{T0}} C_{N_{\dot{\alpha}}}$$

$$Z_{\delta} = -\frac{\rho S V_{T0}^2}{2m} C_{N_{\delta}}$$

$$M_u = \frac{\rho S \bar{c} U_0}{I_y} \left[\frac{M}{2} C_{m_M} + C_m - \frac{W_0}{2U_0} C_{m_{\dot{\alpha}}} \right]$$

$$M_u^* = M_u + \frac{I_{th}}{I_y} T_u$$

$$M_w = \frac{\rho S \bar{c} U_0}{2I_y} \left[C_{m_{\dot{\alpha}}} + \frac{2W_0}{U_0} \left(C_m + \frac{M}{2} C_{m_M} \right) \right]$$

$$M_{\dot{w}} = \frac{\rho S \bar{c}^2}{4I_y} \frac{U_0}{V_{T0}} C_{m_{\dot{\alpha}}}$$

$$M_q = \frac{\rho S \bar{c}^2 V_{T0}}{4I_y} C_{m_q}$$

$$M_{\delta} = \frac{\rho S \bar{c} V_{T0}^2}{2I_y} C_{m_{\delta}}$$

$$T_u = \frac{1}{am} \frac{\partial T}{\partial M}$$

A.4.2 Lateral Derivatives

$$Y_v = \frac{\rho S V_{T0}}{2m} C_{Y_{\beta}}$$

$$Y_{\delta} = \frac{\rho S V_{T0}^2}{2m} C_{Y_{\delta}}$$

$$Y_{\delta}^* = \frac{1}{V_{T0}} Y_{\delta}$$

$$L_{\beta} = \left(\frac{\rho S V_T^2 b^2}{2 I_x} \right) C_{l_{\beta}}$$

$$L_p = \left(\frac{\rho S V_T b^2}{4 I_x} \right) C_{l_p}$$

$$L_r = \left(\frac{\rho S V_T b^2}{4 I_x} \right) C_{l_r}$$

$$L_{\delta} = \left(\frac{\rho S V_T^2 b^2}{2 I_x} \right) C_{l_{\delta}}$$

$$N_{\beta} = \left(\frac{\rho S V_T^2 b^2}{2 I_z} \right) C_{n_{\beta}}$$

$$N_p = \left(\frac{\rho S V_T b^2}{4 I_z} \right) C_{n_p}$$

$$N_r = \left(\frac{\rho S V_T b^2}{4 I_z} \right) C_{n_r}$$

$$N_{\delta} = \left(\frac{\rho S V_T^2 b^2}{2 I_z} \right) C_{n_{\delta}}$$

$$L_{\beta}' = (L_{\beta} + I_{xz} N_{\beta}/I_x)G$$

$$L_p' = (L_p + I_{xz} N_p/I_x)G$$

$$L_r' = (L_r + I_{xz} N_r/I_x)G$$

$$L_{\delta}' = (L_{\delta} + I_{xz} N_{\delta}/I_x)G$$

$$N_{\beta}' = (N_{\beta} + I_{xz} L_{\beta}/I_z)G$$

$$N_p' = (N_p + I_{xz} L_p / I_z) G$$

$$N_r' = (N_r + I_{xz} L_r / I_z) G$$

$$N_\delta' = (N_\delta + I_{xz} L_\delta / I_z) G$$

where

$$G \equiv \frac{1}{1 - \frac{I_{xz}^2}{I_x I_z}}$$

APPENDIX B

TURBULENCE FILTERS AND INPUT-OUTPUT RELATIONSHIPS

Under the assumptions on the statistical properties of turbulence cited in Section 2.1, it has been shown (47) that the power spectral density of any aircraft system output quantity of interest, $\Phi_0(\omega)$, can be related to the input power spectral density $\Phi_i(\omega)$ through $|G(\omega)|^2$, the square of the modulus of the appropriate transfer function

$$\Phi_0(\omega) = |G(\omega)|^2 \Phi_i(\omega) \quad (\text{B.1})$$

at a given unit sinusoidal frequency ω . The root-mean-square value of the output, σ , is then given by the integral of the output power spectral density taken over all spectral frequencies:

$$\sigma = \left[\int_0^{\infty} \Phi_0(\omega) d\omega \right]^{\frac{1}{2}} . \quad (\text{B.2})$$

The root-mean-square value, identical to the variance for a process with zero mean, is one of the most useful quantities in describing the magnitude of response. The average frequency of exceeding a peak response level can also be related to the power spectral density.

Formulations for the power spectral density of the components of atmospheric turbulence are given in Reference 32. Two forms are generally used-- the Dryden and Von Karman. Although the Von Karman description has been shown to more closely match actual measured spectra, the Dryden form has the advantage of being spectrally

factorable. Thus, the transfer function, expressed in Laplace notation, for filtering a white-noise input is available. For this reason, an approximation to the Dryden form is used in this study. The turbulence transfer functions are defined as follows:

$$G_{\Delta}^{wg} = \sigma_w \sqrt{\frac{L_w}{\pi V_{T0}}} \frac{1 + \left(\frac{\sqrt{3} L_w}{V_{T0}}\right) s}{\left(1 + \frac{L_w}{V_{T0}} s\right)^2}, \quad (B.3)$$

$$G_{\Delta}^{qg} = G_{\Delta}^{wg} \cdot \frac{\left(\frac{1}{V_{T0}}\right) s}{\left(1 + \frac{4b}{\pi V_{T0}} s\right)}, \quad (B.4)$$

$$G_{\Delta}^{\beta g} = \left(\frac{1}{V_{T0}}\right) \sigma_{vg} \sqrt{\frac{L_v}{\pi V_{T0}}} \frac{1 + \left(\frac{\sqrt{3} L_v}{V_{T0}}\right) s}{\left(1 + \frac{L_v}{V_{T0}} s\right)^2}, \quad (B.5)$$

$$G_{\Delta}^{rg} = -G_{\Delta}^{\beta g} \cdot \frac{s}{1 + \left(\frac{3b}{\pi V_{T0}}\right) s}, \quad (B.6)$$

$$G_{\Delta}^{pg} = \sigma_w \sqrt{\frac{1}{L_w V_{T0}}} \frac{\sqrt{0.8 \left(\frac{\pi L_w}{4b}\right)^{1/3}}}{1 + \left(\frac{4b}{\pi V_{T0}}\right) s}, \quad (B.7)$$

where

L_w, L_v are the characteristic gust lengths for vertical and lateral turbulence fields, respectively,

b is the reference wing span of the aircraft, and

V_{T0} is the total steady-state velocity of the aircraft.

Note that the expressions for q_g , r_g , p_g are strictly valid only for very low frequencies. For clear air turbulence, at altitudes above 533 meters (1750 feet), L_v and L_w are taken equal to 533 meters (1750 feet). For lower altitudes, the suggested values are $L_w = h$ meters and $L_v = 36.2 h^{1/3}$ meters. The probability of exceeding a given σ_{wg} once turbulence has been encountered is given by

$$\hat{P}(\sigma_w) = \exp\left(-\frac{1}{2} \frac{\sigma_w^2}{c^2}\right), \quad (\text{B.8})$$

where $c = 0.7$ m/sec (2.3 ft/sec).

Finally, the following similarity relationship is given in Reference 32:

$$\frac{\sigma_v^2}{L_v} = \frac{\sigma_w^2}{L_w} \quad (\text{B.9})$$

APPENDIX C

JETSTAR DATA

JetStar Power Approach Configuration

S	= 50.4 m ² (542.5 ft ²)
\bar{c}	= 3.3 m (10.9 ft)
b	= 16.4 m (53.75 ft)
V _{T0}	= 72.1 m/sec (236.7 ft/sec)
h	= 305 m (1000 ft)
W	= 142300 N (32,000 lb)
I _x	= 84900 kg-m ² (62400 slug-ft ²)
I _y	= 272000 kg-m ² (200000 slug-ft ²)
I _z	= 204000 kg-m ² (150000 slug-ft ²)
I _{xz}	= 750 kg-m ² (550 slug-ft ²)
W/S	= 2824 N/m ² (59.0 lb/ft ²)

Dimensional Stability Derivatives

(X_B axis aligned with fuselage reference line)

α ₀	= 11°
θ ₀	= 11°
C _{L0}	= 0.88
X _u *	= -0.0058 1/sec
X _w	= 0.1040 1/sec
X _w *	= 0.0
X _q	= 0.0 m/sec (0.0 ft/sec)
X _{δ_e}	= 1.0298 m/sec ² /rad (3.3787 ft/sec ² /rad)
X _{δ_f}	= 0.3877 m/sec ² /rad (1.2719 ft/sec ² /rad)

$$\begin{aligned}
Z_u^* &= -0.0991 \text{ 1/sec} \\
Z_w &= -0.9192 \text{ 1/sec} \\
Z_{\dot{w}} &= 0.0 \\
Z_q &= 0.0 \text{ m/sec (0.0 ft/sec)} \\
Z_{\delta_e} &= -5.2981 \text{ m/sec}^2/\text{rad (-17.3823 ft/sec}^2/\text{rad)} \\
Z_{\delta_f} &= -1.9944 \text{ m/sec}^2/\text{rad (-6.5434 ft/sec}^2/\text{rad)} \\
M_u^* &= 0.0062 \text{ 1/m-sec (0.0019 1/ft-sec)} \\
M_w &= -0.0266 \text{ 1/m-sec (-0.0081 1/ft-sec)} \\
M_{\dot{w}} &= 0.0 \text{ 1/m (0.0 1/ft)} \\
M_q &= -0.9180 \text{ 1/sec} \\
M_{\delta_e} &= -2.5798 \text{ 1/sec}^2 \\
M_{\delta_f} &= -0.1131 \text{ 1/sec}^2 \\
Y_v &= -0.1226 \text{ 1/sec} \\
Y_{\delta_a}^* &= -0.0061 \text{ 1/sec} \\
Y_{\delta_r}^* &= 0.0473 \text{ 1/sec} \\
Y_{\delta_{sfg}}^* &= 0.0167 \text{ 1/sec} \\
L_{\beta}^{\prime} &= -4.0765 \text{ 1/sec}^2 \\
L_p^{\prime} &= -0.9763 \text{ 1/sec} \\
L_r^{\prime} &= 0.3842 \text{ 1/sec} \\
L_{\delta_a}^{\prime} &= 1.3736 \text{ 1/sec}^2 \\
L_{\delta_r}^{\prime} &= 0.6888 \text{ 1/sec}^2 \\
L_{\delta_{sfg}}^{\prime} &= 0.2681 \text{ 1/sec}^2 \\
N_{\beta}^{\prime} &= 0.8736 \text{ 1/sec}^2 \\
N_p^{\prime} &= -0.1655 \text{ 1/sec} \\
N_r^{\prime} &= -0.1617 \text{ 1/sec}
\end{aligned}$$

$$N_{\delta_a} = 0.0932 \text{ 1/sec}^2$$

$$N_{\delta_r} = -0.6051 \text{ 1/sec}^2$$

$$N_{\delta_{sfg}} = 0.0493 \text{ 1/sec}^2$$

Surface Actuator Dynamics

$$G_{\delta_e} = \frac{1}{(1 + s/100)^2}$$

$$G_{\delta_{dlf_c}} = \frac{1}{(1 + s/40)^2}$$

$$G_{\delta_{a_c}} = \frac{1}{(1 + s/50)^2}$$

$$G_{\delta_{r_c}} = \frac{1}{(1 + \frac{2(0.25)}{27} s + \frac{s^2}{27^2})}$$

$$G_{\delta_{sfg_c}} = \frac{1}{(1 + s/30)^2}$$

Maximum Deflections and Rates for Force Control Surfaces

Direct Lift Flaps: $\delta_{\max} = \pm 27^\circ$; $\dot{\delta}_{\max} = \pm 52^\circ/\text{sec}$

Side Force Generators: $\delta_{\max} = \pm 24^\circ$; $\dot{\delta}_{\max} = \pm 37^\circ/\text{sec}$

APPENDIX D

FORMULATION OF TRANSFER FUNCTIONS FOR MULTI-LOOP FEEDBACK CONTROL SYSTEMS

The theoretical framework for expanding the transfer function formulation to include multi-loop control feedback loops is presented by McRuer et al. For negative feedback systems, the rules are as follows:

1. The effective numerator is equal to:
 - a. The open loop numerator;
 - b. Plus the sum of all the feedback transfer functions, each one multiplied by the appropriate coupling numerator;
2. The effective denominator is equal to:
 - a. The open-loop denominator;
 - b. Plus the sum of all the feedback transfer functions, each one multiplied by the appropriate numerator;
 - c. Plus the sum of all the feedback transfer functions taken two at a time, each pair multiplied by the appropriate coupling numerator. (Reference 48, page 95.)

Thus, for two loops closed (e.g., $q_1 \rightarrow \delta_1$, $q_2 \rightarrow \delta_2$), the effective transfer function for output q_i due to input of δ_j is written as:

$$G_{\delta_j}^{q_i} = \frac{N_{\delta_j}^{q_i} + G_{q_1}^{\delta_1} N_{\delta_j \delta_1}^{q_i q_1} + G_{q_2}^{\delta_2} N_{\delta_j \delta_2}^{q_i q_2}}{\Delta + G_{q_1}^{\delta_1} N_{\delta_1}^{q_1} + G_{q_2}^{\delta_2} N_{\delta_2}^{q_2} + G_{q_1}^{\delta_1} G_{q_2}^{\delta_2} N_{\delta_1 \delta_2}^{q_1 q_2}}, \quad (D.1)$$

where Δ is the open-loop characteristic denominator. Numerators of the form $N_{\delta_j}^{q_i}$ are formed by simply applying Cramer's rule to the aircraft equations of motion written in the Laplace variable s (i.e., replacing the column corresponding to q_i by the input vector δ_j). Coupling numerators of the form $N_{\delta_j \delta_k}^{q_i q_\ell}$ are formed by computing the determinant of the matrix of the aircraft equations of motion with the two columns corresponding to q_i and q_ℓ replaced by the control vectors corresponding to δ_j and δ_k simultaneously. If $\delta_j = \delta_k$ or $q_i = q_\ell$, the determinant is defined as zero.

For the Longitudinal Ride Smoothing System, with unequalized feedbacks $a_z \rightarrow \delta_f$, $\theta \rightarrow \delta_e$, the transfer function of interest is:

$$G_{w_g}^{a_z} = \frac{N_{w_g}^{a_z} - K_\theta N_{w_g}^{a_z \theta} \delta_e}{\Delta_1 - K_{a_z} N_{\delta_f}^{a_z} - K_{a_z} N_{\delta_e}^\theta + K_{a_z} K_\theta N_{\delta_f}^{a_z \theta} \delta_e}, \quad (D.2)$$

where $K_{a_z} > 0$ and $K_\theta > 0$.

For the Lateral Ride Smoothing System, with unequalized feedbacks $a_y \rightarrow \delta_{sfg}$, $r \rightarrow \delta_r$, the transfer function of interest is:

$$G_{\beta_g}^{a_y} = \frac{N_{\beta_g}^{a_y} - K_r N_{\beta_g}^{a_y r} \delta_r}{\Delta_2 + K_{a_y} N_{\delta_{sfg}}^{a_y} - K_r N_{\delta_r}^r - K_{a_y} K_r N_{\delta_{sfg}}^{a_y r} \delta_r}, \quad (D.3)$$

where $K_{ay} > 0$ and $K_r > 0$.

Expressions for Δ_1 , N_{wg}^{az} , $N_{\delta f}^{az}$, $N_{\delta e}^{\theta}$, Δ_2 , $N_{\delta sfg}^{ay}$, $N_{\delta r}^r$ can be found in Reference 46.

For the JetStar aerodynamics, the following coupling numerators were derived:

$$\begin{aligned}
 N_{wg\delta e}^{az\theta} &= s^2 \{ M_{\delta e} Z_w - M_w Z_{\delta e} \} \\
 &+ s \{ M_{\delta e} (X_w Z_u^* - X_u Z_w^*) \\
 &+ X_{\delta e} (M_u Z_w^* - M_w Z_u^*) \\
 &+ Z_{\delta e} (M_w X_u^* - M_u X_w^*) \} \quad (D.4)
 \end{aligned}$$

$$\begin{aligned}
 N_{\delta f\delta e}^{az\theta} &= s^2 \{ M_{\delta e} Z_{\delta f} - M_{\delta f} Z_{\delta e} \} \\
 &+ s \{ M_{\delta f} (X_u Z_{\delta e}^* - X_{\delta e} Z_u^*) \\
 &+ X_{\delta f} (M_{\delta e} Z_u^* - M_u Z_{\delta e}^*) \\
 &+ Z_{\delta f} (M_u X_{\delta e}^* - M_{\delta e} X_u^*) \} \quad (D.5)
 \end{aligned}$$

$$\begin{aligned}
 N_{\beta g\delta r}^{ayr} &= s^3 V_{T0} \{ N_{\delta r} Y_v - N_{\beta} Y_{\delta r}^* \} \\
 &+ s^2 V_{T0} \{ Y_v (L_{\delta r} N_p^* - L_p N_{\delta r}^*) + Y_{\delta r}^* (L_p N_{\beta}^* - L_{\beta} N_p^*) \}
 \end{aligned}$$

(D.6) 183

$$\begin{aligned}
N_{\delta_{sfg}}^{ayr} = & s^3 V_{T0} \{N_{\delta_r} 'Y_{\delta_{sfg}} * - N_{\delta_{sfg}} 'Y_{\delta_r} *\} \\
& + s^2 V_{T0} \{Y_{\delta_r} *(L_p 'N_{\delta_{sfg}} ' - L_{\delta_{sfg}} 'N_p ')\} \\
& + Y_{\delta_{sfg}} *(L_{\delta_r} 'N_p ' - L_p 'N_{\delta_r} ')\} \\
& + s V_{T0} \sin \theta_0 \{Y_v (L_{\delta_{sfg}} 'N_{\delta_r} ' - L_{\delta_r} 'N_{\delta_{sfg}} ')\} \\
& + Y_{\delta_r} *(L_{\beta} 'N_{\delta_{sfg}} ' - L_{\delta_{sfg}} 'N_{\beta} ')\} \\
& + Y_{\delta_{sfg}} *(L_{\delta_r} 'N_{\beta} ' - L_{\beta} 'N_{\delta_r} ')\} \\
& + g \cos \theta_0 \{Y_v (L_{\delta_{sfg}} 'N_{\delta_r} ' - L_{\delta_r} 'N_{\delta_{sfg}} ')\} \\
& + Y_{\delta_r} *(L_{\beta} 'N_{\delta_{sfg}} ' - L_{\delta_{sfg}} 'N_{\beta} ')\} \\
& + Y_{\delta_{sfg}} *(L_{\delta_r} 'N_{\beta} ' - L_{\beta} 'N_{\delta_r} ')\}. \tag{D.7}
\end{aligned}$$

The handling qualities parameter n/α is defined as the steady-state normal acceleration change per unit change in angle of attack for an incremental elevator deflection at constant speed (36). This factor, written in terms of the dimensional stability derivatives defined previously, is expressed as:

$$\frac{n}{\alpha} \equiv - \frac{U_0 \hat{N}_{\delta_e}^{az'}(s)}{g \hat{N}_{\delta_e}^{w'}(s)} \quad (\text{g/rad}) \tag{D.8}$$

evaluated at $s \equiv 0$ (45). The notation \hat{N} implies that the short-period approximation is used to evaluate the above transfer functions. From the rules given, it follows that:

$$\hat{N}_{\delta_e}^{a_z'} = \hat{N}_{\delta_e}^{a_z} , \quad (D.9)$$

$$\hat{N}_{\delta_e}^{w'} = \hat{N}_{\delta_e}^w - G_{a_z}^{\delta_f} N_{\delta_e \delta_f}^{w a_z} , \quad (D.10)$$

where

$$\hat{N}_{\delta_e}^{a_z'} = g \sin \theta_0 (M_w Z_{\delta_e} - M_{\delta_e} Z_w) \quad (D.11)$$

$$\hat{N}_{\delta_e}^w = -g \sin \theta_0 M_{\delta_e} \quad (D.12)$$

$$\hat{N}_{\delta_e \delta_f}^{w a_z} = g \sin \theta_0 (M_{\delta_f} Z_{\delta_e} - M_{\delta_e} Z_{\delta_f}) . \quad (D.13)$$

Thus,

$$\frac{n}{\alpha} = - \frac{U_0}{g} \left\{ \frac{M_w Z_{\delta_e} - M_{\delta_e} Z_w}{-M_{\delta_e} - G_{a_z}^{\delta_f} (M_{\delta_f} Z_{\delta_e} - M_{\delta_e} Z_{\delta_f})} \right\} \quad (\text{g/rad}) \quad (D.14)$$

For the JetStar

$$M_w Z_{\delta_e} \ll M_{\delta_e} Z_w , \text{ and} \quad (D.15)$$

$$M_{\delta_f} Z_{\delta_e} \ll M_{\delta_e} Z_{\delta_f} . \quad (D.16)$$

APPENDIX E

STOL DATA

Power Approach Configuration

	<u>Buffalo</u>	<u>S-11</u>
S	= 87.8 m ² (945 ft ²)	55.7 m ² (600 ft ²)
\bar{c}	= 3.1 m (10.3 ft)	3.0 m (9.8 ft)
b	= 29.3 m (96.0 ft)	20.2 m (66.2 ft)
V _{T0}	= 38.6 m/sec (126.5 ft/sec)	36.0 m/sec (118.2 ft/sec)
h	= 305 m (1000 ft)	305 m (1000 ft)
W	= 145400 N (32683 lb)	213500 N (48000 lb)
I _x	= 375800 kg-m ² (276300 slug-ft ²)	289000 kg-m ² (213000 slug-ft ²)
I _y	= 303400 kg-m ² (223100 slug-ft ²)	315000 kg-m ² (232500 slug-ft ²)
I _z	= 625500 kg-m ² (459900 slug-ft ²)	546000 kg-m ² (402500 slug-ft ²)
I _{xz}	= 40100 kg-m ² (29500 slug-ft ²)	42200 kg-m ² (31150 slug-ft ²)
W/S	= 1656 N/m ² (34.6 lb/ft ²)	3833 N/m ² (80 lb/ft ²)

Dimensional Stability Derivatives

(X_B axis aligned with fuselage reference line)

	<u>Buffalo</u>	<u>S-11</u>
α ₀	= -2.4°	4.9°
θ ₀	= -2.4°	4.9°
C _{L0}	= 1.85	4.79
X _u *	= -0.0859 1/sec	-0.0200 1/sec
X _w	= 0.1396 1/sec	0.0935 1/sec
X _w *	= -0.00035	0.0
X _q	= 0.0 m/sec (0.0 ft/sec)	0.0 m/sec (0.0 ft/sec)

	<u>Buffalo</u>	<u>S-11</u>
$X_{\delta e}$	= 0.0 m/sec ² /rad (0.0 ft/sec ² /rad)	0.8869 m/sec ² /rad (2.9098 ft/sec ² /rad)
$X_{\delta f}$	= -2.2855 m/sec ² /rad (-7.4985 ft/sec ² /rad)	-1.8745 m/sec ² /rad (6.1500 ft/sec ² /rad)
Z_u^*	= -0.5503 1/sec	-0.5055 1/sec
Z_w	= -0.8216 1/sec	-0.4829 1/sec
$Z_{\dot{w}}$	= -0.0083	0.0
Z_q	= -1.7774 m/sec (-5.8313 ft/sec)	0.0 m/sec (0.0 ft/sec)
$Z_{\delta e}$	= -3.0533 m/sec ² /rad (-10.0175 ft/sec ² /rad)	-10.5619 m/sec ² /rad (-34.6519 ft/sec ² /rad)
$Z_{\delta f}$	= -5.7892 m/sec ² /rad (-18.9935 ft/sec ² /rad)	-2.5452 m/sec ² /rad (-8.3504 ft/sec ² /rad)
M_u^*	= 0.0023 1/m-sec (0.00069 1/ft-sec)	0.00062 1/m-sec (0.00019 1/ft-sec)
M_w	= -0.0539 1/m-sec (-0.01644 1/ft-sec)	-0.0073 1/m-sec (-0.002238 1/ft-sec)
$M_{\dot{w}}$	= -0.0055 1/m (-0.001678 1/ft)	0.0 1/m (0.0 1/ft)
M_q	= -1.3817 1/sec	-0.9014 1/sec
$M_{\delta e}$	= -2.0152 1/sec ²	-1.4203 1/sec ²
$M_{\delta f}$	= -0.02612 1/sec ²	0.0276 1/sec ²
Y_v	= -0.1577 1/sec	-0.1600 1/sec
$Y_{\delta a}^*$	= 0.000194 1/sec	-0.00551 1/sec
$Y_{\delta r}^*$	= 0.0570 1/sec	0.0349 1/sec
$Y_{\delta sfg}^*$	= 0.03133 1/sec	0.03354 1/sec
L_{β}^i	= -0.7881 1/sec ²	-0.9411 1/sec ²
L_p^i	= -1.4553 1/sec	-0.3533 1/sec
L_r^i	= 1.1771 1/sec	0.6986 1/sec

	<u>Buffalo</u>	<u>S-11</u>
$L_{\delta_a}^i$	$= 0.3138 \text{ 1/sec}^2$	0.7476 1/sec^2
$L_{\delta_r}^i$	$= 0.2776 \text{ 1/sec}^2$	0.2116 1/sec^2
$L_{\delta_{sfg}}^i$	$= 0.0 \text{ 1/sec}^2$	0.0 1/sec^2
N_{β}^i	$= 0.4590 \text{ 1/sec}^2$	0.6372 1/sec^2
N_p^i	$= -0.1988 \text{ 1/sec}$	-0.1389 1/sec
N_r^i	$= -0.2985 \text{ 1/sec}$	-0.0957 1/sec
$N_{\delta_a}^i$	$= 0.0133 \text{ 1/sec}^2$	0.1583 1/sec^2
$N_{\delta_r}^i$	$= -0.6527 \text{ 1/sec}^2$	-0.3647 1/sec^2
$N_{\delta_{sfg}}^i$	$= 0.0 \text{ 1/sec}^2$	0.0 1/sec^2

REFERENCES

1. Phillips, William H.: Gust Alleviation, in "Performance and Dynamics of Aerospace Vehicles." NASA Langley Research Center. NASA SP-258, 1971, pp. 521-530, 548.
2. Zbrozek, F.; Smith, K. W.; and White, D.: Preliminary Report on a Gust Alleviator Investigation on a Lancaster Aircraft. Reports and Memoranda No. 2972, British A.R.C., August 1953.
3. Zbrozek, F. K. Theoretical Analysis of a Gust Alleviator Used on a Lancaster Aircraft and Comparison with Experiment. RAE Report No. AERO 2645, January 1961.
4. Hirsch, R. L'Absorption des Rafales sur Avions et Résultats des Essais en Vol d'un Appareil Experimental. Doc-Air-Espace, no. 105, July 1967, pp. 41-56.
5. Phillips, William H.; and Kraft, C. C., Jr.: Theoretical Study of Some Methods for Increasing the Smoothness of Flight Through Rough Air. NACA Technical Note 2416, July 1951.
6. Kraft, Christopher C., Jr.; and Assadourian, A.: Experimental Study of an Angle-of-Attack Vane Mounted Ahead of the Nose of an Airplane for Use as a Sensing Device for an Acceleration Alleviator. NACA Technical Note 2415, February 1951.
7. Boucher, Robert W.; and Kraft, C. C., Jr.: Analysis of a Vane-Controlled Gust-Alleviation System. NACA Technical Note 3597, April 1956.
8. Kraft, Christopher C., Jr.: Initial Results of a Flight Investigation of a Gust-Alleviation System. NACA Technical Note 3612, April 1956.
9. Hunter, Paul A.; Kraft, C. C., Jr.; and Alford, W. L.: A Flight Investigation of an Automatic Gust-Alleviation System in a Transport Airplane. NASA TN D-532, January 1961.
10. Schott, Russell L.; and Hamer, H. A.: Flight Investigation of Some Effects of a Vane-Controlled Gust-Alleviation System on the Wing and Tail Loads of a Transport Airplane. NASA TN D-643, January 1961.
11. Barker, L. Keith; and Sparrow, G. W.: Analysis of Effects of Spanwise Variations of Gust Velocity on a Vane-Controlled Gust-Alleviation System. NASA TN D-6126, April 1971.
12. Barker, L. Keith: Effects of Spanwise Variation of Gust Velocity on Alleviation System Designed for Uniform Gust Velocity Across Span. NASA TN D-6346, June 1971.

13. Barker, L. Keith; Crawford, D. J.; and Sparrow, G. W.: Effect of Limited Amplitude and Rate of Flap Motion on Vane-Controlled Gust-Alleviation System. NASA TN D-6723, March 1972.
14. Oehman, Waldo I.: Analytical Study of the Performance of a Gust Alleviation System for a STOL Airplane. NASA TN D-7201, 1973.
15. Phillips, William H.: Study of a Control System to Alleviate Aircraft Response to Horizontal and Vertical Gusts. NASA TN D-7278, December 1973.
16. Oehman, Waldo I.: Analytical Study of the Performance of a Gust Alleviation System with a Vane Sensor. NASA TN D-7431, February 1974.
17. Tobak, Murray: On the Minimization of Airplane Responses to Random Gusts. NACA Technical Note 3290, October 1957.
18. Coupry, Gabriel: Some Results on Gust Alleviation, in "Proceedings, Royal Aeronautical Society, International Conference on Atmospheric Turbulence, London, England," May 18-21, 1971. (A71-29785)
19. Tsumura, Toshihiro; Nakagawa, K.; and Murotsu, Y. Investigation of Gust-Alleviation System for Transport Airplanes. Osaka Prefecture University Bulletin, Series A, Engineering and Natural Sciences, vol. 14, no. 2, 1965, pp. 59-80.
20. Nakagawa, Kenji; Murotsu, Y.; and Fujiwara, N.: The Optimization of Airplane Gust-Alleviation System. Osaka Prefecture University Bulletin, Series A, Engineering and Natural Sciences, vol. 15, no. 2, 1966, pp. 35-48.
21. Holloway, R. B.; Thompson, G. O.; and Rohling, W. J.: Prospects for Low Wing-Loading STOL Transports with Ride Smoothing. AIAA J. of Aircraft, vol. 9, no. 8, August 1972, pp. 525-530.
22. Gordon, C. K.; and Dodson, R. O.: STOL Ride Control Feasibility Study--Technical Report. NASA CR-2276, December 1972.
23. Hess, Ronald: An Application of Optimal Stochastic Control Theory to the Problem of Aircraft Gust Alleviation. Ph.D. Dissertation, University of Cincinnati, College of Engineering, July 1970.
24. Clement, Russell Lee: A Parameter Optimization to Aircraft Gust Alleviation. M.S. (A.E.) Thesis, Naval Postgraduate School, March 1972.
25. Hess, Ronald A.: Some Results of Suboptimal Gust Alleviation. AIAA J. of Aircraft, vol. 9, no. 5, May 1972, pp. 380-381.

26. McClean, R.: The Optimization of an Autopilot for an Airplane Subjected to Random Atmospheric Turbulence. UTIA Technical Note No. 45, University of Toronto, Institute of Aerophysics, November 1960.
27. Hiff, K. W.: Identification and Stochastic Control with Application to Flight Control in Turbulence. Ph.D. Dissertation, University of California at Los Angeles; UCLA-ENG-7340, May 1973.
28. Swaim, Robert L.: Aircraft Elastic Mode Control. AIAA J. of Aircraft, vol. 8, no. 2, February 1971, pp. 65-71.
29. Smith, Ralph E.; Lum, E. L.; and Yamamoto, T. G.: Application of Linear Optimal Theory to Control of Flexible Aircraft Ride Qualities. AFFDL-TR-67-136, Air Force Flight Dynamics Laboratory, January 1968.
30. Morris, R. L.; Hanke, C. R.; Pasley, L. H.; and Rohling, W. J.: The Influence of Wing Loading on Turbofan Powered-STOL Transports with and without Externally Blown Flaps. NASA CR-2320, November 1973.
31. McRuer, Duane; Ashkenas, Irving; and Graham, Dunstan. Aircraft Dynamics and Automatic Control. Naval Air Systems Command, Department of the Navy, Washington, D.C., August 1968. Chapter 4: Vehicle Equations of Motion.
32. Chalk, C. R.; Neal, T. P.; Harris, T. M.; Pritchard, F. E.; and Woodcock, R. J.: Background Information and User Guide for MIL-F-8785B(ASG), Military Specification, Flying Qualities of Piloted Airplanes. AFFDL-TR-69-72, Air Force Flight Dynamics Laboratory, 1969. Section 3.7, Atmospheric Disturbances.
33. Pratt, Kermit G.: Response of Flexible Airplanes to Atmospheric Turbulence, in "Performance and Dynamics of Aerospace Vehicles." NASA Langley Research Center. NASA-SP-258, 1971, pp. 450-460.
34. Stone, Ralph W., Jr.: Ride Quality Overview, in "Symposium on Vehicle Ride Quality." NASA-TM X-2620, October 1972.
35. Jacobson, Ira D.; and Richards, L. G.: Ride Quality Evaluation II: Modelling of Airline Passenger Comfort. STOL Memorandum Report 403217, Dept. of Engineering Science and Systems, Univ. of Virginia, Charlottesville, December 1974.
36. Anonymous: Military Specification--Flying Qualities of Piloted Airplanes. MIL-F-8785B(ASG), August 7, 1965.
37. Barnes, A. G.: C.S.A.S. Design for Good Handling Qualities in Turbulence, in "Flight in Turbulence." AGARD Conference Proceedings No. 140, Paper No. 21, May 1973.

38. Cooper, G. E.; and Harper, R. P., Jr.: The Use of Pilot Rating in the Evaluation of Aircraft Handling Qualities. NASA TN D-5153, April 1969.
39. Stapleford, R. L.; McRuer, D. T.; Hoffman, L. G.; and Teper, G. L.: A Practical Optimization Design Procedure for Stability Augmentation Systems. AFFDL-TR-70-11, Air Force Flight Dynamics Laboratory, 1970.
40. Clark, Daniel C.; and Kroll, John: General Purpose Airborne Simulator--Conceptual Design Report. NASA CR-544, August 1966.
41. Musick, R. O.; and Wagner, C. A.: A Flight Simulator Control System Using Electric Torque Motors. AIAA Paper 75-105, AIAA 13th Aerospace Sciences Meeting, Pasadena, California, January 20-22, 1975.
42. Myers, Albert; and Evans, Martha: SIM II Users Guide. Programming Branch, NASA Flight Research Center, Edwards, California, May 22, 1974.
43. Washington, Harold P.; and Gibbons, John T.: Analytical Study of Takeoff and Landing Performance for a Jet STOL Transport Configuration with Full-Span, Externally Blown, Triple-Slotted Flaps. NASA TN D-7441, October 1973.
44. Powers, Bruce G.; and Kier, David A.: Simulator Evaluation of the Low-Speed Flying Qualities of an Experimental STOL Configuration with an Externally-Blown Flap Wing or an Augmentor Wing. NASA TN D-7454, October 1973.
45. Heffley, Robert K.; and Jewell, W. F.: Aircraft Handling Qualities Data. NASA CR-2144, December 1972.
46. Szalai, Kenneth J.: Validation of a General Purpose Airborne Simulator for Simulation of Large Transport Aircraft Handling Qualities. NASA TN D-6431, October 1971.
47. Etkin, Bernard: Dynamics of Flight. John Wiley and Sons, Inc., 1959. (Chapter 10.)
48. McRuer, D. T.; Ashkenas, I. L.; and Pass, H. R.: Analysis of Multiloop Vehicular Control Systems. Air Force Flight Dynamics Laboratory Technical Documentary Report ASD-TDR-62-1014, March 1964.

DISTRIBUTION LIST

Copy No.

1 - 2	NASA Scientific and Technical Information Facility P.O. Box 8757 Baltimore/Washington International Airport Maryland 21240
3 - 5	Life Sciences Division NASA/Flight Research Center P.O. Box 273 Edwards, California 93523 Attention: Mr. Thomas Wolf
6 - 7	I. D. Jacobson
8 - 9	Maris Lapins
10	A. R. Kuhlthau
11 - 12	E. H. Pancake Clark Hall
13	I. A. Fischer
14	RLES Files
15 - 30	A. T. Symmers

UNIVERSITY OF VIRGINIA

School of Engineering and Applied Science

The University of Virginia's School of Engineering and Applied Science has an undergraduate enrollment of approximately 1,000 students with a graduate enrollment of 350. There are approximately 120 faculty members, of whom, about 90% hold a doctorate. Excellence in graduate education is aided and supplemented by a research program approximating \$3 million per year. This relatively high level of participation in sponsored research is one factor which helps our faculty consistently to maintain high quality graduate education at all degree levels.

As research is an integral part of the educational program, research interests parallel academic specialties. These interests range from the traditional engineering departments of Chemical, Civil, Electrical and Mechanical to include departments of Biomedical Engineering, Engineering Science & Systems, Materials Science, Nuclear Engineering, and Applied Mathematics & Computer Science. In addition to these departmental interests, there are interdepartmental groups in the areas of Automatic Controls and Applied Mechanics. All departments are authorized to offer the doctorate while the Biomedical and Materials Science Departments are graduate degree granting departments only.

The School of Engineering and Applied Science, is an integral part of an outstanding University, which has strong professional Schools of Law, Medicine, and Business Administration. In addition, the College of Arts and Sciences has strong basic science departments in Mathematics, Physics, Chemistry, and other departments relevant to the engineering research program. This not only provides an excellent scholarly climate, but also enhances the school's potential for creating truly interdisciplinary teams in the pursuit of our basic goals of education, research, and public service.

Inside this cover are listed some of the present research activities of the department from which this report originates. For more information on this or other areas, address the department chairman or Dean J. E. Gibson, Commonwealth Professor and Dean, School of Engineering and Applied Science, University of Virginia, Charlottesville, Virginia 22901.